2015

Polycystin-2 (PKD2), Eccentric (XNTA), and Meckelin (MKS3) in the Ciliated Model Organism Paramecium tetraurelia

Megan Smith Valentine
University of Vermont

POLYCYSTIN-2 (*PKD2*), ECCENTRIC (*XNTA*), AND MECKELIN (*MKS3*) IN THE CILIATED MODEL ORGANISM *PARAMECIUM TETRAURELIA*

A Dissertation Presented

by

Megan Smith Valentine

to

The Faculty of the Graduate College

of

The University of Vermont

In Partial Fulfillment of the Requirements
for the Degree of Doctor of Philosophy
Specializing in Biology

October, 2015

Defense Date: June 4th, 2015
Dissertation Examination Committee:

Judith Van Houten, Ph.D., Advisor
Alan Howe, Ph.D., Chairperson
Anthony Morielli, Ph.D.
Jim O. Vigoreaux, Ph.D.
Cynthia J. Forehand, Ph.D., Dean of the Graduate College

Abstract

Paramecium tetraurelia is a ciliated single cell used as a model organism for the study of ciliopathies. Ciliopathies are mammalian diseases involving the dysfunction of cilia, including cilia maintenance, construction, and signaling. *P. tetraurelia* and its cilia provides an excellent non-canonical system for the investigation and elucidation of proteins important for the structure, maintenance and function of cilia and ciliary beating. We utilize features of this cell such as its 1000's of cilia and highly organized and patterned cell surface to observe changes in swimming behavior or disruptions in the ordered cell surface which are not feasible in mammalian cells. Here, we present research on three proteins in *Paramecium*, two of which are homologs to human ciliopathy genes. Using combinations of epitope-tagging, RNA interference (RNAi), immunofluorescence, immunoprecipitations, LC-MS/MS analysis and electrophysiology, we have attempted to elucidate the location, function, and potential interacting partners of these three proteins.

The first protein, meckelin (MKS3), is a contributing factor in Meckel-Gruber syndrome, among other ciliopathies. Using epitope tagging, we identified the location of the Mks3 protein above each basal body. Depletion of *MKS3* using RNAi leads to global loss of cilia, a severe disruption in the surface organization and a mislocalization of basal bodies out of the anterior-posterior axis of the cell. We show that depletion of Mks3 leads to abnormal backward swimming in ionic stimuli and depleted secretion of trichocysts. Based on our data, we propose two functions for Mks3 in *P. tetraurelia*. The first function is a transition zone component important for proper regulation of ciliary protein content, consistent with MKS3 function in other organisms. The depletion of *MKS3* led to global ciliary loss, but also an imbalance in the ciliary ion channels that was different from the loss of cilia due to interference with intraflagellar transport as observed in cells depleted of *IFT88*. The second novel role for MKS3 is as a transient connection to the kinetodesmal fiber which is important for basal body guidance when daughter basal bodies migrate away from the mother basal body before cell division.

We also examine the contribution of the non-selective cation channel Polycystin-2 (Pkd2) in *Paramecium* to Mg^{2+} permeability and Mg^{2+}-induced behavior. When mutated in humans, Pkd2 leads to 15% of the cases of Autosomal Dominant Polycystic Kidney Disease (ADPKD). When *PKD2* is depleted using RNAi in *Paramecium*, cells show short backward swimming in Mg^{2+} solutions, a resistance to heavy metal paralysis, and depleted membrane permeability to Mg^{2+}. The channel-like protein XntA which is unique to *Paramecium* and *Tetrahymena*, is also important for these phenotypes. Therefore, we utilized the *Paramecium* XntA1 mutant in our studies, which lacks Mg^{2+}-induced behavior. We demonstrate that both Pkd2 and XntA are present in the cell membrane and in the cilia. Co-IP assays show that the IP of XntA-myc co-IPs the Pkd2-FLAG channel, but not vice versa, possibly because of an occluded FLAG epitope due to protein interactions. To tease apart the contributions of Pkd2 in the cilia and the cell membrane, electrophysiology was used to measure membrane potential of ciliated and deciliated cells. Depletion of *BBS8* eliminates Pkd2 in the cilia, allowing us to examine Pkd2 activity restricted to the cell membrane of ciliated cells. Depletion of Pkd2 or XntA decreases membrane permeability to Mg^{2+}. When Pkd2 was restricted to the cell membrane via *BBS8* depletion, the membrane permeability to Mg^{2+} increased, much like over-expressing the Pkd2 protein. Depletion of Pkd2, especially in the deciliated XntA1 mutant, leads to a dramatic decrease in Mg^{2+} membrane permeability. Based on these data, we propose that Pkd2 is the Mg^{2+} channel in *Paramecium* and XntA is not a channel, but is perhaps important for stabilizing Pkd2 in membrane microdomains.

We have uncovered novel function roles for the proteins mentioned here, leading to a broader understanding of their function. These studies also highlight to usefulness and importance of the model organism *Paramecium tetraurelia* to the study of human ciliopathy genes.

Citations

Material from this dissertation has been published in the following form:

*Picariello, T., *Valentine, M.S., Yano, J., and Van Houten, J.. (2014). Reduction of Meckelin Leads to General Loss of Cilia, Ciliary Microtubule Misalignment, and Distorted Cell Surface Organization. *Cilia*, 3:2.

*These authors contributed equally to this work.

Acknowledgements

I cannot begin to express my appreciation and gratitude to my supervisor, advisor, and mentor, Dr. Judith Van Houten, University Distinguished Professor. You have taught me so much and I am forever indebted to you for the opportunities and experiences you have provided me. I have great admiration for you. You have been a role model and an inspiration. I would also like to thank my other committee members, Dr. Alan Howe, Dr. Jim Vigoreaux, and Dr. Tony Morielli. You have been helpful and supportive and your insight and interest in my research have been very encouraging. Even though two of you were on my Master's committee, you continued to see me through this next stage. I also appreciate Dr. Morielli's guidance with my latest adventure of learning electrophysiology. I truly appreciate all of you and your insights.

I cannot move forward without thanking Dr. Junji Yano. There is not a student whom has graduated or left Dr. Van Houten's lab that hasn't learned something from "The Master of Microinjection." I have learned a great deal from Dr. Yano and never would have been able to complete my work without his patience and help. I would also like to thank other members of the Van Houten lab, past and present. This includes Heather Czapla, Carlie Wilson, Cassandra Love (Jacobs), Mallory Romanovitch, Dilhan Weeraratne, Sukanya Lodh, Meagan Keiser, Anbazhagan Rajendran, Wade Bell, Samsudeen Ponissery Saidu, among others.

I would like to thank all of the individuals whom have provided technical assistance, including Dr. Todd Clason for DeltaVision microscopy. Also, Michele Von Turkovich and Jan Schwarz for SEM and TEM assistance and training. I would like to thank Julia Fields, Dr. Wai Lam and Dr. Bin Deng for all their help with sample preparation and LC-MS/MS analysis and support. Thank you to Jeremy Arenos and Dr. Jon Vick for their help with getting me off the ground with starting electrophysiology work.

My family and friends have been my help behind the scenes. Especially my mom and dad. The pursuit of a Ph.D. was partially my dad's idea. Without him and his guidance, I would never have made it to where I am now. My mother has also been a great source of strength and continued support. I appreciate all the long runs, talks, support, and love from all my parents and my brother. Although we don't talk much, my brother is another inspiration in my life. My husband Scott has been supportive throughout this process and I truly appreciate his patience and most of all, his encouragement. My daughter has been a constant source of laughter and light through this whole process, a true source of joy. I also want to thank my Uncle Jim for his support and "tough love." Also, I want to thank my late grandparents Jack and Kathleen. I wish you were here. Lastly, all my friends - who constantly ask me when I will be done! From my Reach the Beach Van-mates to my college hallmates, they have all helped in some way. I especially want to thank my closest friends, Jess C., Jess G., Heather K., KP, Cindy, Noel, and everyone else along the way whom has offered a run, a hug or a laugh, and a swift kick in the butt when required, thank you. This has been a journey, a challenge, and a test. I have enjoyed the ride.

Table of Contents

List of Tables

List of Figures

Chapter 1

Chapter 2

Chapter 3

Chapter 1: Comprehensive Literature Review

I. *Paramecium tetraurelia*

Structure

Paramecium tetraurelia is a ciliated single-celled eukaryotic protist that lives in fresh water (Figure 1.1). These cells can be seen by the naked eye and are 100 to 200 μm in length. Paramecia have a highly organized cell surface which is structured into hexagonal units called cortical ridges. Each of the repeated cortical units contains one or two basal bodies with a cilium arising and a parasomal sac. Parasomal sacs are used for endo- and/or exo-cytosis, but whether the function is endocytosis, exocytosis, or both, is debated (Flotenmeyer et al., 1999, Plattner and Kissmehl, 2003, Allen, 1988, Allen and Fok, 1980). Just beneath the cell membrane are alveolar sacs which are membrane-bound calcium storage organelles. These sacs are believed to connect between units, but have small openings for the basal bodies and for the trichocysts (Allen, 1971). The alveolar sacs provide the majority of the calcium needed for the secretion of the trichocysts (Stelly et al., 1991), although some calcium is also supplied from the extracellular space (Iwadate and Kikuyama, 2001). Trichocysts are membrane-bound organelles containing an inner and outer sheath. They can be ejected from the cell in the event of a predator encounter (Buonanno et al., 2013). Below the alveolar sacs lies the epiplasm. The epiplasm is a continuous amorphous layer containing perforations near the crests of the cortical ridges. It also has 9 equidistant-spaced perforations around the outside of the bottom (proximal) surface of the basal body (Allen, 1971).

Behavior

The behavior of paramecia was first described by Jennings (Jennings, 1906). He described in depth both their forward swimming patterns as well as the "avoidance reaction". The avoidance reaction occurs when a *Parameicum* encounters an unfavorable environment or a

physical barrier (Jennings, 1906). The avoidance reaction is a rapid and coordinated change in the ciliary beat pattern which is dependent upon calcium (Machemer and Eckert, 1973). This reaction results in a rapid backward movement of the cell, quickly followed by a reorientation, at which point the cell swims off in another direction.

Ionic changes in the environment can cause swimming reversal by bringing the membrane potential of the cell above threshold for an action potential. Calcium that enters the cilia during the action potential causes a change in the ciliary power stroke from a power stoke toward the posterior of the cell to a power stroke toward the anterior, resulting in backward movement of the cell (Machemer and Eckert, 1973). The calcium enters the cilia through the voltage-dependent calcium channels (Ca_V) which are found exclusively in the ciliary membrane (Dunlap, 1977). These action potentials are graded (Eckert and Brehm, 1979). Rapidly after the calcium enters the cilia, an outward potassium current is produced (Eckert and Brehm, 1979). The efflux of potassium ions occurs through the Ca^{2+}-dependent K^+ channels and the voltage-dependent K^+ channels (Figure 1.2). The majority of these channels are expected to reside in the ciliary membrane to respond to high intraciliary calcium levels (Brehm et al., 1978). The cell will maintain the ciliary power stroke toward the anterior of the cell, and therefore backward swimming, as long as the calcium remains high in the cilia (Brehm et al., 1978, Eckert, 1972).

The electrical potential across the membrane of *Paramecium* governs both the swimming speed and direction of the cell (Van Houten, 1979). Paramecia accumulate in areas of attractants presumably in a search for their food. Paramecia are unable to orient and migrate directly toward an attractant in a taxis as shown by *Dictyostelium* (Gerisch, 1982) and *C. elegans* (Bargmann, 2006). Paramecia display a chemokinesis, a behavior by which the cells move up a gradient of attractant by a biased random walk (Van Houten, 1979). Paramecia have a resting membrane potential of approximately -25 to -40 mV (Machemer and Eckert, 1973, Machemer and

Ogura, 1979, Preston and Van Houten, 1987, Brehm et al., 1978, Van Houten, 1979). As a cell encounters strong attractants, the membrane will hyperpolarize (become more negative) by 8 to 10 mV and the cell will swim fast and smoothly forward (Van Houten, 1979). A strong repellent, such as barium, will cause the cell to depolarize (become more positive) by up to 25 mV, instituting more frequent turning and possibly bouts of long backward swimming and ciliary reversal.

The receptors and channels necessary for these chemical cues are located in the cell membrane, the cilia or both. The GPI-anchored (glycosyl phosphatidylinositol) folate receptor is located at the tips and the bases of the cilia (Valentine et al., 2012, Weeraratne, 2007). Some receptors are concentrated in the cilia and are not expected to be abundant in the cell membrane, as in the case of the glutamate receptors (Valentine, unpublished data (Jacobs, 2007, Romanovitch, 2012, Van Houten et al., 2000)). These receptors contribute to the membrane potential changes that occur through second-messenger pathways. For the glutamate receptors, the membrane becomes more negative by the activation of a K^+ conductance and is maintained at hyperpolarized levels by the plasma membrane calcium ATPase pumps (PMCAs; calcium extrusion). The ciliary adenylyl cyclase that is also a potassium channel is activated by glutamate, and cyclic AMP is a second messenger for this pathway. Protein Kinase A (PKA) is activated by the cAMP. The substrate activated by the PKA is thought to be the PMCAs which are activated by PKA phosphorylation (Van Houten et al., 2000, Schultz et al., 1992). These changes in membrane potential help facilitate the swimming speed and direction of the ciliary beat to assist *Paramecium* in locating their food (Van Houten, 1979).

Cell Membrane and Cilia

The cell surface membrane of *Paramecium* is often referred to as the "pellicle." The "pellicle" of *Paramecium* is comprised of the plasma membrane, the alveolar sacs, and the

epiplasm. These components are very difficult to separate (Allen, 1988). The plasma membrane is contiguous with the ciliary membrane, although they are compositionally different (Brehm et al., 1978, Capdeville, 1993). The difference between the plasma membrane and the ciliary membrane is true for both lipid and protein content. The cilia contain more phosphonolipids, ester lipids, and sphingophospholipids than the cell membrane (Kaneshiro, 1987, Rhoads and Kaneshiro, 1979). The channels and receptors differ between the two membranes. For example, the voltage-dependent calcium channels are exclusively found in the cilia (Dunlap, 1977) while the channels responsible for the mechanosensitivity of the cell reside in the cell membrane (Ogura and Machemer, 1980). The rectifier channels and those channels responsible for the resting conductances of the cell are also expected to be in the cell membrane (Machemer and Ogura, 1979).

The entire surface of *Paramecium* is covered in cilia. There are approximately 1000 of them on each cell (Machemer and Ogura, 1979). These organelles are 10 μm in length and 0.2 μm wide (Machemer and Eckert, 1973). Cilia account for approximately 50% of the surface area of the cell. Conveniently, the cilia can be easily removed from the cell through an ethanol treatment and trituration (Machemer and Ogura, 1979) or treating the cell with 4 mM chloral hydrate (Dunlap, 1977). Neither of these deciliation methods are permanent. The paramecia will regrow their cilia over a period of hours, regaining full length and function in 10 hours. Deciliation also permits the return of the graded calcium action potentials, although the return of channel function is not linear. It has been inferred from electrophysiology studies that the distribution of the Ca_V channels is non-uniform along the cilium, with more channels concentrated at the distal end (Dunlap, 1977). After deciliation, the capacitance of the cell is decreased by 50% but the resting membrane potential remains unaltered (Machemer and Ogura, 1979). When the cell is deciliated, the cilia break above the axosome, leaving the proposed transition zone and ciliary necklace with the cell body (Machemer and Ogura, 1979, Satir et al., 1976).

Basal Bodies and Duplication

Basal bodies are highly conserved structures analogous to centrioles located just below the cell surface that anchor the cilia (reviewed in (Beisson and Wright, 2003)). A basal body is composed of nine triplets of microtubules that form a circle approximately 220 μm in diameter and 400 μm long. The tubules, A, B, and C, form a cartwheel pattern where the A tubule is connected to the C tubule of the neighboring triplet by a fiber. At the base of the cilium, the triplet becomes a doublet of microtubules, as the A and B tubules continue to form the backbone of the cilium, referred to as the axoneme (Ringo, 1967). Radial spokes and inner and outer dynein arms fill the center of the axoneme along with a central pair of microtubules in some cases. The radial spoke proteins are essential to the beating and bending of the cilium. Cilia are analogous to flagella, similar in structure and function to flagella. The best described flagella are in the green algae, *Chlamydomonas* (Yang et al., 2006).

Basal bodies are anchored in place below the cell surface by numerous rootlets. These rootlets help to stabilize the basal body during ciliary beating and also in the division process (Iftode, 1996, Iftode and Fleury-Aubusson, 2003). There are three rootlets that emanate from the basal bodies in *P. tetraurelia*. As if a face of a clock, the striated rootlet (also known as the kinetodesmal fiber) emanates from ~10 o'clock and projects anteriorly, connecting with other kinetodesmal fibers traversing numerous cortical units. A post ciliary rootlet projects at 7 o'clock and the transverse microtubule projects at 5 o'clock. Some cortical units contain two basal bodies. In the case of two basal body units, the anterior of the two basal bodies is considered a daughter basal body. The daughter basal body attaches to the kinetodesmal fiber and has a post ciliary rootlet, but no transverse microtubule and no cilium arising from it (Iftode and Fleury-Aubusson, 2003, Iftode et al., 1989). (See Figure 1.3 for a schematic illustration.)

The basal bodies, along with the other components in the cell, must duplicate when *Paramecium* divides. The process of division is highly ordered and binary, producing two identical daughter cells. Division begins by a cell becoming larger and producing extra basal bodies. A fission furrow will form around the center of the cell and a new oral apparatus develops. There are two waves of duplication of the basal bodies. The first wave has two rounds of duplication. In the first round, a new basal body is produced in each cortical unit. The second round creates another new basal body in each cortical unit. The second round of duplication mostly takes place around the central midline of the cell, yielding three or four basal body units which then separate and reform the cortical ridges to delineate each unit. During division, the cytoskeletal structures, such as the kineties and the epiplasm, are broken down and elongated, then rebuilt with the cortical units (Iftode, 1989, Iftode and Fleury-Aubusson, 2003, Ruiz et al., 2005).

Paramecium as a Model Organism

Paramecium is an excellent model organism not just because they are easy to grow and maintain, but they are also amenable to techniques such as electrophysiology and RNA interference (RNAi) by feeding. These cells survive easily at room temperature (20 to 25°C) and divide approximately every six hours. They can grow to great densities, upwards of 30,000 cells per mL, which can be collected. The cilia and cell bodies can be collected separately for biochemistry studies (Wright and van Houten, 1990, Adoutte et al., 1980). The genome for *Paramecium* has been sequenced and annotated (ParameciumDB, http://paramecium.cgm.cnrs-gif.fr/) (Arnaiz et al., 2007, Arnaiz and Sperling, 2011). There are numerous behavioral mutants available for study, many of which, the affected protein has been identified (reviewed in (Kung and Saimi, 1982, Preston and Kung, 1994b, Preston and Kung, 1994a)). There are many reasons, not just the ones mentioned here, that make *Paramecium* an attractive model organism.

II. The *Paramecium* Mutant *eccentric* and Mg^{2+}

Paramecium Reproduction and Creating a Mutant

Paramecia cells contain one somatic polyploidy macronucleus and two germ line diploid micronuclei. Paramecia cells are able to divide both sexually and asexually. These cells divide asexually by binary fission, creating two identical daughter cells. This process usually takes place when the cells are well fed in a bacteria-rich environment. *Paramecium* can also exchange genetic material by reproducing sexually through conjugation. During conjugation, two paramecia cells of opposing mating types join and exchange genetic material. After the two cells fuse, the micronuclei undergo meiosis and are exchanged between the cells. The micronuclei then fuse and the old macronuclei of the conjoined cells are degraded. To complete conjugation, each cell duplicates its micronuclei, develops a new macronucleus, then the cells separate (Cronkite, 1974). In the last process of reproduction, cells are able to undergo autogamy, which produces a diploid cell that is homozygous for all genes (reviewed in (Kung et al., 1975)). The process of autogamy is very useful in genetic studies of these cells.

The multiple nuclei of these cells makes site-directed mutagenesis nearly impossible. However, by forcing paramecia cells through the process of autogamy after the application of a general mutagen, a genetically homozygous diploid cell is produced (Kung et al., 1975). Autogamy is the rearrangement of the somatic macronucleus. It is a unique form of sexual reproduction that the cell is able to perform by itself. During autogamy, the cell degrades the polyploid macronucleus. The germ line micronuclei then go through meiosis to first separate into haploid micronuclei which then duplicate. Of the four haploid meiotic products, three will randomly degrade. The cell then progresses to mitosis where the one remaining haploid nucleus divides and reunites to form a diploid cell. This division process produces a cell that is completely homozygous in all genes. The resulting cell is genetically a diploid, but expresses the

genes phenotypically because the genes are identical (Kung et al., 1975). The process of autogamy after a mutagen is applied provides a stable cell line with two identical copies of each gene. The cell lines can then be screened for mutants with the desired phenotype.

A commonly used mutagen applied to paramecia cell populations is *N*-methyl-*N'*-nitro-*N*-nitrosoguanidine (MNNG). The mutagen MNNG can add methyl groups to guanine residues, creating 7-methyguanine (Craddock, 1968). After the application of MNNG, approximately 50% of the paramecia will die (Preston and Kung, 1994a). Those paramecia that do survive and successfully go through autogamy can then be used for behavioral tests or screens. The cells that have gone through autogamy would phenotypically display their genotype, as already described for autogamy (Kung et al., 1975). Methods to rapidly screen large groups of cells for changes in behavior allow for the desired phenotypes to be identified and isolated. The methods used often rely on the ability of the cells to react to gravity by swimming upward in solution as well as to the reaction to ionic stimuli (Preston and Kung, 1994b, Kung, 1971).

Screening for Mg^{2+} Mutants

Paramecia cells are reactive in Mg^{2+} solutions and will swim backward or jerk when they are exposed to 5 mM $MgCl_2$. A Mg^{2+} current in *Paramecium* was first described in 1990 (Preston, 1990). Soon after, researchers sought to isolate mutants defective in their reaction to Mg^{2+}. After exposing a population of cells to the mutagen MNNG and allowing the cells to go through autogamy, the population was screened for cells unreactive to Mg^{2+} solutions. The initial screening involved placing the mutagenized cells in a trough of a galvanotactic chamber. A 40V pulse was applied to the trough every 50 msec at a frequency of 4 Hz. The controlled application of an electrical pulse oriented the cells such that their anterior end was pointed toward the cathode of the trough. When Mg^{2+} was added to the trough, the cells would react, and swim backward toward the anode unless they were deficient in their response to Mg^{2+}, in which case

the cells would swim forward toward the cathode. The unreactive cells, those that swam forward, were then cultured as single-cells for analysis (Preston and Kung, 1994b).

Although Preston and colleagues screened the mutants for cells that were unreactive in Mg^{2+}, some cells were just generally unresponsive to depolarizing ions. Other cell types that were isolated included "pawn" mutants and "atalantas." These mutants are unable to reverse their cilia, therefore the deficiency was not Mg^{2+}-specific. Because *pawns* and *atalantas* cannot swim backward, they made it through the initial galvanotactic chamber screening using Mg-solutions because they were unable to reverse their cilia (Kung and Naito, 1973). Preston and colleagues tested the newly created mutants in different ionic stimuli other than those containing Mg^{2+}. They also used back-crossing of these newly created mutants with other mutant lines to determine the genetic relationship of these newly mutated genes (Preston and Kung, 1994b).

***Eccentric* Mutants (XntA and XntB)**

The Mg^{2+}-resistant mutants that were isolated harbor recessive mutations of two different single mutations. The first demonstrated a strong resistance to Mg^{2+}-induced behavior, these were referred to as XntA mutants (XntA1, XntA2, and XntA3). The second group was weakly resistant to Mg^{2+}, referred to as XntB. The name "eccentric" comes from the odd behavior of these cells which was very distinguishable from the wild type cells. The *eccentric* mutants, while swimming in culture fluid, would display complex turns and bouts of long and rapid backward swimming. The abnormal behavior was described as being eccentric, hence the mutant's name, *eccentric* (Xnt) (Preston and Kung, 1994b, Preston and Kung, 1994a).

The eccentric mutants have phenotypes other than an absence of Mg^{2+}-induced behavior. The Xnt mutants are also resistant to $NiCl_2$ ciliary paralysis. *Paramecium* incubated in heavy metals have been shown to decrease their ciliary motion or even become paralyzed, unable to

move the cilia (Naitoh, 1966). Similarly, in mammalian cells, a concentration of 100 μM $NiCl_2$ caused reduced metabolism in the cells and ciliary paralysis of rat, guinea pig, and hamster tracheal explants. The exposure to $NiCl_2$ did not change the morphology of the cilia (Gabridge et al., 1982). When wild type and XntA paramecia were incubated for 24 hours in a 50 μM $NiCl_2$ solution, all the wild type cells were dead or paralyzed while the XntA mutants were unaffected (Preston and Kung, 1994b). The XntB mutants were also found to be resistant to this paralysis, but to a lesser extent than the XntA mutants. The conclusion was that Ni^{2+} must enter the cells through the same channel or using the same proteins as Mg^{2+} (Preston and Kung, 1994b).

There are two other phenotypes of XntA mutants that are not heavily researched or discussed. These mutants have a very fast deactivation of the calcium-dependent sodium current. This can be observed as very short backward swimming in sodium-tetraethylammonium (TEA) solutions or by using voltage clamp in the presence of 10 mM TEA with 10 mM NaCl. The step-depolarization of the XntA cells elicits tail currents that decay twice as fast as wild type tail currents under the same conditions (Preston and Kung, 1994a). XntA mutants also have a slow deactivation of the depolarization-activated calcium current. These mutants show long backward swimming in high K^+ solutions, twice that of the wild type cells (Preston and Kung, 1994b, Preston and Kung, 1994a). Under voltage clamp, the inactivation of the depolarization-activated K^+ current is seen in a slow recovery after depolarization steps from -40 mV to -10 mV (Preston and Kung, 1994a).

Paramecium Intracellular Mg^{2+} Concentrations and $I_{Mg(Ca)}$

Over 300 enzymatic reactions require Mg^{2+}, including binding ATP and ATP synthesis, synthesis of proteins, fat, and nucleic acids, and neurotransmitter release, to name a few (Maguire and Cowan, 2002). Therefore, the intracellular concentration of Mg^{2+} ions is very tightly regulated. Techniques are still being developed to detect and calculate the concentrations of

intracellular free Mg^{2+}. The commonly accepted intracellular concentration of free Mg^{2+} in mammalian cells is 0.3 mM (Maguire and Cowan, 2002). Not much different is the intracellular free Mg^{2+} concentration in *Paramecium*, calculated to be 0.4 mM (Preston, 1990, Preston, 1998). *Paramecium* also has an unknown intracellular Mg^{2+} store that has a concentration of 8 mM, far higher than the intracellular concentration. These concentrations were determined using a Mg^{2+}-specific dye, Mag-fura-2 (Preston, 1998).

The membrane of *Paramecium* is permeable to Mg^{2+} and will depolarize. The concentration of Mg^{2+} must be 0.5 mM or higher for a significant depolarization to occur producing an action potential (Preston, 1990). The action potential is prolonged in solutions containing Mg^{2+} because of the calcium-dependent Mg^{2+} conductance ($I_{Mg(Ca)}$). The XntA mutants lack the $I_{Mg(Ca)}$, showing no Mg^{2+}-induced behavior (backward swimming) and very little membrane depolarization, ~1 mV (Preston and Kung, 1994b, Preston and Kung, 1994a, Haynes et al., 2002). Upon depolarizing *Paramecium* using voltage clamp in the presence of Ca^{2+} and Mg^{2+}, Ca^{2+} and Mg^{2+} will enter the cell. Once the cell is returned to -30 mV, a typical resting potential for the cell, a tail current occurs. The tail current is the closing of the Mg^{2+} channel and its current has been determined to purely Mg^{2+}; it does not occur when Mg^{2+} is removed from the bath. The tail current is 1-2 nA and is calcium-dependent (Preston, 1990). The source of the Ca^{2+} needed for this conductance comes from the ciliary voltage-gated Ca^{2+} channels (VGCCs) (Dunlap, 1977). If the paramecia cells are deciliated, they no longer elicit I_{Mg} under physiological conditions. Similarly, *pawn B* mutants, which do not have VGCC's in the cilia, also do not elicit I_{Mg} under physiological conditions (Preston, 1990, Preston and Kung, 1994a, Preston, 1998).

XntA Protein and Gene (*XNTA*)

In 2002, the gene that cured the XntA mutants was found using phenotypic curing of the mutant after microinjection of fragments of the DNA library of wild type cells. The locus was

eventually mapped to a 2,427 bp fragment of DNA that cured the mutant when injected, but not the mutant equivalent of the same fragment. The DNA sequence was eventually determined using reverse transcriptase PCR (RT-PCR). The gene for *XNTA* is 1,707 bp long and contains two introns. The other XntA mutants were cured by expressing this same gene, but the XntB mutant was not (Haynes et al., 2002). The gene is translated into a predicted protein of 550 amino acids with 11 predicted transmembrane spanning domains. The protein can be divided into two regions, α1 and the α2, which are separated by a long intracellular domain. The α1 and the α2 regions show low levels of homology to the Na^+/Ca^{2+} exchanger (NCX) and $Na^+/Ca^{2+}/K^+$ exchanger (NCKX) proteins, respectively. The intracellular domain contains a possible PEST sequence, which may target the protein for early degradation. The mutation creating XntA1 is a deletion at cysteine 111 which generates a premature stop (Haynes et al., 2002). The premature stop would severely truncate the protein, most likely rendering it useless.

The function of the XntA protein is unknown. XntA is described as a possible Mg^{2+}-specific channel-like exchanger protein. However, the authors do not specifically name the protein as a channel or as an exchanger (Haynes et al., 2002). Although the authors were successful in curing the mutant with the *XNTA* wild type gene for I_{Mg} and Mg^{2+}-induced behavior, they did not address either of the other behavioral phenotypes. The authors did not test the backward swimming in high K^+ or Na/TEA nor did they examine the heavy metal paralysis resistance of the XntA mutant (Haynes et al., 2002). It has been speculated that the XntA protein may be a regulatory protein of the Mg^{2+} influx (Haynes et al., 2002) or that eccentric mutants may be a phosphatase or kinase mutant (Preston and Kung, 1994a, Preston and Kung, 1994b). There is still much more to learn about the function and regulation of the XntA protein in *Paramecium* and its contribution to the conductance of Mg^{2+}.

III. Cilia and Ciliopathies

Cilia Structure

Cilia are membrane-bound organelles that protrude from the surface of eukaryotic cells. A cell may have one or many cilia. Cilia behave as an "antennae," sensing the surrounding environment and sending signals back to the cell. These organelles are typically characterized as "9+0" or "9+2." Primary non-motile cilia are typically a "9+0" configuration, lacking a central pair of microtubules. Motile cilia are typically a "9+2" configuration and contain the central pair of microtubules (reviewed in (Fliegauf et al., 2007)). There are exceptions to these rules, as embryonic nodal cilia, which are motile with a configuration of "9+0," are important for left-right asymmetry determination (Nonaka et al., 1998). Non-motile kinocilia in the inner ear have a "9+2" arrangement (Flock and Duvall, 1965). Motile cilia can also be sensory, as seen in *Paramecium*. Numerous receptors that are important for locating food and interacting with the surrounding environment are found in the cilia of this cell (Weeraratne, 2007, Jacobs, 2007).

Cilia do not contain the necessary machinery for protein production. Therefore, they require proteins to be trafficked in from the cell to the cilium and along the axoneme. The axoneme runs up the center of the cilium and contains the 9 outer pairs of A and B microtubules, and in some cases, the central pair of tubules as well. The A and B tubules are extensions from the basal body (Ringo, 1967). Cilia develop from the base to the tip (Johnson and Rosenbaum, 1992) using the B tubule as a highway for cargo movement up and down the cilium (Kozminski et al., 1993). This transport system is called intraflagellar transport (IFT), first described in *Chlamydomonas* (Kozminski et al., 1993). IFT moves the cargo in trains from the base to the tip using anterograde transport with kinesin-2 motor proteins (Kozminski et al., 1995). The cargo return from the tip to the base using retrograde transport and cytoplasmic dynein (Pazour et al., 1999, Porter et al., 1999). For review of IFT and cargo interactions, see (Bhogaraju et al., 2013).

A barrier exists between the cilia and the cell membrane called the transition zone. The transition zone separates the ciliary compartment from the inside of the cell. As already mentioned, the membrane of the cell surface and the cilia are contiguous, but they are compositionally different. The transition zone is important to keep these compartments separate by creating a selective filter, only allowing certain proteins to enter the cilium. This zone in cilia with a "9+2" arrangement spans from the basal body, where the C tubule terminates, to where the central pair of tubules begins in the cilium (Garcia-Gonzalo et al., 2011, Aubusson-Fleury et al., 2012). Proteins in this zone form a filter that allows the selective passage of proteins into and out of the cilium, regulating the contents (Figure 1.4). The filter is a complex and includes the tectonic (Tctn) proteins, specifically Tctn 1, which is essential for ciliogenesis in some cell types. Other proteins that comprise this filter in mammalian cells include MKS1, Tmem267, MKS3, Cep290, Cc2d2a, B9d1, and Tctn 2 (Garcia-Gonzalo et al., 2011). In *Paramecium*, the conserved centrosomal FOP family protein (FGFR1 Oncogene Partner) FOR20 is required for the building of the transition zone, as well as the centrin protein Cen2 (Aubusson-Fleury et al., 2012).

Ciliary Defects and Ciliopathies

When cilia are defective or dysfunctional, the resulting pathology or disease is referred to as a ciliopathy. The most common physiological abnormalities that arise from these diseases include, but are not limited to, cystic kidneys, retinal degeneration, anosmia, liver fibrosis, obesity, developmental delay, situs inversus, and infertility (reviewed in (Hildebrandt et al., 2011)). Although the commonality among ciliopathies are dysfunctional cilia, these diseases are very tissue- and cell-type specific. Some ciliopathies can be treated with medication, gene therapy or transplantations while others can be fatal.

Advances in genetic screening have allowed much better diagnosis of patients with ciliopathies. Large data bases of gene mutations are available for some diseases as well as

information forums and support groups. Genetic testing is also available for many ciliopathy diseases (see http://pkdb.mayo.edu, http://www.med.unc.edu/pulmonary/specialties/areas-and-programs/pcd, or http://www.rarediseases.org/rare-disease-information/rare-diseases/byID/20/printFullReport). The list of genes contributing to ciliopathies is ever-growing, emphasizing the importance of research on ciliary dysfunction to better understand the contributions made by these ciliopathy proteins in their mutated and non-mutated forms. It is important to identify the genes and proteins involved as well as identify their location, role within the cell, as well as potential interacting partners within the systems and cells of which they reside.

Meckel-Gruber Syndrome and MKS3

Meckel-Gruber Syndrome (MKS) is a ciliopathy disease caused by mutations in at least three proteins leading to renal dysplasia, encephalocele, and polydactyly (Salonen and Norio, 1984, Salonen and Paavola, 1998). MKS is a rare recessive disorder with world-wide rates ranging between 1 in 13,250 and 1 in 140,000 births. Geographic areas such as Finland, the Middle East, and North Africa have higher rates of incident, 1:9,000 (Salonen and Norio, 1984). MKS can be diagnosed early using an ultrasound at 11 to 12 weeks of gestation to detect developmental abnormalities (Sepulveda et al., 1997). There is no treatment for this disease and in severe cases of this syndrome, individuals may die before birth or may only live a few hours after birth (Salonen and Paavola, 1998).

The MKS3 protein, or TMEM67, is one of the contributors to the MKS ciliopathy when it is mutated. The MKS3 protein is highly conserved among organisms. In humans MKS3 is 995 amino acids in length, with a molecular weight of 108 kD. The protein is postulated to have three or seven transmembrane spanning regions, although more current publications characterize the protein as containing three (Dawe et al., 2007, Smith et al., 2006, Dawe et al., 2009). MKS3 is a

component of the transition zone complex in mammalian cells, important for forming a filtration barrier separating the ciliary compartment from that of the rest of the cell (Garcia-Gonzalo et al., 2011, Chih et al., 2012, Czarnecki and Shah, 2012, Williams et al., 2011). MKS3 has also been shown to play a role in the positioning of basal bodies and the formation of cilia (Dawe et al., 2007). Continued research aims to further understand the MKS3 protein and its multiple roles in the positioning of basal bodies and functioning as a ciliary gate-geeping transition zone complex protein.

Autosomal Dominant Polycystic Kidney Disease (ADPKD)

Autosomal dominant polycystic kidney disease, or ADPKD, is one of the most common and potentially lethal inherited human diseases in the world. ADPKD is characterized by kidney cysts, rendering the kidney non-functional in approximately 45 to 50% of patients by the age of 60 (Gabow, 1993). Typically ADPKD is inherited as autosomal dominant gene mutations. Spontaneous mutations leading to the disease occur in less than 10% of the cases (Gabow, 1993). The first gene identified in ADPKD was *PKD1*, or polycystin-1, located on the short arm of chromosome 16 (Reeders et al., 1985). Later, the second gene was identified, *PKD2* or polycystin-2 (TRPP2 or Pkd2), on chromosome 4 (Mochizuki et al., 1996). A third gene is thought to exist, but has yet to be identified (Daoust et al., 1995).

Currently, a database to report the mutations and families associated and affected by ADPKD is available (http://pkdb.mayo.edu). As of February 1st, 2015, there are 2,322 families in the ADPKD database with 2,055 reported mutations in *PKD1*. Another 463 families with the disease containing 278 different mutations in *PKD2* (ADPKD, 2014). Mutations in *PKD1* also account for earlier-onset of end-stage renal failure (ESRF) from the disease compared to mutations in *PKD2*. On average, ESRF for individuals with mutations in *PKD1* occur at 58.1 years of age while those individuals with mutations in *PKD2* have renal failure onset on average

at 79.7 years of age (Cornec-Le Gall et al., 2013). Also, truncation mutations are far more severe with an earlier onset of ESRF. Truncation mutations of *PKD1* led to ESRF at age 55.6 compared to 67.9 years of age for those mutations which were in-frame or missense (Cornec-Le Gall et al., 2013).

Mutations in the *PKD* genes cause varying degrees of severity of ADPKD. The mutations can cause missense mutations, splice site mutations, truncations, and can be as simple as amino acid substitutions. Rarely are large deletions of *PKD1* observed, accounting for approximately 4% of the cases of ADPKD (Ariyurek et al., 2004). Unfortunately the *PKD1* gene is very complex, duplicated multiple times on chromosome 16, so identifying mutations in *PKD1* typically requires direct sequencing. Mutations in the *PKD1* and *PKD2* genes can be analyzed to predict the severity of the mutation. Interestingly, two mutations predicted to be "benign" mutations identified in the *PKD1* gene manifested as extremely severe in the patients with the mutations. In these "benign" cases, the manifestation of the disease was apparent at birth and at 3 months of age (Hoefele et al., 2011). In the same study, another predicted "benign" mutation in the *PKD2* gene led to early onset of renal failure, however, the amino acid that was altered was shown to be highly conserved evolutionarily (Hoefele et al., 2011). Other mutations in the *PKD2* gene that lead to more severe manifestations of the disease are truncation mutations that occur at the C-terminus. These truncation mutations effect the trafficking of the Pkd2 protein and are often used in research, which will be discussed shortly (Cai et al., 1999, Tsiokas et al., 1997b, Hanaoka et al., 2000).

Mutations in Pkd1 and Pkd2 mostly affect the kidneys, but other organs, such as the liver and pancreas can develop cysts. Also, because *PKD1* and *PKD2* are expressed in vascular smooth muscle, mitrial valve prolapses, artery dissections and aneurysms are not uncommon. Brain aneurysms can also occur (Reviewed in (Torres et al., 2007)). Annual healthcare costs for

treatment per patient (data collected from 2003 to 2006) range from $26,521 to $140,139. The annual cost of dialysis, the most common form of treatment for the disease, is $131,890 per patient. In-hospital stays for a kidney transplant, which is currently the only way to stop the progression of the disease, costs $119,931 (Lentine et al., 2010). Recently, the use of tolvaptan, a vasopressin receptor agonist which has been approved as a treatment for hyponatremia (low blood sodium), has been investigated to slow the progression of the disease by slowing cyst growth and development. There are risks to taking this medication, however. Liver function and uric acid levels must be monitored and thirst and frequent urination can be a problem (Torres et al., 2012).

Mammalian Pkd1 and Pkd2

The *PKD1* and *PKD2* genes and their proteins were identified and described in the mid-1980's 1990's. The Pkd1 protein was described in 1995. Its sequencing was complicated by chromosomal rearrangements that take place on chromosome 16 (Hughes et al., 1995). Pkd1 is a 450 to 460 kD protein, approximately 4300 amino acids in length (Hildebrandt et al., 2011, Chapin and Caplan, 2010, Hughes et al., 1995). The protein sequence contains a very long extracellular N-terminus consisting of over 2500 amino acids followed by 11 transmembrane spanning domains and very short intracellular C-terminus (Hughes et al., 1995). The large extracellular domain contains two leucine-rich repeats, followed by 16 repeats that resemble IgG folds, and a calcium-dependent lectin domain. The last 1000 amino acids before the transmembrane domains contains an amino acid sequence that is similar to that of the guanylyl cyclase receptor for egg jelly, as seen in sea urchin spermatozoa. In human fetal kidney cells, the Pkd1 protein co-localizes with the catenins and E-cadherin, suggesting it is important for protein-protein and protein-carbohydrate interactions and junctions between cells (Huan and van Adelsberg, 1999).

Although Pkd1 is considered a transient receptor potential (TRP)-like protein, it is not a member of the TRP superfamily (Giamarchi and Delmas, 2007).

The human *PKD2* gene, located in chromosome 4, encodes a 968-amino acid protein which spans the membrane 6 times (Mochizuki et al., 1996). The Pkd2 protein contains intracellular N- and C- termini with a C-terminal EF-hand (Mochizuki et al., 1996). The full-length human version contains a 34-amino acid endoplasmic reticulum (ER) retention sequence located at the C-terminus that contains two phosphorylation sites (Cai et al., 1999). A pore loop exists between the fifth and sixth transmembrane domains that is predicted to have a helix-loop structure with three negatively charged amino acids in the loop structure (Nomura et al., 1998). These conserved negatively charged amino acids are important for the conductance of calcium ions. The structure and negatively charged amino acids are similar to the α1 region of the voltage gated calcium channels (Nomura et al., 1998).

Pkd2 is a member of the transient receptor potential channels (TRP channels), a member of the P-type family (Giamarchi and Delmas, 2007). Pkd2 is a non-selective cation channel, permeable to Ca^{2+}, Mg^{2+}, K^{+}, Na^{+}, Cs^{+} and Ba^{2+} (Gonzalez-Perrett et al., 2001, Koulen et al., 2002, Hanaoka et al., 2000). These conductances were demonstrated using patch-clamp studies of reconstituted proteins from human term syncytiotrophoblast (hST) cells (Gonzalez-Perrett et al., 2001), ER vesicles from LLC-PK porcine kidney cells expressing human Pkd2 (Koulen et al., 2002), and Chinese hamster ovary cells expressing human Pkd1 and Pkd2 (Hanaoka et al., 2000). Pkd2 showed more permeability to Ca^{2+} over monovalent ions (Gonzalez-Perrett et al., 2001), which was in agreement with earlier studies (Hanaoka et al., 2000). Gonzalez-Perrett and colleagues also demonstrated that this channel was blocked by the Anti-PKD2 antibody, made to recognize the last C-terminal 258 amino acids of human Pkd2 (amino acids 710 to 968), and also by the addition of La^{3+}, Gd^{3+}, pH reduction and by Ca^{2+} itself (Gonzalez-Perrett et al., 2001).

Localization of Pkd2

The Pkd2 protein has been found in the endoplasmic reticulum (ER) (Cai et al., 1999, Bae et al., 2006, Kottgen et al., 2005), the cell membrane (Gonzalez-Perrett et al., 2001, Hanaoka et al., 2000, Pazour et al., 2002, Luo et al., 2003), and the ciliary membrane (Nauli et al., 2003, Huang et al., 2007, Pazour et al., 2002). Pkd2 is found in the ER where it is trafficked to other parts of the cell or in some cases, returned to the ER. One study used a collection of different cells lines and demonstrated that Pkd2 remains in the ER due to an ER-retention or ER-"retrieval" signal (Cai et al., 1999). When human full-length Pkd2 is expressed in human embryonic kidney cells (HEK293), a short 34 amino acid sequence between glutamic acid 787 and glycine 821 prevents Pkd2 from leaving the ER (Cai et al., 1999) or causes Pkd2 to be quickly returned to the ER from the cis-Golgi in a COPII-dependent manner (Hoffmeister et al., 2011, Cai et al., 1999). By expressing truncated versions of the Pkd2 sequence in LLC-PK or HEK293 cells (R742X, R787X, and R872X), this group demonstrated that full length Pkd2 and the R872X version, both that contain the ER "retrieval" signal, remained in the ER. However, the two truncated Pkd2 versions without this "retrieval" sequence (R742X and R787X) were found in the cell membrane (Cai et al., 1999).

In some cell types, the Pkd2 protein requires recruitment by the Pkd1 protein to traffic to different membranes. Investigation of full length human *PKD1* and *PKD2* expressed in Chinese Hamster Ovary (CHO) cells suggested Pkd2 required Pkd1 for Pkd2 location in the cell membrane and channel activity. When expressed alone, full length Pkd2 was found inside the cell and the truncated Pkd2 protein R742X was found in the cell membrane (Cai et al., 1999, Hanaoka et al., 2000). Full length *PKD2* had to be co-expressed with *PKD1* in CHO cells for Pkd2 to be found in the cell membrane. Interestingly, when the truncated Pkd2 (R742X) was co-expressed with Pkd1, no currents were produced in the CHO cells suggesting no channel activity

even though both proteins were found in the cell membrane. The truncated Pkd2 (R742X) does not co-IP with the Pkd1 protein (Hanaoka et al., 2000). These data support the interaction of Pkd1 and Pkd2 at the C-terminus of Pkd2 and also suggest, as the authors mentioned, that even full length Pkd2 containing the ER-retrieval signal can traffic to the cell membrane (Hanaoka et al., 2000). Other work has shown that the Pkd1 and Pkd2 proteins interact between amino acid positions 871 to 968 at the C-terminus of Pkd2 (Hanaoka et al., 2000, Tsiokas et al., 1997a) which may interfere with the ER-retrieval signal, "masking" it (Cai et al., 1999).

Pkd2 is also located in the cilia, and, because of the involvement in ADPKD, some researchers sought to examine Pkd2 trafficking and localization in the cilia of kidney cells. Initial studies looked at the localization of the Pkd2 protein in cultured human and mouse kidney cells. Using the YCC2 antibody (Cai et al., 1999), the Pkd2 protein was clearly localized to the cilia and the cell body (Pazour et al., 2002). In another study using mouse kidney cells, the Pkd1 protein was localized to the primary cilium. In the kidney cells from a mouse with a truncated version of the Pkd1 protein, *Pkd1*$^{del34/del34}$ (Nauli et al., 2003), Pkd1 was no longer in the kidney cilia. These mice express a truncated form of Pkd1 which has deleted exon 34, truncating the Pkd1 protein near amino acid 3467 (Delmas et al., 2004). The same study localized the Pkd2 protein to the primary cilium in the wild type kidney cells but not in the mutant kidney cells from the *Pkd1*$^{del34/del34}$ mice (Nauli et al., 2003). These results suggested Pkd2 requires full length Pkd1 in the mouse kidney cilia in order for Pkd2 to traffic there.

Another study of Pkd2 using a knockout mouse shed light on the movement of Pkd2 from the cilia back to the cell (Pazour et al., 2002). When Pazour and colleagues examined the *Tg737*^{orpk} mouse, a commonly used mouse model for kidney disease, they found that Pkd2 immunofluorescence was elevated in the cilia of the kidney cells from the *Tg737*^{orpk} compared to the wild type littermates. It turns out the gene mutated in the *Tg737*^{orpk} mice is IFT88

(intraflagellar transport protein 88) which is a vital component to anterograde transport and the B complex. Pazour and colleagues concluded that Pkd2 does not require IFT88 for transport into the cilia, but it does for the cycling of this protein back to the cell body. The cilia of these mutant mice were short, contained high levels of Pkd2 staining, and had bulges at their tips (Pazour et al., 2002).

There are instances where Pkd2 relies on other proteins for trafficking to the cell membrane, to the cilia, and out of the cilia, as we have discussed. However, there are also examples of Pkd2 trafficking independently of other proteins. In the nematode *C. elegans*, the homologue for Pkd2 (pkd-2) does not require the Pkd1 homologue (lov-1) to traffic into the ciliated neurons. Although both of these proteins are involved in the same pathway, they do so through independent trafficking (Barr et al., 2001). Another example is in the green algae *Chlamydomonas reinhardtii*. In this flagellated cell, Pkd2 is translated into a 210 kD protein. However, it must be cleaved into two smaller proteins, 120 and 90 kD, before entering the cilia. Pkd2 does not depend on the presence of Pkd1 for this to occur (Huang et al., 2007). What is apparent from all of these studies is the versatility of the Pkd2 protein. The multitude of differences highlights the adaptability of Pkd2 and that its location and movement between membranes is very cell-type and species specific.

Pkd2 and Pkd1 Interactions

We have already mentioned the interactions of the Pkd1 and Pkd2 proteins. Because of their dual involvement in ADPKD, these two proteins are commonly co-expressed in cells for study. The interactions of Pkd1 and Pkd2 have been demonstrated to occur at the C-terminus of both proteins. Using the Yeast two Hybrid screening system, the last 226 amino acids of Pkd1 were used as bait while the final 289 amino acids of Pkd2 were used as prey. Pkd1 interacted with Pkd2 at the last 97 amino acids of Pkd2 but not with other prey proteins or with itself

(Tsiokas et al., 1997a). The authors determined that Pkd1 and Pkd2 interact at their C-termini. The same study demonstrated that amino acids 742 to 871 of Pkd2 are important for Pkd2 homodimerization. This section of amino acids in Pkd2 contains a proposed coiled-coil domain and is independent of the proposed Pkd1 interacting domain (Tsiokas et al., 1997a).

The large C-terminal region of human Pkd2 (amino acids 679 to 968) was later analyzed using a coiled-coil prediction program, PCOILS (http://toolkit.tuebingen.mpg.de/pcoils). Two domains were identified. The first, CC1 (E769-L796) scored lower than the second predicted domain, CC2 (S835-A873) (Giamarchi et al., 2010). Similar to the work just mentioned by Tsiokas and colleagues (Tsiokas et al., 1997a), the later part of the C-terminus is essential for interactions with the Pkd1 protein, meaning deletions or mutations to the CC2 domain (S835 to A873) abolish heteromers with PKD1. However, deletions or mutations to CC2 do not interfere with Pkd2 forming homomultimers. The vast majority of the predicted CC2 domain, described as being essential for Pkd1 interaction (Giamarchi et al., 2010), is absent from the original domain described by Tsiokas and colleagues (1997). When addressed by the authors, Giamarchi *et al* (2010) suggested that the CC2 domain, although essential for Pkd1 interaction, is not the direct binding site for Pkd1, which is the area just distal to the CC2 domain, described by Tsiokas *et al* (1997). Instead, the CC2 domain most likely helps facilitate the interaction of these two proteins and is required for their interaction (Giamarchi et al., 2010).

Pkd2 and Other Interacting Proteins

Research has shown that the Pkd2 protein interacts with proteins other than Pkd1. Interaction includes formation of heterotetramers (Kobori et al., 2009) which requires a cysteine residue at position 632. The cysteine is located in the third extracellular loop, where it forms important disulfide bonds between Pkd2 monomers (Feng et al., 2011). This cysteine, when mutated to an alanine or an arginine (C632A or C632R), and expressed in HEK293 cells did not

demonstrate any problems with Pkd1 interactions. However, when these mutated forms of Pkd2 were expressed in HEK293 cells, there was a diminished activity of the Pkd2-dependent calcium release from the ER (Feng et al., 2011). Another study in HEK293 cells demonstrated that co-expression of *PKD1* and *PKD2* allowed these two proteins to from a junction. The same study showed the Pkd1 protein in the cell membrane will interact with the Pkd2 protein in the ER where Pkd2 will function as an intracellular calcium release channel (Giamarchi et al., 2010). Also in the ER, Pkd2 has been shown to activate and interact with the Ryanodine receptor (RyR), acting as an intracellular calcium release channel (Nauli et al., 2003, Anyatonwu et al., 2007, Koulen et al., 2002).

The Pkd2 protein also acts in a complex with TRPV4, a member of the Vanilloid subfamily of the TRP channels. The full length human genes encoding TRPP2 (Pkd2) and TRPV4 were expressed in MDCK cells and *Xenopus* oocytes. The TRPV4 channel co-localized with Pkd2 in the cilia of the MDCK cells. The expression of these two genes in oocytes showed an increased conductance in response to osmotic swelling compared to single-expressing oocytes and the wild type control cells. Interestingly, Kottgen *et al* (2008) observed that TRPV4 was important in the MDCK cells for fluid-flow mechanosensation, but that it was not necessary in mice or zebrafish for the same fluid-flow detection. Another finding of this study was that heterozygous $TRPV4^{+/-}$ and $TRPP2^{+/-}$ mice showed a reduction in temperature sensitivity, tolerating 46°C, 2°C higher than the control animals' 44°C in tail-immersion tests. (A tail immersion test is a gently restrained animal whose tail is place in a water bath for a maximum of 300 seconds and the time until the tail is flicked by the animal is recorded)(Kottgen et al., 2008). These data suggest the two proteins, Pkd2 and TRPV4, are important for mechanosensation and thermosensation. Further investigation of epitope tagged versions of human Pkd2 and TRPV4 with atomic force microscopy (AFM) support Pkd2 and TRPV4 function as a heterotetramer with a 2:2 stoichiometry (Stewart et al., 2010).

The Pkd2 protein also interacts with the TRPC1 protein. Co-expression of epitope tagged Pkd2 and TRPC1 proteins in HEK293 cells, again using AFM, demonstrated these two proteins form a heterotetramer with a 2:2 stoichiometry (Kobori et al., 2009). The Pkd2 and TRPC1 channels were first shown to interact in the late 1990s by another group (Tsiokas et al., 1999). The initial study co-expressed full length versions of N- and C-terminally epitope tagged Pkd2 and TRPC1 proteins, respectively, in HEK293T cells. The Pkd2 and TRPC1 proteins were shown to co-immunoprecipitate, suggesting an interaction. Truncated versions of these expressed proteins suggest the interaction occurs at their C-termini (Tsiokas et al., 1999). The interaction of Pkd2 with TRPC1 and TRPC4 were also demonstrated in glomerular mesangial cells (MC) where these proteins were shown to physically interact to form a calcium-permeable channel in the membrane (Du et al., 2008).

The Pkd2 protein has also been shown to interact with non-TRP channels. Just mentioned was the interaction of Pkd2 with the ryanodine receptors of the ER to form intracellular calcium release channels (Nauli et al., 2003, Koulen et al., 2002, Anyatonwu et al., 2007). Pkd2 has also been shown to interact with 1,4,5-triphosphate receptors (IP_3R) of the ER (Li et al., 2005, Sammels et al., 2010). In LLC-PK1 cells expressing mouse wild type full-length *PKD2*, co-immunoprecipitation (co-IP) assays show that Pkd2 co-immunoprecipitates with IP_3R1 and IP_3R3. The reciprocal experiments are also consistent, that IP specifically for IP_3R1 and IP_3R3 co-IP the Pkd2 channel. Using patch clamp experiments, the same group demonstrated that these proteins act as an IP_3- or Ca^{2+}– induced calcium release pathway that helps to regulate intracellular calcium concentrations (Sammels et al., 2010).

Regulation of the Pkd2 Channel

The Pkd2 channel is shown to be an important component for intracellular calcium release in some cells. Pkd2 can also be regulated by intracellular calcium levels. Using LLC-PK1

cells expressing human *PKD2*, cells were harvested and their isolated ER microsomes were reconstituted in lipid bilayers. These reconstituted membranes were then used for single channel recordings which found that the Pkd2 channel activity was responsive to changes in calcium levels (Koulen et al., 2002). Pkd2 is regulated by calcium using the second of its two predicted EF hands, which is thought to be the calcium sensor and important for calcium binding (Koulen et al., 2002). A second study demonstrated that mutations in this second EF hand make the Pkd2 protein insensitive to intracellular calcium levels (Kuo et al., 2014). Normally, Pkd2 is functional between 100 nM and 10 μM calcium (Kuo et al., 2014, Koulen et al., 2002). When the C-terminal EF hands of Pkd2 bind calcium, it makes a conformational change which is expected to control gating of the channel (Celic et al., 2012).

Pkd2 can be regulated by kinases and phosphatases as well. This regulation can be a change in activity due to a phosphorylation/dephosphorylation event or these changes in phosphorylation state can affect the trafficking of the protein. For example, in the nematode *C. elegans*, phosphorylation at S534 by CKII in the male sensory ciliated neurons is facilitated by the *C. elegans* version of Pkd1, *lov-1*. This phosphorylation activates the channel that leads to an increase in intraciliary calcium levels. The excess calcium then activates *tax-6*, the *C. elegans* homologue of calcineurin (CaN). The *tax-6* protein in turn dephosphorylates Pkd2, deactivating it (Hu et al., 2006). The constitutive phosphorylation of Pkd2 at S534 in *C. elegans* also leads to a loss of this protein from the male sensory neurons, which are modified cilia. The mutation of S534 to an alanine (S534A), which prevents phosphorylation, does not interfere with the localization of $Pkd2^{S534A}$ to the cilia. A second form of Pkd2, where S534 is changed to an aspartic acid (S534D), is a "phospho-mimetic" and does not traffic to the cilia (Hu et al., 2006). The phosphorylation is not always important for trafficking of Pkd2, however. In mammalian renal epithelial cells, CKII phosphorylation of Pkd2 at S812 has been shown to regulate the protein's

activity and calcium sensitivity. However, it does not appear to be important for the trafficking of the protein (Cai et al., 2004).

IV. The BBSome and Trafficking to the Cilia

The BBSome Complex

The mammalian BBSome complex is comprised of eight proteins: BBS1, 2, 4, 5, 7, 8, 9 and BBIP10 (Nachury et al., 2007). This complex of proteins forms an electron-dense coat around vesicles and is morphologically distinct from other coat complexes, such as those formed by COPI, COPII, and clathrin. The BBSome prefers acidic phospholipids, especially multiphosphorylated phosphatidylinositol phosphates, for recruitment to liposomes. The BBSome is recruited to liposomes by BBS3/Arl6, which is an Arf-like GTPase (Jin et al., 2010). To determine how the members of this complex assemble before recruitment, the different BBSome components were expressed in HEK293T cells in various combinations for IPs and co-IPs. Four of the proteins have β-propeller domains (BBS1, 2, 7, and 9) which are important for protein-protein interactions; two proteins have tetratricopeptide repeat domains (BBS4 and 8) (Zhang et al., 2012). A thorough analysis of these BBSome components expressed in the HEK293T cells in various combinations resulted in an explanation of the assembly order of this coat complex of proteins. BBS9 is considered the central scaffold of the complex while BBS2 and 7 are core components. BBS1 also has a strong association with BBS2 and 7, but it is added to the complex later in assembly, along with BBS5 and 8 (Zhang et al., 2012).

To reach the cilia, the BBSome complex requires recruitment by other proteins. BBS4 is thought to be the final addition to the complex and is the last component added before the BBSome moves to the cilia (Zhang et al., 2012, Nachury et al., 2007). Once at the base of the

cilium, the BBSome requires the GTPase Rab8 and the guanine nucleotide exchange factor Rabin 8 for association with IFT particles at the base of the cilia (Nachury et al., 2007). After the addition of BBS4, the conserved centriolar satellite protein SSX2IP (synovial sarcoma X breakpoint-2 interacting protein) is necessary for the recruitment of the BBSome into the cilia. In retinal pigment epithelial cells (RPE-1 cells) induced to grow cilia, SSX2IP was knocked down using small interfering RNA (siRNA) and the immunofluorescence of BBS components in the cilia were observed. When SSX2IP was depleted, Rab8-GFP, which enters the cilia with the BBSome (Nachury et al., 2007), was reduced significantly in the cilia compared to the control treated cells (Klinger et al., 2014). Once in the cilia, the BBSome traffics up and down the cilium using IFT (Nachury et al., 2007, Williams et al., 2014).

Trafficking by the BBSome

Certain proteins have been shown to require the BBSome for trafficking to the cilia, but so far, not to the cell membrane. The somatostatin receptor 3 (SST3), a seven-transmembrane spanning G-protein coupled receptor, has been shown to be BBSome-dependent for its trafficking to the cilia. Recently, in RPE-1 cells depleted in SSX2IP and therefore ciliary BBS components, the SST3 does not reach the cilia (Klinger et al., 2014). In BBS4$^{-/-}$ and BBS2$^{-/-}$ mice, the same is true. Neurons from these knockout mice lack the SSTR3 and melanin-concentrating hormone receptor-1 (Mchr-1) in the cilia of central neurons. The receptors will return to the neurons if the wild type BBS gene is expressed in the cells, showing the dependence of these G-protein coupled receptors on the BBSome for ciliary trafficking (Berbari et al., 2008).

There are other ciliary membrane proteins that are dependent on the BBSome for ciliary localization. These other proteins are not seven transmembrane spanning proteins, but include Pkd2 (Valentine et al., 2012, Hoffmeister et al., 2011) and a potassium channel, SK1a (Valentine et al., 2012). Other studies have demonstrated that Pkd2 relies on BBSome trafficking to reach the

cilia. First, the study by Hoffmeister and colleagues (2012) used IMPDH (inosine-5'-monophosphate dehydrogenase) to interfere with GTP production in LLC-PK cells expressing human full-length *PKD2*. Without GTP, the GTPase Rab8 would not be fully functional. As mentioned, the BBSome requires Rab8 for ciliary entry (Nachury et al., 2007). The treatment of the expressing cells with IMPDH prevented Pkd2 from reaching the cilia, but the smoothened protein, which does not rely on the BBSome for ciliary trafficking, was unaffected (Hoffmeister et al., 2011). A second study demonstrated that the depletion of BBSome components, namely *BBS7*, *8*, or *9*, using RNAi in *P. tetraurelia* prevented Pkd2 from reaching the cilia. Although the Pkd2 protein appears at the cell surface (Valentine et al., 2012). Lastly, a *bbs-7* mutant of *C. elegans* with a mutation in *my13* shows abnormal male mating behavior. Further investigation using *my13* mutant worms expressing PKD2-GFP showed the Pkd2 protein accumulated at the base of the cilia (Braunreiter et al., 2014).

Ciliary Targeting Signals

The idea of ciliary targeting signals or sequences has been proposed for numerous proteins. For example, rhodopsin contains a VxPx motif at the C-terminus of the protein, that when truncated, prevents this protein from reaching the cilia (Mazelova et al., 2009). A similar proposed sequence in the human Pkd2 protein is sufficient for ciliary trafficking. The N-terminal R_6VxP motif, if mutated (R6G, V7A and P9A), prevents Pkd2 from trafficking to the cilia of epithelial cells. Interestingly, the same study placed the first 72 amino acids of Pkd2 onto the N-terminus of PKD2L1, which does not localize to the cilia normally. When this chimeric form of PKD2L1 was expressed in epithelial cells, the protein was found in the cilia (Geng et al., 2006). Although these two sequences are very similar, they are found at separate termini. Other proposed CTS sequences have been suggested, but there seems to be little consistency among

them, suggesting that these sequences may be species-specific or may require a combination of signals or proteins for recognition and trafficking.

V. Experimental Approach

RNA interference (RNAi)

The use of RNA interference (RNAi) has become a highly utilized technique for the study of gene function in numerous cell types. This technique to deplete cells of targeted mRNA was first published in the nematode *C. elegans* (Fire et al., 1998). RNAi is now widely used in other organisms, including but not limited to, *Paramecium* (Valentine et al., 2012, Picariello et al., 2014, Galvani and Sperling, 2002), Zebrafish (Andrews et al., 2014), *Chlamydomonas* (Kim and Cerutti, 2009), *Drosophila* (Clemens et al., 2000), and in mammalian cells (reviewed in (Sui et al., 2002)). The use of RNAi techniques provides a study model that is a knock down, not a knock out. A knock out, especially in the case of *Paramecium*, is not usually available and would be challenging to create. Using RNAi is simple in concept, providing a knock down model for study quite rapidly, sometimes only taking a few weeks to obtain results. However, as with any technique, there can be some pitfalls that need to be taken into account.

The basic idea of RNAi is to rely on a cell's own natural defenses to degrade endogenous mRNA which results in depleted protein amounts. The introduction of large amounts of double-stranded RNA (dsRNA) will trigger this response. By introducing dsRNA to a cell, the enzyme complex Dicer will be activated. Dicer is an RNase-III protein with endoribonuclease activity first described in *Drosophila* that cuts the long strands of dsRNA into smaller 21 to 25 length strands of dsRNA (Bernstein et al., 2001). These smaller dsRNA fragments then catalyze the formation of the RNA-Induced Silencing complex, RISC. One of the most important components

of this complex is the endonuclease activity which is Mg^{2+}-dependent (Schwarz et al., 2004) and the protein Argonaute (Ago). RISC is responsible for binding the small dsRNA fragments and unwinding them to create single strands. The small single strand of anti-sense RNA then guides the RISC complex to the complementary strand of RNA. Once bound, in an ATP-dependent fashion, the mRNA strand is cut by the PIWI domain of the Ago protein (reviewed in (Pratt and MacRae, 2009)).

When using RNAi as a research approach, there are drawbacks that need to be considered. One potential pitfall are inexact matching of the siRNAs to the mRNA which would result in the wrong mRNA strand being degraded. Although miss-matching is a concern, it is not expected to occur very often. One study has demonstrated that the first and last two positions of the siRNA are the most tolerant of mismatches with A:C and C:A mismatches being the most common (Du et al., 2005). There can also be off-target effects where a mismatch occurs or the same sequence exists in an mRNA that is not the target strand. This incorrect recognition then leads to the degradation of the wrong mRNA strand. Prediction programs are in place that help with RNAi construct design to prevent this from occurring. *Drosophila* has a search engine (http://www.flyrnai.org/DRSC-TOO.html) as well as *Paramecium* (http://paramecium.cgm.cnrs-gif.fr/cgi/tool/alignment/off_target.cgi). Both of these sites allow the user to search the genome using the sequence(s) to be used for RNAi. The search engine will then provide the user an analysis including the potential off-target sequences. In some search engines, the user is also given the opportunity to select the stringency of the filter, selecting the length of the proposed siRNAs or the number of mismatches that will be tolerated.

Once the RNAi is designed and produced, for it to be effective it much be introduced into the cells. Methods to get the dsRNA into the cells include soaking, feeding, electroporation, transfection, injection, among others. The method of introduction is also dependent upon the

organism being studied (reviewed in (Agrawal et al., 2003)). In *P. tetraurelia,* RNAi by feeding is the most commonly used method because it is both simple and effective. Typically between 60 and 80% of the population of cells exposed to the dsRNA show an effect of the RNAi (Galvani and Sperling, 2002). Although we are also able to use injection for expressing dsRNA within paramecia, injection methods are far more time consuming and the plasmid that expresses the dsRNA is diluted over time with the division of the cells (Galvani and Sperling, 2002), which occurs approximately every six hours. Another method that is similar to RNAi is the use of an Antisense plasmid. The plasmid is created to transcribe the antisense sequence for the mRNA to be depleted (Yano et al., 2003). RNAi by feeding is a simple and quick method where paramecia are fed bacteria filled with dsRNA. The bacteria are specially created *E. coli* variants called Ht115 bacteria that are RNase-III deficient are used. These bacteria are able to produce massive amounts of the dsRNA without degrading it. Paramecia that have been purged to remove contaminating bacteria from their surface and release from their cytoproct can be added to cultures containing the special RNase-III deficient bacteria which they ingest, releasing the dsRNA into the cell.

To produce the dsRNA in the bacteria, the Ht115 bacteria cells are transformed with an engineered plasmid that contains two opposing T7 promoters and a lacZ domain for induction with isopropyl-beta-D-thiogalactopyranosidase (IPTG). The plasmid also contains ampicillin resistance for selective pressure during bacterial transformation. Restriction enzyme sites between the two T7 promoters allows the sequence of interested to be ligated into place.

Over-expression of Exogenous Proteins in *Paramecium*

Paramecia are very amenable to the over-expression of genes and genes with an epitope tag added to the 5′- or 3′- end. The sequenced genome allows an entire gene from start to finish to be amplified and cloned into an expression plasmid. The plasmid pPXV has been instrumental

in the tagging and expression of genes in *Paramecium* for study. This plasmid (Figure 1.5) contains calmodulin promoters to ensure the gene is highly expressed. Calmodulin is a calcium binding protein that is highly expressed in cells. By using these promoters when engineering this plasmid ensures that the sequence in between them is expressed at very high levels. The plasmid also contains *Tetrahymena* telomeres which flank the promoters and the sequence so that the linear plasmid is maintained within the macronucleus of the cell. In between the two promoters are a few restriction enzyme sites to allow for the insertion of the gene of interest.

The pPXV plasmid has been altered to provide different epitope tags and restriction enzyme cut sites. The epitope tags have allowed the use of commercial antibodies to bind to and immunoprecipitate (IP) the proteins that are being expressed. We have created an N- and C-terminal three-fold repeat of the FLAG epitope (DYKDDDDK) and a three-fold repeat of the myc epitope (EQKLISEEDL). Lastly, we created an N-terminal 3×myc tag with a C-terminal 3×FLAG tag (See Figure 1.5 for plasmid maps). We are able to amplify genes of interest utilizing restriction enzyme cut sites and using long primers that create restriction enzyme cut sites and the 5′- and 3′- ends of the genes with PCR. The PCR products and the pPXV plasmid can be processed with the desired restriction enzymes. The plasmid and PCR products can be ligated together and introduced into the macronucleus by microinjection after the plasmid-product is linearized.

There are few antibodies available to identify *Paramecium* proteins. The evolutionary distance between most of the available mammalian antibodies and *Paramecium* protein sequences is too great for many antibodies to recognize the *Paramecium* proteins. However, antibodies against highly conserved proteins, such as tubulin, or antibodies that were developed against proteins in closely related organisms, such as the anti-centrin antibody made against a *Tetrahymena* centrin protein (kind gift of Dr. Mark Winey, University of Colorado, Boulder, CO)

have proven successful in recognizing *Paramecium* proteins. The use of these easily engineered epitope sequences expressed on the 5'- or 3'- end of a gene has greatly enhanced our ability to locate and visualize proteins within a cell.

Although the pPXV expression plasmid has been instrumental in our research and has elevated our findings to new levels, the use of an injected plasmid with no selective pressure prevents some challenges. First, the paramecia cells must be well-fed and cannot be allowed to go through autogamy. During autogamy, the macronucleus is broken down and reformed using the micronuclei. The destruction of the macronucleus would also destroy the exogenous plasmid (Godiska et al., 1987). Once the plasmid is injected, the cells are maintained as individual clones and are screened by genomic extraction and PCR to amplify the endogenous gene and the exogenous plasmid for comparison. Only those cells that contain the injected plasmid in a level the same or higher than the endogenous gene are maintained.

The over-expression of the gene can sometimes cause a dominant negative effect, interfering with the function of the endogenous protein and generating a silencing effect. The placement of the epitope tag can also prevent the proper placement of the expressed protein or interfere with the function or the trafficking. The ability to have the epitope tag expressed at the N- or the C- terminus of the protein has allowed for some flexibility. Once the plasmid is injected, it is typically stably expressed for three to six weeks. By using this technique, we are able to use techniques including, but not limited to, immunoprecipitation (IP), co-IP, purification for LC-MS/MS, Western blot, and immunofluorescence.

Swimming Assays and Electrophysiology

The speed the cilia beat and therefore the speed the cell swims is governed by the membrane potential of the cell. The membrane of these cells is permeable to ions in the

environment, some ions more than others. *Paramecium's* membrane potential is primarily determined by K^+, allowing the cell to act like a potassium electrode. The membrane is also permeable to Na^+ and Mg^{2+}, but it is very selective concerning the passage of Ca^{2+} and Cl^- (Hansma, 1979, Machemer-Rohnisch and Machemer, 1989, Naitoh, 1968, Naitoh et al., 1972, Preston, 1990).

Paramecia cells, when depolarized beyond threshold, open the voltage-gated calcium channels of the cilia causing an action potential. The opening of these channels allows Ca^{2+} to enter the cilia and will reverse the beating of the cilia sending the cell backward. As long as Ca^{2+} remains high in the cilia, the cell will continue to move backward. The influx of Ca^{2+} is countered by the efflux of K^+ by the fast-acting voltage dependent K^+ conductance and the slower activated Ca^{2+}-dependent K^+ conductance (Brehm et al., 1978, Satow and Kung, 1980). The action potential is prolonged by the ions in the solution bathing the cell resulting in prolonged backward swimming. Therefore, we use the length of time the cell spends swimming backward (seconds) as a proxy measurement of ion conductance. Short backward swimming therefore indicates a reduced conductance of an ion while prolonged backward swimming may indicate a larger conductance of an ion.

The permeability of the membrane to certain ions determines the resting membrane potential of *Paramecium*. Already mentioned is that the resting membrane potential of the cells is mostly governed by K^+. However, if the concentration of K^+ remains constant and a new ion is introduced to the cell, the cell may depolarize or hyperpolarize the membrane depending on the permeability of the membrane to that ion. If no change in the membrane potential occurs, or perhaps only small changes occur, that may indicate that the membrane is impermeable to that ion, as in the case of ciliated XntA1 mutants to Mg^{2+} (Preston and Kung, 1994a). Therefore, by

observing changes in membrane potential in potassium solution with and without an additional ion can be used to measure the permeability of the membrane to that ion.

Measuring membrane potential (V_m) is relatively straight forward. It can be performed on either ciliated or deciliated cells. Paramecia can be temporarily deciliated by trituration in a 5% ethanol v/v bath (Machemer and Ogura, 1979). A pulled glass electrode is back-filled with 500 mM KCl and the resistance is then tested in the resting bath the cell will be placed in. Typically the resistance is between 40 and 100 MΩ. The main chamber bath is connected to a smaller reference bath filled with 3 M KCl using a 3% agar in 3 M KCl bridge. The recording chamber bath on the stage of an inverted microscope can then be drained and a single cell placed in the center with very little fluid. A micromanipulator is used to impale the cell membrane with the glass recording electrode. After the cell is impaled, the bath chamber is quickly, but gently, filled with the resting solution. Figure 1.6 shows a ciliated and deciliated *Paramecium* on the end of a glass electrode for recording. The bath requires a peristaltic pump for a controlled and steady flow rate so the cell is not disturbed, which could activate mechanoreceptors. The membrane potential of the cell is recorded continuously.

Experimental Approach

We have utilized the ciliated cell *Paramecium* for the study of ciliopathies and to better understand the role of proteins in a non-canonical system. In the second chapter, which was published in 2014 (Picariello et al., 2014), we have again used *Paramecium* to elucidate other roles of a ciliopathy gene, this time *MKS3*. The highly ordered cell surface and sub-surface structures of *Paramecium* has allowed for the possible identification of a new role for the MKS3 protein. In *Paramecium*, this protein may be involved as a transition zone component, but we also hypothesize that the Mks3 protein is vital to the guidance of daughter basal bodies as they migrate away from their mother basal body before cell duplication process begins. Using RNAi

and epitope-tagging, we have localized the Mks3 protein in *Paramecium* and have used LC-MS/MS analysis and GST-fusion proteins to identify the potential interaction with the kinetodesmal fibers below the cell surface. It is this interaction that may cause basal bodies to migrate off their path leading to a disrupted cell surface.

The third chapter of this work examines the non-specific channel protein Pkd2, a protein that when mutated in humans, can lead to Autosomal Dominant Polycystic Kidney Disease (ADPKD). Although we found three possible orthologs for Pkd2 in *Paramecium* using human and mouse sequences, we are focusing on two paralogs. Based on preliminary findings that RNAi to deplete cells of *PKD2* led to short backward swimming in Mg^{2+} solutions, we include the use of the *Paramecium* mutant *eccentric* (XntA1) in our studies. We use a combination of techniques involving epitope-tagging and RNAi to examine the Pkd2 channel function, trafficking, and location in *Paramecium*. We hypothesize that Pkd2 and XntA are both involved in Mg^{2+}-induced behavior and that the Pkd2 protein is the Mg^{2+} channel in *Paramecium*.

Lastly, this review and our use of *Paramecium tetraurelia* highlights the importance of using a non-mammalian system to elucidate new roles and functions of proteins that are involved in ciliopathies. These studies help to understand the full potential of the discussed proteins and to identify novel roles and potential interacting partners. The continued pursuit of knowledge surrounding these genes, namely *PKD2*, may contribute to new studies and disease treatments. *Paramecium* continues to prove itself as an approachable, useful and powerful model for the study of human ciliopathy genes.

References

ADOUTTE, A., RAMANATHAN, R., LEWIS, R. M., DUTE, R. R., LING, K. Y., KUNG, C. & NELSON, D. L. 1980. Biochemical studies of the excitable membrane of Paramecium tetraurelia. III. Proteins of cilia and ciliary membranes. *J Cell Biol,* 84**,** 717-38.

ADPKD 2014. Autosomal Dominant Polycystic Kidney Disease: Mutation Database. *PKD Foundation Web site*.

AGRAWAL, N., DASARADHI, P. V., MOHMMED, A., MALHOTRA, P., BHATNAGAR, R. K. & MUKHERJEE, S. K. 2003. RNA interference: biology, mechanism, and applications. *Microbiol Mol Biol Rev,* 67**,** 657-85.

ALLEN, R. D. 1971. Fine structure of membranous and microfibrillar systems in the cortex of Paramecium caudatum. *J Cell Biol,* 49**,** 1-20.

ALLEN, R. D. 1988. Chapter 2: Cytology. *Paramecium***,** 4-40.

ALLEN, R. D. & FOK, A. K. 1980. Membrane recycling and endocytosis in Paramecium confirmed by horseradish peroxidase pulse-chase studies. *J Cell Sci,* 45**,** 131-45.

ANDREWS, O. E., CHA, D. J., WEI, C. & PATTON, J. G. 2014. RNAi-mediated gene silencing in zebrafish triggered by convergent transcription. *Sci Rep,* 4**,** 5222.

ANYATONWU, G. I., ESTRADA, M., TIAN, X., SOMLO, S. & EHRLICH, B. E. 2007. Regulation of ryanodine receptor-dependent calcium signaling by polycystin-2. *Proc Natl Acad Sci U S A,* 104**,** 6454-9.

ARIYUREK, Y., LANTINGA-VAN LEEUWEN, I., SPRUIT, L., RAVINE, D., BREUNING, M. H. & PETERS, D. J. 2004. Large deletions in the polycystic kidney disease 1 (PKD1) gene. *Hum Mutat,* 23**,** 99.

ARNAIZ, O., CAIN, S., COHEN, J. & SPERLING, L. 2007. ParameciumDB: a community resource that integrates the Paramecium tetraurelia genome sequence with genetic data. *Nucleic Acids Res,* 35**,** D439-44.

ARNAIZ, O. & SPERLING, L. 2011. ParameciumDB in 2011: new tools and new data for functional and comparative genomics of the model ciliate Paramecium tetraurelia. *Nucleic Acids Res,* 39**,** D632-6.

AUBUSSON-FLEURY, A., LEMULLOIS, M., DE LOUBRESSE, N. G., LALIGNE, C., COHEN, J., ROSNET, O., JERKA-DZIADOSZ, M., BEISSON, J. & KOLL, F. 2012. The conserved centrosomal protein FOR20 is required for assembly of the transition zone and basal body docking at the cell surface. *J Cell Sci,* 125**,** 4395-404.

BAE, Y. K., QIN, H., KNOBEL, K. M., HU, J., ROSENBAUM, J. L. & BARR, M. M. 2006. General and cell-type specific mechanisms target TRPP2/PKD-2 to cilia. *Development,* 133**,** 3859-70.

BARGMANN, C. I. 2006. Chemosensation in C. elegans. *WormBook***,** 1-29.

BARR, M. M., DEMODENA, J., BRAUN, D., NGUYEN, C. Q., HALL, D. H. & STERNBERG, P. W. 2001. The Caenorhabditis elegans autosomal dominant polycystic kidney disease gene homologs lov-1 and pkd-2 act in the same pathway. *Curr Biol,* 11**,** 1341-6.

BEISSON, J. & WRIGHT, M. 2003. Basal body/centriole assembly and continuity. *Curr Opin Cell Biol,* 15**,** 96-104.

BERBARI, N. F., LEWIS, J. S., BISHOP, G. A., ASKWITH, C. C. & MYKYTYN, K. 2008. Bardet-Biedl syndrome proteins are required for the localization of G protein-coupled receptors to primary cilia. *Proc Natl Acad Sci U S A,* 105**,** 4242-6.

BERNSTEIN, E., CAUDY, A. A., HAMMOND, S. M. & HANNON, G. J. 2001. Role for a bidentate ribonuclease in the initiation step of RNA interference. *Nature,* 409**,** 363-6.

BHOGARAJU, S., ENGEL, B. D. & LORENTZEN, E. 2013. Intraflagellar transport complex structure and cargo interactions. *Cilia,* 2**,** 10.

BRAUNREITER, K., HAMLIN, S. & LYMAN-GINGERICH, J. 2014. Identification and characterization of a novel allele of Caenorhabditis elegans bbs-7. *PLoS One,* 9**,** e113737.

BREHM, P., DUNLAP, K. & ECKERT, R. 1978. Calcium-dependent repolarization in Paramecium. *J Physiol,* 274**,** 639-54.

BUONANNO, F., HARUMOTO, T. & ORTENZI, C. 2013. The defensive function of trichocysts in Paramecium tetraurelia against metazoan predators compared with the chemical defense of two species of toxin-containing ciliates. *Zoolog Sci,* 30**,** 255-61.

CAI, Y., ANYATONWU, G., OKUHARA, D., LEE, K. B., YU, Z., ONOE, T., MEI, C. L., QIAN, Q., GENG, L., WIZTGALL, R., EHRLICH, B. E. & SOMLO, S. 2004. Calcium dependence of polycystin-2 channel activity is modulated by phosphorylation at Ser812. *J Biol Chem,* 279**,** 19987-95.

CAI, Y., MAEDA, Y., CEDZICH, A., TORRES, V. E., WU, G., HAYASHI, T., MOCHIZUKI, T., PARK, J. H., WITZGALL, R. & SOMLO, S. 1999. Identification and characterization of polycystin-2, the PKD2 gene product. *J Biol Chem,* 274**,** 28557-65.

CAPDEVILLE, Y., CHARRET, R., ANTONY, C., DELORME, J., NAHON, P., AND ADOUTTE, A. 1993. Ciliary and Plasma Membrane Proteins in *Paramecium*: Description, Localization, and Intracellular Transit. *Advances in Cell and Molecular Biology of Membranes,* 2A**,** 181-226.

CELIC, A. S., PETRI, E. T., BENBOW, J., HODSDON, M. E., EHRLICH, B. E. & BOGGON, T. J. 2012. Calcium-induced conformational changes in C-terminal tail of polycystin-2 are necessary for channel gating. *J Biol Chem,* 287**,** 17232-40.

CHAPIN, H. C. & CAPLAN, M. J. 2010. The cell biology of polycystic kidney disease. *J Cell Biol,* 191**,** 701-10.

CHIH, B., LIU, P., CHINN, Y., CHALOUNI, C., KOMUVES, L. G., HASS, P. E., SANDOVAL, W. & PETERSON, A. S. 2012. A ciliopathy complex at the transition zone protects the cilia as a privileged membrane domain. *Nature Cell Biology,* 14**,** 61-U97.

CLEMENS, J. C., WORBY, C. A., SIMONSON-LEFF, N., MUDA, M., MAEHAMA, T., HEMMINGS, B. A. & DIXON, J. E. 2000. Use of double-stranded RNA interference in Drosophila cell lines to dissect signal transduction pathways. *Proceedings of the National Academy of Sciences of the United States of America,* 97**,** 6499-6503.

CORNEC-LE GALL, E., AUDREZET, M. P., CHEN, J. M., HOURMANT, M., MORIN, M. P., PERRICHOT, R., CHARASSE, C., WHEBE, B., RENAUDINEAU, E., JOUSSET, P., GUILLODO, M. P., GRALL-JEZEQUEL, A., SALIOU, P., FEREC, C. & LE MEUR, Y. 2013. Type of PKD1 mutation influences renal outcome in ADPKD. *Journal of the American Society of Nephrology,* 24**,** 1006-13.

CRADDOCK, V. M. 1968. The reaction of N-methyl-N'-nitro-N-nitrosoguanidine with deoxyribonucleic acid. *Biochem J,* 106**,** 921-2.

CRONKITE, D. L. 1974. Genetics of chemical induction of conjugation in Paramecium aurella. *Genetics,* 76**,** 703-14.

CZARNECKI, P. G. & SHAH, J. V. 2012. The ciliary transition zone: from morphology and molecules to medicine. *Trends in Cell Biology,* 22**,** 201-210.

DAOUST, M. C., REYNOLDS, D. M., BICHET, D. G. & SOMLO, S. 1995. Evidence for a third genetic locus for autosomal dominant polycystic kidney disease. *Genomics,* 25**,** 733-6.

DAWE, H. R., ADAMS, M., WHEWAY, G., SZYMANSKA, K., LOGAN, C. V., NOEGEL, A. A., GULL, K. & JOHNSON, C. A. 2009. Nesprin-2 interacts with meckelin and mediates ciliogenesis via remodelling of the actin cytoskeleton. *J Cell Sci,* 122**,** 2716-26.

DAWE, H. R., SMITH, U. M., CULLINANE, A. R., GERRELLI, D., COX, P., BADANO, J. L., BLAIR-REID, S., SRIRAM, N., KATSANIS, N., ATTIE-BITACH, T., AFFORD, S. C., COPP, A. J., KELLY, D. A., GULL, K. & JOHNSON, C. A. 2007. The Meckel-Gruber Syndrome proteins MKS1 and meckelin interact and are required for primary cilium formation. *Hum Mol Genet,* 16**,** 173-86.

DELMAS, P., NAULI, S. M., LI, X., COSTE, B., OSORIO, N., CREST, M., BROWN, D. A. & ZHOU, J. 2004. Gating of the polycystin ion channel signaling complex in neurons and kidney cells. *FASEB J,* 18**,** 740-2.

DU, J., DING, M., SOURS-BROTHERS, S., GRAHAM, S. & MA, R. 2008. Mediation of angiotensin II-induced Ca2+ signaling by polycystin 2 in glomerular mesangial cells. *Am J Physiol Renal Physiol,* 294**,** F909-18.

DU, Q., THONBERG, H., WANG, J., WAHLESTEDT, C. & LIANG, Z. 2005. A systematic analysis of the silencing effects of an active siRNA at all single-nucleotide mismatched target sites. *Nucleic Acids Res,* 33**,** 1671-7.

DUNLAP, K. 1977. Localization of calcium channels in Paramecium caudatum. *J Physiol,* 271**,** 119-33.

ECKERT, R. 1972. Bioelectric control of ciliary activity. *Science,* 176**,** 473-81.

ECKERT, R. & BREHM, P. 1979. Ionic mechanisms of excitation in Paramecium. *Annu Rev Biophys Bioeng,* 8**,** 353-83.

FENG, S., RODAT-DESPOIX, L., DELMAS, P. & ONG, A. C. 2011. A single amino acid residue constitutes the third dimerization domain essential for the assembly and function of the tetrameric polycystin-2 (TRPP2) channel. *J Biol Chem,* 286**,** 18994-9000.

FIRE, A., XU, S., MONTGOMERY, M. K., KOSTAS, S. A., DRIVER, S. E. & MELLO, C. C. 1998. Potent and specific genetic interference by double-stranded RNA in Caenorhabditis elegans. *Nature,* 391**,** 806-11.

FLIEGAUF, M., BENZING, T. & OMRAN, H. 2007. Mechanisms of disease - When cilia go bad: cilia defects and ciliopathies. *Nature Reviews Molecular Cell Biology,* 8**,** 880-893.

FLOCK, A. & DUVALL, A. J., 3RD 1965. The Ultrastructure of the Kinocilium of the Sensory Cells in the Inner Ear and Lateral Line Organs. *J Cell Biol,* 25**,** 1-8.

FLOTENMEYER, M., MOMAYEZI, M. & PLATTNER, H. 1999. Immunolabeling analysis of biosynthetic and degradative pathways of cell surface components (glycocalyx) in Paramecium cells. *Eur J Cell Biol,* 78**,** 67-77.

GABOW, P. A. 1993. Autosomal dominant polycystic kidney disease. *N Engl J Med,* 329**,** 332-42.

GABRIDGE, M. G., DOUGHERTY, E. P., GLADD, M. F. & MECCOLI, R. A. 1982. Effects of heavy metals on structure, function, and metabolism of ciliated respiratory epithelium in vitro. *In Vitro,* 18**,** 1023-32.

GALVANI, A. & SPERLING, L. 2002. RNA interference by feeding in Paramecium. *Trends Genet,* 18**,** 11-2.

GARCIA-GONZALO, F. R., CORBIT, K. C., SIREROL-PIQUER, M. S., RAMASWAMI, G., OTTO, E. A., NORIEGA, T. R., SEOL, A. D., ROBINSON, J. F., BENNETT, C. L., JOSIFOVA, D. J., GARCIA-VERDUGO, J. M., KATSANIS, N., HILDEBRANDT, F. & REITER, J. F. 2011. A transition zone complex regulates mammalian ciliogenesis and ciliary membrane composition. *Nat Genet,* 43**,** 776-84.

GENG, L., OKUHARA, D., YU, Z., TIAN, X., CAI, Y., SHIBAZAKI, S. & SOMLO, S. 2006. Polycystin-2 traffics to cilia independently of polycystin-1 by using an N-terminal RVxP motif. *J Cell Sci,* 119**,** 1383-95.

GERISCH, G. 1982. Chemotaxis in Dictyostelium. *Annu Rev Physiol,* 44**,** 535-52.

GIAMARCHI, A. & DELMAS, P. 2007. Activation Mechanisms and Functional Roles of TRPP2 Cation Channels. *In:* LIEDTKE, W. B. & HELLER, S. (eds.) *TRP Ion Channel Function in Sensory Transduction and Cellular Signaling Cascades.* Boca Raton (FL).

GIAMARCHI, A., FENG, S., RODAT-DESPOIX, L., XU, Y., BUBENSHCHIKOVA, E., NEWBY, L. J., HAO, J., GAUDIOSO, C., CREST, M., LUPAS, A. N., HONORE, E., WILLIAMSON, M. P., OBARA, T., ONG, A. C. & DELMAS, P. 2010. A polycystin-2 (TRPP2) dimerization domain essential for the function of heteromeric polycystin complexes. *EMBO J,* 29**,** 1176-91.

GODISKA, R., AUFDERHEIDE, K. J., GILLEY, D., HENDRIE, P., FITZWATER, T., PREER, L. B., POLISKY, B. & PREER, J. R., JR. 1987. Transformation of Paramecium by microinjection of a cloned serotype gene. *Proc Natl Acad Sci U S A,* 84**,** 7590-4.

GONZALEZ-PERRETT, S., KIM, K., IBARRA, C., DAMIANO, A. E., ZOTTA, E., BATELLI, M., HARRIS, P. C., REISIN, I. L., ARNAOUT, M. A. & CANTIELLO, H. F. 2001. Polycystin-2, the protein mutated in autosomal dominant polycystic kidney disease (ADPKD), is a Ca2+-permeable nonselective cation channel. *Proc Natl Acad Sci U S A,* 98**,** 1182-7.

HANAOKA, K., QIAN, F., BOLETTA, A., BHUNIA, A. K., PIONTEK, K., TSIOKAS, L., SUKHATME, V. P., GUGGINO, W. B. & GERMINO, G. G. 2000. Co-assembly of polycystin-1 and -2 produces unique cation-permeable currents. *Nature,* 408**,** 990-4.

HANSMA, H. G. 1979. Sodium uptake and membrane excitation in Paramecium. *J Cell Biol,* 81**,** 374-81.

HAYNES, W. J., KUNG, C., SAIMI, Y. & PRESTON, R. R. 2002. An exchanger-like protein underlies the large Mg2+ current in Paramecium. *Proc Natl Acad Sci U S A,* 99**,** 15717-22.

HILDEBRANDT, F., BENZING, T. & KATSANIS, N. 2011. Ciliopathies. *N Engl J Med,* 364**,** 1533-43.

HOEFELE, J., MAYER, K., SCHOLZ, M. & KLEIN, H. G. 2011. Novel PKD1 and PKD2 mutations in autosomal dominant polycystic kidney disease (ADPKD). *Nephrol Dial Transplant,* 26**,** 2181-8.

HOFFMEISTER, H., BABINGER, K., GURSTER, S., CEDZICH, A., MEESE, C., SCHADENDORF, K., OSTEN, L., DE VRIES, U., RASCLE, A. & WITZGALL, R. 2011. Polycystin-2 takes different routes to the somatic and ciliary plasma membrane. *J Cell Biol,* 192**,** 631-45.

HU, J., BAE, Y. K., KNOBEL, K. M. & BARR, M. M. 2006. Casein kinase II and calcineurin modulate TRPP function and ciliary localization. *Mol Biol Cell,* 17**,** 2200-11.

HUAN, Y. & VAN ADELSBERG, J. 1999. Polycystin-1, the PKD1 gene product, is in a complex containing E-cadherin and the catenins. *J Clin Invest,* 104**,** 1459-68.

HUANG, K., DIENER, D. R., MITCHELL, A., PAZOUR, G. J., WITMAN, G. B. & ROSENBAUM, J. L. 2007. Function and dynamics of PKD2 in Chlamydomonas reinhardtii flagella. *J Cell Biol,* 179**,** 501-14.

HUGHES, J., WARD, C. J., PERAL, B., ASPINWALL, R., CLARK, K., SAN MILLAN, J. L., GAMBLE, V. & HARRIS, P. C. 1995. The polycystic kidney disease 1 (PKD1) gene encodes a novel protein with multiple cell recognition domains. *Nat Genet,* 10**,** 151-60.

IFTODE, F., ADOUTTE, A., AND FLEURY, A. 1996. The Surface Pattern of Paramecium tetraurelia in interphase: An Electron Microscopic Study of Basal Body Variability, Connections with Associated Ribbons and their Epiplasmic Environment. *European Journal of Protistology,* 32**,** 1.

IFTODE, F., COHEN, J., RUIZ, F., RUEDA, A. T., CHENSHAN, L., ADOUTTE, A. & BEISSON, J. 1989. Development of Surface Pattern during Division in Paramecium .1. Mapping of Duplication and Reorganization of Cortical Cytoskeletal Structures in the Wild-Type. *Development,* 105**,** 191-211.

IFTODE, F., COHEN, J., RUIZ, F., RUEDA, A. T., CHEN-SHAN, L., ADOUTE, A., AND BEISSON, J. 1989. Development of surface pattern during division in Paramesium. *Development,* 105**,** 191-211.

IFTODE, F. & FLEURY-AUBUSSON, A. 2003. Structural inheritance in Paramecium: ultrastructural evidence for basal body and associated rootlets polarity transmission through binary fission. *Biol Cell,* 95**,** 39-51.

IWADATE, Y. & KIKUYAMA, M. 2001. Contribution of calcium influx on trichocyst discharge in Paramecium caudatum. *Zoological Science,* 18**,** 497-504.

JACOBS, C. L. 2007. NMDA receptor associated protein in Paramecium and it involvement in glutamate chemoresponse. *MS thesis*.

JENNINGS, H. S. 1906. *Behavior of the lower organisms,* New York,, The Columbia university press, The Macmillan company, agents; etc.

JIN, H., WHITE, S. R., SHIDA, T., SCHULZ, S., AGUIAR, M., GYGI, S. P., BAZAN, J. F. & NACHURY, M. V. 2010. The conserved Bardet-Biedl syndrome proteins assemble a coat that traffics membrane proteins to cilia. *Cell,* 141**,** 1208-19.

JOHNSON, K. A. & ROSENBAUM, J. L. 1992. Polarity of flagellar assembly in Chlamydomonas. *J Cell Biol,* 119**,** 1605-11.

KANESHIRO, E. S. 1987. Lipids of Paramecium. *J Lipid Res,* 28**,** 1241-58.

KIM, E. J. & CERUTTI, H. 2009. Targeted gene silencing by RNA interference in Chlamydomonas. *Methods Cell Biol,* 93**,** 99-110.

KLINGER, M., WANG, W., KUHNS, S., BARENZ, F., DRAGER-MEURER, S., PEREIRA, G. & GRUSS, O. J. 2014. The novel centriolar satellite protein SSX2IP targets Cep290 to the ciliary transition zone. *Mol Biol Cell,* 25**,** 495-507.

KOBORI, T., SMITH, G. D., SANDFORD, R. & EDWARDSON, J. M. 2009. The transient receptor potential channels TRPP2 and TRPC1 form a heterotetramer with a 2:2 stoichiometry and an alternating subunit arrangement. *J Biol Chem,* 284**,** 35507-13.

KOTTGEN, M., BENZING, T., SIMMEN, T., TAUBER, R., BUCHHOLZ, B., FELICIANGELI, S., HUBER, T. B., SCHERMER, B., KRAMER-ZUCKER, A., HOPKER, K., SIMMEN, K. C., TSCHUCKE, C. C., SANDFORD, R., KIM, E., THOMAS, G. & WALZ, G. 2005. Trafficking of TRPP2 by PACS proteins represents a novel mechanism of ion channel regulation. *EMBO J,* 24**,** 705-16.

KOTTGEN, M., BUCHHOLZ, B., GARCIA-GONZALEZ, M. A., KOTSIS, F., FU, X., DOERKEN, M., BOEHLKE, C., STEFFL, D., TAUBER, R., WEGIERSKI, T., NITSCHKE, R., SUZUKI, M., KRAMER-ZUCKER, A., GERMINO, G. G., WATNICK, T., PRENEN, J., NILIUS, B., KUEHN, E. W. & WALZ, G. 2008. TRPP2 and TRPV4 form a polymodal sensory channel complex. *J Cell Biol,* 182**,** 437-47.

KOULEN, P., CAI, Y., GENG, L., MAEDA, Y., NISHIMURA, S., WITZGALL, R., EHRLICH, B. E. & SOMLO, S. 2002. Polycystin-2 is an intracellular calcium release channel. *Nat Cell Biol,* 4**,** 191-7.

KOZMINSKI, K. G., BEECH, P. L. & ROSENBAUM, J. L. 1995. The Chlamydomonas kinesin-like protein FLA10 is involved in motility associated with the flagellar membrane. *J Cell Biol,* 131**,** 1517-27.

KOZMINSKI, K. G., JOHNSON, K. A., FORSCHER, P. & ROSENBAUM, J. L. 1993. A motility in the eukaryotic flagellum unrelated to flagellar beating. *Proc Natl Acad Sci U S A,* 90**,** 5519-23.

KUNG, C. 1971. Genic mutants with altered system of excitation in Paramecium aurelia. II. Mutagenesis, screening and genetic analysis of the mutants. *Genetics,* 69**,** 29-45.

KUNG, C., CHANG, S. Y., SATOW, Y., HOUTEN, J. V. & HANSMA, H. 1975. Genetic dissection of behavior in paramecium. *Science,* 188**,** 898-904.

KUNG, C. & NAITO, Y. 1973. Calcium-induced ciliary reversal in the extracted models of "Pawn", a behavioral mutant of Paramecium. *Science,* 179**,** 195-6.

KUNG, C. & SAIMI, Y. 1982. The physiological basis of taxes in Paramecium. *Annu Rev Physiol,* 44**,** 519-34.

KUO, I. Y., KEELER, C., CORBIN, R., CELIC, A., PETRI, E. T., HODSDON, M. E. & EHRLICH, B. E. 2014. The number and location of EF hand motifs dictates the calcium dependence of polycystin-2 function. *FASEB J,* 28**,** 2332-46.

LENTINE, K. L., XIAO, H., MACHNICKI, G., GHEORGHIAN, A. & SCHNITZLER, M. A. 2010. Renal function and healthcare costs in patients with polycystic kidney disease. *Clin J Am Soc Nephrol,* 5**,** 1471-9.

LI, Y., WRIGHT, J. M., QIAN, F., GERMINO, G. G. & GUGGINO, W. B. 2005. Polycystin 2 interacts with type I inositol 1,4,5-trisphosphate receptor to modulate intracellular Ca2+ signaling. *J Biol Chem,* 280**,** 41298-306.

LUO, Y., VASSILEV, P. M., LI, X., KAWANABE, Y. & ZHOU, J. 2003. Native polycystin 2 functions as a plasma membrane Ca2+-permeable cation channel in renal epithelia. *Mol Cell Biol,* 23**,** 2600-7.

MACHEMER-ROHNISCH, S. & MACHEMER, H. 1989. A Ca paradox: Electric and behavioural responses of Paramecium following changes in external ion concentration. *Eur J Protistol,* 25**,** 45-59.

MACHEMER, H. & ECKERT, R. 1973. Electrophysiological control of reversed ciliary beating in Paramecium. *J Gen Physiol,* 61**,** 572-87.

MACHEMER, H. & OGURA, A. 1979. Ionic conductances of membranes in ciliated and deciliated Paramecium. *J Physiol,* 296**,** 49-60.

MAGUIRE, M. E. & COWAN, J. A. 2002. Magnesium chemistry and biochemistry. *Biometals,* 15**,** 203-10.

MAZELOVA, J., ASTUTO-GRIBBLE, L., INOUE, H., TAM, B. M., SCHONTEICH, E., PREKERIS, R., MORITZ, O. L., RANDAZZO, P. A. & DERETIC, D. 2009. Ciliary targeting motif VxPx directs assembly of a trafficking module through Arf4. *EMBO J,* 28**,** 183-92.

MOCHIZUKI, T., WU, G., HAYASHI, T., XENOPHONTOS, S. L., VELDHUISEN, B., SARIS, J. J., REYNOLDS, D. M., CAI, Y., GABOW, P. A., PIERIDES, A., KIMBERLING, W. J., BREUNING, M. H., DELTAS, C. C., PETERS, D. J. & SOMLO, S. 1996. PKD2, a gene for polycystic kidney disease that encodes an integral membrane protein. *Science,* 272**,** 1339-42.

NACHURY, M. V., LOKTEV, A. V., ZHANG, Q., WESTLAKE, C. J., PERANEN, J., MERDES, A., SLUSARSKI, D. C., SCHELLER, R. H., BAZAN, J. F., SHEFFIELD, V. C. & JACKSON, P. K. 2007. A core complex of BBS proteins cooperates with the GTPase Rab8 to promote ciliary membrane biogenesis. *Cell,* 129**,** 1201-13.

NAITOH, Y. 1966. Reversal response elicited in nonbeating cilia of paramecium by membrane depolarizatin. *Science,* 154**,** 660-2.

NAITOH, Y. 1968. Ionic control of the reversal response of cilia in Paramecium caudatum. A calcium hypothesis. *J Gen Physiol,* 51**,** 85-103.

NAITOH, Y., ECKERT, R. & FRIEDMAN, K. 1972. A regenerative calcium response in Paramecium. *J Exp Biol,* 56**,** 667-81.

NAULI, S. M., ALENGHAT, F. J., LUO, Y., WILLIAMS, E., VASSILEV, P., LI, X., ELIA, A. E., LU, W., BROWN, E. M., QUINN, S. J., INGBER, D. E. & ZHOU, J. 2003. Polycystins 1 and 2 mediate mechanosensation in the primary cilium of kidney cells. *Nat Genet,* 33**,** 129-37.

NOMURA, H., TURCO, A. E., PEI, Y., KALAYDJIEVA, L., SCHIAVELLO, T., WEREMOWICZ, S., JI, W., MORTON, C. C., MEISLER, M., REEDERS, S. T. & ZHOU, J. 1998. Identification of PKDL, a novel polycystic kidney disease 2-like gene whose murine homologue is deleted in mice with kidney and retinal defects. *J Biol Chem,* 273**,** 25967-73.

NONAKA, S., TANAKA, Y., OKADA, Y., TAKEDA, S., HARADA, A., KANAI, Y., KIDO, M. & HIROKAWA, N. 1998. Randomization of left-right asymmetry due to loss of nodal cilia generating leftward flow of extraembryonic fluid in mice lacking KIF3B motor protein. *Cell,* 95**,** 829-37.

OGURA, A. & MACHEMER, H. 1980. Distribution of Mechanoreceptor Channels in the Paramecium Surface-Membrane. *Journal of Comparative Physiology,* 135**,** 233-242.

PAZOUR, G. J., DICKERT, B. L. & WITMAN, G. B. 1999. The DHC1b (DHC2) isoform of cytoplasmic dynein is required for flagellar assembly. *J Cell Biol,* 144**,** 473-81.

PAZOUR, G. J., SAN AGUSTIN, J. T., FOLLIT, J. A., ROSENBAUM, J. L. & WITMAN, G. B. 2002. Polycystin-2 localizes to kidney cilia and the ciliary level is elevated in orpk mice with polycystic kidney disease. *Curr Biol,* 12**,** R378-80.

PICARIELLO, T., VALENTINE, M. S., YANO, J. & VAN HOUTEN, J. 2014. Reduction of meckelin leads to general loss of cilia, ciliary microtubule misalignment and distorted cell surface organization. *Cilia,* 3**,** 2.

PLATTNER, H. & KISSMEHL, R. 2003. Molecular aspects of membrane trafficking in paramecium. *Int Rev Cytol,* 232**,** 185-216.

PORTER, M. E., BOWER, R., KNOTT, J. A., BYRD, P. & DENTLER, W. 1999. Cytoplasmic dynein heavy chain 1b is required for flagellar assembly in Chlamydomonas. *Mol Biol Cell,* 10**,** 693-712.

PRATT, A. J. & MACRAE, I. J. 2009. The RNA-induced silencing complex: a versatile gene-silencing machine. *J Biol Chem,* 284**,** 17897-901.

PRESTON, R. R. 1990. A magnesium current in Paramecium. *Science,* 250**,** 285-8.

PRESTON, R. R. 1998. Transmembrane Mg2+ currents and intracellular free Mg2+ concentration in Paramecium tetraurelia. *J Membr Biol,* 164**,** 11-24.

PRESTON, R. R. & KUNG, C. 1994a. Inhibition of Mg2+ current by single-gene mutation in Paramecium. *J Membr Biol,* 139**,** 203-13.

PRESTON, R. R. & KUNG, C. 1994b. Isolation and characterization of paramecium mutants defective in their response to magnesium. *Genetics,* 137**,** 759-69.

PRESTON, R. R. & VAN HOUTEN, J. L. 1987. Chemoreception in Paramecium tetraurelia: acetate and folate-induced membrane hyperpolarization. *J Comp Physiol A,* 160**,** 525-35.

ROMANOVITCH, M. 2012. The L-glutamate receptor in Paramecium tetraurelia. *MS thesis*.

REEDERS, S. T., BREUNING, M. H., DAVIES, K. E., NICHOLLS, R. D., JARMAN, A. P., HIGGS, D. R., PEARSON, P. L. & WEATHERALL, D. J. 1985. A highly polymorphic DNA marker linked to adult polycystic kidney disease on chromosome 16. *Nature,* 317**,** 542-4.

RHOADS, D. E. & KANESHIRO, E. S. 1979. Characterizations of Phospholipids from Paramecium-Tetraurelia Cells and Cilia. *Journal of Protozoology,* 26**,** 329-338.

RINGO, D. L. 1967. Flagellar motion and fine structure of the flagellar apparatus in Chlamydomonas. *J Cell Biol,* 33**,** 543-71.

RUIZ, F., GARREAU DE LOUBRESSE, N., KLOTZ, C., BEISSON, J. & KOLL, F. 2005. Centrin deficiency in Paramecium affects the geometry of basal-body duplication. *Curr Biol,* 15**,** 2097-106.

SALONEN, R. & NORIO, R. 1984. The Meckel syndrome in Finland: epidemiologic and genetic aspects. *Am J Med Genet,* 18**,** 691-8.

SALONEN, R. & PAAVOLA, P. 1998. Meckel syndrome. *J Med Genet,* 35**,** 497-501.

SAMMELS, E., DEVOGELAERE, B., MEKAHLI, D., BULTYNCK, G., MISSIAEN, L., PARYS, J. B., CAI, Y., SOMLO, S. & DE SMEDT, H. 2010. Polycystin-2 activation by inositol 1,4,5-trisphosphate-induced Ca2+ release requires its direct association with the inositol 1,4,5-trisphosphate receptor in a signaling microdomain. *J Biol Chem,* 285**,** 18794-805.

SATIR, B., SALE, W. S. & SATIR, P. 1976. Membrane renewal after dibucaine deciliation of Tetrahymena. Freeze-fracture technique, cilia, membrane structure. *Exp Cell Res,* 97**,** 83-91.

SATOW, Y. & KUNG, C. 1980. Ca-induced K+-outward current in Paramecium tetraurelia. *J Exp Biol,* 88**,** 293-303.

SCHULTZ, J. E., KLUMPP, S., BENZ, R., SCHURHOFF-GOETERS, W. J. & SCHMID, A. 1992. Regulation of adenylyl cyclase from Paramecium by an intrinsic potassium conductance. *Science,* 255**,** 600-3.

SCHWARZ, D. S., TOMARI, Y. & ZAMORE, P. D. 2004. The RNA-induced silencing complex is a Mg2+-dependent endonuclease. *Curr Biol,* 14**,** 787-91.

SEPULVEDA, W., SEBIRE, N. J., SOUKA, A., SNIJDERS, R. J. & NICOLAIDES, K. H. 1997. Diagnosis of the Meckel-Gruber syndrome at eleven to fourteen weeks' gestation. *Am J Obstet Gynecol,* 176**,** 316-9.

SMITH, U. M., CONSUGAR, M., TEE, L. J., MCKEE, B. M., MAINA, E. N., WHELAN, S., MORGAN, N. V., GORANSON, E., GISSEN, P., LILLIQUIST, S., ALIGIANIS, I. A., WARD, C. J., PASHA, S., PUNYASHTHITI, R., MALIK SHARIF, S., BATMAN, P. A., BENNETT, C. P., WOODS, C. G., MCKEOWN, C., BUCOURT, M., MILLER, C. A., COX, P., ALGAZALI, L., TREMBATH, R. C., TORRES, V. E., ATTIE-BITACH, T., KELLY, D. A., MAHER, E. R., GATTONE, V. H., 2ND, HARRIS, P. C. & JOHNSON, C. A. 2006. The transmembrane protein meckelin (MKS3) is mutated in Meckel-Gruber syndrome and the wpk rat. *Nat Genet,* 38**,** 191-6.

STELLY, N., MAUGER, J. P., CLARET, M. & ADOUTTE, A. 1991. Cortical alveoli of Paramecium: a vast submembranous calcium storage compartment. *J Cell Biol,* 113**,** 103-12.

STEWART, A. P., SMITH, G. D., SANDFORD, R. N. & EDWARDSON, J. M. 2010. Atomic force microscopy reveals the alternating subunit arrangement of the TRPP2-TRPV4 heterotetramer. *Biophys J,* 99**,** 790-7.

SUI, G., SOOHOO, C., AFFAR EL, B., GAY, F., SHI, Y., FORRESTER, W. C. & SHI, Y. 2002. A DNA vector-based RNAi technology to suppress gene expression in mammalian cells. *Proc Natl Acad Sci U S A,* 99**,** 5515-20.

TORRES, V. E., CHAPMAN, A. B., DEVUYST, O., GANSEVOORT, R. T., GRANTHAM, J. J., HIGASHIHARA, E., PERRONE, R. D., KRASA, H. B., OUYANG, J., CZERWIEC, F. S. & INVESTIGATORS, T. T. 2012. Tolvaptan in patients with autosomal dominant polycystic kidney disease. *N Engl J Med,* 367**,** 2407-18.

TORRES, V. E., HARRIS, P. C. & PIRSON, Y. 2007. Autosomal dominant polycystic kidney disease. *Lancet,* 369**,** 1287-301.

TSIOKAS, L., ARNOULD, T., ZHU, C., KIM, E., WALZ, G. & SUKHATME, V. P. 1999. Specific association of the gene product of PKD2 with the TRPC1 channel. *Proc Natl Acad Sci U S A,* 96**,** 3934-9.

TSIOKAS, L., KIM, E., ARNOULD, T., SUKHATME, V. P. & WALZ, G. 1997a. Homo- and heterodimeric interactions between the gene products of PKD1 and PKD2. *Proceedings of the National Academy of Sciences of the United States of America,* 94**,** 6965-6970.

TSIOKAS, L., KIM, E., ARNOULD, T., SUKHATME, V. P. & WALZ, G. 1997b. Homo- and heterodimeric interactions between the gene products of PKD1 and PKD2. *Proc Natl Acad Sci U S A,* 94**,** 6965-70.

VALENTINE, M. S., RAJENDRAN, A., YANO, J., WEERARATNE, S. D., BEISSON, J., COHEN, J., KOLL, F. & VAN HOUTEN, J. 2012. Paramecium BBS genes are key to presence of channels in Cilia. *Cilia,* 1**,** 16.

VAN HOUTEN, J. 1979. Membrane potential changes during chemokinesis in Paramecium. *Science,* 204**,** 1100-3.

VAN HOUTEN, J. L., YANG, W. Q. & BERGERON, A. 2000. Chemosensory signal transduction in paramecium. *J Nutr,* 130**,** 946S-9S.

WEERARATNE, S. D. 2007. GPI receptors in folate chemosensortransduction in Paramecium tetraurelia. *PhD Thesis*.

WILLIAMS, C. L., LI, C. M., KIDA, K., INGLIS, P. N., MOHAN, S., SEMENEC, L., BIALAS, N. J., STUPAY, R. M., CHEN, N. S., BLACQUE, O. E., YODER, B. K. & LEROUX, M. R. 2011. MKS and NPHP modules cooperate to establish basal body/transition zone membrane associations and ciliary gate function during ciliogenesis. *Journal of Cell Biology,* 192**,** 1023-1041.

WILLIAMS, C. L., MCINTYRE, J. C., NORRIS, S. R., JENKINS, P. M., ZHANG, L., PEI, Q., VERHEY, K. & MARTENS, J. R. 2014. Direct evidence for BBSome-associated intraflagellar transport reveals distinct properties of native mammalian cilia. *Nat Commun,* 5**,** 5813.

WRIGHT, M. V. & VAN HOUTEN, J. L. 1990. Characterization of a putative Ca2(+)-transporting Ca2(+)-ATPase in the pellicles of Paramecium tetraurelia. *Biochim Biophys Acta,* 1029**,** 241-51.

YANG, P., DIENER, D. R., YANG, C., KOHNO, T., PAZOUR, G. J., DIENES, J. M., AGRIN, N. S., KING, S. M., SALE, W. S., KAMIYA, R., ROSENBAUM, J. L. & WITMAN, G. B. 2006. Radial spoke proteins of Chlamydomonas flagella. *J Cell Sci,* 119**,** 1165-74.

YANO, J., RACHOCHY, V. & VAN HOUTEN, J. L. 2003. Glycosyl phosphatidylinositol-anchored proteins in chemosensory signaling: antisense manipulation of Paramecium tetraurelia PIG-A gene expression. *Eukaryot Cell,* 2**,** 1211-9.

ZHANG, Q., YU, D., SEO, S., STONE, E. M. & SHEFFIELD, V. C. 2012. Intrinsic protein-protein interaction-mediated and chaperonin-assisted sequential assembly of stable bardet-biedl syndrome protein complex, the BBSome. *J Biol Chem,* 287**,** 20625-35.

Figure 1.1. Scanning Electron Micrograph of *Paramecium tetraurelia*.

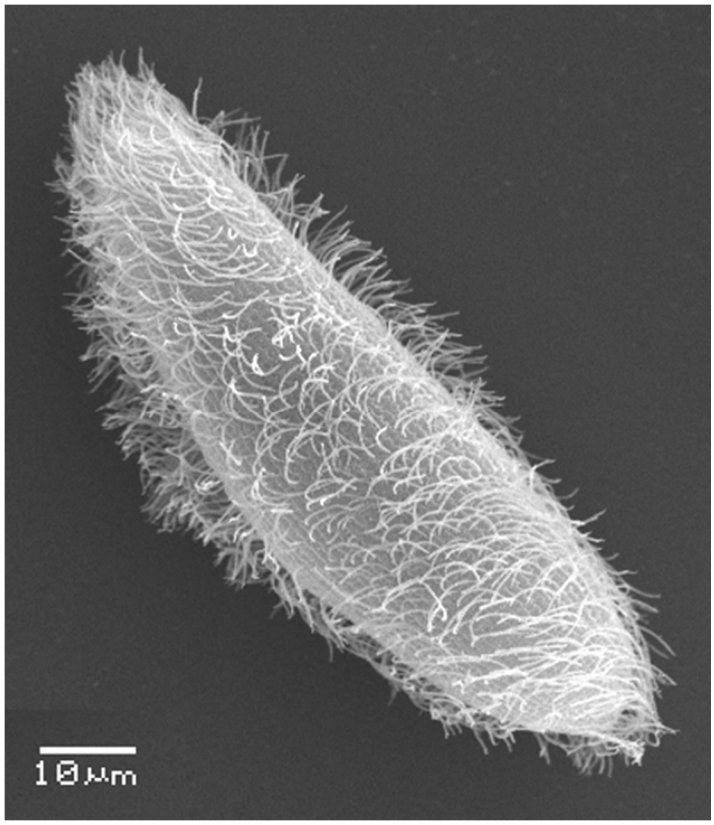

Figure 1.2. Swimming behavior and membrane potential of *P. tetraurelia*. Paramecia typically display forward swimming with the ciliary power stroke toward the posterior of the cell. This occurs with the membrane at rest, which is about -30 mV. When the cell encounters a repellent, high ionic concentrations, or sometimes a random event, the membrane will become depolarized enough to produce an action potential. This depolarization beyond threshold cause the voltage gated calcium channels of the cilia to open allowing calcium to enter. The depolarization is countered by the activation of the calcium-dependent and voltage-dependent potassium channels. As long as calcium remains high, the cilia will remain with their power stroke toward the anterior of the cell, causing backward swimming. Once the calcium is remove and the membrane potential returns to its resting state, the cilia will revert back to the power stroke toward the posterior of the cell and forward swimming. This figure was adapted from Figure 1 in (Kung et al., 1975).

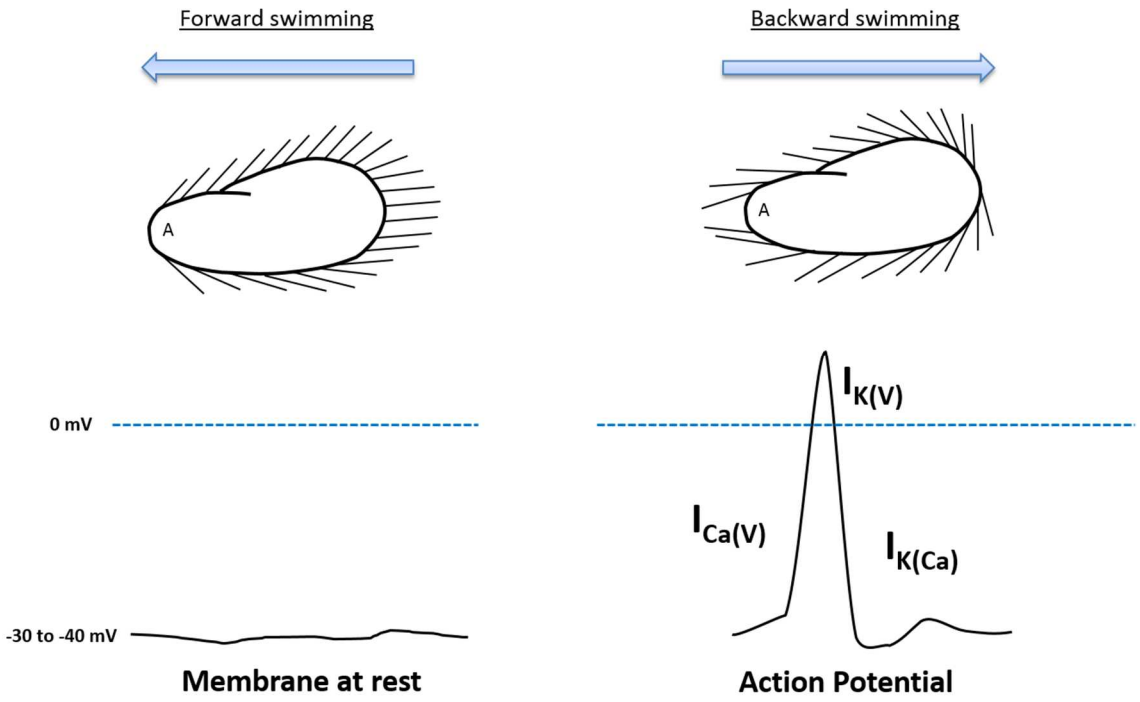

Figure 1.3. Schematic depiction of a *Paramecium* one (A) and two (B) basal body units with accompanying rootlets. The cortical units of *Paramecium* contain one (A) or two (B) basal bodies (red). (A) One basal body units contain a single basal body with a striated rootlet or kinetodesmal fiber (green), a transverse microtubule (purple), and a post ciliary rootlet emanating from the basal body. (B) Two basal body units contain a mother basal body and a daughter basal body. The mother basal body is structured like the basal bodies in (A) and the daughter basal body is attached to the striated rootlet and contains the transverse microtubule, but not a post ciliary rootlet. Anterior to posterior orientation can be seen on the right.

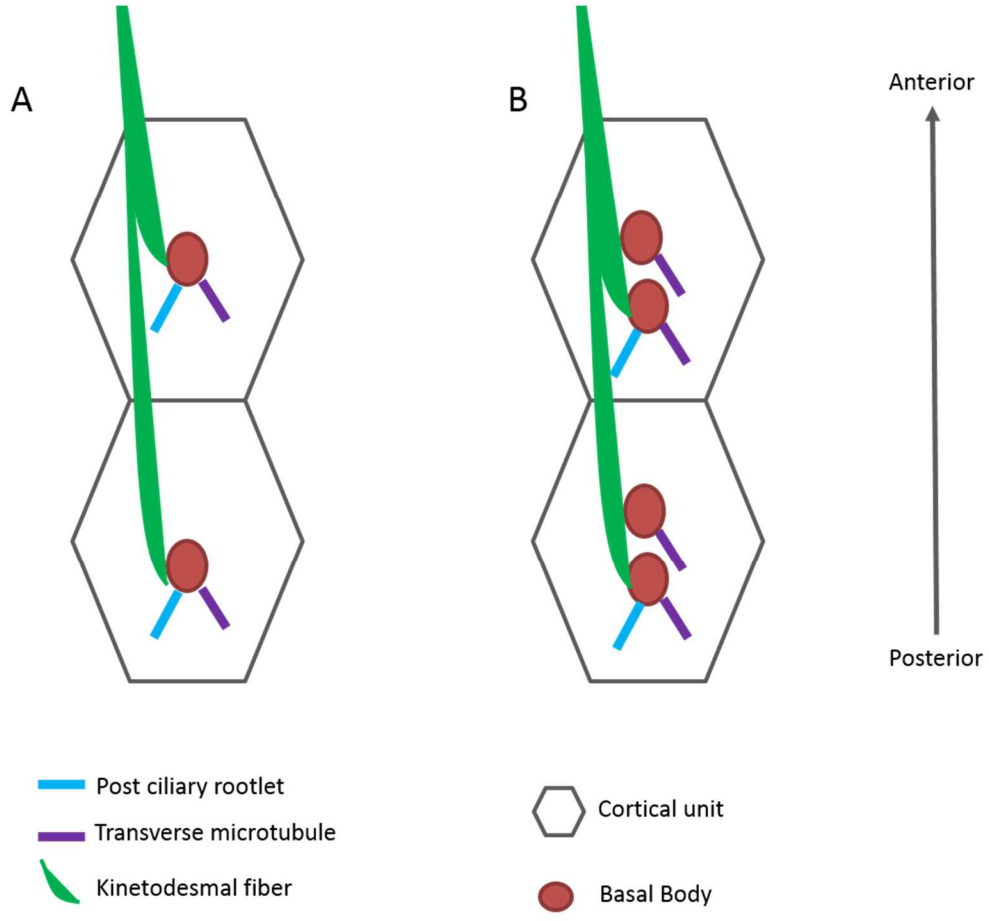

Figure 1.4. Structure of a *Paramecium* cilium and basal body. (A) A schematic line illustration of a paramecium cilium. Basal body is comprised of nine triplets of microtubules below the cell surface (red). The transition zone (yellow bracket) is shaded in yellow and is the area between where the C tubules of the basal body triplet terminate and the central pair of microtubules in the axoneme of the cilium begins. The cilium proper is approximately 10 µm in length (green bracket). Anterograde and retrograde directions of intraflagellar transport (IFT) are indicated by the blue arrows. Illustration not drawn to scale. **(B)** A transverse section through a paramecium basal body (red bracket), transition zone (shaded in yellow) and the beginning of a cilium (green bracket). Large empty spaces (as) on either side are the alveolar sacs. Scale bar is 50 nm.

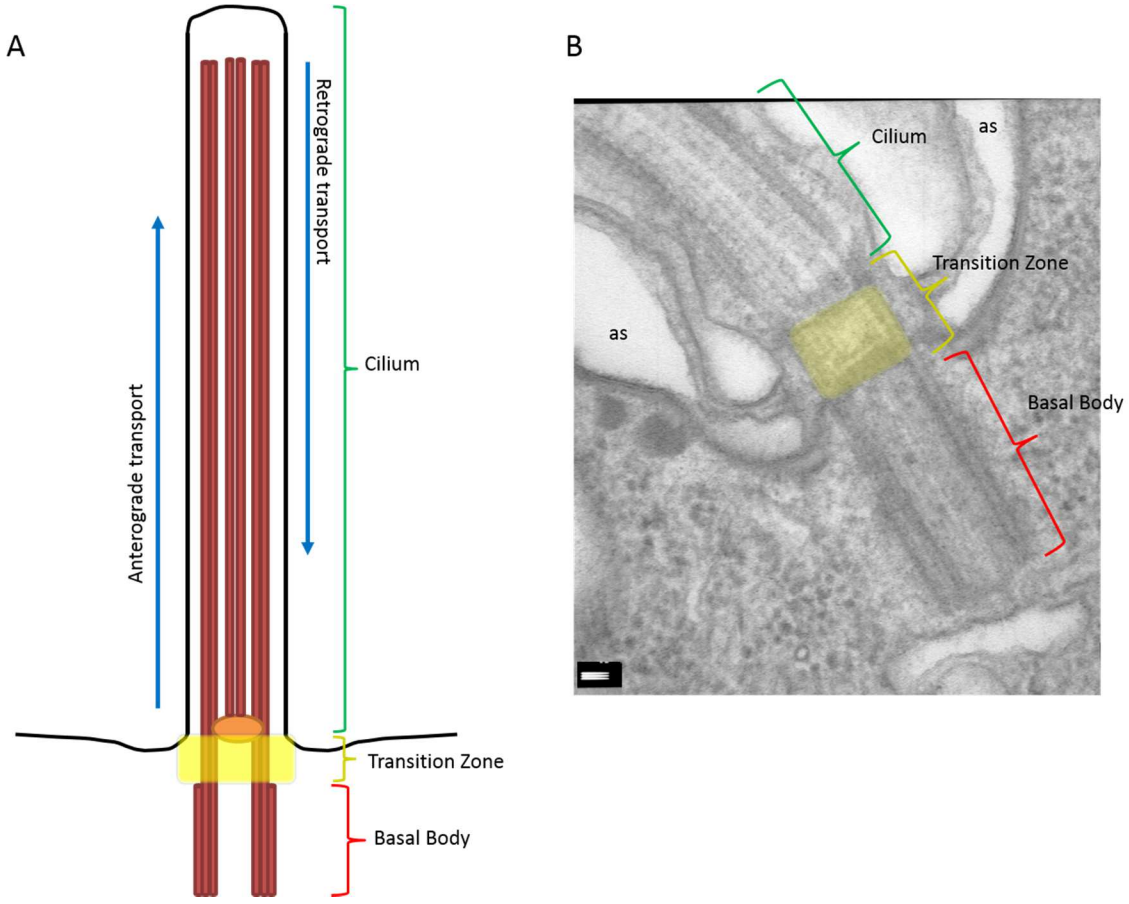

Figure 1.5. Plasmid maps for pPXV over-expression plasmids. **(A)** Plasmid map for N-terminal epitope tag FLAG $(DYKDDDDK)^{x3}$ or myc $(EQKLISEEEDL)^{x3}$. **(B)** Plasmid map for C-terminal epitope tag FLAG or myc. **(C)** Plasmid map for N-terminal myc epitope tag and C-terminal FLAG epitope tag. All epitope tags are in the pPXV plasmid (Gift of W. John Haynes). The plasmid contains *Tetrahymena* telomeres (blue), a Not I linearization site, calmodulin promoters (green), and ampicillin resistance (pink). All plasmid maps show relevant restriction enzyme cut sites for insertion of the gene of interest.

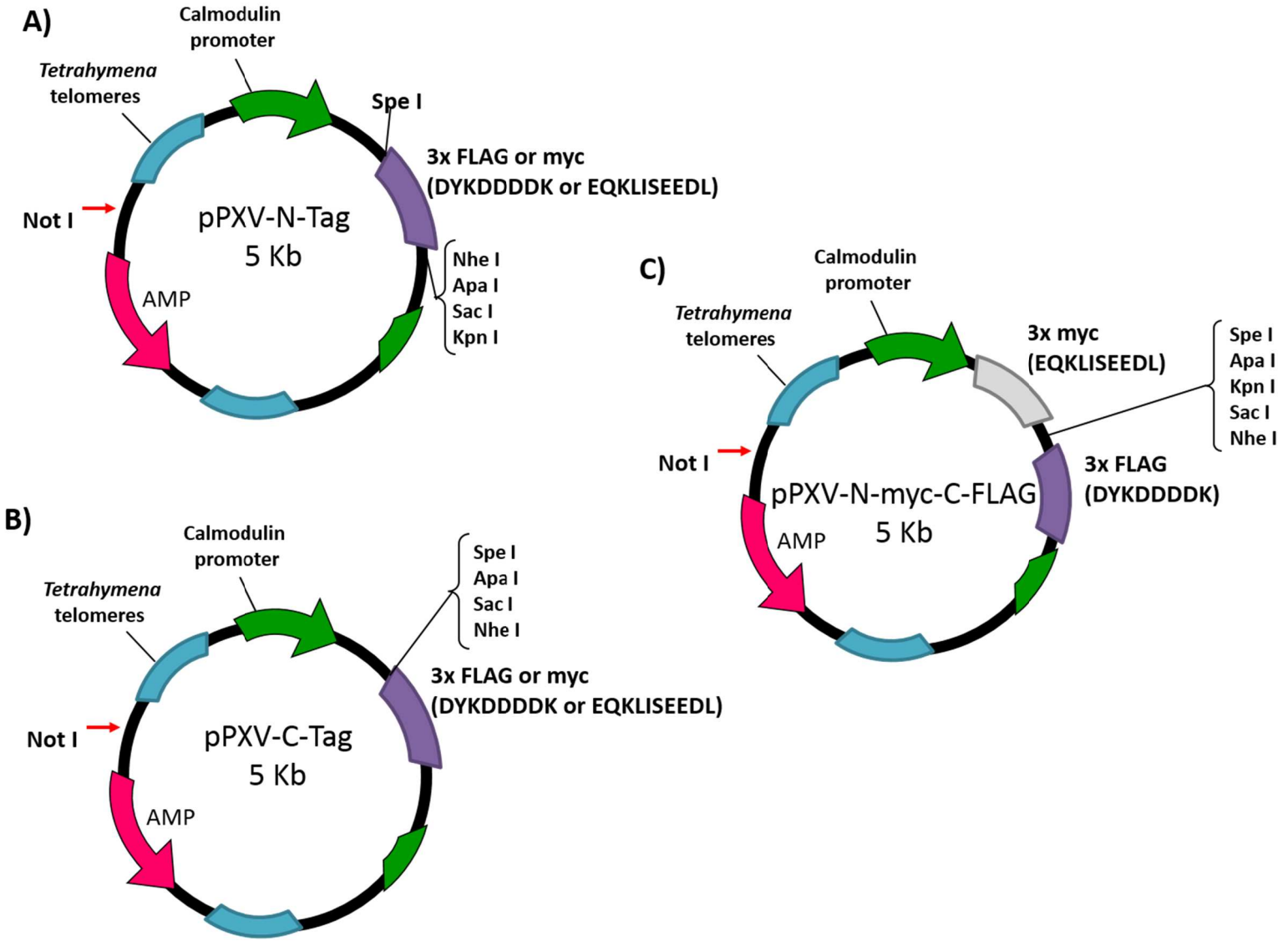
A)
Calmodulin promoter
Tetrahymena telomeres
Spe I
3x FLAG or myc (DYKDDDDK or EQKLISEEDL)
Not I
pPXV-N-Tag
5 Kb
Nhe I
Apa I
Sac I
Kpn I
AMP
B)
Calmodulin promoter
Tetrahymena telomeres
Spe I
Apa I
Sac I
Nhe I
3x FLAG or myc (DYKDDDDK or EQKLISEEDL)
Not I
pPXV-C-Tag
5 Kb
AMP
C)
Calmodulin promoter
Tetrahymena telomeres
3x myc (EQKLISEEDL)
Spe I
Apa I
Kpn I
Sac I
Nhe I
Not I
3x FLAG (DYKDDDDK)
pPXV-N-myc-C-FLAG
5 Kb
AMP

Figure 1.6. Electrophysiology recording from a ciliated and deciliated cell.

Chapter 2: Reduction of Meckelin Leads to General Loss of Cilia, Ciliary Microtubule Misalignment, and Distorted Cell Surface Organization

Reduction of Meckelin Leads to General Loss of Cilia, Ciliary Microtubule Misalignment, and Distorted Cell Surface Organization

Tyler Picariello*
E-mail: Tyler.Picariello@uvm.edu

Megan Smith Valentine*
E-mail: Megan.Valentine@uvm.edu

Junji Yano
E-mail: Junji.Yano@uvm.edu

Judith Van Houten
E-mail: Judith.Vanhouten@uvm.edu

University of Vermont, Department of Biology, Burlington, VT 05405 USA

** These authors contributed equally to this work*

Correspondence:
J. Van Houten
University of Vermont
Department of Biology
120A Marsh Life Science
Burlington, VT 05405 USA
Phone: 802-656-0704
Fax: 802-656-2914
Judith.Vanhouten@uvm.edu

Abstract

Background. Meckelin (MKS3), a conserved protein linked to Meckel Syndrome, assists in the migration of centrioles to the cell surface for ciliogenesis. We explored for additional functions of MKS3p using RNA interference (RNAi) and expression of FLAG epitope tagged protein in the ciliated protozoan *Paramecium tetraurelia*. This cell has a highly organized cell surface with thousands of cilia and basal bodies that are grouped into one or two basal body units delineated by ridges. The highly systematized nature of the *P. tetraurelia* cell surface provides a research model of MKS and other ciliopathies where changes in ciliary structure, subcellular organization and overall arrangement of the cell surface can be easily observed. We used cells reduced in *IFT88* for comparison, as the involvement of this gene's product with cilia maintenance and growth is well understood.

Results. FLAG-MKS3p was found above the plane of the distal basal body in the transition zone. Approximately 95% of those basal bodies observed had staining for FLAG-MKS3. The RNAi phenotype for *MKS3* depleted cells included global shortening and loss of cilia. Basal body structure appeared unaffected. On the dorsal surface, the basal bodies and their associated rootlets appeared rotated out of alignment from the normal anterior-posterior rows. Likewise, cortical units were abnormal in shape and out of alignment from normal rows. A GST pull down using the MKS3 coiled-coil domain suggests previously unidentified interacting partners.

Conclusions. Reduction of MKS3p shows that this protein affects development and maintenance of cilia over the entire cell surface. Reduction of MKS3p is most visible on the dorsal surface. The anterior basal body is attached to and moves along the striated rootlet of the posterior basal body in preparation for duplication. We propose that with reduced MKS3p, this attachment and guidance of the basal body is lost. The basal body veers off course, causing basal body rows to be misaligned and units to be misshapen. Rootlets form normally on these misaligned basal bodies but are rotated out of their correct orientation. Our hypothesis is further supported by the identification of novel interacting partners of MKS3p including a kinetodesmal fiber protein, KdB2.

Background

Ciliopathies are human disorders caused by abnormalities in the assembly, maintenance, or function of cilia and include developmental defects leading to cystic kidneys, vision problems, polydactyly, obesity, encephalocele, and even death (reviewed in [1]). In order to improve our understanding of the wide array of cellular processes affected in these disorders, the function and involvement of the genes and gene products involved in ciliopathies should be defined [2-4]. Toward this end, we have investigated the protein Meckelin (MKS3) in *Paramecium tetraurelia*, a multi-ciliated cell.

MKS3 is one of at least three genes commonly associated with the ciliopathy Meckel Syndrome (MKS), and has been found to be dysfunctional in other ciliopathy syndromes including Bardet-Biedl [5], COACH [6, 7] and Joubert [8]. The three most common characteristics of MKS are renal dysplasia, encephalocele, and polydactyly [9, 10]. The MKS disease is autosomal recessive and has high occurrence rates in Finland, the Middle East, North Africa, and Asia [9-12].

Recently it was shown that MKS3 is a component of a multi-protein complex that contributes to the function of the transition zone to separate the ciliary compartment from the rest of the cell [13]. Other cellular disruptions caused by a reduction of MKS3 have not been closely examined, such as changes in the sub-surface scaffolding or in cell surface polarity and surface organization.

P. tetraurelia have large numbers of cilia and basal bodies arranged in polarized rows of hexagonal cortical units whose shape is created by a ridge of surface membrane covering an outer lattice. Each cortical unit contains one or two basal bodies. There is one cilium in each of these polarized cortical units (even in units with two basal bodies) as well as one parasomal sac (site of endo- and exo- cytosis) [14-16], and secretory vesicles (trichocysts) at the apex of the

ridges [17-19]. Basal bodies have rootlets emanating from them in a stereotypical orientation relative to the anterior-posterior axis of the cell. The rootlets most likely help secure basal bodies and distribute the forces generated by the beating cilia [20, 21]. In units with one basal body, there is a striated rootlet coursing anteriorly, and a transverse and post ciliary rootlet projecting at 5 and 7 o' clock, respectively. In units with two basal bodies, the posterior basal body has a cilium and all three rootlets while the anterior basal body has no cilium and only a transverse microtubule [21, 22].

The division process in *Paramecium* is complex and begins with basal body duplication. As the cell elongates, it accommodates for new basal bodies and cilia. The organization of the cortical units and their contents are determined by the "old" already existing units [23]. Disrupting this organization or development of these cortical units causes growth arrest and even cell death [19, 24, 25]. It is this highly repetitive patterned surface organization that allows identification of subtle changes in ciliary and surface organization in *P. tetraurelia*.

The results of epitope tagging and RNA interference (RNAi) to perturb the ciliopathy protein MKS3 in *Paramecium tetraurelia* presented here suggest previously unidentified-roles for this protein in maintaining the cell and ciliary membrane surface and cytoskeletal organization. Tagged MKS3 protein is consistently found above the plane of the basal body, in the transition zone of *Paramecium*, which spans from the proximal surface of the epiplasm to the ciliary necklace [26, 27]. Dawe and others [28] have published observations of short and missing cilia upon reduction of *MKS3* mRNA levels, similar to our findings of short and missing cilia with RNAi. Our study shows new findings, most notably that reduction of *MKS3* causes misalignment of longitudinal rows of basal bodies, rotation of the orientation of basal bodies with their microtubule rootlets, and distortion of the cell and ciliary surfaces. We also have evidence of new potential interacting partners of MKS3 relevant to these microtubule rootlets, suggesting

important interactions of MKS3 with these structures. The depletion of Intraflagellar Transport 88 (*IFT88*) mRNA, used as a control to observe global ciliary loss, causes short and missing cilia but does not cause disarray of basal body rows or of the cell surface. We propose that MKS3p in *Paramecium* acts as a transient guide in the movement of basal bodies prior to duplication through an interaction with the microtubule rootlet system and that its localization at the base of the cilium is consistent with an involvement at the transition zone as a filter.

Materials and Methods

Stocks, Cultures and Chemicals

Cells (*Paramecium tetraurelia*; 51-s, sensitive to killer) were grown in wheat grass medium inoculated with *Klebsiella pneumoniae* or *Aerobacter aerogenes* (adapted from [29]). All chemicals were from Sigma-Aldrich (St. Louis, MO, USA) unless otherwise noted.

Sequence Analysis and Construct Design

BLAST searches in the *Paramecium* Annotated Genome were completed using the human sequence for TMEM67 (Q5HYA8) for *MKS3* and the human IFT88 (NP_783195) and Mouse Tg737 (NP_033402) sequences for *IFT88* orthologs. Searches identified GSPATG00015939001 as a potential ortholog for *MKS3* which was used to create the RNAi construct. Five potential orthologs (GSPATG00038505001, GSPATG00021390001, GSPATG00011771001, GSPATG00022644001, and GSPATG00039556001) were identified for *IFT88*. The construct to target *IFT88* mRNA was designed from GSPATG00038505001. Homology of these genes to those in other organisms can be seen in Supplemental Tables 2.1 and 2.2.

All constructs were created from genomic DNA, which was collected using organic extraction. Briefly, 100 µL of cells were mixed 1:1 with Denaturing Buffer (Promega, Madison, WI, USA), mixed 1:1 with phenol:chloroform:isoamyl alcohol (25:24:1), and centrifuged for 5 minutes at 12,000 x g (Eppendorf Centrifuge 5424, Hauppauge, NY, USA). The aqueous phase was removed, and mixed 1:1 with chloroform:isoamyl alcohol (24:1) and spun again. The DNA was precipitated 2:1 with cold isopropanol for 20 min at -20°C and spun for 10 minutes at 4°C (Eppendorf Centrifuge 5424, Hauppauge, NY, USA). Pellets were rinsed twice with 75% ethanol, dried, and resuspended in water.

FLAG-tag of *MKS3*

To localize MKS3p, we added the coding sequence for a three-fold repeated FLAG (DYKDDDDK) sequence to the 5′ end of the genomic DNA sequence for GSPATG00015939001 in the pPXV plasmid using the restriction enzymes Apa I and Sac I (USB/Affymetrix, Cleveland, OH, USA). These cut sites were created using large primers to add them to either end of the sequence: forward (5′- gcggggcccatgctaatttatatcg -3′) and reverse (5′-cgcgagctctcatattagaaacctttgtc -3′). Platinum®*Pfx* Polymerase (Invitrogen/Life Technologies, Grand Island, NY, USA) was used per the vendor's instructions to amplify the sequence. A total of 75 ng of genomic DNA was used in each PCR reaction: 94°C for five minutes; 5 cycles of 94°C for 1 minute, 40°C for 1 minute, 68°C for 3 minutes; 5 cycles of 94°C for 1 minute, 48°C for 1 minute, 68°C for 3 minutes; 10 cycles of 94°C for 1 minute, 58°C for 1 minute, 68°C for 3 minutes; 17 cycles of 94°C for 1 minute, 65°C for 1 minute, 68°C for 3 minutes; once cycle of 68°C for 15 minutes (Techne TC-4000 Thermal Cycler, Krackeler Scientific, Albany, NY, USA). The products were cleaned using the PrepEasy™ Gel Extraction kit (Affymetrix, Cleveland, OH, USA). The resulting DNA was treated with restriction enzymes, cleaned again using the PrepEasy™ Gel Extraction kit and ligated into the pPXV-5′-3xFLAG plasmid using the Ligate-IT™ kit

(Affymetrix). The mixture was then transformed into OneShot® competent cells (Invitrogen/Life technologies, Grand Island, NY, USA) and the resulting colonies were screened for positives. Positive clones were sequenced at the Vermont Cancer Center DNA Analysis Facility (University of Vermont, Burlington, VT).

Plasmid Injection

Approximately 200 µg of pPXV-3xFLAG-*MKS3* was linearized with Not I (Affymetrix) overnight at 37°C and then cleaned using an organic extraction method modified from that described earlier. This procedure required 2 washes in phenol:chloroform:isoamyl alcohol (25:24:1) followed by 2 washes of chloroform:isoamyl alcohol (24:1). The final pellet was resuspended in 50 µL of MilliQ water and the concentration was checked using a spectrophotometer (Agilent Technologies, Santa Clara, CA, USA). The sample was spun at 16,000 x g (Eppendorf Centrifuge 5424) for 10 minutes to pellet debris. The top 45 µL was carefully removed and placed in a fresh RNase/DNase-free 1.5 mL Eppendorf tube and was again dried in a speed vac. The final pellet was resuspended in MilliQ water to obtain a concentration between 3 and 9 µg/µL and stored at 4°C until injection.

Approximately 20 cells which had recently undergone autogamy were placed under high temperature silicon oil to immobilize them. Approximately 5 to 50 pg of the plasmid was injected into the macronucleus of each cell using a pulled capillary and a Narishige micromanipulator (Narishige International USA, Inc., East Meadow, NY, USA). Individual injected cells were transferred to 750 µL of inoculated culture fluid in depression slides and incubated in a humidifying chamber at RT for two days, allowing the cells to recover and divide. Cells were then transferred to test tubes with inoculated culture fluid and maintained at 15°C as individual clones. Genomic DNA was extracted from the clone cultures as described previously (see Sequence analysis and Construct design) and tested with PCR using plasmid-specific

primers: the forward primer for the plasmid pPXV (5′- taagatgaatggaatataatg -3′) and a reverse primer (5′- gaaaacccaagccaatcaatac – 3′), which was sequence-specific for *MKS3*. One µL (approximately 400 ng) of DNA was used in each PCR reaction: one cycle of 95°C for 5 minutes followed by 30 cycles of 95°C for 1 minute, 40°C for 1 minute, and 72°C for 3 minutes, followed by one last 15 minute cycle at 72°C.

Localization, Visualization, and Analysis of FLAG-MKS3p

We tested small cultures of individual clones to ascertain whether the cells expressed the protein and where it was localized. A 10 mL culture of injected cells was added to 50 mL of inoculated culture fluid and grown at 22°C for approximately 48 to 72 h. The cells were immunostained and imaged as described below. Images were analyzed for colocalization using SoftWoRx™ Pro software (Applied Precision, Issaquah, WA, USA). Experiments were repeated 5 times.

To isolate pellicle membrane and whole cilia membrane, wild type (51-S) cells expressing FLAG (control) or FLAG-*MKS3* (Test) were maintained in large culture (3 to 6 L of culture fluid) at 22°C until at a density of 8,000 to 12,000 cells per mL. For pellicle membrane, cells were harvested as described in [30]. In separate experiments, cilia were separated from cell bodies and collected as described in [31] up to the point of separation of the ciliary membrane from the axoneme. Protein concentrations were determined using a BCA Protein Assay (Thermo Scientific, Rockford, IL, USA) and equalized between the test and control. Samples were separated on a 12% SDS-PAGE gel after adding 1 µL B-Mercaptoethanol and boiling for 5 minutes. One hundred µg of pure pellicle membrane and 400 µg of whole cilia were loaded along with 10 µL Pierce 3-color prestained protein molecular weight marker (Thermo Scientific). Proteins were transferred onto nitrocellulose membrane (Pall Gelman Corp., Krackeler Scientific, Albany, NY, USA) and blocked for one hour using 5% non-fat dry milk, 2% Telost gelatin from

fish, 3% Normal Goat serum (Vector Labs, Burlingame, CA, USA), in TBS-T (15 mM Tris-Cl, 140 mM NaCl, 0.1% v/v Tween-20, pH 7.5). Blots were probed with a 1:2500 dilution of rabbit Anti-FLAG M2 clone or 1:10,000 mouse Anti-Tubulin in the blocking buffer. Blots were incubated overnight while rocking at 4°C. Buffers were removed, the blots rinsed three times in TBS-T and then incubated for 1 h in 1:10,000 goat Anti-rabbit or Anti-mouse AP-conjugate secondary antibody. Blots were rinsed again four times in TBS-T, 15 minutes each wash, and developed using NBT/BCIP Alkaline Phosphatase (Moss, Inc., Pasadena, MD, USA).

RNAi by feeding construct

Constructs for RNAi were created from genomic DNA using the following primers: *MKS3* forward, 5'- gaaaacccaagccaatcaatac -3' and reverse, 5'- ggtcgacaatctgaaggataag -3'; *IFT88* forward, 5'- caattaaggaaaaccacctg-3' and reverse, 5'- aaaactaacaggattgtcatct-3'. All PCR conditions began with an initial step at 95°C for 5 minutes and ended with a final stage of 72°C for 20 minutes. The *MKS3* RNAi construct was amplified by 30 cycles of 95°C for 1 minute, 52°C for 1 minute, and 72°C for 2 minutes. The *IFT88* construct was amplified by 5 cycles of 95°C for 1 minute, 47°C for 1 minute, and 72°C for 2.25 minutes; followed by 25 cycles of 95°C for 1 minute, 50°C for 1 minute, and 72°C for 2.25 minutes (Techne Thermal Cycler). The final PCR products were analyzed on a 0.75 or 1.0 % agarose gel (Invitrogen/Life Technologies, Grand Island, NY, USA) and visualized with ethidium bromide. Resulting PCR products were cloned directly into pCR®2.1-TOPO® vector (Invitrogen/Life Technologies), transformed into OneShot® cells (Invitrogen/Life Technologies), and sequenced. Correct sequences were cut from the pCR®2.1-TOPO® vector and ligated into the double-T7 promoter vector L4440 (AddGene, Cambridge, MA, USA) using the Ligate-IT™ Kit (USB/Affymetrix, Cleveland, OH, USA), as per the kit instructions. *Escherichia coli* strain Ht115 (DE3), which lacks RNase-III, were transformed with 50 ng of plasmid DNA for either *MKS3* or *IFT88*. As a control, Ht115 cells were transformed with

L4440 with no insert. Bacterial cultures were maintained with tetracycline (12.5 µg/mL) and ampicillin (AMP) (100 µg/mL).

RNAi by Feeding

Overnight cultures of Ht115(DE3) transformed with RNAi or control plasmids were used to inoculate 50 mL of LB-AMP (100 µg/mL) and grown until the $O.D._{595}$ reached 0.3 to 0.4, at which point, IPTG (Isopropyl β-D-1-thiogalactopyranoside) (RPI, Corp., Mount Prospect, IL, USA) was added to a final concentration of 0.125 mg/mL. Cultures were incubated with shaking for 3 h at 37°C to induce the production of double-strand RNA. Paramecia that had recently undergone autogamy were collected by centrifugation and resuspended in 10 mL of Dryl's solution (1 mM Na_2HPO_4, 1 mM NaH_2PO_4, 1.5 mM $CaCl_2$, 2 mM Na-citrate, pH 6.8) to purge bacteria from their surface and food vacuoles.

The induced bacteria were collected by centrifugation at 4,000 x g (Beckman J2-21 centrifuge, JA-14 rotor, Beckman Coulter, Brea, CA, USA) at 4°C and resuspended in 100 mL of wheat culture medium containing an additional 8 µg/mL stigmasterol, 0.125 mg/mL IPTG (RPI, Corp.), and 100 µg/mL AMP. Approximately 50 to 100 of the purged paramecia were added to the control culture. In the case of the *MKS3* and *IFT88* RNAi cultures, 4000 and 8000 cells were added to 100 mL, respectively. Cultures were maintained at 28°C, and after 24 h, an additional 0.125 mg/mL of IPTG (RPI, Corp.) and 800 µg of stigmasterol were added. Growth rates of cultures were determined by counting cells at 24, 48, and 72 h of growth. All experiments were repeated a minimum of three time and all cultures were harvested or observed after approximately 72 h of growth, unless noted.

Immunofluorescence

100 mL of cultured cells were collected by centrifugation (IEC clinical centrifuge, Damon/IEC Division, Needham Heights, MA, USA) and rinsed twice in 100 mL of Dryl's solution. The cell volume was reduced to approximately 100 µL in a 1.5 mL Eppendorf tube before 1 mL of PHEM buffer [60 mM PIPES (1,4-Piperazinediethanesulfonic acid), 25 mM HEPES (2-[4-(2-hydroxyethyl)piperazin-1-yl] ethanesulfonic acid), 2 mM $MgCl_2$, 10 mM EGTA (ethylene glycol tetraacetic acid), and 0.1% or 0.5% Triton X-100) was added. Cells sat undisturbed for 1 to 4 minutes, spun at 250 x g (IEC Clinical centrifuge), the supernatant was removed and the pellet (cells) was mixed with 1 mL of Fixation buffer [2% or 4% paraformaldehyde (Electron Microscopy Sciences, Hatfield, PA, USA), 2 mM $NaH_2PO_4 \cdot H_2O$, 8 mM Na_2HPO_4, 150 mM NaCl, pH 7.5]. Samples were undisturbed for 10 minutes or rocked for 1 h at RT and washed three times in 1 mL of Blocking Buffer (2 mM $NaH_2PO_4 \cdot H_2O$, 8 mM Na_2HPO_4, 150 mM NaCl, 10 mM EGTA, 2 mM $MgCl_2$, 0.1% Tween-20, 1% or 3% BSA, pH 7.5).

Primary antibodies for the immunostaining for localization were: FLAG-MKS3: mouse Anti-FLAG, M2 clone at a 1:300 dilution (Sigma), Anti-centrin at a 1:1000 dilution (Anti-*Tetrahymena* centrin, gift from Dr. Mark Winey, University of Colorado, Boulder, CO). For ciliary measurements we used mouse Anti-alpha-tubulin at a dilution of 1:200 (Sigma). For visualization of basal bodies we used Anti-centrin at a dilution of 1:1000. For cortical unit visualization we used Anti-2F12 at a dilution of 1:200 (Gift, Dr. Jean Cohen, Gif-sur-Yvette, France). For the visualization of the kinetodesmal fibers, we used Anti-KDF at a 1:400 dilution (gift from Dr. Janine Beisson, Centre de Génétique Moléculaire, Gif-sur-Yvette, France) and Anti-Glu-α-Tubulin at a 1:500 dilution (Synaptic Systems, Goettingen, Germany). Primary antibodies in 100 µL of blocking buffer were mixed with the cells and rocked at RT for 1 h. Cells were washed three times in blocking buffer or Wash buffer (2 mM $NaH_2PO_4 \cdot H_2O$, 8 mM Na_2HPO_4, 150

mM NaCl, 0.1% Tween-20, 1% BSA, pH 7.5). The cells were mixed with 100 µL of blocking buffer with a 1:200 dilution of secondary antibodies. Secondary antibodies (Molecular Probes/Invitrogen, Grand Island, NY, USA) included: AlexaFluor® goat anti-mouse 488 or 555 and AlexaFluor® goat anti-rabbit 488 or 568. After 30 minutes to 1 h of incubation while rocking, cells were washed three to five times with blocking or wash buffer and, to the final 20 µL of cells, one drop (~15 µL) of VectaShield® (Vector Labs, Burlingame, CA, USA) was added. Tubes were wrapped in aluminum foil and stored at 4°C until use.

Imaging of the immunostained cells was done using a DeltaVision® Restoration Microscopy System (Applied Precision, Issaquah, WA, USA) consisting of an inverted Olympus IX70 microscope and a Kodak CH350E camera. Seven µL of prepared cells were placed under a glass coverslip and imaged at 20-22°C using either a PlanApo 60x or 100x /1.40 oil-immersion objective and deconvolved and analyzed using SoftWoRx® Pro software (Applied Precision).

Co-localization of FLAG-MKS3 and Centrin (basal bodies) was analyzed using SoftWoRx® Pro software or ImageJ [32]. Eleven cells were analyzed for the co-localization of these two proteins. To examine the staining patterns and calculate the number of basal bodies with FLAG-MKS3 staining, 15 µm x 15 µm grids were chosen from both the ventral and the dorsal surface of each of three cells. Basal bodies within that grid were counted and noted whether they had FLAG-MKS3 staining. A total of 463 basal bodies were analyzed on these three cells.

Scanning Electron Microscopy (SEM)

200 mL of RNAi cultured cells were collected by brief centrifugation at 800 x g (IEC Clinical centrifuge, Damen Division, Needham Heights, MA, USA), washed twice in Dryl's solution, and fixed as described in Lieberman et al. [33]. After critical point drying, cover slips

were glued onto an aluminum chuck using colloidal graphite cement and allowed to dry in a desiccator overnight. The samples were sputter coated and stored in a desiccator until imaged using a JEOL 6060 Scanning Electron Microscope (JEOL USA, Peabody, MA, USA).

Transmission EM

100 mL of RNAi cultured cells were collected by brief centrifugation at 800 x g (IEC Clinical Centrifuge), washed twice in 100 mL Dryl's, and approximately 100 µL of the cell pellet was removed and placed in 1.5 mL Eppendorf tubes. One mL of Fixation Solution A (1% gluteraldehyde (Electron Microscopy Sciences, Hatfield, PA, USA), 0.05M sodium cacodylate, pH 7.2) was added, rocked for 30 minutes on ice, and washed three times for 10 minutes under the same conditions. Cells were resuspended in post-fix Solution B (1% gluteraldehyde (Electron Microscopy Sciences), 0.05M sodium cacodylate buffer, 1% osmium tetroxide, pH 7.2) and again washed and rinsed as described. Cells were pre-embedded in 2% agarose (Invitrogen/Life Technologies) in 0.05M sodium cacodylate buffer, allowed to set, then sliced into 1 mm x 1 mm blocks. Blocks were placed in glass vials with 50% ethanol and rocked on a specimen rotator for 30 minutes during each of the following washes: 50% ethanol, 70%, 90%, two times with 100%, the two washes in propylene oxide. Cells were left overnight on specimen rotator in 1:1 propylene oxide and Spurr's solution (Electron Microscopy Sciences). The next day, samples were placed in fresh Spurr's (Electron Microscopy Sciences) for 6 h, and placed in flat embedding molds with fresh Spurr's (Electron Microscopy Sciences) at 60°C for 48 h. Sections were cut to 90 nm thick, placed on copper 200 mesh grids, contrasted on droplets of 2% Uranyl acetate in 50% ethanol for 6 minutes followed by lead citrate (120 mM sodium citrate, 2.66% lead nitrate and 0.65 % sodium hydroxide in water) for 4 minutes. Sections were imaged using a JEOL JEM-1210 Electron microscope. These studies were repeated 3 times.

GST Pull Down and Mass Spectrometry Analysis

The coiled-coil domain of MKS3 was expressed with a GST tag for use in a GST pull down. The construct was created by amplifying position +2183 to +2273 of GSPATG00015939001 using the following forward and reverse primers, respectively: 5'-gcgggatccatgaattttgtcgatctc-3' and 5'-gcggaattctgatggattttctccatg-3'. The PCR product was treated with BamHI and EcoRI (New England Biolabs, Ipswich, MA, USA), cleaned using gel purification and the PrepEasy™ Gel Extraction Kit (Affymetrix, Santa Clara, CA, USA), then ligated into pGEX-2TK (GE Healthcare Life Sciences) using the Ligate-IT™ kit (Affymetrix). The pGEX-2TK plasmid had already been opened using the same restriction enzymes, treated with 1U of calf-intestinal alkaline phosphatase at 37°C for 5 minutes to remove the phosphate groups followed by heat-inactivation with 5 mM Na_2EDTA at 72°C for 20 minutes. The GST-MKS3 coiled-coil domain and GST were expressed in BL-21 cells and bound to glutathione sepharose beads (GE Healthcare Life Sciences, Pittsburg, PA, USA) as described in [34]. After beads were collected from bacterial cell lysates, they were washed in a 1 M $MgCl_2$ buffer to remove bacterial proteins from the GST and GST-MKS3 proteins. Protein-bound beads were stored at 4°C in PBS buffer for up to 2 weeks.

51-s *Paramecium tetraurelia* were cultured and harvested as described in [35] for whole cell extract (WCE). Glutathione sepharose beads (GE Healthcare Life Sciences) were prepared by washing three times in LAP200 (50 mM HEPES, 200 mM KCl, 1 mM EGTA, 1 mM $MgCl_2$, pH=7.4) buffer with 1% Triton X-100. 200 µL of washed beads were added to 20 ml WCE. This pre-cleared WCE was then split in half and incubated with 200 µL of glutathione sepharose beads attached to either GST or GST-MKS3. Beads in the supernatant were allowed to rock on ice at 4°C for 1 h. Control and test beads were recovered and washed 3x in LAP200 buffer with 1% Triton X-100. Samples were run on a 7-14% gradient acrylamide gel, silver stained and gel slices were trypsin digested as described in [35].

Samples were analyzed by LC-MS/MS on a linear ion trap (LTQ) Mass Spectrometer (Thermo Fisher). Half the material was loaded onto a 100 um x 120 mm capillary column packed with MAGIC C18 (5 um particle size, 20 nm pore size, Michrom Bioresources, CA) at a flow rate of 500 nL/min. Peptides were separated by a gradient of 5-35% CH_3CN/ 0.1% formic acid over 30 minutes, 40-100% CH_3CN /0.1% formic acid in 1 minute, and 100% CH_3CN for 10 minutes.

Product ion spectra were searched using the SEQUEST search engine on Proteome Discoverer 1.4 (Thermo Fisher Scientific, MA) against a curated *Paramecium tetraurelia* database with sequences in forward and reverse orientations. The 13 raw files from "control" and the 13 raw files from "test" samples were searched as one contiguous input file and a single result file was generated for each. The database was indexed to allow for full trypsin enzymatic activity, two missed cleavages, and peptides between the MW of 350-5000. Search parameters set the mass tolerance at 2 Da for precursor ions and 0.8 Da for fragment ions. The result files were then searched against the Scaffold software 4.0.5 (Proteome Software, OR). Cross-correlation (Xcorr) significance filters were applied to limit the false positive rates to less than 1% in both data sets. The Xcorr values were as follows: (+1): 1.8, (+2): 2.7, (+3): 3.3, (+4): 3.5. Other filters applied were a minimum peptide cutoff of 2 as well as DeltaCN >0.1. Ultimately, the confidence parameters resulted in 0% false discovery rate (FDR) at the protein and peptide level for both the control and test results.

Results

Sequence Analysis

The sequence for *MKS3* in *Paramecium* (GSPATG00015939001, $4e^{-57}$, 23% identical) was found using the human sequence for TMEM67 (Q5HYA8) and the annotated *Paramecium* genome

(ParameciumDB, http://paramecium.cgm.cnrs-gif.fr/). *Paramecium MKS3* (TMEM67) codes for 2906 nucleic acids and 951 amino acids. The RNAi construct design for *Paramecium MKS3* comprises bases from position +1101 to +2019.

Five potential homologues for *IFT88* were found using the human IFT88 (NP_783195) and mouse Tg737 (NP_033402) sequences. The best match was GSPATP00038505001 (e^{-146}, 38% identical), which codes for 2341 nucleic acids, and 743 amino acids. The RNAi construct for *Paramecium IFT88* spans position +48 to +2121. Using a feature of ParameciumDB to identify potential off-target effects [36], we found that the *MKS3* RNAi plasmid will target only GSPATG00015939001, while the RNAi plasmid for *IFT88* will target all five homologues, but no other gene sequences outside this gene family. Included in the supplemental material are tables comparing *Paramecium* IFT88 and MKS3 (Supplemental Tables 2.1 and 2.2) with sequences from other organisms. To further document the conservation of these proteins in *Paramecium*, amino acid alignments of full length and conserved regions in each protein have also been included in Supplemental Figures 2.1 and 2.2.

FLAG-MKS3p Immunostaining and Localization

We used a 5'-3xFLAG-tag (FLAG-*MKS3*) expression vector to produce FLAG-MKS3p in order to localize the MKS3 protein. Control paramecia were derived from cells that were injected with the empty FLAG vector in order to confirm that cells were unaffected by the expressed FLAG peptide. Cells were permeabilized, stained with Anti-centrin and Anti-FLAG, and imaged. In Figure 2.1, images are stacks to ensure that basal bodies and FLAG-MKS3p staining are visible. Cells expressing FLAG or FLAG-*MKS3* showed similar centrin staining patterns across the cell surface (Figure 2.1A). The control cells show almost no staining by Anti-FLAG but the FLAG-*MKS3* expressing cells show very clear FLAG staining near the basal bodies and faint staining in the cilia (Figure 2.1A and arrows in 2.1C). Supplemental Movie 2.1 demonstrates this

pattern of FLAG-MKS3p staining above the staining of centrin; when scanning through the same cell, starting from the surface, the green FLAG staining can be seen prior to the red staining of the centrin. Figure 1B also demonstrates the FLAG-MKS3p staining at the distal side of the centrin staining, i.e. above the staining of the basal body. The Anti-centrin antibody recognizes *Tetrahymena* Centrin 1, which is homologous to *Paramecium* Centrin 2, which is found in the basal body along the shaft [25]. The transition zone of the *Paramecium* cilium has been defined as stretching from the basal body, near the proximal surface of the epiplasm, to the base of the cilium where the triplets of microtubules become doublets and the central pair of microtubule doublets begins [26, 27]. The localization of the MKS3 protein is therefore consistent with that of the transition zone for these cells.

To quantify the basal body and FLAG-MKS3 staining, 15 μm x 15 μm squares on the dorsal and ventral surface of 3 different cells expressing FLAG-*MKS3* were randomly chosen. Of the 463 basal bodies observed, 95.2 ± 2.2 % of them had FLAG-*MKS3* staining. These data suggest that where a basal body is present, we would expect to find MKS3 protein. To quantify the extent of co-localization of the centrin and FLAG-MKS3p staining, the images were analyzed using the softWoRx® software to obtain a Pearson's coefficient (*r*). Eleven FLAG-MKS3p cells showed an average co-localization score of 0.46 ± 0.11 (*r* ± SD), indicating partial co-localization. FLAG-MKS3p staining is clearly seen in the oral groove (Figure 2.1A, yellow arrows), but we were unable to differentiate individual basal bodies in this region due to their close packing and the spatial limitations of fluorescence microscopy. Therefore these oral groove basal bodies were not included in our analysis.

Ultrastructure

We utilize RNAi by feeding of paramecia because of its ease of use and the creation of knock-outs by homologous recombination is not possible. RNAi allows us to observe the cells in

a depleted state of a targeted protein quickly and effectively in a wild type background. RNAi that is estimated to be 80% effective [37]. RNAi allows us to leave variable amounts of the targeted protein in the cells and thereby protect them from lethal effects of complete loss of MKS3p. We found that very aggressive RNAi treatment quickly leads to cell death. In this way, RNAi has an advantage for us over gene knock out.

Scanning electron micrographs (SEM) show that the control cells were covered in cilia and displayed a highly organized cell surface with one cilium protruding from each cortical unit (Figure 2.2A, B). The cilia on the control cells appeared normal as shown in the representative cell in Figure 2.2A. The *MKS3* depleted cells displayed very short and sparse cilia (Figure 2.2C-2.2F) and look dramatically different from the controls. The cilia that were present did not resemble the control cilia; they had wrinkled surfaces and bulges at the tips (Figure 2.2E and 2.2F). Of the 23 *MKS3* depleted cells observed, 56.5% displayed the "blebby" cilia. This was not observed on any of the control cells. (The control cell in Figure 2.2A was fixed with the metachronal wave intact, but the *MKS3* depleted cell in Figure 2.2B was not, which is far more common. This difference between the two cells is not a consequence of the reduction of *MKS3* mRNA.) The disturbance to the cell and cilia surface by reduction of *MKS3* mRNA is more evident at higher magnification (Figure 2.2D and 2.2F). We used RNAi to reduce mRNA for *IFT88* that is known to cause loss of cilia by failure of intraflagellar transport (IFT), a mechanism that is specific to ciliary development and maintenance. The *IFT88* depleted cells displayed a normal patterned cell surface (Figure 2.2G and 2.2H), with very few and short cilia present on the surface of the majority of the cells (Figure 2.2G; yellow arrows).

MKS3 RNAi resulted in cells that appear, by SEM examination (Figure 2.2), to have missing or shortened cilia everywhere on the cell except in the oral groove. The reduction of

MKS3 using RNAi also causes severe distortions in the cell surface in contrast to the surfaces of cells depleted of *IFT88* that show missing cilia, but no other disruptions.

Transmission EM (TEM) was employed to examine the ultrastructure of basal bodies to determine whether they were structurally equivalent in control and *MKS3* depleted cells. This demonstrates that the loss of cilia that we observed were not due to their inability to properly form basal bodies. Cross-sections of basal bodies observed using TEM were measured for both height and width using ImageJ software [32]. No differences were observed between control basal bodies that were 379.6 ± 42.4 nm in length and 202.9 ± 22.8 nm wide (± SD, *N*=13) and *MKS3* depleted basal bodies that were 367.7 ± 35.5 nm long and 191.8 ± 21.9 nm wide (± SD, *N*=14). In addition, no obvious differences in basal body docking were observed.

Immunofluorescence: Basal Bodies and Cortical Units

Immunostaining of the *MKS3* depleted cells with Anti-centrin revealed a basal body pattern that differed from that of the control and *IFT88* depleted cells. The images in Figure 3 are stacks of Z-sections, approximately 10 μm thick, to ensure all basal bodies could be visualized. The representative views shown are of the anterior dorsal surface of the cells. The control cell shows rows of basal bodies that run from anterior to posterior (Figure 2.3). The basal body rows at the midline of the typical *MKS3* depleted cell show disorganization and twisting (Figure 2.3, white arrows). Distortions of rows can be seen elsewhere on the dorsal side of the cells but are most commonly observed at the dorsal midline. The control and *IFT88* depleted cells maintain straight organized rows.

The ridges of the cortical units were highlighted using Anti-2F12 and observed at 60x magnification (Figure 2.4). Light staining of a basal body can be seen at the center of each unit. The dorsal surface of a control cell (Figure 2.4A) demonstrates the high level of organization of

the cortical units. An area of the control cell has been enlarged (yellow box) to better highlight this (Figure 2.4a). The lower images in Figure 2.4a-2.4c have been traced for clarity and are to the right of each image. The contractile vacuole pores are pointed out using gray arrows. The two *MKS3* depleted cells (Figure 2.4B and 2.4C) show two major types of differences from the control: an insertion of cortical units that incorporates a short row into another row of units (a kinety) (Figure 2.4B; yellow arrows) and clustering of basal bodies that should be organized in a row (Figure 2.4C; yellow arrows). The *MKS3* depleted cell with the insertion of an abbreviated kinety has a basal body for almost every cortical unit (Figure 2.4b) while the complete surface disruption, the clustering, shows a chaotic organization of the cortical units, some of which are missing a basal body (Figure 2.4c). Of the *MKS3* depleted cells observed, 70% show kinety disruptions. Of those, 90% showed clusters of basal bodies as shown in Figure 2.4C and 10% showed an insertion of a partial kinety row, as shown in Figure 2.4B. These changes in ridge patterns were always observed on the dorsal surface of the cell often near the midline and never at the extreme poles of the cell in over 30 control and 70 *MKS3* depleted cells observed.

Each cortical unit has one or two basal bodies with its corresponding microtubule rootlets. The transverse microtubule (TM) and the post ciliary microtubule (PCM) are oriented at 5 o'clock and 7 o'clock, with the anterior end of the cell pointing to 12 o'clock. We examined the orientation of TMs and PCMs using an Anti-α-tubulin antibody and the basal bodies using the *Tetrahymena* Anti-centrin antibody. The *MKS3* depleted cells lost most of their cilia, which facilitated the imaging of the basal bodies and cortical microtubule cytoskeleton. However, the cilia on control cells obscured the image of the cortical microtubules that were visualized with the Anti-α-tubulin antibody. Therefore, we used *IFT88* depleted cells as a control because they lose their cilia but do not lose alignment of basal bodies in orderly rows of cortical units (Figure 2.3). Figure 2.5 shows representatives of both *IFT88* (2.5A) and *MKS3* (2.5B) depleted cells. Basal bodies of the control *IFT88* depleted cell showed organized rows and microtubule rootlets that

maintain their polarity and orientation. In contrast, the representative *MKS3* depleted cell showed twisting of a basal body row and with it, a new alignment of the TM and PCM rootlets. The organized pattern of the *IFT88* depleted cell has been enlarged (Figure 2.5A; yellow box) and traced to show the basal bodies (red) and their microtubule rootlets (black). The same has been done for the *MKS3* depleted cell (Figure 2.5B; yellow box) where the orientation of the microtubule rootlets, as well as the basal bodies, can clearly be seen. The angle between the TM and PCM ribbons that emanate from the basal body was maintained in the *MKS3* depleted cells (Figure 2.5C), but the orientation of the rootlets relative to the anterior-posterior axis was changed. Both of the images of representative cells shown in Figure 2.5 are of the dorsal surfaces and the enlarged areas are from near the dorsal midline. Note that the microtubule rootlet misalignments coincide with basal body misalignments, but not *vice versa*. The third rootlet, the striated rootlet (SR), also called kinetodesmal fiber, was visualized using Anti-Kinetodesmal fiber (KDF) [38] and the basal bodies with Anti-Glu-α-Tubulin. Figure 2.6A shows a control RNAi fed cell with basal bodies (red) forming clear organized rows, or kineties, along the cell. Emanating from the left side of each basal body is a striated rootlet (green). These fibers extend toward the anterior pole of the cell and will span two or more cortical units [22]. The control cell clearly demonstrates the anterior orientation of the SRs. In the case of two basal body units, this fiber only projects from the posterior of that basal body pair (Figure 2.6A; yellow arrows; the large red structures in Figure 2.6A and 2.6B are the contractile vacuoles and are not the subject of this study). In the *MKS3* depleted cell, within the areas of basal body misalignment, the SRs do not always project toward the anterior and often veer in oblique directions (Figure 2.6B, b, and b'). The basal bodies are no longer maintained in their kinety rows, and much like the twisted orientation of the PCMs and TMs from Figure 2.5, the SRs are chaotic in their orientations. These data, in conjunction with the TM and PCM data (Figure 2.5), suggest that these rootlets develop

from the basal body normally, but the basal body has lost its orientation and does not maintain its position along the anterior-posterior axis of the cell (See also Supplemental Figure 2.3).

Mass Spectrometry and potential interacting partners

Whole cell extract was collected from wild type cells, solubilized, and probed using either expressed GST or expressed GST fused with the coiled-coil domain of MKS3. Samples were separated on SDS-PAGE gels, silver stained, and the entire test (GST-MKS3 coiled-coil) and control (GST) lanes were analyzed by tandem mass spectrometry. We only considered those proteins unique to the test lane. In total, five proteins unique to the test sample were identified (Table 2.I). These proteins had a minimum of two unique peptides and included two *Paramecium* centrin binding proteins (PtCenBP1), a SERCA pump (PtSERCA1), a Ran-GTPase activating protein, and a kinetodesmal fiber protein (KdB2).

Discussion

Reduced *MKS3* leads to abnormal and missing cilia

We expressed FLAG tagged MKS3 protein to localize it within the *Paramecium* cell and used feeding RNAi to explore for new functions of this protein. *IFT88* served as a control for our approach because reduction of *IFT88* mRNA would inhibit ciliary transport and help us to determine whether short and missing cilia were sufficient to explain the RNAi phenotype for MKS3. Both *IFT88* and *MKS3* depleted cells showed shortening and loss of cilia over the entire cell except in the oral groove. These results for *MKS3* depletion are in agreement with those of Dawe et al. [28], who reported that siRNA duplexes against *MKS3* caused short or missing cilia in inner medullary collecting duct cells (IMCD3). In the same study, siRNA duplexes were used against *IFT88* in IMCD3 cells, leaving >90% of the cells without a primary cilium. The authors

concluded that loss of MKS3 disrupts polarity of centrioles and their migration to the cell surface for cilium formation [28]. Other studies have found a variety of changes in ciliary number and length, possibly because of differences among cell types and methods of interfering with MKS3 expression through reduction in amount or mutation [28, 39-42].

We found that aspects other than short and missing cilia differed between the *Paramecium MKS3* RNAi phenotypes and *IFT88* RNAi phenotypes. For example, the cilia that remain on the *IFT88* depleted cells appeared short but not misshapen, while those on *MKS3* depleted cells were short with bulging membranes, giving a "blebby" appearance, especially at the tips.

In other systems, MKS3 (TMEM67) functions as part of the filter or as a gate keeper in the transition zone, the region between the basal body and the ciliary necklace [13, 43-45]. Failure of transition zone function to control ciliary structure and membrane composition can lead to short and bulbous cilia [46] similar to our observed "blebby" cilia on cells depleted of *MKS3* by RNAi. Our immunofluorescence data of paramecia expressing FLAG-*MKS3* suggest that FLAG-MKS3p is in the transition zone, which in *Paramecium* has been defined as an area which spans from the epiplasm to the base of the cilium below the ciliary necklace [26, 27] (Figure 2.1 and Supplemental Movie 2.1). The antibody we used to label basal bodies recognizes *Tetrahymena* Centrin 1, which is most homologous to *Paramecium* Centrin 2, and stains the full length of the *Paramecium* basal body below the cell surface [25]. The transverse section through the surface of the cell shows Anti-FLAG labeling for FLAG-MKS3p near the cell surface and at or above the distal end of the basal body. This location of MKS3p in *P. tetraurelia* is also consistent with the observations by Dawe et al. [28] who were the first to show the localization of MKS3p at the base of the primary cilium at the transition zone in IMCD3 and HEK293 cells transfected with N-terminal tagged proteins. Other groups have made similar findings [13, 47].

We propose that the depletion of MKS3p from the transition zone accounts for the loss of cilia and blebbing of the membrane of the short remaining cilia by causing a failure of the transition zone to regulate ciliary structure and membrane composition. We have also data that suggest the presence of MKS3p in the distal portion of the cilium (Western blot, Supplemental Figure 2.4). The cilia for the Western blot preparations are severed from the cell body above the ciliary necklace, which means that if MKS3p is in the cilia the proteins on blot come from above the transition zone [48].

New phenotypes of *MKS3* mRNA depletion suggest interaction with basal body striated rootlet (SR)

The repetitive stereotypical rows of cortical units of *P. tetraurelia* allowed us to identify subtle deviations due to reduction of MKS3p. RNAi for *MKS3* led to basal bodies out of kinety rows on the dorsal surface, mostly at the midline. The disorganized basal bodies were in patches, mostly in clusters or less often in small extra rows, and with misshapen morphology of cortical ridges. These phenotypes were not seen in the *IFT88* depleted cells indicating that the shortening and loss of cilia are not sufficient to explain these changes in *MKS3* depleted paramecia.

Cortical units across the surface of *Paramecium* contain either one or two basal bodies (mono- or di- kinetids respectively). In preparation for cell division, basal bodies duplicate and the cell must enlarge and elongate. This first stage of division involves the conversion of all dikinetids to monokinetids [21], with the exception of those in the invariant zones at the extreme anterior and posterior ends of the cells [21, 22]. This conversion of di- to mono- kinetids is the earliest stage in preparation for cell division and once complete, the cell will begin basal body duplication and formation of the fission furrow at the midline of the cell [21]. For both the conversion of di- to mono- kinetids and basal body duplication, where a new basal body is produced anterior to the parental basal body, the anterior basal bodies or the new basal bodies

move away from the parental basal bodies using the striated rootlet (SR) as a guide, thus maintaining orderly rows [21, 22]. While basal bodies in all areas outside the "invariant" zones must duplicate for cell division, we do not see a distortion of the kinety rows of basal bodies except on the dorsal side and primarily at the midline. Therefore, we propose that the *MKS3* RNAi phenotype of disorientation of basal bodies and rootlet orientations that we observe is primarily from failure of the anterior basal body of two basal body units to appropriately migrate along the SR and thereby maintain a straight kinety row. The conversion from di- to mono-kinetids is prior to basal body duplication happens first on the dorsal surface of the cell, where a large number of randomly distributed dikinetids exist [20], and at the midline because the anterior movement is in advance of basal body duplication, which begins at the midline.

The posterior basal body in the dikinetid has a cilium and full complement of rootlets (TM, PCM and SR) projecting in stereotypical orientations. The anterior basal body of the pair has no cilium and only the transverse microtubules associated with it. In addition to the rootlets, a set of three cytoskeletal "nodes" link the basal bodies of a dikinetid to each other and to the striated rootlet [20, 21]. While moving, the anterior basal body remains linked to the SR, which extends for two or more cortical units toward the anterior and appears to act as a guide that keeps the migrating basal bodies aligned with the cortical row. Once the anterior basal body has separated from the posterior basal body it develops a PCM and a SR in addition to its preexisting TM [21]. A schematic of this process is shown in Figure 2.7.

We propose that misguidance in the early movement of the anterior basal body of dikinetids can account for the observed RNAi phenotype of misalignments primarily near the dorsal midline. We also propose that all newly forming basal bodies which also use the SR as a guide could require MKS3p for their attachments to the SR. We expect that only the errors in anterior basal body movements in the di-kinetics are noticed in *MKS3* RNAi depleted cells

because they occur early, before basal body duplication, and because cells stop growing and do not proceed further with basal body duplication and cell division. Indeed, these RNAi treated cells stop growing after 24 h of RNAi feeding (data not shown).

This hypothesis of interaction of MKS3p with the SR is strongly supported by the results of a GST pull down assay. Using the MKS3p coiled coil domain as bait, we have identified a kinetodesmal fiber protein (KdB2: GSPATG00008129001).

MKS3p bait also pulls down two *Paramecium* Centrin binding protein 1s (PtCenBP1: GSPATG00034434001 and GSPATG00034433001) which has been shown to be the main component of the infraciliary lattice (ICL). The ICL is a contractile cortical cytoskeletal network that is nucleated from the basal body region [49, 50]. An interaction of MKS3p and PtCenBP1 could help to stabilize the basal body within the cortical unit allowing a cilium to be properly established.

GST pull down results included a Ran GTPase activating protein 1 (RanGAP: GSPATG00009639001). An interaction of RanGAP1 with MKS3p is interesting if the ciliary pore functions in a fashion similar to the nuclear pore complex, which has been suggested [51, 52]. A RanGTP/GDP gradient between the cilia and cell compartments has been suggested to be involved in for the entrance of select proteins into the cilia, such as Kif17, in mammalian cells [53]. The interaction of MKS3 with RanGAP may prove to be a reflection of MKS3p function in the transition zone and part of the explanation for loss and deformation of cilia in *MKS3* depletion.

It might be suggested that the misalignment phenotypes in *MKS3* depleted cells results from inappropriate development of the rootlets around the basal body. We do not favor this explanation because in areas of disruption, the PCM and TM rootlets form with a normal angle

between them and kinetodesmal fibers develop. These results suggest that the entire basal body unit with rootlets appears to be mis-directed and not aligned with the anterior-posterior axis of a kinety as opposed to a dysfunction in rootlet development.

We did not identify a second location for MKS3 in our immunofluorescence studies of tagged MKS3p outside the transition zone. Although physical interactions of basal bodies and the SR were identified in structural studies [21], the transient nature of the attachments have made it difficult to identify the interacting components. Our findings open a new opportunity to dissect these transient but critical interactions.

Conclusion

There appear to be dual roles for MKS3 in *Paramecium*. We have shown that MKS3p in *P. tetraurelia* is located at the cell surface near each basal body's transition zone where it most likely helps to filter and import (or retain) proteins into the cilia. When MKS3p is reduced from this location, cilia are lost and the cell surface and ciliary membranes become distorted. Secondly, a pool of MKS3 may be required in di-kinetid units to guide the anterior basal body of the separating pair along the striated rootlet. A reduction in this pool of MKS3 may lead to the basal body becoming twisted and misaligned from its polarized row.

Abbreviations

AMP	Ampicillin
DIC	Differential Interference Contrast
ER	Endoplasmic reticulum
EGTA	*ethylene glycol tetraacetic acid*
HEK293	Human Embryonic kidney cell line
HEPES	2-[4-(2-hydroxyethyl)piperazin-1-yl]ethanesulfonic acid
IMCD3	Inner medullary collecting duct cell line
IFT	Intraflagellar transport
IPTG	Isopropyl-beta-D-thiogalactopyranoside
MKS3	Meckelin
MKS	Meckel-Gruber Syndrome
MKS3p	MKS3 protein
PIPES	1,4-Piperazinediethanesulfonic acid
PCM	Post ciliary microtubule
RNAi	RNA interference
SEM	Scanning Electron Microscopy
SD	Standard deviation
SR	Striated Rootlet or kinetodesmal fiber
STDEM	Standard error of the mean
TEM	Transmission electron microscopy
TM	Transverse microtubule

Authors Contributions

TP: Anti-2F12, Anti-KDF, and tubulin rootlet immunostaining data and diagrams. GST-MKS3 coiled-coil domain construct creation, expression, and pull-down, MS/MS analysis, figure preparation, organization, preparation and critical reading of manuscript, project and experimental design.

MSV: Creation of the *IFT88* RNAi plasmid and FLAG-*MKS3* plasmid, basal body staining, FLAG-MKS3 protein localization, SEM, TEM, database searches, manuscript preparation, figure preparation, statistical analysis, experiment and project design.

JY: All plasmid injections, experimental guidance and project design, and critical reading of manuscript.

JVH: Principal investigator for the project, experiment and project design, manuscript preparation and critical reading of manuscript.

Acknowledgements

We would like to thank Dr. Jean Cohen and France Koll for the *MKS3* RNAi plasmid and the Anti-2F12 antibody, Dr. Janine Beisson for the Anti-KDF antibody, and Dr. Joel Rosenbaum for his critical suggestions and discussions of this manuscript. At the University of Vermont, Dr. Todd Clason from the COBRE imaging center with the DeltaVision Microscope; Michele von Turkovich for her assistance with SEM, TEM and critical point drying of samples; Jan Schwarz for assistance with TEM and to Dr. Mark Winey for donation of the Anti-centrin antibody. We would also like to thank Julia Fields for her assistance with the MS/MS sample preparation and analysis. *The project described was supported in part by NIH NIGMS Grants* P20 GM103449 Vermont Genetics Network-Vermont INBRE Proteomics Facility; *2 P20 RR016435-06; and RO1 GM59988.*

Competing interests: The authors declare that they have no competing interests.

References

1. D'Angelo A, Franco B: **The dynamic cilium in human diseases**. *PathoGenetics* 2009, **2**(1):3.

2. Pazour GJ, Dickert BL, Vucica Y, Seeley ES, Rosenbaum JL, Witman GB, Cole DG: **Chlamydomonas IFT88 and its mouse homologue, polycystic kidney disease gene tg737, are required for assembly of cilia and flagella**. *J Cell Biol* 2000, **151**(3):709-718.

3. Pedersen LB, Rosenbaum JL: **Intraflagellar transport (IFT) role in ciliary assembly, resorption and signalling**. *Curr Top Dev Biol* 2008, **85**:23-61.

4. Sharma N, Berbari NF, Yoder BK: **Ciliary dysfunction in developmental abnormalities and diseases**. *Current topics in developmental biology* 2008, **85**:371-427.

5. Leitch CC, Zaghloul NA, Davis EE, Stoetzel C, Diaz-Font A, Rix S, Alfadhel M, Lewis RA, Eyaid W, Banin E *et al*: **Hypomorphic mutations in syndromic encephalocele genes are associated with Bardet-Biedl syndrome**. *Nature genetics* 2008, **40**(4):443-448.

6. Brancati F, Iannicelli M, Travaglini L, Mazzotta A, Bertini E, Boltshauser E, D'Arrigo S, Emma F, Fazzi E, Gallizzi R *et al*: **MKS3/TMEM67 mutations are a major cause of COACH Syndrome, a Joubert Syndrome related disorder with liver involvement**. *Human mutation* 2009, **30**(2):E432-442.

7. Gleeson JG, Keeler LC, Parisi MA, Marsh SE, Chance PF, Glass IA, Graham Jr JM, Maria BL, Barkovich AJ, Dobyns WB: **Molar tooth sign of the midbrain-hindbrain junction: occurrence in multiple distinct syndromes**. *American journal of medical genetics Part A* 2004, **125A**(2):125-134; discussion 117.

8. Baala L, Romano S, Khaddour R, Saunier S, Smith UM, Audollent S, Ozilou C, Faivre L, Laurent N, Foliguet B *et al*: **The Meckel-Gruber syndrome gene, MKS3, is mutated in Joubert syndrome**. *American journal of human genetics* 2007, **80**(1):186-194.

9. Salonen R, Norio R: **The Meckel syndrome in Finland: epidemiologic and genetic aspects**. *American journal of medical genetics* 1984, **18**(4):691-698.

10. Salonen R, Paavola P: **Meckel syndrome**. *Journal of medical genetics* 1998, **35**(6):497-501.

11. Holmes LB, Driscoll SG, Atkins L: **Etiologic heterogeneity of neural-tube defects**. *The New England journal of medicine* 1976, **294**(7):365-369.

12. Chen CP: **Meckel syndrome: genetics, perinatal findings, and differential diagnosis**. *Taiwanese journal of obstetrics & gynecology* 2007, **46**(1):9-14.

13. Williams CL, Li C, Kida K, Inglis PN, Mohan S, Semenec L, Bialas NJ, Stupay RM, Chen N, Blacque OE *et al*: **MKS and NPHP modules cooperate to establish basal body/transition zone membrane associations and ciliary gate function during ciliogenesis**. *J Cell Biol* 2011, **192**(6):1023-1041.

14. Allen RD, Fok AK: **Membrane recycling and endocytosis in Paramecium confirmed by horseradish peroxidase pulse-chase studies**. *Journal of cell science* 1980, **45**:131-145.

15. Flotenmeyer M, Momayezi M, Plattner H: **Immunolabeling analysis of biosynthetic and degradative pathways of cell surface components (glycocalyx) in Paramecium cells**. *European journal of cell biology* 1999, **78**(1):67-77.

16. Plattner H, Kissmehl R: **Molecular aspects of membrane trafficking in Paramecium**. *Int Rev Cytol* 2003, **232**:185-216.

17. Sonneborn TM: **Gene action in development**. *Proc R Soc Lond B Biol Sci* 1970, **176**(44):347-366.

18. Allen RD: **Fine structure of membranous and microfibrillar systems in the cortex of Paramecium caudatum**. *J Cell Biol* 1971, **49**(1):1-20.

19. Iftode F, Cohen, J., Ruiz, F., Rueda, A. T., Chen-Shan, L., Adoute, A., and Beisson, J.: **Development of surface pattern during division in Paramesium**. *Development* 1989, **105**:191-211.

20. Iftode F, Adoutte, A., and Fleury, A.: **The Surface Pattern of Paramecium tetraurelia in interphase: An Electron Microscopic Study of Basal Body Variability, Connections with Associated Ribbons and their Epiplasmic Environment**. *Eur J Protistol* 1996, **32**(Suppl. 1):12.

21. Iftode F, Fleury-Aubusson A: **Structural inheritance in Paramecium: ultrastructural evidence for basal body and associated rootlets polarity transmission through binary fission**. *Biology of the cell / under the auspices of the European Cell Biology Organization* 2003, **95**(1):39-51.

22. Iftode F, Cohen J, Ruiz F, Rueda AT, Chenshan L, Adoutte A, Beisson J: **Development of Surface Pattern during Division in Paramecium .1. Mapping of Duplication and Reorganization of Cortical Cytoskeletal Structures in the Wild-Type**. *Development* 1989, **105**(2):191-211.

23. Beisson J, Sonneborn TM: **Cytoplasmic Inheritance of the Organization of the Cell Cortex in Paramecium Aurelia**. *Proceedings of the National Academy of Sciences of the United States of America* 1965, **53**:275-282.

24. Ruiz F, Beisson, J., Rossier, J., Dupuis-Williams, P.: **Basal Body duplication in Paramecium requires gamma-tubulin**. *Current Biology* 1999, **9**:43-46.

25. Ruiz F, Garreau de Loubresse N, Klotz C, Beisson J, Koll F: **Centrin deficiency in Paramecium affects the geometry of basal-body duplication**. *Current biology : CB* 2005, **15**(23):2097-2106.

26. Aubusson-Fleury A, Lemullois M, de Loubresse NG, Laligne C, Cohen J, Rosnet O, Jerka-Dziadosz M, Beisson J, Koll F: **The conserved centrosomal protein FOR20 is required for assembly of the transition zone and basal body docking at the cell surface**. *Journal of cell science* 2012, **125**(Pt 18):4395-4404.

27. Dute R, Kung C: **Ultrastructure of the proximal region of somatic cilia in Paramecium tetraurelia**. *J Cell Biol* 1978, **78**(2):451-464.

28. Dawe HR, Smith UM, Cullinane AR, Gerrelli D, Cox P, Badano JL, Blair-Reid S, Sriram N, Katsanis N, Attie-Bitach T *et al*: **The Meckel-Gruber Syndrome proteins MKS1 and meckelin interact and are required for primary cilium formation**. *Human molecular genetics* 2007, **16**(2):173-186.

29. Sasner JMaVH, J. L.: **Evidence for a *Paramecium* folate chemoreceptor**. *Chemical Senses* 1989, **14**(4):587-595.

30. Wright MV, van Houten JL: **Characterization of a putative Ca2(+)-transporting Ca2(+)-ATPase in the pellicles of Paramecium tetraurelia**. *Biochimica et biophysica acta* 1990, **1029**(2):241-251.

31. Adoutte A, Ramanathan R, Lewis RM, Dute RR, Ling KY, Kung C, Nelson DL: **Biochemical studies of the excitable membrane of Paramecium tetraurelia. III. Proteins of cilia and ciliary membranes**. *J Cell Biol* 1980, **84**(3):717-738.

32. Rasband WS: **ImageJ**. In: *US National Institute of Health.* 1997-2009.

33. Lieberman SJ, Hamasaki T, Satir P: **Ultrastructure and motion analysis of permeabilized Paramecium capable of motility and regulation of motility**. *Cell motility and the cytoskeleton* 1988, **9**(1):73-84.

34. Saha M, Carriere A, Cheerathodi M, Zhang X, Lavoie G, Rush J, Roux PP, Ballif BA: **RSK phosphorylates SOS1 creating 14-3-3-docking sites and negatively regulating MAPK activation**. *The Biochemical journal* 2012, **447**(1):159-166.

35. Valentine MS, Rajendran, A., Yano, J., Weeraratne, S.D., Beisson, J., Cohen, J., Koll, F., Van Houten, J.L.: ***Paramecium* BBS genes are key to presence of channels in cilia**. *Cilia* 2012, **In Press**.

36. Li H, Durbin R: **Fast and accurate short read alignment with Burrows-Wheeler transform**. *Bioinformatics* 2009, **25**(14):1754-1760.

37. Galvani A, Sperling L: **RNA interference by feeding in Paramecium**. *Trends in genetics : TIG* 2002, **18**(1):11-12.

38. Sperling L, Keryer G, Ruiz F, Beisson J: **Cortical morphogenesis in Paramecium: a transcellular wave of protein phosphorylation involved in ciliary rootlet disassembly**. *Developmental biology* 1991, **148**(1):205-218.

39. Cook SA, Collin GB, Bronson RT, Naggert JK, Liu DP, Akeson EC, Davisson MT: **A mouse model for Meckel syndrome type 3**. *J Am Soc Nephrol* 2009, **20**(4):753-764.

40. Tammachote R, Hommerding CJ, Sinders RM, Miller CA, Czarnecki PG, Leightner AC, Salisbury JL, Ward CJ, Torres VE, Gattone VH, 2nd *et al*: **Ciliary and centrosomal defects associated with mutation and depletion of the Meckel syndrome genes MKS1 and MKS3**. *Human molecular genetics* 2009, **18**(17):3311-3323.

41. Smith UM, Consugar M, Tee LJ, McKee BM, Maina EN, Whelan S, Morgan NV, Goranson E, Gissen P, Lilliquist S *et al*: **The transmembrane protein meckelin (MKS3) is mutated in Meckel-Gruber syndrome and the wpk rat**. *Nature genetics* 2006, **38**(2):191-196.

42. Dawe HR, Adams M, Wheway G, Szymanska K, Logan CV, Noegel AA, Gull K, Johnson CA: **Nesprin-2 interacts with meckelin and mediates ciliogenesis via remodelling of the actin cytoskeleton**. *Journal of cell science* 2009, **122**(Pt 15):2716-2726.

43. Czarnecki PG, Shah JV: **The ciliary transition zone: from morphology and molecules to medicine**. *Trends in cell biology* 2012, **22**(4):201-210.

44. Chih B, Liu P, Chinn Y, Chalouni C, Komuves LG, Hass PE, Sandoval W, Peterson AS: **A ciliopathy complex at the transition zone protects the cilia as a privileged membrane domain**. *Nat Cell Biol* 2012, **14**(1):61-72.

45. Garcia-Gonzalo FR, Reiter JF: **Scoring a backstage pass: mechanisms of ciliogenesis and ciliary access**. *J Cell Biol* 2012, **197**(6):697-709.

46. Garcia-Gonzalo FR, Corbit KC, Sirerol-Piquer MS, Ramaswami G, Otto EA, Noriega TR, Seol AD, Robinson JF, Bennett CL, Josifova DJ *et al*: **A transition zone complex regulates mammalian ciliogenesis and ciliary membrane composition**. *Nature genetics* 2011, **43**(8):776-784.

47. Adams M, Simms RJ, Abdelhamed Z, Dawe HR, Szymanska K, Logan CV, Wheway G, Pitt E, Gull K, Knowles MA *et al*: **A meckelin-filamin A interaction mediates ciliogenesis**. *Human molecular genetics* 2012, **21**(6):1272-1286.

48. Satir B, Sale WS, Satir P: **Membrane renewal after dibucaine deciliation of Tetrahymena. Freeze-fracture technique, cilia, membrane structure**. *Experimental cell research* 1976, **97**:83-91.

49. Beisson J, Clerot JC, Fleury-Aubusson A, Garreau de Loubresse N, Ruiz F, Klotz C: **Basal body-associated nucleation center for the centrin-based cortical cytoskeletal network in Paramecium**. *Protist* 2001, **152**(4):339-354.

50. Gogendeau D, Beisson J, de Loubresse NG, Le Caer JP, Ruiz F, Cohen J, Sperling L, Koll F, Klotz C: **An Sfi1p-like centrin-binding protein mediates centrin-based Ca2+ -dependent contractility in Paramecium tetraurelia**. *Eukaryot Cell* 2007, **6**(11):1992-2000.

51. Kee HL, Verhey KJ: **Molecular connections between nuclear and ciliary import processes**. *Cilia* 2013, **2**(1):11.

52. Fan S, Margolis B: **The Ran importin system in cilia trafficking**. *Organogenesis* 2011, **7**(3):147-153.

53. Dishinger JF, Kee HL, Jenkins PM, Fan S, Hurd TW, Hammond JW, Truong YN, Margolis B, Martens JR, Verhey KJ: **Ciliary entry of the kinesin-2 motor KIF17 is regulated by importin-beta2 and RanGTP**. *Nat Cell Biol* 2010, **12**(7):703-710.

Table 2.I. Unique proteins to the test lane from GST-MKS3 coiled coil domain pull down.

Paramecium DB Accession number	Molecular Weight	Peptides (control)	Peptides (test)	Name
GSPATG00034434001	146 kDa	0	2	PtCenBP1
GSPATG00020240001	115 kDa	0	2	PtSERCA1
GSPATG00034433001	85 kDa	0	2	PtCenBP1
GSPATG00009639001	39 kDa	0	2	Ran-GTPase activating protein 1
GSPATG00008129001	36 kDa	0	3	KdB2

Figure 2.1. Localization of FLAG-MKS3p. Cells expressing FLAG (control) or FLAG-*MKS3* were immunostained with Anti-Centrin (red) and Anti-FLAG (green); representative cells are shown here. The oral grove (mouth) is indicated by yellow arrows (A). FLAG staining in the test cell expressing FLAG-*MKS3* (A) shows a punctate pattern at each basal body with partial co-localization (B). This staining is above the plane of the basal body (C) (See also Supplemental Figure 4 for Western blots and Supplemental Movie 1 for individual Z sections). Images are stacks of Z sections, either 10 to 15 μm (A and B) or 4 μm (C) thick. Scale bars are 15 μm (A), 5 μm (B), or 2 μm (C).

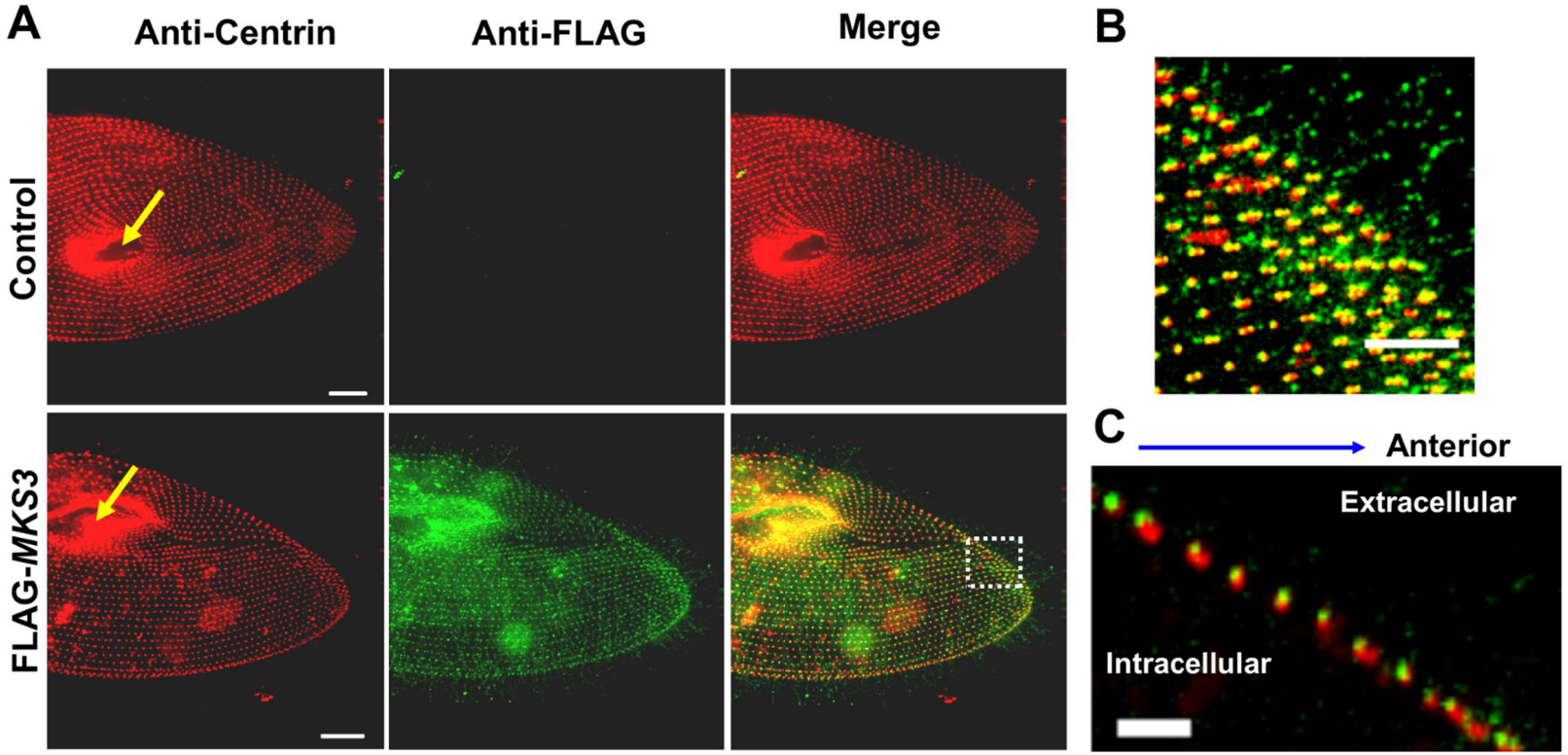
A
Anti-Centrin
Anti-FLAG
Merge
Control
FLAG-MKS3
B
C
Anterior
Extracellular
Intracellular

Figure 2.2. *MKS3* depleted cells have sparse cilia and distorted cell and ciliary surfaces. SEMs of representatives of control (A and B), *MKS3* depleted (C-F), and *IFT88* depleted (G and H) cell populations (the cell in G has been rotated). Whole cell images of control (A), *MKS3* depleted (C and E), and *IFT88* depleted (G) cells. Scale bars: 10 μm. The control cell (A) is covered in cilia while the *MKS3* depleted cells show sparse and short cilia (C and E). The *IFT88* depleted cell (G) has almost no cilia remaining, although a few short cilia are visible (yellow arrows). Higher magnifications of the cell surfaces from A, C, E, and G, (yellow boxes) are shown in B, D, F and H, respectively (scale bars: 2μm). Control cell surface (B) shows cilia arising from the cortical units while the *MKS3* depleted cells show short and missing cilia (D and F). Over 50% of the MKS3 depleted cells had cilia that were severely misshapen and "blebby." The cell surface of these cells also becomes heavily wrinkled and distorted (F). The *IFT88* depleted cell (H) shows normal organization of cortical units.

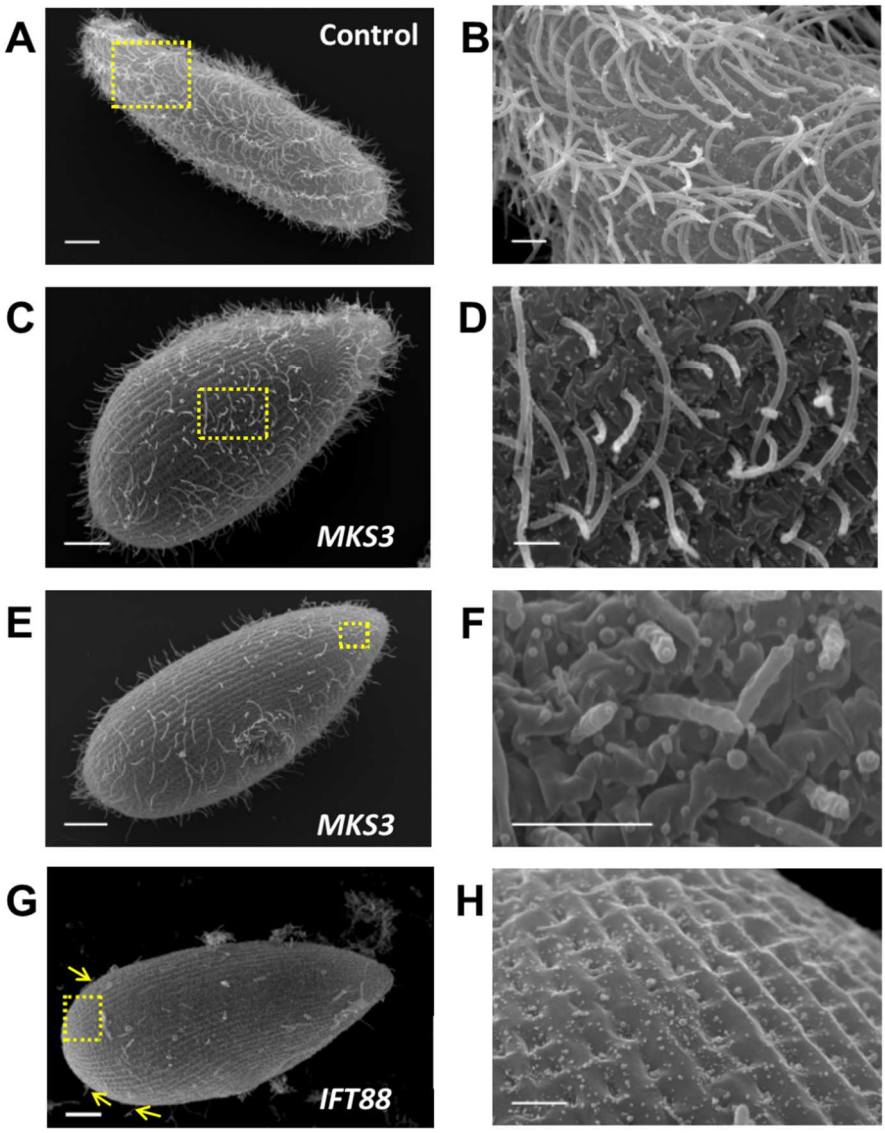
A
Control
B
C
MKS3
D
E
MKS3
F
G
IFT88
H

Figure 2.3. Basal bodies of *MKS3* depleted cells are misaligned primarily at the dorsal midline. Cells were stained using Anti-centrin to visualize the basal bodies. Images represent stacks of Z sections, approximately 10 μm thick. The images shown are the dorsal surface of the anterior side of the cell. Basal bodies should be arranged in organized rows, as seen in the control and *IFT88* depleted cells. The *MKS3* depleted cell (center panel) shows the basal bodies not aligned and no longer in straight rows (white arrows) at the midline of the cell. Scale bars: 10 μm.

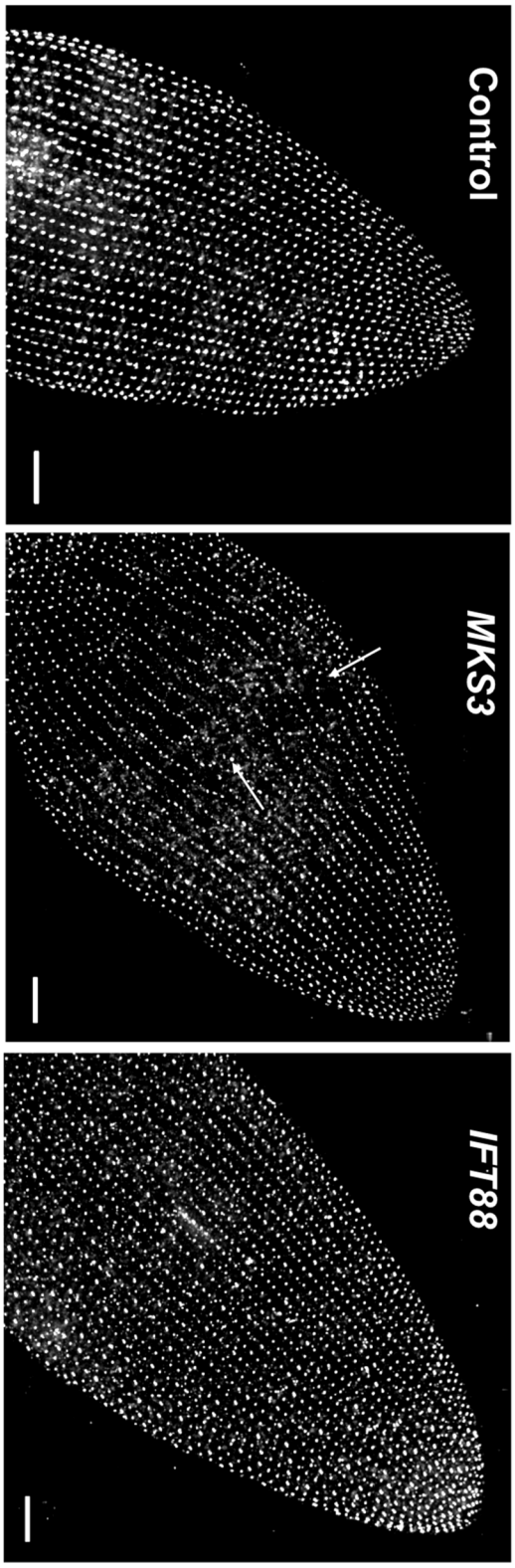
Control
MKS3
IFT88

Figure 2.4. Disruptions of the cortical units correspond to the areas of basal body misalignment. Control (A) and *MKS3* depleted cells (B and C) were stained using Anti-2F12 to visualize the cortical ridges. These images are of the dorsal surface and are stacks of Z sections, approximately 10 μm thick. The green bright spots are the intense fluorescence of the oral grooves. The control cell (A) shows the high degree of organization of the outer lattice across the cell surface. The presence of a basal body in each unit can be seen in the enlarged area (a; yellow box) and the traced image below (black dot inside hexagonal unit). The *MKS3* depleted cells illustrate an insertion of several cortical units forming an abbreviated kinety (B, b; yellow arrows) or a disruption type caused by the insertion of multiple cortical units resulting in the formation of a cluster (C, c; yellow arrows). The contractile vacuole pores are pointed out using gray arrows. Scale bars: 10 μm.

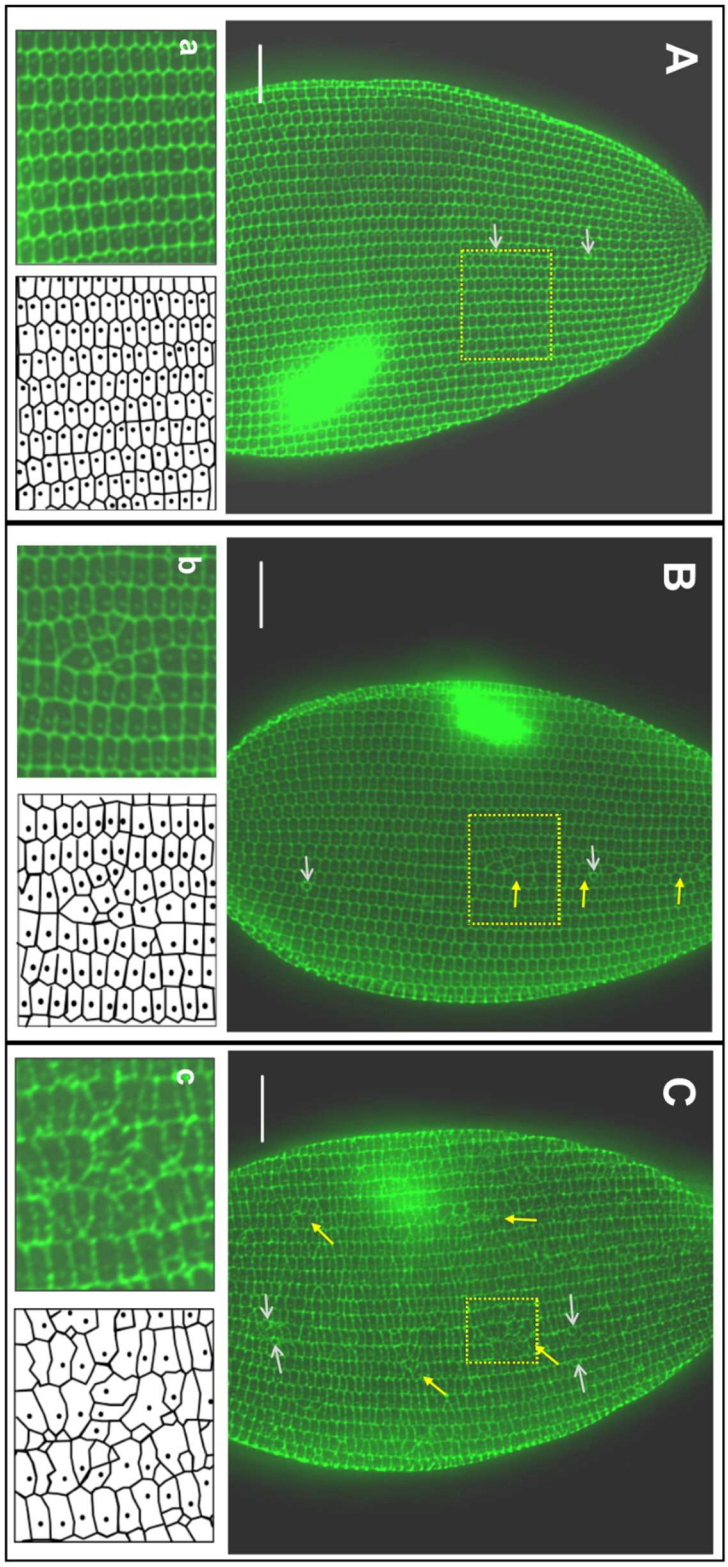
A
B
C
a
b
c

Figure 2.5. The microtubule ribbons have an altered orientation in *MKS3* depleted cells. *IFT88* (A) and *MKS3* (B) depleted cells were stained using Anti-centrin (red; basal bodies) and Anti-tubulin (green; microtubule rootlets). Images are stacks of Z sections approximately 10 μm thick. All images are the anterior dorsal surface. Areas in (A) and (B) (yellow box) have been enlarged and below each is a tracing to depict the basal body (red) and the emanating rootlets (black). The rootlets are organized into the basal body rows (kineties) as a 5 o'clock (TM) and 7 o'clock (PCM) orientation relative to the basal body. In the disrupted region of the *MKS3* depleted cell (B), the microtubule rootlets are present and maintain the angle between them (C), but do not maintain the regular orientation along the anterior-posterior cell axis as seen in the control cell. Scale bars: 10 μm. The angles between the TM and PCM were measured (C) and these angles were maintained in the MKS3 depleted cells (35 cells from both test and control cells; error bars are ± SD).

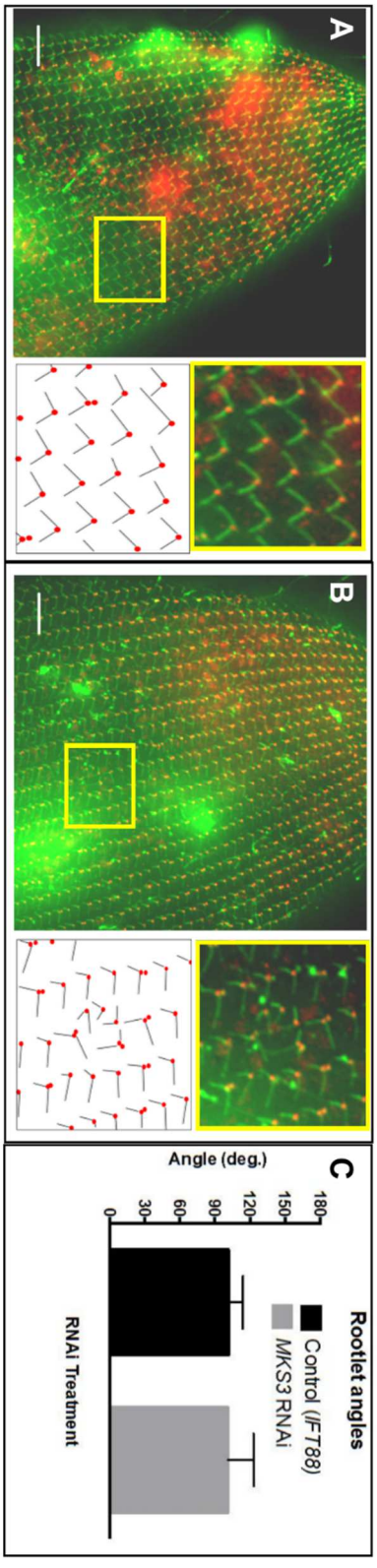
A
B
C
Angle (deg.)
0
30
60
90
120
150
180
Rootlet angles
Control (IFT88)
MKS3 RNAi
RNAi Treatment

Figure 2.6. Chaotic orientation of the striated rootlet (SR) in *MKS3* depleted cells. Control (A) and *MKS3* depleted (B) cells were stained with Anti-Glu-α-Tubulin (red; basal bodies) and Anti-KDF (green; striated rootlets). Yellow arrows in (A) and (B) indicate the contractile vacuoles on the dorsal surface of these cells. SRs project from the basal bodies; in two basal body units, SRs project only from the posterior basal body (a; dotted yellow arrows). SRs project toward the anterior of the cell in a highly organized manner along the kinety. Cells depleted of *MKS3* depict chaotic organization of the SRs, which project in every direction (b and b'). Scale bar is 10 µm.

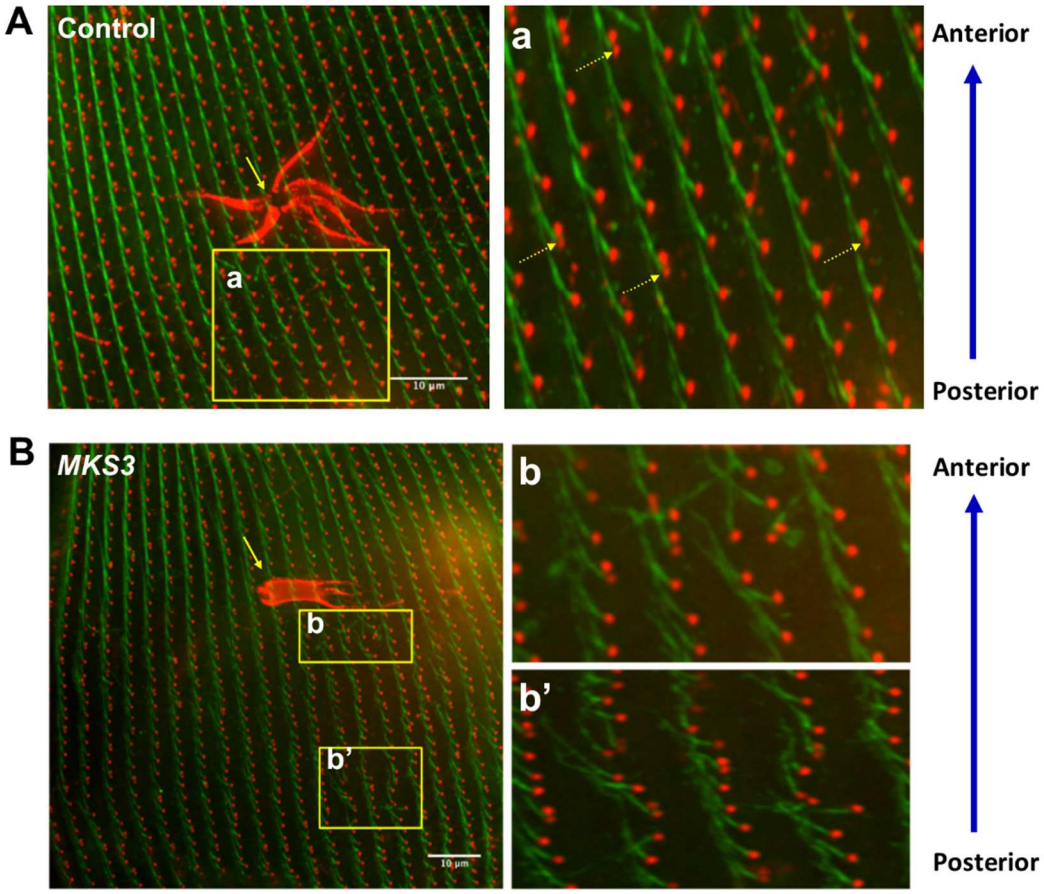

Figure 2.7. The upper portion of the panel diagrams the normal transition of a dikinetid to a monokinetid in a control cell prior to basal body duplication. In this case, the anterior basal body of the pair is linked to and uses the SR as a guide during movement. MKS3p is shown at each basal body near the cell surface (Transition zone associated MKS3p) and also at the attachment of the anterior basal body to the SR (striated rootlet associated MKS3p). We propose that this second location of MKS3p is temporary because MKS3p is not required as a guide once the anterior basal body has moved away from the posterior one sufficiently to develop its rootlets and foster the growth of another basal body. The lower portion of the panel diagrams the transition from a dikinetid to a monokinetid in *MKS3* depleted cells. We propose that in the absence of MKS3p, the anterior basal body loses its 'mooring' and can no longer utilize the SR as a guide for migration. Without guidance the basal body wanders out of alignment resulting in skewed rootlets, disorganized basal body rows, and muddled cortical ridge organization.

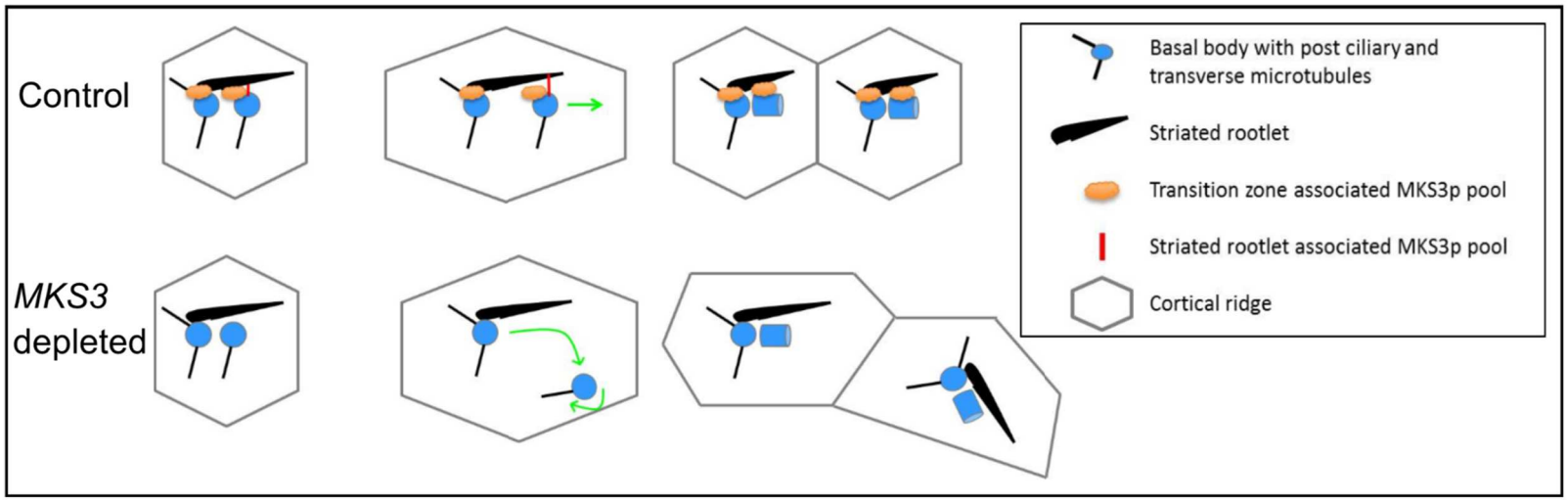
Control
MKS3
depleted
Basal body with post ciliary and transverse microtubules
Striated rootlet
Transition zone associated MKS3p pool
Striated rootlet associated MKS3p pool
Cortical ridge

Supplement Table 2.1.Comparison of *Paramecium* IFT88 with other organisms.

Gene (GSPATG…)	Nucleic acids	Amino acids	Best non-ciliate match	e-value	*Chlamydomonas* match (XP_001700100.1)	Human match IFT88 Isoform 2 (NP_006522.2)
00038505001	2341	743	*Salmo Salar* (ACN11151)	$1.00e^{-150}$	$2e^{-170}$ (42% identical)	$6e^{-168}$ (38% identical)
00021390001	2319	726	*Salmo Salar* (ACN11151)	$4.00e^{-145}$	$1e^{-163}$ (42% identical)	$2e^{-159}$ (40% identical)
00011771001	2346	736	*Salmo Salar* (ACN11151)	$2.00e^{-136}$	$1e^{-153}$ (39% identical)	$3e^{-156}$ (37% identical)
00022644001	2342	730	*Danio rerio* (CAQ14425)	$7.00e^{-128}$	$2e^{-138}$ (37% Identical)	$9e^{-140}$ (35% Identical)
00039556001	1727	566	*Salmo Salar* (ACN11151)	$1.00e^{-107}$	$9e^{-116}$ (39% identical)	$2e^{-116}$ (38% identical)

Supplement Table 2.II. Comparison of *Paramecium* MKS3 with other organisms.

Gene (GSPATG…)	Nucleic acids	Amino acids	Best non-ciliate match	e-value	*Mus musculus* (NP_808529.2)	Human match (NP_001135773.1)
00015939001	2906	951	*Rattus norvegicus* (NP_001101386.3)	$8e^{-164}$ (24% identical)	$5e^{-60}$ (24% identical)	$2e^{-56}$ (25% identical)

Supplemental Movie 2.1

Movie is the FLAG-*MKS3* injected cell shown in Figure 1 and begins outside the cell, with the anterior on the right. As the movie plays, each frame is one z-section, showing the FLAG stain (green) in the frame before the centrin stain (red). Notice the FLAG stain appears before (above) the basal bodies, which are positioned slightly below the membrane, and is positioned to the side and posterior.

(Go to: http://www.ciliajournal.com/content/3/1/2 , Additional File 5: Movie S1 to view)

Supplemental Figure 2.1

An alignment of the full-length *Paramecium,* Mouse and Human MKS3 amino acid sequences are shown (A). Shown in (B), the cysteine rich domain and coiled coil domain show conservation across all species. The *Paramecium* cysteine rich domain shows 23% identity to both the Mouse and Human sequences and the majority of the cysteines in this region are conserved across all three species. The MKS3 coiled coil domain of *Paramecium* shows 59% identity to the Mouse MKS3 coiled coil domain and 55% identity to the Human MKS3 coiled coil domain. For all alignments, red indicates 100% amino acid identity, green indicates and amino acid consensus match and white indicates a mismatch.

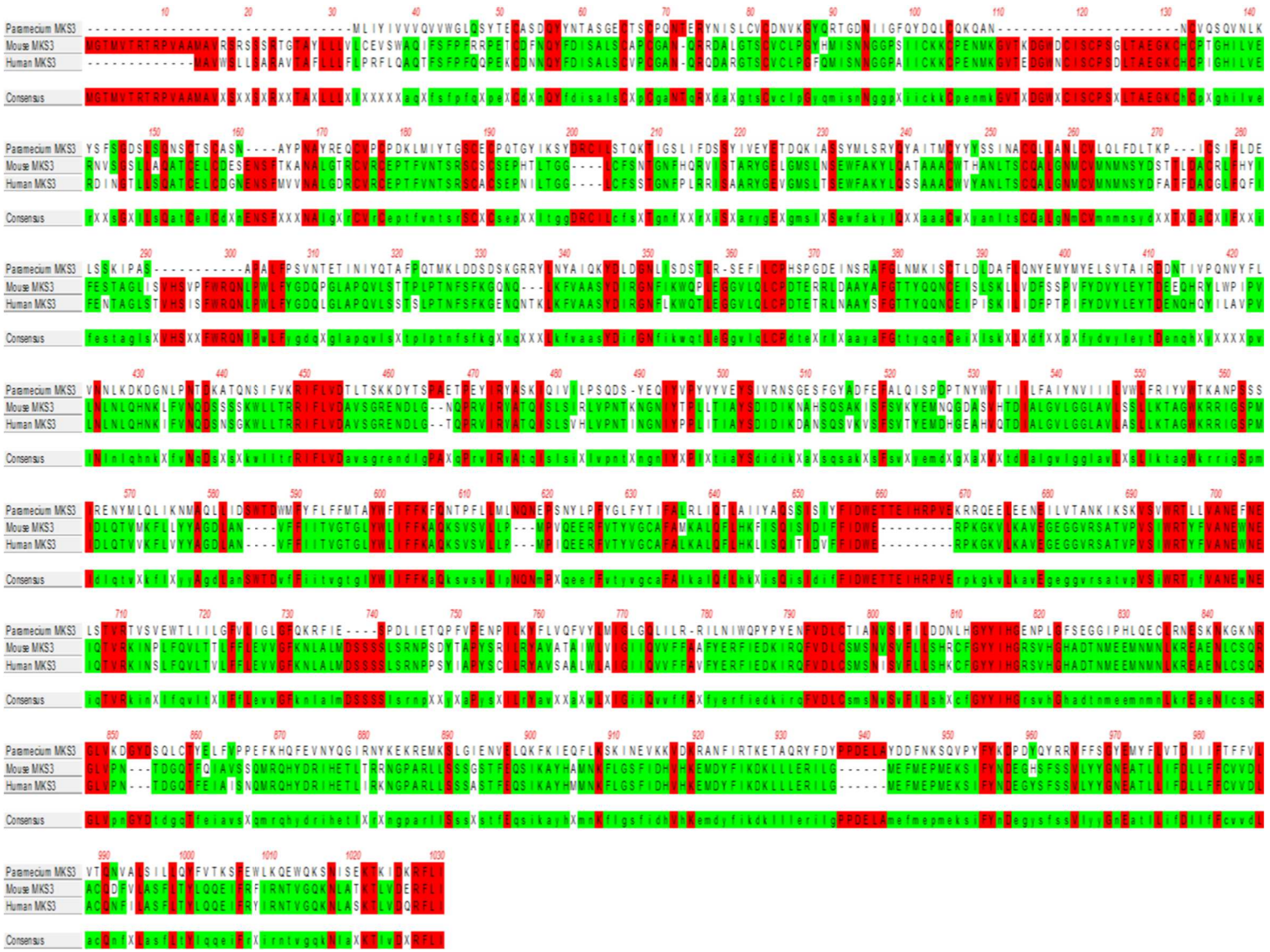
Paramecium MKS3
Mouse MKS3
Human MKS3
Consensus

Cysteine Rich Domain

Coiled Coil Domain

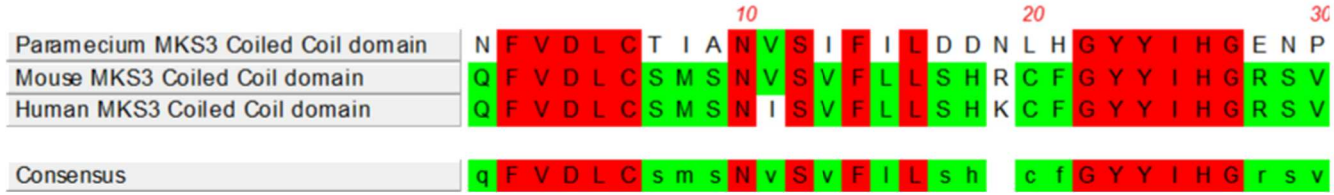

Supplemental Figure 2.2

An alignment of the full-length *Paramecium,* Mouse and Human IFT88 amino acid sequences are shown (A). Four of the predicted tetratricopeptide repeat (TPR) domains of IFT88 are conserved in the *Paramecium* sequence and are shown in (B). TPR1 shows 44% and 42% identity, TPR2 shows 45% and 51% identity, TPR3 shows 54% and 53% identity and TPR4 shows 43% and 44% identity to the Mouse and Human TPR domains, respectively. For all alignments, red indicates 100% amino acid identity, green indicates and amino acid consensus match and white indicates a mismatch.

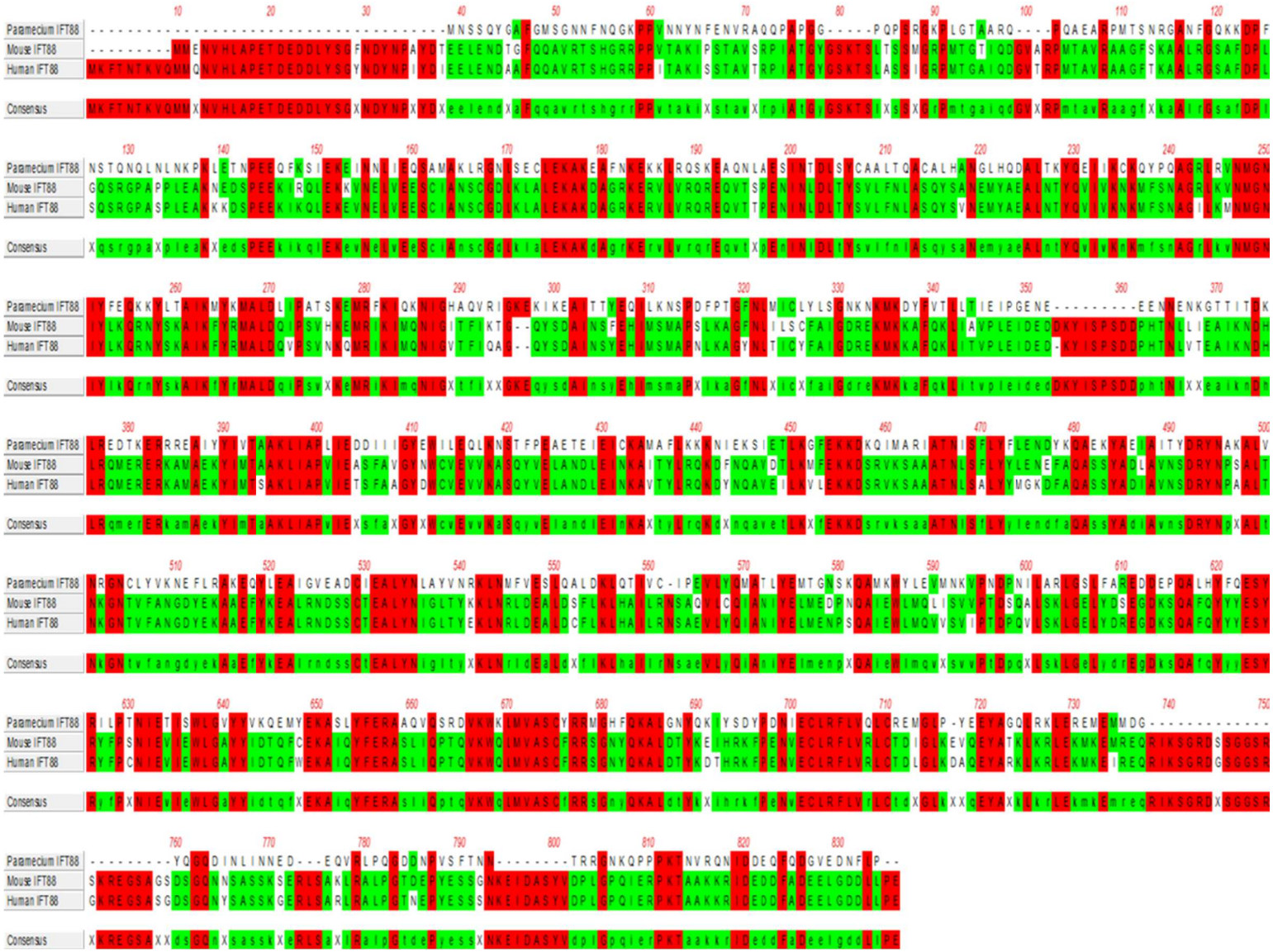
Paramecium IFT88
Mouse IFT88
Human IFT88
Consensus

B

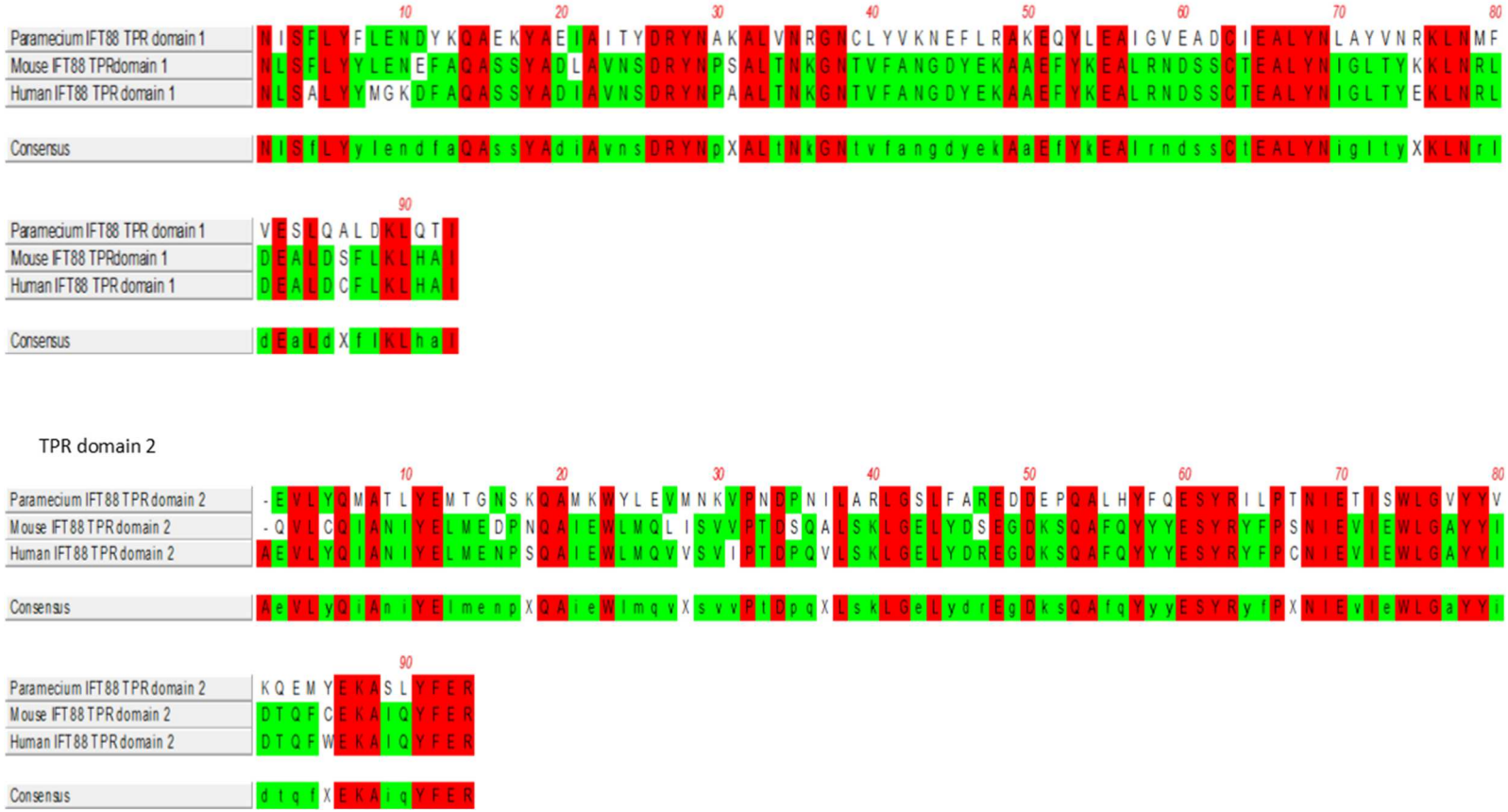
Paramecium IFT88 TPR domain 1
Mouse IFT88 TPRdomain 1
Human IFT88 TPR domain 1
Consensus
Paramecium IFT88 TPR domain 1
Mouse IFT88 TPRdomain 1
Human IFT88 TPR domain 1
Consensus
TPR domain 2
Paramecium IFT88 TPR domain 2
Mouse IFT88 TPR domain 2
Human IFT88 TPR domain 2
Consensus
Paramecium IFT88 TPR domain 2
Mouse IFT88 TPR domain 2
Human IFT88 TPR domain 2
Consensus

TPR domain 3

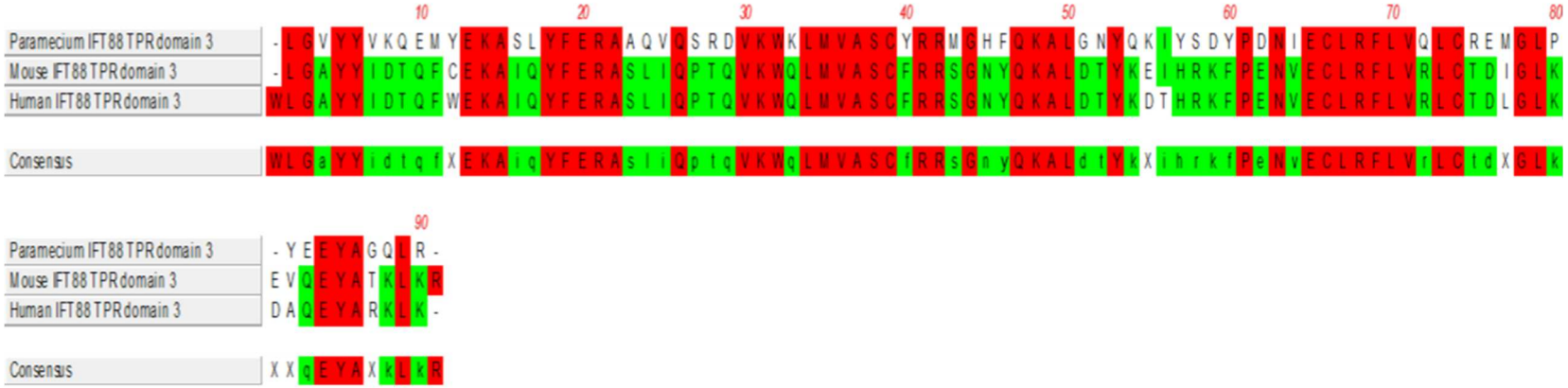

TPR domain 4

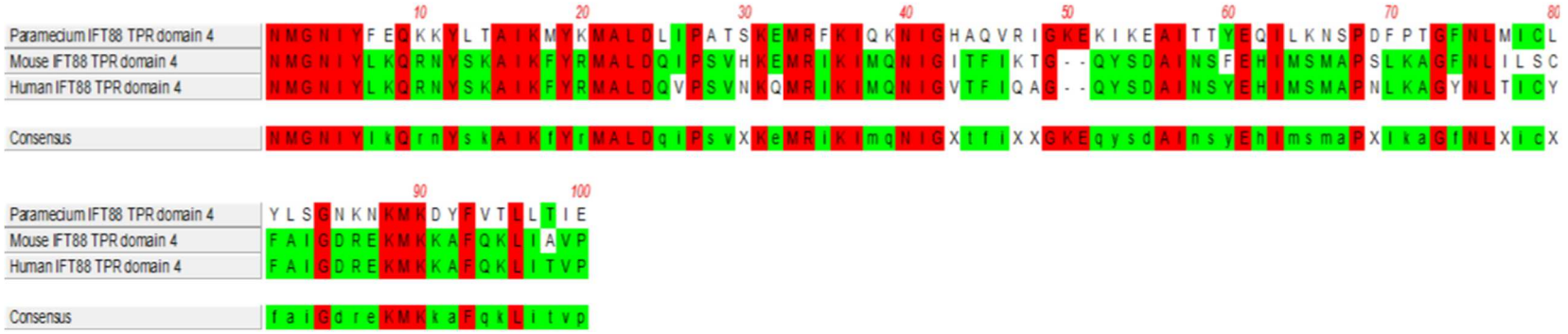

Supplemental Figure 2.3

Images of control and *MKS3* RNAi cells stained with Anti-KDF (green) and Anti-Glu-α-tubulin (red) that show a larger section of the dorsal surface. Normal kinety and kinetodesmal fiber alignment can be seen across the entire surface of the control cell. The *MKS3* depleted cell shows clustering disruptions in multiple regions of the dorsal surface (yellow arrows).

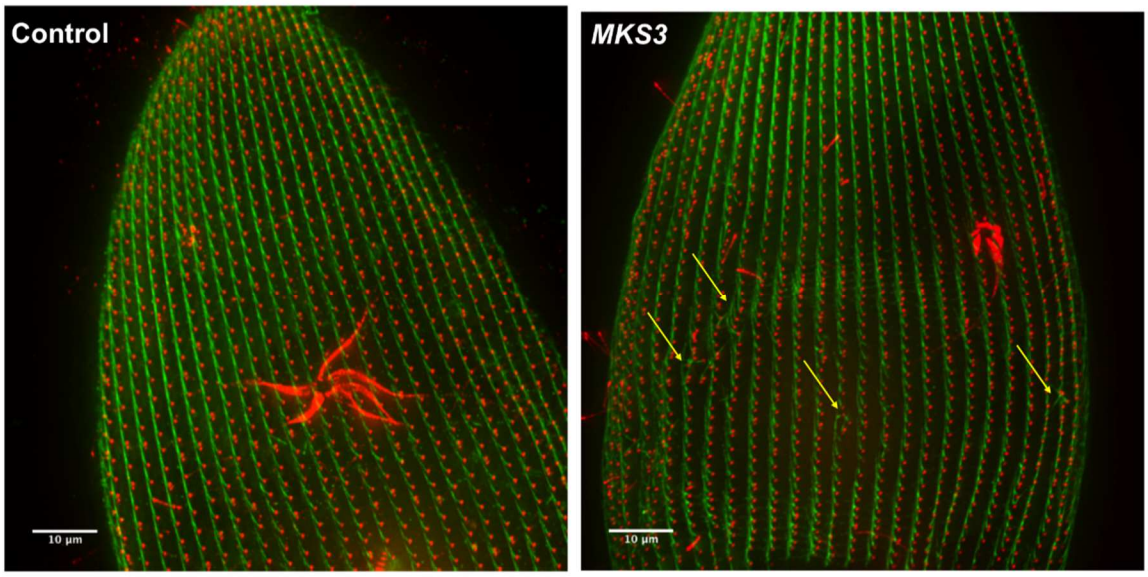

Supplemental Figure 2.4

To help determine the localization of this protein, we examined its presence in isolated whole cilia and pure cell (pellicle) membrane from cells expressing FLAG-*MKS3* or, as a control, FLAG. The isolated proteins were then separated on SDS-PAGE and transferred to nitrocellulose. The nitrocellulose blots were then probed using Anti-FLAG or Anti-Tubulin (Tubulin Loading Control). The FLAG-MKS3 protein can be seen at 105 kDa in the cell membrane (blue arrowhead) and at 105 and 77 kDa in the whole cilia (Cilia; blue arrowheads). There are non-specific bands present in both the test and control lane, in the whole cilia blot (Cilia; gray arrowheads, ~107 kDa), most likely due to the large amount of protein loaded (250 µg). Anti-tubuling blot is a representative loading control indicating the test and control samples contained the same amount of protein.

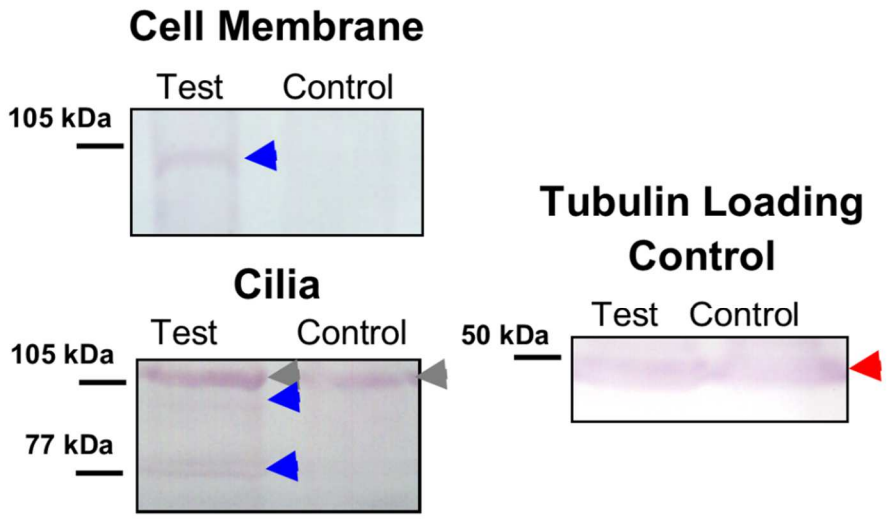

Chapter 3: A Novel Role for Polycystin-2 (Pkd2) in *P. tetraurelia* as a Probable Mg^{2+} Channel Necessary for Mg^{2+}-Induced Behavior

A Novel Role for Polycystin-2 (Pkd2) in *P. tetraurelia* as a Probable Mg^{2+} Channel Necessary for Mg^{2+}-Induced Behavior

Authors: Megan Smith Valentine, Junji Yano, Judith Van Houten

Affiliations: University of Vermont, Department of Biology, 120 Marsh Life Science, 109 Carrigan Drive, Burlington, VT 05405 USA.

Running Head: Polycystin-2 and Mg^{2+} in *Paramecium tetraurelia*

Common Abbreviations: Pkd2, Polycystin-2 or TRPP2; Pkd1, Polycystin-1; RNAi, RNA interference; TEA, tetraethyl ammonium; $(\Delta)V_m$, (change in) membrane potential; AP, action potential; Mg/TEA, 5 mM $MgCl_2$ with 25 mM TEA; Na/TEA, 10 mM NaCl with 25 mM TEA; SEM, standard error of the mean; CM, cell membrane; WC, whole cilia; IP, immunoprecipitation; I_{Mg}, magnesium current; $I_{Mg(Ca)}$, calcium-dependent magnesium current.

Abstract

Polycystin-2 (Pkd2), a non-selective cation channel, is a versatile human ciliopathy gene. Known for its interactions with other TRP channels and Pkd1, we used the ciliated organism *Paramecium tetraurelia* to explore the location and activity of Pkd2 in a non-canonical system lacking most of the previously published interacting partners. Combinations of RNAi, over-expression, and epitope-tagging were utilized for immunofluorescence, behavior assays, and electrophysiology. Depletion of Pkd2 led to a similar phenotype as *eccentric* (XntA1), a *Paramecium* mutant lacking the calcium-dependent Mg^{2+} conductance. Pkd2 and XntA localize to the cilia and cell membrane, but are not dependent on one another for trafficking. Restricting Pkd2 to the cell membrane by depleting cells of *BBS8* did no inhibit Mg^{2+}-induced behavior and mostly increased depolarizations in Mg^{2+} solutions. The XntA protein co-IP's Pkd2 from cell membrane and cilia, further supporting their cooperation. Electrophysiology of ciliated and deciliated cells showed that depletion and over-expression of Pkd2 led to smaller and larger depolarizations in Mg^{2+} solutions, respectively. We propose that Pkd2 in *P. tetraurelia* collaborates with XntA for Mg^{2+}-induced behavior and membrane permeability to Mg^{2+}. Furthermore, we propose Pkd2 is sufficient and necessary for I_{Mg}, membrane permeability to Mg^{2+}, and that Pkd2 is a Mg^{2+} channel.

Introduction

Polycystin-2 (Pkd2 or TRPP2) is a member of the transient receptor potential family of proteins which contains at least 56 members grouped into seven subfamilies. The 56 members of the TRP family share the structural homology of six predicted transmembrane-spanning regions with a pore region between S5 and S6 (Giamarchi and Delmas, 2007, Tsiokas et al., 1999). Three of the subfamilies, TRPC, TRPV, and TRPM which comprise the canonical, vanilloid, and melastatins, are related in their predicted structure and in their sequence homology. The remaining subfamilies are more divergent in their sequence and predicted structures including the TRPP subfamily of polycystins. In humans, there are eight members of the TRPP subfamily, one of which is TRPP2, or Pkd2 (Giamarchi and Delmas, 2007). Mutations in the human *PKD2* gene or protein lead to 15% of the cases of Autosomal Dominant Polycystic Kidney Disease (ADPKD) (Gonzalez-Perrett et al., 2001), one of the leading causes of adult-onset renal failure in the United States and affecting one out of every 800 live births (Wilson, 2004).

Pkd2 is a versatile ciliopathy protein from an ever-growing list of genes that when mutated, leads to the dysfunction of cilia (reviewed in (Hildebrandt et al., 2011)). The Pkd2 channel is a non-selective cation channel (Hanaoka et al., 2000). Human Pkd2 protein expressed in reconstituted human term syncytiotrophoblasts (hst), Chinese hamster ovary (CHO) cells, or LLC-PK porcine kidney cells is capable of conducting Na^+, Ca^{2+}, K^+, Cs^+, Ba^{2+} or Mg^{2+} ions (Gonzalez-Perrett et al., 2001, Koulen et al., 2002, Hanaoka et al., 2000). The Pkd2 channel operates as a homo- or hetero- tetramer (Kobori et al., 2009, Zhang et al., 2013, Stewart et al., 2010, Feng et al., 2011, Zhang et al., 2009) with an ion-passing pore of at least 11 Å (Anyatonwu et al., 2007).

The Pkd2 protein is promiscuous, with numerous interacting partners, one of which is another ciliopathy protein, Polycystin-1 (Pkd1) (Tsiokas et al., 1997, Hanaoka et al., 2000,

Giamarchi et al., 2010, Nauli et al., 2003, Delmas et al., 2004). Pkd1 is not considered a member of the TRP superfamily. At ~468 kD, Pkd1 is a large protein with an extensive extracellular N-terminus (over 2500 amino acids) followed by 11 predicted membrane spanning domains and an intracellular C-terminus (Hughes et al., 1995). The other 85% of ADPKD cases not caused by mutations in Pkd2, come from mutations in Pkd1 (Igarashi and Somlo, 2002). In addition to interacting with Pkd1, the Pkd2 channel interacts with other channels and proteins, including other TRP channels such as TRPC1 (Tsiokas et al., 1999, Du et al., 2014, Bai et al., 2008, Zhang et al., 2009), TRPC4 (Du et al., 2008), and TRPV4 (Kottgen et al., 2008, Du et al., 2014, Zhang et al., 2013). Pkd2 will also bind to itself (Zhang et al., 2009, Feng et al., 2011). Non-TRP family proteins that Pkd2 has been shown to interact with include the inositol 1, 4, 5-triphosphate (IP3) receptor (Li et al., 2005) and ryanodine receptor (RyR3) (Anyatonwu et al., 2007), both for intracellular calcium release.

The location of mammalian Pkd2 is cell-type specific and membrane-specific. Pkd2 has been shown to localize to and be active in the cell membrane (Gonzalez-Perrett et al., 2001, Luo et al., 2003, Hanaoka et al., 2000), the cilia (Yoshiba et al., 2012, Nauli et al., 2003) and the endoplasmic reticulum (ER) (Cai et al., 1999, Bae et al., 2006). Pkd2 has been shown to require Pkd1 for its trafficking to another membrane. In Chinese hamster ovary (CHO) cells expressing human *PKD1* and *PKD2*, the Pkd1 protein recruits Pkd2 to the cell membrane where these proteins form a functional channel (Hanaoka et al., 2000). In mouse embryonic kidney cells, changes in fluid stress cause Pkd1 to activate Pkd2 present in the ciliary membrane (Nauli et al., 2003). There are instances of Pkd2 not requiring Pkd1 for trafficking to the cell membrane or cilia. This is demonstrated in *C. elegans*, where the homologue of Pkd1, *lov-1*, is not required for *pkd-2* to be trafficked to the membrane of ciliated neurons (Barr et al., 2001). Another instance is in the green algae *Chlamydomonas reinhardtii* where the Pkd2 protein is cleaved from a 210 kD

protein into two smaller 120 and 90 kD proteins before entering the cilia completely independent of Pkd1 (Huang et al., 2007).

The trafficking of Pkd2 within cells, to the Golgi, the cell membrane, and the cilia membrane requires different routes and accompanying proteins. The full length human Pkd2 sequence contains an ER retention signal at the C-terminus (amino acids E^{787} to S^{820}). When expressed in HEK293 cells, Pkd2 is retained in the ER. When the retention signal is masked or is absent, Pkd2 moves to the cell membrane (Cai et al., 1999) or returns it to the ER after briefly traveling to the Golgi via COPII (Hoffmeister et al., 2011). In *Xenopus* oocytes expressing human Pkd2 and mutated forms of human Pkd2, the phosphofurin acidic cluster sorting proteins (PACS) 1 brings Pkd2 back from the cell membrane to the Golgi and PACS2 is needed to transport Pkd2 to the ER along with COPII (Kottgen et al., 2005). The movement of Pkd2 between membranes is clearly part of the regulatory or recycling system for the Pkd2 channel.

Another mode of transportation for Pkd2 is the BBSome coat complex which is vital for the transport of Pkd2 from the Golgi to the cilia. The BBSome complex consists of 8 proteins, BBS1, 2, 4, 5, 7, 8, 9 and BBIP10 (Nachury et al., 2007). The formation of this coat is regulated by Arl6GTP, an Arf-like GTPase, also known as BBS3. The coat itself is electron-dense and morphologically distinct from coats formed by COPI, COPII, and clathrin (Jin et al., 2010). The depletion of BBSome coat complex components, namely *BBS7, 8,* or *9*, leaves Pkd2 unable to traffic to the cilia, but the protein appears present at the cell surface (Valentine et al., 2012). Hoffmeister and colleagues suggest Pkd2 traffics to different points within the Golgi before being trafficked to the ER, cell membrane, or cilia (Hoffmeister et al., 2011). If Pkd2 is destined for the cell membrane, it will travel through the Golgi. However, if Pkd2 is destined for the cilia, it will leave from the *cis*-Golgi in a Rab8a-dependent manner. Pkd2 then reaches and enters the cilia in a BBSome-dependent process (Hoffmeister et al., 2011). These studies provide evidence of

multiple trafficking pathways and the dependence of Pkd2, at least in some cases, on other proteins for its localization and function.

The single-cell ciliated eukaryote *Paramecium tetraurelia* provides a useful platform for further investigations of the Pkd2 protein and its potential interacting partners. These cells are covered in a thousand or more cilia that can be easily separated from the cell bodies for investigation. The cells are amenable to RNA interference (RNAi) and over-expression of epitope-tagged proteins for localization studies using immunoprecipitation or immunofluorescence. Electrophysiology and behavioral assays are often used to investigate ion channel function or cell attraction (Van Houten, 1979, Van Houten et al., 2000, Machemer and Eckert, 1973, Machemer and Ogura, 1979). The fully annotated genome is available and searchable for homologous proteins as well as RNAi off-target sequences (ParameciumDB, paramecium.cgm.cnrs-gif.fr/) (Arnaiz et al., 2007, Arnaiz and Sperling, 2011). Interestingly, paramecia do not have homologous sequences for Pkd1, but do have sequences homologous to Pkd2, which we use and discuss in this study. We provide here the results of RNAi and epitope-tagged protein studies to investigate potential and novel interacting partners for the Pkd2 protein in both the cell membrane and the cilia. We demonstrate that the unique *Paramecium* protein eccentric, XntA (Haynes et al., 2002, Preston and Kung, 1994b, Preston and Kung, 1994a), is a potential interacting partner for Pkd2. Both of these proteins are located in the cell membrane and in the cilia and function in Mg^{2+}-induced behavior for these cells. Further, we propose that Pkd2 is the magnesium channel in the cell membrane and most likely in the cilia, demonstrating for the first time *in vivo* that Pkd2 functions as a magnesium-permeable channel.

Materials and Methods

Cell Culture

All research was done using *Paramecium tetraurelia*, 51-s (sensitive to killer) or the mutant XntA1 (Haynes et al., 2002, Preston and Kung, 1994b, Preston and Kung, 1994a). Paramecia stocks were maintained at 15°C, 22°C, or at room temperature. Culture media, discussed in (Sasner and Vanhouten, 1989), was inoculated with *Klebsiella pneumoniae* or *Aerobacter aerogenes* and incubated at 37°C for 24 to 48 hours prior to use, unless otherwise noted (see RNAi experiments).

All chemicals were obtained through Sigma (St. Louis, MO), unless otherwise noted.

BLAST searches, RNAi Construct Design and mRNA Depletion Using RNAi by Feeding

The sequence for *XNTA* (PTETG4300006001) is published (Haynes et al., 2002). This is a very unique nucleic acid sequence with no other closely related sequences within the *Paramecium* genome. To find potential homologues of Pkd2, the *Paramecium* Genome (ParameciumDB) was searched using the human and mouse sequences for Pkd2, Accession numbers NP_000288 and NP_032887, respectively. Three potential *PKD2* sequences were identified (GSPATG00005599001, GSPATG00024265001, and GSPATG00012640001) which we identify as *PKD2a*, *PKD2b* and *PKD2L*. *PKD2a* and *PKD2b* are paralogs, over 84% identical at the nucleic acid level. The sequence designed for RNA interference (RNAi) targets both of these paralogs. *PKD2L* is less similar, 47% identical at the nucleic acid level to *PKD2a* and *b*. PKD2L is not presented in this study.

Primers used to create the RNAi construct for *PKD2* were: forward 5′-GGCAGCTAATTATTAAGGAAC-3′ and reverse 5′-CAGAATTTATTCCCTACTTTTC-3′ which amplify position +781 to +2613 in GSPATG000055990001. The primers used to create the RNAi

construct for *XNTA* (PTETG4300006001) were forward 5′-ATGACCTACAGAGAATTAGTCCC-3′ and reverse 5′-GTAAATCCTTTAGCTAATGC-3′ and amplify position +1 to +1559. Constructs were created from genomic DNA isolated using organic extraction as described previously (Picariello et al., 2014).

The PCR conditions to create the RNAi constructs were: 95°C for 5 min; 5 cycles of 95°C for 1 min, 42°C for 1 min and 72°C for 3 min; 27 cycles of 95°C for 1 min, 43°C for 1 min and 72°C for 3 min; and final extension of 20 min at 72°C. Single bands were identified in 1% agarose gels stained with ethidium bromide. Two µL of the PCR products were cloned into the TOPO®pCR 2.1® cloning vector (Invitrogen/Life Technologies, Grand Island, NY) as per the kits instructions. OneShot ™Competent cells were transformed with the plasmid on LB plates containing ampicillin (AMP) and 40 ug/mL of X-GAL [5-bromo-4-chloro-3-indolyl-beta-D-galactopyranoside (RPI corp., Mount Prospect, IL)].

Plasmid Extraction and RNA interference (RNAi) Construct Creation

Potential positive colonies were grown overnight while shaking at 37°C and plasmids were extracted using the Wizard® Plasmid extraction kit (Promega, Madison, WI) as per the kit instructions. DNA was eluted using 25 µL of MilliQ water and the concentration was determined using an Agilent spectrophotometer (Agilent, Santa Clara, CA) (O.D. of 260 and 280 nm) and stored at -20°C for later use. Twenty µL of the plasmid at a concentration of 50 ng/µL was sequenced (Vermont Genetics Center DNA Facility, University of Vermont, Burlington, VT) using a commercial M13 forward primer. Positive inserted sequences were removed from TOPO®pCR2.1® plasmid (Life Technologies) using the restriction enzymes SacI and XhoI (New England BioLabs, Ipswich, MA). Fragments were ligated into the double-T7 promoter RNAi plasmid L4440 (Addgene, Cambridge, MA) using the Ligate-IT™ Rapid ligation kit (Affymetrix)

as previously described (Valentine et al., 2012). The RNAi construct for *BBS8* was created previously and is described in Valentine et al., 2012.

Preparation of RNAi Cultures

RNase-III deficient Ht115 *E. coli* bacteria were used for RNAi experiments to express double-stranded RNA. Overnight Ht115 bacteria cultures that had been transformed with the test (*PKD2*, *XNTA*, or *BBS8* sequence in L4440) RNAi plasmid or the control plasmid (L4440 vector) were used to inoculate a 50 mL culture (50 mL of LB with 100 μg/mL of AMP). That culture was grown to an $O.D._{600}$ of between 0.3 to 0.4, at which point the bacteria were induced by adding 125 μg/mL IPTG (isopropylthio-β-galactoside; RPI, corp.). Cultures were induced for 4 hours then the bacteria were pelleted by spinning the cultures in at 3440 x g (JA-14 rotor; 5000 RPM) (Beckman-Coulter, Brea, CA) for 10 minutes at 4°C. The supernatant was discarded and the pellet resuspended in 100 mL of wheat grass medium supplemented with 100 μg/mL AMP, 125 μg/mL IPTG, and 8 μg/mL stigmasterol. A 50 to 100 mL culture of starved paramecia cells were collected and allowed to swim for at least one hour in 10 mL Dryl's solution [1 mM Na_2HPO_4 (Thermo Fisher Scientific, Pittsburgh, PA), 1 mM NaH_2PO_4 (Thermo Fisher Scientific), 1.5 mM $CaCl_2$, 2 mM Na-citrate, pH 6.8] to purge them of bacteria. One hundred to 250 of the purged cells were then used to start the RNAi cultures which were incubated at 22°C or room temperature. The cultures were supplemented with an additional 125 μg/mL IPTG and 100 μg/mL AMP at 24 and 48 hours.

For the large-scale *BBS8* depleted cell study, cells were grown in 1.5 L cultures. Bacteria were grown in 250 mL LB-AMP cultures from a 10 mL overnight culture to the same density before inducing with IPTG. Induced bacteria were pelleted as before. RNAi cultures were started with 10,000 to 14,000 purged cells and maintained at room temperature. Cultures were re-fed every 24 hours by resuspending the collected pellets of freshly induced test and control bacteria

in the large culture flasks. Paramecia cultures were again supplemented with fresh AMP and IPTG. Three 1.5 L flasks were maintained for each cell type (FLAG expressing paramecia fed L4440 RNAi; *PKD2*-FLAG expressing paramecia fed L4440 RNAi; and *PKD2*-FLAG expressing paramecia fed *BBS8* RNAi). Cells were tested for behavior (backward swimming assays, see below) before harvesting. One of the flasks of each cell type was used to isolate cell membrane while the other two flasks of each cell type were used to harvest cilia (see procedures below).

Backward Swimming Assays

Solutions to test for backward swimming were made containing the base buffer 1 mM calcium citrate and ~1.3 mM Tris Base (Satow and Kung, 1976, Valentine et al., 2012). Additional salts were then added and the pH adjusted to 7.02 to 7.05 using 100 mM Tris Base. The following solutions were made using the base buffer: 30 mM KCl, 25 mM TEA (tetraethylammonium chloride) with 10 mM NaCl (Na/TEA); 25 mM TEA with 5 mM $MgCl_2$ (Mg/TEA); and the resting buffer contained 4 mM KCl.

To test behavior, the RNAi-fed or over-expressing paramecia were allowed to grow for 72 hours at room temperature or 22°C. Cells were transferred, approximately 25 at a time, to 500 µL of resting buffer (4 mM KCl in base buffer) and allowed to acclimate for at least 15 minutes. Cells were transferred one at a time using specially made glass micropipettes to 100 µL of a test solution and the time each cell spent swimming backward was timed using a stop watch. Once the cells returned to a forward swimming pattern, the stop watch was stopped and the time recorded. Test solutions were changed after ~5 cells had been tested in it. All tests were done in glass depression slides using dissecting microscopes.

Heavy Metal Resistance

To test cells for heavy metal resistance, $NiCl_2$ was used because of previous work done with this solution (Preston and Kung, 1994b). Paramecia cells fed the RNAi bacteria for 72 hours were tested for short backward swimming in 25 mM TEA with 5 mM $MgCl_2$ to ensure the RNAi was effective. The cells were briefly washed in depression slides of Dryl's solution and placed in resting buffer (see above). A total of 30 cells per cell type were placed in three separate wells of a depression slide; there were ten cells in each well. The wells contained varying concentrations of $NiCl_2$ (25, 50, 100, and 250 μM) in the base buffer above. The depression slides were maintained in a humidification chamber to prevent excessive drying. The number of cells swimming in each of the depressions was counted every 30 minutes. That number when then compared to the starting number of cells in that depression.

Creation of -FLAG and -myc Tagged Proteins

The creation of the N-terminal and C-terminal FLAG tag in the pPXV plasmids have been described previously (Valentine et al., 2012, Picariello et al., 2014). The C-terminal myc tag was created in a similar manner as previously published (Valentine et al., 2012). Briefly, a 3× myc sequence (three repeats of EQKLISEEDL) was inserted into the pPXV plasmid (Courtesy of W John Haynes, University of Wisconsin, Madison, WI) that had been treated with the restriction enzymes Nhe I and Kpn I (New England BioLabs). The following primers were used to create the insert: Top primer 5′-CTAGC[GAACAAAAATTGATTTCAGAAGAAGATTTG]$^{\times 3}$GGTAC-3′ and bottom primer 5′-C[CAAATCTTCTTCTGAAATCAATTTTTGTTC]$^{\times 3}$G-3′ which were annealed together and ligated into the linearized pPXV plasmid. Resulting colonies of bacteria were screened and two plasmids were selected to be sequenced using the pPXV sequence-specific primer, pPXV 5′: 5′-TAAGATGAATGGAATATAATG-3′. Correct plasmids were then mutated using the QuikChange Site-Directed Mutagenesis kit (Stratagene/Agilent, Santa Clara, CA) to

create a stop codon as per the kits instructions. The following primer was used for the mutation (sequence in parentheses is the existing sequence, bold letters indicate the mutation): 5'-CAGAAGAAGATTTG**TGA**(GGT)ACCCTTATCTAAATGAAC-3'.

The epitope-tagged sequences used in this study were created using the following primers. *PKD2*-FLAG (pPXV-FLAG, C-terminal FLAG tag): Forward, 5'-GCGGGGCCCATGAAAAACCTATAGG-3', reverse, 5'CGCGAGCTCATTTTCTGTTGCAGAATTTATTCCC-3', using the enzymes Apa I and Sac I. The PCR conditions were 95°C for 5 minutes; 5 cycles of 95°C for 1 min, 47°C for 1 min, 72°C for 3 min; 25 cycles of 95°C for 1 min, 49°C for 1 min, 72°C for 3 min; and then 72°C for 15 min and was done using a standard Taq polymerase (Affymetrix). *XNTA*-myc (pPXV-myc, C-terminal myc tag): Forward, 5'-GCGACTAGTATGACCTACAGAGAATTAG-3', reverse, 5'-CGCGCTAGCCTTTTAAATATTCAATCC-3', Spe I and Nhe I. The PCR conditions were 94°C for 2 min; 5 cycles of 94°C for 30 sec, 38°C for 30 sec, 68°C for 3 min 30 sec; 5 cycles of 94°C for 30 sec, 45°C for 30 sec, 68°C for 3 min 30 sec; 10 cycles of 94°C for 30 sec, 55°C for 30 sec, 68°C for 3 min 30 sec; 23 cycles of 94°C for 30 sec, 60°C for 30 sec, 68°C for 3 min 30 sec and was performed using the proof-reading Taq polymerase *Pfx* (Life Technologies). *XNTA*-FLAG (pPXV-FLAG, C-terminal FLAG tag) was created using the same primers, PCR conditions, and restriction enzymes as the *XNTA*-myc plasmid. FLAG-*PKD2* (pPXV N-FLAG, N-terminal FLAG tag): Forward, 5'-GCGGGGCCCATGAAAAACCTATAGGGG-3', reverse, 5'-CGCGGTACCTCAATTTTCTGTTGCAG-3', using the restriction enzymes Apa I and Kpn I. The PCR conditions were as follows: 94°C for 2 min; 5 cycles of 94°C for 30 sec, 46°C for 30 sec, 68°C for 3 min 30 sec; 5 cycles of 94°C for 30 sec, 50°C for 30 sec, 68°C for 3 min 30 sec; 10 cycles of 94°C for 30 sec, 55°C for 30 sec, 68°C for 3 min 30 sec; 17 cycles of 94°C for 30 sec, 59°C for 30 sec, 72°C for 3 min 30 sec and was performed using the proof-reading Taq polymerase *Pfx* (Life Technologies). In all cases, the resulting plasmids were sequenced from start to finish using

sequence-specific primers as well as the pPXV5′ primer (already described) and pPXV 3′, 5′-TTATTTAAGTGTTGTTCATTTA-3′.

The preparation of the plasmid for injection and screening of the injected paramecia was done as previously described (Picariello et al., 2014, Valentine et al., 2012). Sequence-specific primers used to screen the isolated genomic DNA from those injected cells were as follows: *PKD2*-FLAG and FLAG-*PKD2*, endogenous used *PKD2* 5′ untranslated region (UTR) 5′GGTGAGTCTTTGTAGGATT-3′ and *PKD2* RT R 5′-CTTATTCTATACCTTCAATTG-3′ and exogenous used the same reverse primer and pPXV 5′. *XNTA*-FLAG and *XNTA*-myc, endogenous primers were *XNTA* RT F 5′-CTTGAAATGCCTAAAGAATC-3′ and *XNTA* 3′UTR 5′-AGATATTGTTCTTAAATGAAC-3′, exogenous used the same forward primer and pPXV3′ reverse primer.

Immunofluorescence

Cells were cultured for immunofluorescence at 22°C or at room temperature. Cells were collected and immunostained as previously published (Valentine et al., 2012). Antibodies used for immunostaining were rabbit anti-centrin, 1:1000 (*Tetrahymena* centrin, gift from Dr. Mark Winey, University of Colorado, Boulder, CO) and mouse anti-Flag, M2 clone, 1:300 (Sigma). Secondary antibodies used were AlexaFluor® goat anti-mouse 488, AlexaFluor® goat anti-rabbit 488, AlexaFluor® goat anti-mouse 555, and AlexaFluor® goat anti-rabbit 568 (Molecular Probes/Life Technologies). Cells were examined and images recorded using the DeltaVision Restoration Microscopy System (Applied Precision, LLC, Issaquah, WA). This system consists of an inverted Olympus IX70 microscope and a Kodak CH350E camera (system and analysis equipment available through the Neuroscience COBRE Program, University of Vermont, Burlington, VT). All images were taken using a 60x oil-immersion objective and images were deconvolved and analyzed using SoftWoRx Pro software (Applied Precision).

Cell and Membrane Isolations

For all preparations, control cells were expressing the epitope tag(s) and test cells were expressing the desired plasmid(s). Cells were grown in 1.5 L volumes of fortified wheatgrass medium at 22°C or room temperature until cell densities reached approximately 8,000-12,000 cells per mL.

I. Cell Membrane:

Cell membranes were collected as previously published (Wright and van Houten, 1990) with some changes. Cells were homogenized and washed as previously described, but final cell membrane pellets were resuspended in IP500 buffer without detergents (500 mM NaCl, 100 mM Tris-Cl, 1 mM EDTA, 1 mM EGTA, 0.2 mM sodium vanadate, 10% sucrose, pH 7.5) (Tsiokas et al., 1999) or Lap200 buffer (adapted from (Nachury, 2008, Valentine et al., 2012): 50 mM HEPES, 200 mM KCl, 1 mM EGTA, 1 mM $MgCl_2$, pH 7.8). Protein concentrations were determined using a BCA protein assay (Pierce/Thermo Scientific) followed by equalizing the volume and protein concentrations of the control and test samples. Five µL was removed from each of the test and control samples for a loading control Western blot developed using Anti-Tubulin. Enough Triton X-100 and Nonidet P-40 (NP-40) (Affymetrix) were added to make the final concentrations 1% and 0.5%, respectively. Fresh protease inhibitors, 1 mM PMSF, 1 µg/mL Leupeptin (RPI corp.), and 1 µg/mL Pepstatin A (RPI, corp.), were added to the samples. Samples were rocked on ice in the cold room for one hour before centrifugation at 100,000 × g at 4°C in a Beckman L8-80 Ultracentrifuge for 45 minutes to remove the insoluble proteins. The resulting supernatants were placed in sterile 15 mL disposable centrifuge tubes to be used for immunoprecipitation (IP).

II. Whole Cilia:

To isolate the whole cilia, procedures already published (Adoutte et al., 1980) were modified. Cilia were not heavily vortexed to separate the membranes from the axoneme. Instead, cilia pellets were resuspended in a small volume (100-200 µL) of membrane buffer (8 mM Tris, 50 mM KCl, 5 mM $MgCl_2$, 1 mM EGTA, pH 7.4). The whole cilia were then frozen at -80°C for no more than two weeks after 10 µL was removed for a BCA protein assay to determine the concentration. This was done to ensure enough protein was isolated, a minimum of 1 mg was required for the IPs. For IPs, previously frozen control and test whole cilia samples were pooled from a 2 to 3 preparations to obtain sufficient protein (1 to 5 mg). The samples were brought to equal volumes and concentrations using Lap200 or IP500 buffer (described above). Five µL of protein was removed for a Western blot probed with Anti-tubulin for a loading control. Subsequently, enough Triton X-100 and NP-40 was added to bring the final concentrations to 1% and 0.5%, respectively. Fresh protease inhibitors were added to the concentrations above. As with the cell membrane preparation, whole cilia rocked on ice in the cold room for one hour. This was followed again by centrifugation at 100,000 × g for 45 minutes to remove the insoluble proteins and the supernatant was reserved for IP.

Immunoprecipitations (IP)

IPs were adapted from previously described work (Valentine et al., 2012). Briefly, between 10 to 75 mg of cell membrane protein and 1 to 5 mg of whole cilia were used for solubilizations. Supernatants from the cell membrane and whole cilia isolations described above were pre-cleared with prepared protein A beads (GE Healthcare Life Sciences, Pittsburg, PA). Approximately 30 µL of beads per sample were prepared by washing three times in 1 mL of the appropriate buffer (Lap200 or IP500) containing 1% Triton X-100 and 0.5% NP-40. Fresh protease inhibitors were added to the samples along with 30 µL of prepared Protein A beads and rocked

on ice for one hour at 4°C. Beads were removed using an IEC clinical centrifuge spun at 250 × g for 1 minute. Supernatants were removed and placed in fresh tubes to which new protease inhibitors were added. Freshly prepared affinity agarose, either Anti-FLAG M2 affinity agarose to IP FLAG-tagged proteins or Anti-c-myc affinity agarose to IP myc-tagged proteins (Sigma), were then added. Affinity agaroses were prepared by washing approximately 25 µL of agarose per sample with four 1 mL washes of the appropriate buffer containing detergents and 1% BSA followed by four 1 mL washes of the appropriate buffer with the detergents. Supernatants with affinity agarose were rocked on ice at 4°C for 2 hours. For two consecutive IPs, the agarose from the first IP was removed before adding the second type of affinity agarose. Affinity agarose was collected by centrifuging at 250 × g for 1 minute in an IEC clinical centrifuge. The supernatant was transferred to a new tube (consecutive IP) or discarded (single IP). For consecutive IPs, fresh protease inhibitors were added along with the second affinity agarose. Samples were rocked on ice at 4°C overnight. After IP, the affinity agarose was washed three times with 1 mL of the appropriate buffer containing detergents. After the final wash, as much of the remaining wash was removed as possible before adding 25 – 40 µL of 2× Sample buffer (approximate final concentration: 6.25 mM Tris Base, 1.5% SDS, 1% glycerol, 0.001% Bromophenol Blue, pH 6.8). Samples were stored at -80°C until further use.

SDS-PAGE, Immunoblots, and Silver Staining

Proteins present in the IPs were separated on 7-15% agarose gels followed by transblotting onto BioTrace™ Nitrocellulose paper (Pall Gelman, Port Washington, NY) or silver staining. Before running on the gel, β-mercaptoethanol was added to 1% v/v and samples were boiled for 5 minutes. Samples containing affinity agarose were spun at 14,000 × g for 5 minutes at 4°C to pellet the agarose. Ten µL of PageRuler™ prestained protein ladder (Thermo Fisher Scientific) was added to each gel for estimation of molecular masses and in gels that were silver

stained, 30 µL of diluted Benchmark™ protein ladder (Life Technologies) was used. Gels were run with a constant voltage of 170 mV until the dye front reached or ran off the bottom of the gel. Proteins were transferred to Nitrocellulose at 250 mA for 1 hour 15 min, followed by 390 mA for 1 hour 15 min using a Hoefer TE22 Mighty Small Transfer Tank (Hoefer, Inc., Holliston, MA). Blots were developed using either Enhanced Chemiluminescence (ECL) or alkaline phosphatase (AP). For ECL, blots were blocked in 10 to 20 mL 5% Non-fat Dry milk in TBS-T (15 mM Tris-HCl, 140 mM NaCl, 0.1% w/v TWEEN®-20 (Sigma), pH 7.5). For AP blots, 2% v/v Telost gelatin from fish (Sigma) and 3% Normal Goat Serum (Vector Labs, Burlingame, CA) was added to the milk and TBS-T mixture. Blots were blocked for one hour at room temperature. ECL blots were rinsed three times, 1× 15 minutes, 2× 5 minutes, with approximately 20 mL of TBS-T. Primary antibodies were added directly to the milk blocking buffer for AP blots. For ECL, primary antibodies were added to 10 to 20 mL of TBS-T after rinsing. Primary antibodies and their dilutions included: rabbit or mouse Anti-FLAG M2 clone (Sigma) 1:2500; rabbit or mouse Anti-C-myc (GenScript, Piscataway, NJ), 1:2000; mouse Anti-Tubulin, acetylated (Sigma), 1:10,000. Primary antibody incubation was done overnight at room temperature (TBS-T) or 4°C (milk blocking buffer). The antibody mixture was removed and blots washed three times as before in ~20 mL TBS-T while rocking at room temperature. Secondary antibodies were added in 1:10,000 dilutions in 10 to 20 mL TBS-T and rocked for 1 hour at room temperature. Secondary antibodies used included donkey Anti-rabbit IgG HRP conjugate (GE Healthcare), goat Anti-rabbit IgG AP conjugate (Sigma), goat Anti-mouse IgG HRP conjugate (Thermo Fisher Scientific), and goat Anti-mouse AP conjugate (Sigma). After one hour, blots were washed 4× with ~20 mL TBS-T and then developed using 15 mL BCIP/NBT substrate (Moss, Inc., Pasadena, MD) or SuperSignal West Pico Chemiluminescence Substrate (Thermo Scientific) as per the kit's instructions.

Silver staining was completed as previously described (Valentine et al., 2012) using the FASTSilver™ staining kit (G-Biosciences, St. Louis, MO). After stopping the reaction with 2% acetic acid, gels were stored at 4°C in fresh 2% acetic acid until processed for trypsin digest.

Mass Spectrometry analysis

Samples were analyzed at the Vermont Genetics Network Proteomics Facility at the University of Vermont. The silver stained gel lanes, from both test and control samples, were cut into slices, approximately 15 to 20 slices per lane. The slices were cut into ~ 1mm x 1 mm cubes, placed in sterile low-adhesion Eppendorf tubes and covered with MilliQ water. Silver D-stain™ (G-Biosciences) was used by mixing equal parts component A and component B then placing 500 µL of the mix over the gel slices after the water was removed. Gel slices were incubated at room temperature with occasional vortexing for 20 minutes to remove the silver stain. After 20 minutes, the D-stain™ was removed and more was added if needed. Samples were washed for 15 minutes three to five times in 500 µL 50 mM ammonium bicarbonate at room temperature to remove the yellow D-stain™. Clean samples were spun briefly, any ammonium bicarbonate was removed. 200 µL of 100% acetonitrile was added to dehydrate the gel slices. After 20 minutes, the acetonitrile was removed and an additional 100 µL was added if gel slices were not completely opaque, indicating they were dehydrated. After the samples were completely dehydrated and all acetonitrile removed, the samples were placed in a speed vac for 20 minutes to completely remove the acetonitrile. Approximately 20 µL of trypsin digest solution (40 mM ammonium bicarbonate, 0.6 ng/µL Trypsin, and 5% acetonitrile) was placed on the gel slices (enough to cover them) and samples were placed on ice. After 30 minutes on ice, additional buffer was added (40 mM ammonium bicarbonate and 5% acetonitrile) to ensure gel slides were covered. The samples were incubated at 37°C overnight. The following morning, any fluid was removed and placed in separate 0.6 mL Eppendorf tubes. The gel slices were then covered in

~100 µL extraction solution (5% formic acid and 50% acetonitrile) for 45 minutes at room temperature. After a brief spin in a table-top centrifuge, the extraction buffer was removed and added to the 0.6 mL Eppendorf tube from earlier. The gel slices were then completely dehydrated by adding 100 µL of 100% acetonitrile at room temperature for 15 minutes. The acetonitrile was also removed, added to the same 0.6 mL Eppendorf tubes. If gel slices were not opaque, an additional 100% acetonitrile was added to completely dehydrate the gel slices. The 0.6 mL Eppendorf tubes were then placed in a speed vac to evaporate all the fluid, leaving the peptides behind. Samples were then stored at 4°C until needed for LC-MS/MS.

Samples were analyzed by LC-MS/MS on a linear ion trap (LTQ) Mass Spectrometer (Thermo Fisher Scientific). Half the material was loaded onto a 100 µm x 120 mm capillary column packed with MAGIC C18 (5µm particle size, 20 nm pore size, Michrom Bioresources, Auburn, CA) at a flow rate of 500 nL/min. Peptides were separated by a gradient of 5-35% CH_3CN/0.1% formic acid over 30 minutes, 40-100% CH_3CN/0.1% formic acid in 3.5 minutes, and 100% CH_3CN for 10 minutes.

The product ion spectra were searched using the SEQUEST search engine on Proteome Discoverer 1.4 (Thermo Fisher Scientific) against a curated *Paramecium tetraurelia* database with sequences in the forward and reverse orientations. The raw files from the "control" and "test" samples were searched as one contiguous input file and a single result file was generated for each. The database was indexed to allow for full trypsin enzymatic activity, two missed cleavages and peptides between the MW of 350-5000. Search parameters set the mass tolerance at 2 Da for precursor ions and 0.8 Da for fragment ions. The result files were then searched against the Scaffold software 4.0.5 (Proteome Software, OR). Cross-correlation (Xcorr) significance filters were applied to limit the false positive rates to less than 1% in both data sets. The Xcorr values were as follows: (+1): 1.8, (+2): 2.7, (+3): 3.3, (+4): 3.5. Other filters applied were a minimum

peptide cutoff of 2 as well as DeltaCN>0.1. Ultimately, the confidence parameters resulted in false discovery rate (FDR) of >1% at the protein and peptide level for both the control and test results.

Electrophysiology

Cells used for electrophysiology were in early logarithmic growth phase. Glass electrodes were pulled using a Narishige pipet puller (Japan) using 1 mm borosilicate glass capillary tubes with filament (World Precision Instruments, Sarasota, FL). Pulled electrodes were back-filled with 500 mM KCl. They showed a resistance between 40 and 110 MΩ. Resting membrane potentials were measured using a Warner Intracellular Electrometer IE-251A (Warner Instruments, Hamden, CT) processed through AD Instruments PowerLab 4/35 and LabChart Pro (AD Instruments, Colorado Springs, CO). Cells were placed on a slide mounted to a 2-well chamber. The chambers were connected by a 3M KCl 3% agar bridge. The reference chamber was filled with 3M KCl. The experiment commenced with 5 mM KCl in base buffer (see backward swimming assays) in the main chamber. The fluid in the chamber was under constant flow with a controlled rate of ~3 mL/ min using a Buchler polystaltic pump (Buchler, Fort Lee, NJ). Membrane potential (V_m) was recorded continuously and V_m was noted at 4 minutes after each change of the solution, which is when the V_m had stabilized. All solutions contained the base buffer mentioned in Backward Swimming Assays along with 5 mM KCl, 1 mM KCl, or 0.5 mM $MgCl_2$ with 1 mM KCl. The change in membrane potential (ΔV_m) was calculated as the difference in V_m in 1 mM KCl versus 0.5 or 1 mM $MgCl_2$ with 1 mM KCl.

Both ciliated and deciliated cells were examined. Cells that were deciliated were used within 15 minutes and any deciliated cell that was moving or produced an action potential during or after the recording was not included in the analysis. Cells were deciliated by pipetting

up and down in 5 mM KCl with 5% (v/v) ethanol for 1 minute. Cells were then transferred to fresh 5 mM KCl before being transferred to the chamber for recording.

Results

RNA interference (RNAi) Phenotypes

Paramecium swims by beating its cilia toward the posterior of the cell. The speed of the beating is dependent on the cells membrane potential (V_m), which is governed by the cell's permeability to ions in their environment. The V_m of *Paramecium tetraurelia* is primarily determined by the potassium ion concentration of the bath. This allows *P. tetraurelia* to act like a potassium electrode. The cells are also permeable to Na^+ and Mg^{2+}, but less so to Ca^{2+} and Cl^- ions (Naitoh, 1968, Hansma, 1979, Machemer-Rohnisch and Machemer, 1989, Naitoh et al., 1972).

Depolarization of the cells by high potassium, other cations, or injected current open the voltage gated calcium channels (Ca_V) of the cilia causing an action potential (AP). This AP allows Ca^{2+} to enter the cilia and reach the axoneme in sufficient amounts to change the power stroke of the cilia. The change in power stroke causes transient backward swimming for as long as calcium remains high in the cilia. The K^+ depolarization-induced AP is short, ending quickly by the activation of the K^+ channels of the cilia (Eckert, 1972, Brehm et al., 1978). Since Pkd2 is a non-selective cation channel (Hanaoka et al., 2000), we examined cells depleted of the potential Pkd2 channel in different ionic stimuli to measure the effect of the loss of this channel on the AP-induced backward swimming of the cells. Mg^{2+} depolarization, especially when combined with TEA^+ to inhibit the K^+ channels, prolongs the plateau of the AP and the subsequent backward swimming.

After cells were treated for 72 hours in RNAi bacteria for *PKD2*, their swimming behavior was compared to the control cells fed the empty RNAi vector, L4440. In some cases the data were normalized for comparisons across multiple experiments, as shown in Supplement Table 3.I. All data are written as averages ± standard deviation while all graphs show averages ± standard error of the mean. Because the RNAi construct for *PKD2* targets both *PKD2a* and *PKD2b*, we simply refer to these as *PKD2* depleted cells. The *PKD2* depleted cells showed significantly shorter backward swimming in Mg/TEA compared to control cells (4.8 ± 4.1 sec and 9.6 ± 4.2 sec, respectively). In two other solutions, 30 mM KCl and Na/TEA, the cells were no different compared to the controls (Supplement Table 3.I).

The data suggested a Mg^{2+}-specific phenotype, reminiscent of the *Paramecium* mutant *eccentric* (XntA1) which has no inward Mg^{2+} current (Preston and Kung, 1994b, Preston and Kung, 1994a). The XntA1 mutant (gift of Dr. R. Preston), was created by incubating a population of cells in the mutagen N-methyl-N'-nitro-N-nitrosoguanidine followed by screening the cells for Mg^{2+} behavioral defects (Preston and Kung, 1994b). It is possible that during this incubation with the mutagen, other genes may have been altered. The XntA protein is coined a magnesium-specific channel-like exchanger (Haynes et al., 2002) that is specific to *Paramecium* and *Tetrahymena*. Expression of the wild type *XNTA* gene cures the mutant, returning the Ca-dependent Mg^{2+} current ($I_{Mg(Ca)}$) to the cells and Mg^{2+}-induced behavior (Haynes et al., 2002). Two other swimming behavior changes that are displayed by the XntA1 mutant are long backward swimming in high K^+ and short backward swimming in Na/TEA (Supplement Table 3.I). These were explained previously by a prolonged activation of the Ca^{2+} current and a quickly deactivating Na^+ current, respectively (Preston and Kung, 1994a). However, these other phenotypes were not addressed when the mutants were expressing wild type *XNTA*. Therefore, we are unsure if these behaviors are because of the premature truncation of *XNTA* in the mutant making XntA a non-functional protein or other unknown mutations. For this reason, and

because RNAi is a knock down, not a knock out, an RNAi construct to depleted wild type cells of *XNTA* seemed an appropriate comparison for *PKD2* depletion. The use of both the *XNTA* depleted cells and the XntA1 mutant provide two useful comparisons for *PKD2* depleted cells.

As shown in Figure 3.1A, the depletion of *XNTA* in the wild type background using RNAi shows short backward swimming in Mg/TEA (2.4 ± 2.9 sec) compared to the control cells (9.6 ± 4.2 sec), as expected. The *XNTA* depleted cells also showed long backward swimming in high K^+ and no change in behavior in Na/TEA, which was different than the XntA1 mutant (Supplement Table 3.I). Figure 3.1A does not contain backward swimming data for the XntA1 mutants because these cells have no reaction in Mg/TEA. When both *XNTA* and *PKD2* were depleted at the same time, no additional decrease in backward swimming compared to the *XNTA* depleted cells in Mg/TEA was observed. The *PKD2* + *XNTA* depleted cells swam backward in the Mg/TEA solution for 2.6 ± 3.9 seconds compared to 2.4 ± 2.9 seconds in the *XNTA* depleted cells, but significantly shorter than the *PKD2* depleted cells (4.8 ± 4.1 sec).

A second XntA1 mutant phenotype we investigated was the resistance of the mutant cells to heavy metals. Exposure to heavy metals can cause a decrease in and paralysis of ciliary motion (Naitoh, 1966). In mammalian cells, concentrations of 100 μM $NiCl_2$ cause reduced metabolism and ciliostasis of rat, guinea pig, and hamster tracheal explants with no obvious changes in cell or ciliary morphology (Gabridge et al., 1982). Previous work on the *Paramecium* XntA1 mutant demonstrated these mutants have some resistance to heavy metals. In the case of $NiCl_2$, XntA1 mutants are 10 times more resistant than the wild type cells to ciliary paralysis and death (Preston and Kung, 1994b). Therefore, we compared the resistance to $NiCl_2$ paralysis and death of wild type cells, *PKD2* and *XNTA* depleted wild type cells, and XntA1 mutants. The results are shown in Figure 3.1B. Although other concentrations were tested (25, 50, and 250 μM $NiCl_2$), only 100 μM is shown here. Lower concentrations had little effect on the cells during the

time tested (25 and 50 μM) and the highest concentration (250 μM) was too strong, leading to cell death even in the XntA1 mutant. In Figure 3.1B, all data points at and after 90 minutes were significantly different from the control cells fed the empty RNAi vector (L4440) (asterisk: ANOVA, multiple comparison test, at least $P<0.05$). All samples at and after 150 minutes were significantly different ($P<0.001$) compared to the control cells. There was no significant difference between the survival rates of the *PKD2* or *XNTA* depleted cells and the XntA1 mutants in 100 μM $NiCl_2$.

Over-expression phenotype

Voltage clamp experiments on wild type *Paramecium* have demonstrated that applying physiological changes to the membrane in the presence of calcium and magnesium will cause a robust inward current (1-2 nA) of Mg^{2+} (Haynes et al., 2002). The XntA1 mutants, under the same conditions, elicit no inward Mg^{2+} current (Haynes et al., 2002, Preston and Kung, 1994b, Preston and Kung, 1994a). If the XntA1 mutants are given the *XNTA*$^{+/+}$ gene in a linear plasmid to express, they show a return of I_{Mg} and Mg^{2+}-induced backward swimming (Haynes et al., 2002). We attempted to replicate these experiments by using the XntA1 mutant and wild type cells to express epitope-tagged versions of *XNTA* and *PKD2* or the FLAG epitope. We then examined these expressing cells in a Mg/TEA solution. TEA can be applied externally in the bath to block the fast-acting K^+ conductance which counteracts the influx of calcium ions (Satow, 1978) resulting in prolonged backward swimming. We are using the measurement of backward swimming as measure of ion conductance by proxy.

XntA1 mutants expressing the FLAG plasmid show no Mg^{2+}-induced behavior as shown in Figure 3.2. XntA1 mutants over-expressing *PKD2*-FLAG show a slight return of backward swimming in Mg/TEA, 0.7 ± 1.2 sec (N=60) that is significant compared to the XntA1 mutants expressing FLAG (T-test, asterisk over the bar, $P<0.001$). XntA1 mutants expressing *XNTA*-FLAG

show a strong return of Mg^{2+}-induced behavior, swimming backward for 6.6 ± 4.8 sec (N=60) which is significantly less than wild type cells expressing FLAG (9.5 ± 5.2 sec, N=165)(T-test, $P<0.001$). These data suggest an incomplete curing of the mutant. No difference was observed between wild type cells expressing FLAG and those expressing *PKD2*-FLAG (9.9 ± 6.0 sec, N=30). Wild type cells expressing *XNTA*-FLAG showed an increase in Mg^{2+}-induced behavior, swimming backward for longer than the wild type cells expressing FLAG (14.5 ± 5.4 sec, N=78). When FLAG was expressed on the N-terminus instead of the C-terminus of *PKD2* in wild type cells, Mg^{2+}-induced behavior was inhibited. The expression of FLAG-*PKD2* caused the cells to swim backward for less time than all the other cell types (4.0 ± 3.2 sec, N=127), except the XntA1 mutants expressing FLAG or *PKD2*-FLAG. Wild type cells expressing FLAG-*PKD2* swam backward significantly longer than the XntA1 mutants expressing FLAG or *PKD2*-FLAG.

Localization and trafficking of Pkd2-FLAG and XntA-FLAG / XntA-myc

To localize the Pkd2 and XntA proteins, both immunofluorescence and immunoprecipitation (IP) were used. To determine where Pkd2 and XntA reside, we isolated and solubilized cell membrane (CM) and whole cilia (WC). The resulting eluate was separated by SDS-PAGE followed by a transfer to Nitrocellulose paper. The resulting blots were probed with the appropriate antibodies to recognize Pkd2 (Anti-FLAG) (Figure 3.3A) and XntA (Anti-myc) (Figure 3.3B) from test (T) and control (C) samples. The control cells expressed the appropriate small epitope, either FLAG or myc. Representative loading controls stained with anti-tubulin demonstrate that the solubilization of the CM or WC began with approximately the same amount of protein in the test and control samples (Figure 3.3C). The top panel (Figure 3.3A) shows IPs from cells expressing *PKD2*-FLAG or FLAG. The center panel (Figure 3.3B) shows IPs from cells that were expressing XntA-myc or myc. Cell membrane IP's are on the left (CM IP) and whole cilia IP's are shown on the right (WC IP).

The Anti-FLAG antibody identified bands for Pkd2-FLAG on the CM IP blot at 98, 70, and 55 kD in the test lane only (Figure 3.3A, upper left, black arrows). On the WC IP blot, Anti-FLAG identified Pkd2-FLAG bands at 120, 98 and 70 kD (Figure 3.3A, upper right, black arrows). While the expected size of Pkd2-FLAG is 100 kD, all of the bands have been identified as Pkd2 via LC-MS/MS analysis.

Anti-myc identified multiple XntA-myc bands on both the CM and WC IP blots (Figure 3.3B, grey arrows). The uppermost band in both the CM and WC IP was at 62 kD, which is the expected size of XntA-myc. On the CM IP blot, there was a band present at 46 kD and both the CM and WC IPs show bands at 37-38 kD (Figure 3.3B, grey arrows). Multiple bands are often observed when IP'ing for XntA-myc. The same bands were observed when we IP'd from cells expressing *XNTA*-FLAG (data not shown). The multiple bands for XntA-myc have not been identified through LC-MS/MS analysis, but their identification with two different epitope tags suggests they are XntA. No bands were present in the IP lanes from control cells except in the XntA-myc IP blot from WC. This blot and the IP were both performed using rabbit anti-myc antibodies which showed the heavy chain of the antibody at approximately 55 kD and a few other non-specific bands in both the test and control lanes. These bands should be ignored.

For immunofluorescence, wild type or XntA1 mutant cells expressing FLAG or *PKD2*-FLAG or *XNTA*-FLAG were isolated and stained for the basal bodies (Anti-centrin, gift of Dr. Mark Winey, University of Colorado, Boulder, CO) and the FLAG epitope (Sigma). Figure 3.4 shows the results of the immunofluorescence in wild type cells (Figure 3.4A) or XntA1 mutants (Figure 3.4B). The anti-centrin staining for the basal bodies serves as a sub-cellular reference point. No FLAG staining was seen in the FLAG expressing control cells, which was expected. There was no observable difference between the staining of Pkd2-FLAG and XntA-FLAG in the wild type cells and the XntA1 mutants. In both cases, the XntA-FLAG and Pkd2-FLAG proteins

(red staining) was clearly seen in the cilia and at the cell surface. The cells shown are representative of the populations observed.

Pkd2 has been shown to require other proteins, or signals from those proteins, for its trafficking to the cilia (Nauli et al., 2003) or the cell membrane (Hanaoka et al., 2000). The XntA1 mutants did not appear to have any differences in the localization of Pkd2-FLAG when expressing this protein compared to wild type cells (see Figure 3.4). These data suggest that Pkd2 does not require XntA for ciliary or cell membrane localization. To confirm these findings, we used immunofluorescence to examine wild type cells expressing *PKD2*-FLAG or *XNTA*-FLAG depleted in *XNTA* or *PKD2*, respectively, using RNAi. The immunostained images are shown in Figure 3.5. Included are negative control cells which are wild type cells expressing FLAG. They show very little background staining (red). For a positive control, wild type cells expressing *PKD2*-FLAG or *XNTA*-FLAG fed the empty RNAi vector L4440 (control) show red staining at the cell surface and in the cilia indicating that Pkd2-FLAG and XntA-FLAG locate to those areas of the cell. Cells expressing *PKD2*-FLAG or *XNTA*-FLAG depleted in *XNTA* or *PKD2*, respectively, showed no change in the localization of the FLAG-tagged proteins compared to the respective positive control cells. The efficacy of the depletion of *XNTA* or *PKD2* using RNAi was tested using Mg^{2+}-induced behavior (backward swimming) of the depleted cells compared to both the negative and positive control cells in Mg/TEA. In both *PKD2* or *XNTA* depleted cells, Mg^{2+}-induced behavior was reduced compared to the positive and negative control cells, as indicated by an asterisk (T-test, $P<0.01$) (Figure 3.5), indicating the RNAi was successful.

We have demonstrated here that Pkd2 and XntA do not require each other for trafficking to the cell membrane or the cilia (Figure 3.4 and 3.5). We have demonstrated previously (Valentine et al., 2012) and it has been shown in other studies that Pkd2 requires components of the BBSome, a coat-complex of proteins, to traffic to the cilia but not to the cell surface

(Hoffmeister et al., 2011, Valentine et al., 2012). The BBSome complex transports select proteins from the Golgi to the cilia, such as the G-protein coupled Somatostatin receptor 3 (SSTR3) (Jin et al., 2010, Klinger et al., 2014) and the potassium channel SK1a (Valentine et al., 2012). In order to confirm that Pkd2 was reaching the cell membrane in *Paramecium* depleted of BBS components and that Pkd2 was depleted from the cilia, *Paramecium* cells expressing *PKD2*-FLAG were depleted in *BBS8* using RNAi. We chose to deplete *BBS8* because we did not expect ciliary shortening or loss as observed in *BBS7* or *BBS9* depleted *Paramecium* (Valentine et al., 2012).

The cell membrane and cilia of paramecia expressing *PKD2*-FLAG or FLAG and treated for RNAi were collected and solubilized for IP. The eluates were separated by SDS-PAGE, transblotted, and developed using Anti-FLAG to compare the amount of Pkd2-FLAG in the cell and ciliary membranes with control-fed cells expressing *PKD2*-FLAG and with negative control cells expressing FLAG. We clearly show that Pkd2-FLAG is almost completely absent from the cilia (Figure 3.6B) and is found in the cell membrane when *BBS8* is depleted from the cells (Figure 3.6, black arrows).

To determine if there was an increase in band intensity in the test lanes (*PKD2*-FLAG cells depleted in *BBS8*) compared to the positive control lanes, band intensities were normalized to their respective tubulin loading controls. The normalized intensities were then compared between the test lanes (cells expressing *PKD2*-FLAG depleted in *BBS8*) and the positive control lanes (*PKD2*-FLAG fed empty vector RNAi). This was done for two separate experiments and the data were pooled. There was a slight, but not significant, increase in the intensity of the Pkd2-FLAG bands (120% ± 38%, n=6) in the test lane from the cell membrane IPs. In contrast and in agreement with our previous work (Valentine et al., 2012), the IPs from whole cilia show that the Pkd2-FLAG bands are decreased by 80% in the test lanes compared to the positive control cilia.

These data confirm that Pkd2 requires *BBS8*, a component of the BBSome, to traffic to the cilia. Pkd2 must rely on a different trafficking mechanism to reach the cell membrane.

A phenotype which we observe in paramecia depleted in *BBS7, 8,* or *9* is long backward swimming in both Na/TEA and Mg/TEA. We attributed this prolonged backward swimming to the absence of a rectifying K^+ channel, SK1a (Valentine et al., 2012). The *BBS8* depleted cells used in the experiments also displayed this phenotype (Figure 3.6). The IP data demonstrate that Pkd2 was present in the cell membrane and mostly absent from the cilia. The *BBS8* depleted cells are still able to sufficiently depolarize in the presence of Mg^{2+}, as seen by their Mg^{2+}-induced behavior.

Co-Immunoprecipitation and LC-MS/MS analysis

We asked whether the Pkd2-FLAG and XntA-myc proteins could co-IP, supporting a direct or indirect interaction of these proteins. Cell membrane and whole cilia from wild type cells expressing *PKD2*-FLAG and *XNTA*-myc alongside control cells expressing FLAG and myc were solubilized for IP using FLAG affinity agarose followed by myc affinity agarose. Figure 3.7 shows the results of a representative FLAG IP followed by a myc IP from solubilized cell membrane (Figure 3.7A) and whole cilia (Figure 3.7B). In both experiments, the FLAG affinity agarose was exposed to the solubilized cell component first, then removed. The myc affinity agarose was added to the supernatant second. The resulting nitrocellulose blots were probed using antibodies against FLAG developed with enhanced chemiluminescence (ECL) or myc developed using alkaline phosphatase to locate the Pkd2-FLAG and XntA-myc epitope-tagged proteins. In both the IPs from solubilized cell membrane (3.7A) and solubilized whole cilia (3.7B), the Pkd2-FLAG protein was clearly identified (upper left blots, black arrows). The same multiple bands were seen in the Pkd2-FLAG IP (120, 98, and 70 kD) as shown in Figure 3.3. These bands have all been positively identified as Pkd2 using LC-MS/MS analysis. (In a

previous experiment, these size fragments were sent for LC-MS/MS analysis from a silver stained gel. The peptide sequences confirmed that the majority of the protein in those lanes was Pkd2.) From both the cell membrane and the whole cilia, the FLAG IP for Pkd2-FLAG did not co-IP the XntA-myc protein (lower left blots in Figure 3.7A and 3.7B). However, the consecutive IP from the same supernatant using the myc affinity agarose isolated both the XntA-myc protein (lower blots, right hand side in Figure 3.7A and B) and the Pkd2-FLAG protein (upper blots on the right in Figure 3.7A and B). These results demonstrate that the XntA-myc protein and the Pkd2-FLAG protein co-IP, but only when we use the myc affinity agarose to IP XntA-myc.

In an attempt to identify novel candidate interacting partners for Pkd2, we used cell membrane or whole cilia from wild type cells expressing *PKD2*-FLAG or FLAG followed by solubilization, IP, and LC-MS/MS analysis. We used two different buffers for our cilia IPs and only the IP500 buffer for the cell membrane IP. We used IP500 buffer, a high sodium buffer, because it was used to demonstrate the association of Pkd2 with TRPC1 (Tsiokas et al., 1999). The other buffer, Lap200 (a high potassium buffer), had been used previously to solubilize the Pkd2 protein from whole cilia. Our goal was to successfully solubilize the Pkd2 protein, which can remain attached to the axoneme as in *Chlamydomonas* (Huang et al., 2007, Pazour et al., 2005), while maintaining protein-protein interactions. IP eluates were separated by SDS-PAGE, silver stained, and the entire lane of resulting proteins from both the test and control samples were processed with trypsin for analysis. Resulting peptides were run against a database of *Paramecium* proteins. Identified proteins found in both the test and control samples were removed from the analysis. Proteins reported are unique to the test lane.

Shown in Figure 3.8 is a Venn diagram of the distribution of the identified proteins in the different preparations. Thirty-one proteins were identified in the cell membrane IP and 20 and 50 proteins were identified in the whole cilia Lap200 and IP500 buffer IPs, respectively. Of these,

the Pkd2 protein was found in all three preparations, five proteins overlapped in the two cilia IPs and an additional five overlapped between the cell membrane IP and the two cilia IPs (Figure 3.8A). This small number of proteins that co-IP'd from both the cell membrane and the cilia was expected due to the differences in the composition of the cell membrane and the cilia (Rhoads and Kaneshiro, 1979, Machemer and Ogura, 1979). In total, 89 unique proteins were identified in the two membranes. The types of proteins identified in the two membranes are shown in Figure 3.8B and C. In the two types of membranes, almost half the proteins identified (~45%) were identified as "hypothetical" meaning they have no assigned function. This is not a surprising find since approximately 40% of the annotated proteins of *Paramecium* are uncharacterized, most are species-specific (Zagulski et al., 2004) as in the case of XntA. A complete list of the proteins identified, including peptide number, accession number and protein descripting, are found in Supplement Table 3.II. Notable identified proteins include three intraflagellar transport proteins found in the cilia IPs (IFT 52, 72/74, 81) (GSPATP00006050001, PTETP1200013001, and GSPATP00033046001). We identified a homologue to the *Drosophila* protein mutated in lost boys (*lobo*) (GSPATP00001683001), also known as CG34110, that is a conserved flagellar protein which has been shown to interact with *Drosophila* Pkd2 (Yang et al., 2011). We also identified numerous dyneins (GSPATP00002701001, GSPATP00038423001, GSPATP00029949001, to name a few)(see Supplement Table 3.II for a complete list). Note that the XntA protein was not identified in any of the LC-MS/MS experiments.

Electrophysiology and Membrane Potential (V_m)

To confirm the importance and contribution of the Pkd2 and XntA1 proteins to Mg^{2+}-induced behavior in *Paramecium*, electrophysiology was employed to measure membrane potential (V_m) changes in ciliated and deciliated cells. The changes in membrane potential (ΔV_m) were calculated by first determining the resting V_m in 1 mM KCl in buffer followed by the newly

established resting V_m in 0.5 mM $MgCl_2$ with 1 mM KCl in buffer. The difference between these two V_m's is the calculated ΔV_m. Previous work has shown that wild type cells depolarize by ~10 mV in the presence of 0.5 mM $MgCl_2$ while XntA1 mutants depolarize by 1 ± 7 mV (N=5) in the same concentration of Mg^{2+} (Preston and Kung, 1994a). These previous data prompted us to use 0.5 mM $MgCl_2$ for our recordings. We used cells depleted of *XNTA*, *PKD2,* or *BBS8* or cells over-expressing the FLAG or *PKD2*-FLAG plasmid. These data are presented as averages ± standard deviation (mV) while the histograms (Figure 3.9A and 3.9B) depict averages ± SEM. Table 3.I includes the average ΔV_m of cells ± standard deviations and the results of Mg^{2+}-induced behavior for those cells compared to the appropriate controls (backward swimming phenotypes). Table 3.II provides the ΔV_m's from deciliated cells. We are using ΔV_m as cells were changed between solutions with and without Mg^{2+} as a proxy for membrane permeability to Mg^{2+}. We have not measured membrane permeability or conductance directly. A positive ΔV_m is a depolarization of the cell, therefore we will refer to these changes as depolarizations. A negative ΔV_m is a hyperpolarization of the cell, which we did not observe in this study.

We first replicated previous findings of ciliated wild type and XntA1 mutant cells (Preston and Kung, 1994a). Our data show wild type cells depolarized by 9.8 ± 1.6 mV (N=5) and the XntA1 mutant cells showed little depolarization in Mg^{2+} (1.2 ± 2.2 mV, N=7) (Figure 3.9A). Wild type cells depleted in *PKD2* and *XNTA* showed significantly less depolarization that the wild type cells, 6.9 ± 3.4 mV (N=9) and 4.7 ± 4.9 mV (N=7), respectively. Wild type cells over-expressing FLAG showed no change in depolarization compared to the wild type cells. Wild type cells over-expressing *PKD2*-FLAG depolarized twice as much, 20.9 ± 3.2 mV (N=6), significantly more than all other cell types presented in Figure 3.9A (ANOVA, individual T-test's, $P<0.01$).

When we examined the XntA1 mutants, the mutants expressing FLAG, and those depleted in *PKD2* showed almost no depolarization compared to the XntA1 mutants (Table 3.I and Figure 3.9A). Interestingly, the XntA1 mutants over-expressing *PKD2*-FLAG showed a robust depolarization, no different than the depolarization seen in wild type cells (11.9 ± 3.6 mV, N=6 compared to 9.8 ± 1.6 mV, N=5).

Wild type and XntA1 mutants depleted in *BBS8* were then tested for ΔV_m to examine the contribution of Pkd2 at the cell membrane with and without the XntA protein to Mg^{2+}-induced depolarization. We have demonstrated that cells depleted in *BBS8* have little to no Pkd2 protein in their cilia and are able to swim backward in Mg^{2+} solutions, suggesting there is sufficient Pkd2 in the cell membrane for $I_{Mg(Ca)}$ by proxy. In both wild type and XntA1 mutants depleted of *BBS8*, a larger depolarization was observed compared to their respective controls. Wild type ΔV_m was increased from 9.8 ± 1.6 mV (N=6) to 12.7 ± 2.4 mV (N=6) when *BBS8* was depleted. Surprisingly, the ΔV_m of the XntA1 mutant was increased from 1.2 ± 2.2 mV (N=7) to 6.5 ± 0.8 mV (N=3) (both $P<0.05$, ANOVA, T-tests).

To tease apart the contributions of the cilia and the cell membrane to V_m, we recorded from deciliated cells. Paramecia are easily deciliated in 5 mM KCl with 5% ethanol with mild trituration which has no effect on the resting membrane potential of the cells (Machemer and Ogura, 1979). The amount a deciliated *Paramecium* cell depolarizes in the presence of 0.5 mM $MgCl_2$ has not previously been published. Surprisingly, the deciliated wild type cells showed a depolarization of 17.9 ± 3.8 mV (N=5) and the deciliated XntA1 mutants, 15.7 ± 6.8 (N=8). There is no statistical difference between these values (See Table 3.II and Figure 3.9B). It should be noted that the deciliated wild type cells depolarize by the same amount as the ciliated *BBS8* depleted wild type cells (12.7 ± 2.4 mV, N=6 compared to 17.9 ± 3.8, N=5, $P=0.054$, T-test).

The only changes in depolarization we observed compared to the deciliated wild type cells and deciliated XntA1 mutants were seen in the wild type cells depleted in *PKD2* (10.3 ± 5.3 mV, N=4), the wild type cells over expressing *PKD2*-FLAG (23.9 ± 4.7 mV, N=4), and the XntA1 mutants depleted in *PKD2* (2.9 ± 3.2 mV, N=4) (P<0.05, ANOVA, T-test). The XntA1 mutants over-expressing *PKD2*-FLAG showed no change compared to the XntA1 cells expressing FLAG (See Table 3.II). We did observe that the XntA1 mutants depleted in *BBS8* depolarized by 10.1 ± 3.4 mV (N=6) which was less depolarization than the wild type cells (17.9 ± 3.8 mV, N=5) and wild type cells depleted in *BBS8* (20.3 ± 4.2 mV, N=4). However, the deciliated XntA1 mutants depleted in *BBS8* depolarize by the same amount as the deciliated XntA1 mutants (See Table 3.II).

Lastly, deciliated *PKD2* depleted XntA1 mutants showed almost no depolarization, 2.9 ± 3.2 mV (N=4), which is significantly less than the other deciliated cells (P<0.01, ANOVA, T-tests) and is not significantly different than the ciliated XntA1 mutant cells (P=0.455, T-test) or the ciliated XntA1 cells depleted of *PKD2* (P=0.92, T-test).

Discussion

The depletion of *PKD2* produces phenotypes that resemble, but do not copy, XntA1 mutant phenotypes. The main XntA1 phenotypes are a lack of $I_{Mg(Ca)}$ and resistance to $NiCl_2$ ciliary paralysis (Preston and Kung, 1994b, Preston and Kung, 1994a). These phenotypes were both demonstrated by *PKD2* or *XNTA* depleted cells, suggesting reduced $I_{Mg(Ca)}$. *PKD2* depleted cells showed changes in Mg^{2+} solutions only, suggesting a Mg^{2+}-specific role for Pkd2. The mutants and *XNTA* depleted cells also showed long backward swimming in high K^+, presumably due to a slow deactivation of the Ca^{2+} current (Preston and Kung, 1994b). This may suggest a role for XntA in Ca^{2+}-regulation, which I_{Mg} relies on, although further investigation is needed.

Deciliated cells and *pawn B* mutants, both lacking the voltage-gated calcium channels of the cilia, do not elicit an $I_{Mg(Ca)}$ (Preston, 1990, Preston and Kung, 1994a, Preston, 1998). We have not measured conductance directly, but used ionic stimuli to prolong the AP of cells causing prolonged backward swimming which we used as a proxy for ionic conductance. The short backward swimming in Mg^{2+} suggests a reduced, but not eliminated, $I_{Mg(Ca)}$ in *PKD2* and *XNTA* depleted cells.

Both Pkd2 and XntA are located in the cell membrane and the cilia, but do not require each other for trafficking to these membranes. *Paramecium* Pkd2 does not require XntA or a signal from XntA to traffic to the cilia or the cell membrane, as Pkd2 does in some other cell types (Hanaoka et al., 2000, Nauli et al., 2003). These proteins appear more akin to the *C. elegans* proteins PKD2 and LOV1 than mammalian Pkd2 and Pkd1. In *C. elegans*, PKD2 and LOV1 act in the same pathway for mating behavior, but traffic independently (Barr et al., 2001). In the case of *Paramecium*, Pkd2 and XntA contribute to Mg^{2+}-induced behavior and also traffic independently.

When we IP XntA-myc, Pkd2-FLAG co-precipitates but not *vice versa*. The potential interaction of XntA-myc and Pkd2-FLAG probably blocks the C-terminal FLAG epitope preventing the reciprocal IP. We were able to IP Pkd2-FLAG from the same supernatant but XntA-myc does not co-IP, suggesting a second population of Pkd2 with an unobstructed FLAG epitope. Our analysis of co-IP proteins from Pkd2-FLAG IPs contained no XntA peptides and few proteins with transmembrane domains. Human Pkd2 has been shown to interact with other transmembrane proteins at both its N- and C- terminus (Feng et al., 2011). In an attempt to co-IP transmembrane proteins and possibly XntA, we expressed Pkd2 with the FLAG tag on the N-terminus but unfortunately, Mg^{2+}-induced behavior was disrupted. We propose two populations of Pkd2-FLAG, one with a FLAG epitope that is blocked from interactions with other proteins and one with FLAG available for interactions with other proteins and IP.

Our measurements by proxy of membrane permeability to Mg^{2+} by observing ΔV_m when cells were changed between solutions with and without Mg^{2+} helped to tease apart the contributions of Pkd2 and the cilia to Mg^{2+} permeability. A summary of our findings can be seen in Figure 3.10. We found that our depletion of *XNTA* or *PKD2* produced phenocopies of the mutant, showing less depolarization compared to wild type cells. These data imply a reduced, but not eliminated, membrane permeability to Mg^{2+}. These data, combined with the short backward swimming data we presented for these depleted cells as a proxy for studying $I_{Mg(Ca)}$, newly implicate the Pkd2 protein in both Mg^{2+} permeability and conductance.

Over-expression of *PKD2* showed an increase in Mg^{2+} membrane depolarization and Mg^{2+}-induced behavior in both the wild type cells and mutants. Expression of *PKD2*-FLAG in XntA1 mutants restores the amount the membrane depolarizes in Mg^{2+} to normal wild type levels. Therefore, even without the XntA protein present, the Pkd2 expressed protein allows for Mg^{2+} depolarization and a return of Mg-induced behavior. These data imply that Pkd2 is responsible for Mg^{2+} permeability and that over-expressing Pkd2 in a system without XntA returns some $I_{Mg(Ca)}$.

We became interested in the reaction of deciliated cells when we observed that *BBS8* depletion showed no Pkd2 in the cilia and yet retained Mg^{2+}-induced behavior (Valentine et al., 2012). Our ΔV_m in deciliated cells surprisingly showed that not only did deciliated wild type cells depolarize more than ciliated cells in Mg^{2+}, but that both deciliated XntA1 mutants and *XNTA* depleted cells depolarized as much as deciliated wild type cells. With no functional XntA protein, our expectation was that, ciliated or not, the XntA1 mutants and the *XNTA* depleted cells would not depolarize. Interestingly, ciliated wild type cells depleted of *BBS8* demonstrated the same amount of depolarization as a deciliated wild type cell. These results suggest that Pkd2, when restricted to the cell membrane, is no longer "repressed" or negatively regulated by XntA

in the cilia. These data also suggest that XntA is not a Mg^{2+} channel, that Pkd2 in the cell membrane, or possibly another protein in the cell membrane, is able to become active when the cilia are removed.

Our proposal that Pkd2 is the Mg^{2+} channel in *Paramecium* is further supported by the over-expression of *PKD2*-FLAG in both the wild type and the mutants. In ciliated over-expressing cells we observed larger depolarizations, although we had mixed results for the deciliated cells. Over-expression in the deciliated XntA1 mutants did not additively increase the depolarization in Mg^{2+} solutions over the effects of deciliation alone, which caused unexpectedly high depolarization by itself. Conversely, the depletion of *PKD2* in deciliated wild type cells reduced the depolarization in Mg^{2+} as it did in ciliated wild type cells, but the reduction of *PKD2* in the mutants significantly decreased the depolarization to almost none.

The outcomes of these studies leads to our proposal that Pkd2 is both necessary and sufficient for apparent Mg^{2+} permeability and inferred $I_{Mg(Ca)}$ suggesting Pkd2 is the Mg^{2+} channel. XntA, thought to be the Mg^{2+} channel or transporter, when mutated or depleted in ciliated cells, leads to a loss of Mg^{2+} depolarization and $I_{Mg(Ca)}$. These losses can be overcome with the over-expression of *PKD2*, restriction of Pkd2 to the cell membrane by *BBS8* depletion, or deciliation. In these cases, Pkd2 is able to act alone and effect larger depolarizations. We have established that Pkd2 and XntA can interact directly or indirectly in both the cell membrane and cilia. Although, these interactions are not necessary for Mg^{2+} depolarization and $I_{Mg(Ca)}$. This story seems straight forward, but it doesn't end here. There's a role for cilia in Mg^{2+} permeability and conductance. Our model is the following:

- Pkd2 is in the cilia and the cell membrane and is the channel responsible for the $I_{Mg(Ca)}$.

- Pkd2 in intact cells is somehow negatively regulated by ciliary XntA, reducing Pkd2 channel activity.
- Loss of XntA in ciliated cells leads to a loss of Pkd2 Mg^{2+} channel activity because XntA1 positions Pkd2 in microdomains for function or regulates Pkd2 function by direct or indirect interactions.
- In XntA1 mutants, the XntA protein is lost from the cell, but Pkd2 is not. Depolarization and $I_{Mg(Ca)}$ are lost as part of the mutant phenotype. Why does Pkd2 not function as a channel in these cells until the cilia are removed?

Deciliation or *BBS8* depletion limits the Pkd2 protein to the cell membrane where its activity is increased in wild type cells due to mass action (concentration inside and outside microdomains.) Deciliation of the XntA1 mutant suggests that this Pkd2 is free to be active without encumbrance by XntA1. Deciliated XntA1 mutants with depleted *PKD2* show almost no depolarization, consistent with this model.

Acknowledgements

The authors would like to thank Julia Fields for her assistance with the LC-MS/MS analysis of the samples, Dr. Todd Clason for assistance and maintenance of the DeltaVision microscopy system, and Dr. Anthony Morielli for in-depth discussions of electrophysiology data. Also, we thank Dr. W. John Haynes for the pPXV plasmid, Dr. Robin Preston for the XntA1 mutant cell line, and Dr. Mark Winey for the *Tetrahymena* Anti-centrin antibody. Funding sources include support from IDeA from NIGMS, P20 GM103449 for Vermont Genetics Network Proteomics Facility and by NIH Grant Numbers 5 P30 RR032135 from the COBRE Program of the National Center for Research Resources and 8 P30 GM103498 from the National Institute of General Medical Sciences for Deltavision Microscopy.

References

ADOUTTE, A., RAMANATHAN, R., LEWIS, R. M., DUTE, R. R., LING, K. Y., KUNG, C. & NELSON, D. L. 1980. Biochemical studies of the excitable membrane of Paramecium tetraurelia. III. Proteins of cilia and ciliary membranes. *J Cell Biol,* 84**,** 717-38.

ANYATONWU, G. I., ESTRADA, M., TIAN, X., SOMLO, S. & EHRLICH, B. E. 2007. Regulation of ryanodine receptor-dependent calcium signaling by polycystin-2. *Proc Natl Acad Sci U S A,* 104**,** 6454-9.

ARNAIZ, O., CAIN, S., COHEN, J. & SPERLING, L. 2007. ParameciumDB: a community resource that integrates the Paramecium tetraurelia genome sequence with genetic data. *Nucleic Acids Res,* 35**,** D439-44.

ARNAIZ, O. & SPERLING, L. 2011. ParameciumDB in 2011: new tools and new data for functional and comparative genomics of the model ciliate Paramecium tetraurelia. *Nucleic Acids Res,* 39**,** D632-6.

BAE, Y. K., QIN, H., KNOBEL, K. M., HU, J., ROSENBAUM, J. L. & BARR, M. M. 2006. General and cell-type specific mechanisms target TRPP2/PKD-2 to cilia. *Development,* 133**,** 3859-70.

BAI, C. X., GIAMARCHI, A., RODAT-DESPOIX, L., PADILLA, F., DOWNS, T., TSIOKAS, L. & DELMAS, P. 2008. Formation of a new receptor-operated channel by heteromeric assembly of TRPP2 and TRPC1 subunits. *EMBO Rep,* 9**,** 472-9.

BARR, M. M., DEMODENA, J., BRAUN, D., NGUYEN, C. Q., HALL, D. H. & STERNBERG, P. W. 2001. The Caenorhabditis elegans autosomal dominant polycystic kidney disease gene homologs lov-1 and pkd-2 act in the same pathway. *Curr Biol,* 11**,** 1341-6.

BREHM, P., DUNLAP, K. & ECKERT, R. 1978. Calcium-dependent repolarization in Paramecium. *J Physiol,* 274**,** 639-54.

CAI, Y., MAEDA, Y., CEDZICH, A., TORRES, V. E., WU, G., HAYASHI, T., MOCHIZUKI, T., PARK, J. H., WITZGALL, R. & SOMLO, S. 1999. Identification and characterization of polycystin-2, the PKD2 gene product. *J Biol Chem,* 274**,** 28557-65.

DELMAS, P., NAULI, S. M., LI, X., COSTE, B., OSORIO, N., CREST, M., BROWN, D. A. & ZHOU, J. 2004. Gating of the polycystin ion channel signaling complex in neurons and kidney cells. *FASEB J,* 18**,** 740-2.

DU, J., DING, M., SOURS-BROTHERS, S., GRAHAM, S. & MA, R. 2008. Mediation of angiotensin II-induced Ca2+ signaling by polycystin 2 in glomerular mesangial cells. *Am J Physiol Renal Physiol,* 294**,** F909-18.

DU, J., MA, X., SHEN, B., HUANG, Y., BIRNBAUMER, L. & YAO, X. 2014. TRPV4, TRPC1, and TRPP2 assemble to form a flow-sensitive heteromeric channel. *FASEB J,* 28**,** 4677-85.

ECKERT, R. 1972. Bioelectric control of ciliary activity. *Science,* 176**,** 473-81.

FENG, S., RODAT-DESPOIX, L., DELMAS, P. & ONG, A. C. 2011. A single amino acid residue constitutes the third dimerization domain essential for the assembly and function of the tetrameric polycystin-2 (TRPP2) channel. *J Biol Chem,* 286**,** 18994-9000.

GABRIDGE, M. G., DOUGHERTY, E. P., GLADD, M. F. & MECCOLI, R. A. 1982. Effects of heavy metals on structure, function, and metabolism of ciliated respiratory epithelium in vitro. *In Vitro,* 18**,** 1023-32.

GIAMARCHI, A. & DELMAS, P. 2007. Activation Mechanisms and Functional Roles of TRPP2 Cation Channels. *In:* LIEDTKE, W. B. & HELLER, S. (eds.) *TRP Ion Channel Function in Sensory Transduction and Cellular Signaling Cascades.* Boca Raton (FL).

GIAMARCHI, A., FENG, S., RODAT-DESPOIX, L., XU, Y., BUBENSHCHIKOVA, E., NEWBY, L. J., HAO, J., GAUDIOSO, C., CREST, M., LUPAS, A. N., HONORE, E., WILLIAMSON, M. P., OBARA, T., ONG, A. C. & DELMAS, P. 2010. A polycystin-2 (TRPP2) dimerization domain essential for the function of heteromeric polycystin complexes. *EMBO J,* 29**,** 1176-91.

GONZALEZ-PERRETT, S., KIM, K., IBARRA, C., DAMIANO, A. E., ZOTTA, E., BATELLI, M., HARRIS, P. C., REISIN, I. L., ARNAOUT, M. A. & CANTIELLO, H. F. 2001. Polycystin-2, the protein mutated in autosomal dominant polycystic kidney disease (ADPKD), is a Ca2+-permeable nonselective cation channel. *Proc Natl Acad Sci U S A,* 98**,** 1182-7.

HANAOKA, K., QIAN, F., BOLETTA, A., BHUNIA, A. K., PIONTEK, K., TSIOKAS, L., SUKHATME, V. P., GUGGINO, W. B. & GERMINO, G. G. 2000. Co-assembly of polycystin-1 and -2 produces unique cation-permeable currents. *Nature,* 408**,** 990-4.

HANSMA, H. G. 1979. Sodium uptake and membrane excitation in Paramecium. *J Cell Biol,* 81**,** 374-81.

HAYNES, W. J., KUNG, C., SAIMI, Y. & PRESTON, R. R. 2002. An exchanger-like protein underlies the large Mg2+ current in Paramecium. *Proc Natl Acad Sci U S A,* 99**,** 15717-22.

HILDEBRANDT, F., BENZING, T. & KATSANIS, N. 2011. Ciliopathies. *N Engl J Med,* 364**,** 1533-43.

HOFFMEISTER, H., BABINGER, K., GURSTER, S., CEDZICH, A., MEESE, C., SCHADENDORF, K., OSTEN, L., DE VRIES, U., RASCLE, A. & WITZGALL, R. 2011. Polycystin-2 takes different routes to the somatic and ciliary plasma membrane. *J Cell Biol,* 192**,** 631-45.

HUANG, K., DIENER, D. R., MITCHELL, A., PAZOUR, G. J., WITMAN, G. B. & ROSENBAUM, J. L. 2007. Function and dynamics of PKD2 in Chlamydomonas reinhardtii flagella. *J Cell Biol,* 179**,** 501-14.

HUGHES, J., WARD, C. J., PERAL, B., ASPINWALL, R., CLARK, K., SAN MILLAN, J. L., GAMBLE, V. & HARRIS, P. C. 1995. The polycystic kidney disease 1 (PKD1) gene encodes a novel protein with multiple cell recognition domains. *Nat Genet,* 10**,** 151-60.

IGARASHI, P. & SOMLO, S. 2002. Genetics and pathogenesis of polycystic kidney disease. *J Am Soc Nephrol,* 13**,** 2384-98.

JIN, H., WHITE, S. R., SHIDA, T., SCHULZ, S., AGUIAR, M., GYGI, S. P., BAZAN, J. F. & NACHURY, M. V. 2010. The conserved Bardet-Biedl syndrome proteins assemble a coat that traffics membrane proteins to cilia. *Cell,* 141**,** 1208-19.

KLINGER, M., WANG, W., KUHNS, S., BARENZ, F., DRAGER-MEURER, S., PEREIRA, G. & GRUSS, O. J. 2014. The novel centriolar satellite protein SSX2IP targets Cep290 to the ciliary transition zone. *Mol Biol Cell,* 25**,** 495-507.

KOBORI, T., SMITH, G. D., SANDFORD, R. & EDWARDSON, J. M. 2009. The transient receptor potential channels TRPP2 and TRPC1 form a heterotetramer with a 2:2 stoichiometry and an alternating subunit arrangement. *J Biol Chem,* 284**,** 35507-13.

KOTTGEN, M., BENZING, T., SIMMEN, T., TAUBER, R., BUCHHOLZ, B., FELICIANGELI, S., HUBER, T. B., SCHERMER, B., KRAMER-ZUCKER, A., HOPKER, K., SIMMEN, K. C., TSCHUCKE, C. C., SANDFORD, R., KIM, E., THOMAS, G. & WALZ, G. 2005. Trafficking of TRPP2 by PACS proteins represents a novel mechanism of ion channel regulation. *EMBO J,* 24**,** 705-16.

KOTTGEN, M., BUCHHOLZ, B., GARCIA-GONZALEZ, M. A., KOTSIS, F., FU, X., DOERKEN, M., BOEHLKE, C., STEFFL, D., TAUBER, R., WEGIERSKI, T., NITSCHKE, R., SUZUKI, M., KRAMER-ZUCKER, A., GERMINO, G. G., WATNICK, T., PRENEN, J., NILIUS, B., KUEHN, E. W. & WALZ, G. 2008. TRPP2 and TRPV4 form a polymodal sensory channel complex. *J Cell Biol,* 182**,** 437-47.

KOULEN, P., CAI, Y., GENG, L., MAEDA, Y., NISHIMURA, S., WITZGALL, R., EHRLICH, B. E. & SOMLO, S. 2002. Polycystin-2 is an intracellular calcium release channel. *Nat Cell Biol,* 4**,** 191-7.

LI, Y., WRIGHT, J. M., QIAN, F., GERMINO, G. G. & GUGGINO, W. B. 2005. Polycystin 2 interacts with type I inositol 1,4,5-trisphosphate receptor to modulate intracellular Ca2+ signaling. *J Biol Chem,* 280**,** 41298-306.

LUO, Y., VASSILEV, P. M., LI, X., KAWANABE, Y. & ZHOU, J. 2003. Native polycystin 2 functions as a plasma membrane Ca2+-permeable cation channel in renal epithelia. *Mol Cell Biol,* 23**,** 2600-7.

MACHEMER-ROHNISCH, S. & MACHEMER, H. 1989. A Ca paradox: Electric and behavioural responses of Paramecium following changes in external ion concentration. *Eur J Protistol,* 25**,** 45-59.

MACHEMER, H. & ECKERT, R. 1973. Electrophysiological control of reversed ciliary beating in Paramecium. *J Gen Physiol,* 61**,** 572-87.

MACHEMER, H. & OGURA, A. 1979. Ionic conductances of membranes in ciliated and deciliated Paramecium. *J Physiol,* 296**,** 49-60.

NACHURY, M. V. 2008. Tandem affinity purification of the BBSome, a critical regulator of Rab8 in ciliogenesis. *Methods Enzymol,* 439**,** 501-13.

NACHURY, M. V., LOKTEV, A. V., ZHANG, Q., WESTLAKE, C. J., PERANEN, J., MERDES, A., SLUSARSKI, D. C., SCHELLER, R. H., BAZAN, J. F., SHEFFIELD, V. C. & JACKSON, P.

K. 2007. A core complex of BBS proteins cooperates with the GTPase Rab8 to promote ciliary membrane biogenesis. *Cell,* 129**,** 1201-13.

NAITOH, Y. 1966. Reversal response elicited in nonbeating cilia of paramecium by membrane depolarizatin. *Science,* 154**,** 660-2.

NAITOH, Y. 1968. Ionic control of the reversal response of cilia in Paramecium caudatum. A calcium hypothesis. *J Gen Physiol,* 51**,** 85-103.

NAITOH, Y., ECKERT, R. & FRIEDMAN, K. 1972. A regenerative calcium response in Paramecium. *J Exp Biol,* 56**,** 667-81.

NAULI, S. M., ALENGHAT, F. J., LUO, Y., WILLIAMS, E., VASSILEV, P., LI, X., ELIA, A. E., LU, W., BROWN, E. M., QUINN, S. J., INGBER, D. E. & ZHOU, J. 2003. Polycystins 1 and 2 mediate mechanosensation in the primary cilium of kidney cells. *Nat Genet,* 33**,** 129-37.

PAZOUR, G. J., AGRIN, N., LESZYK, J. & WITMAN, G. B. 2005. Proteomic analysis of a eukaryotic cilium. *J Cell Biol,* 170**,** 103-13.

PICARIELLO, T., VALENTINE, M. S., YANO, J. & VAN HOUTEN, J. 2014. Reduction of meckelin leads to general loss of cilia, ciliary microtubule misalignment and distorted cell surface organization. *Cilia,* 3**,** 2.

PRESTON, R. R. 1990. A magnesium current in Paramecium. *Science,* 250**,** 285-8.

PRESTON, R. R. 1998. Transmembrane Mg2+ currents and intracellular free Mg2+ concentration in Paramecium tetraurelia. *J Membr Biol,* 164**,** 11-24.

PRESTON, R. R. & KUNG, C. 1994a. Inhibition of Mg2+ current by single-gene mutation in Paramecium. *J Membr Biol,* 139**,** 203-13.

PRESTON, R. R. & KUNG, C. 1994b. Isolation and characterization of paramecium mutants defective in their response to magnesium. *Genetics,* 137**,** 759-69.

RHOADS, D. E. & KANESHIRO, E. S. 1979. Characterizations of Phospholipids from Paramecium-Tetraurelia Cells and Cilia. *Journal of Protozoology,* 26**,** 329-338.

SASNER, J. M. & VANHOUTEN, J. L. 1989. Evidence for a Paramecium Folate Chemoreceptor. *Chemical Senses,* 14**,** 587-595.

SATOW, Y. 1978. Internal calcium concentration and potassium permeability in Paramecium. *J Neurobiol,* 9**,** 81-91.

SATOW, Y. & KUNG, C. 1976. A 'TEA+-insensitive' mutant with increased potassium conductance in Paramecium aurelia. *J Exp Biol,* 65**,** 51-63.

STEWART, A. P., SMITH, G. D., SANDFORD, R. N. & EDWARDSON, J. M. 2010. Atomic force microscopy reveals the alternating subunit arrangement of the TRPP2-TRPV4 heterotetramer. *Biophys J,* 99**,** 790-7.

TSIOKAS, L., ARNOULD, T., ZHU, C., KIM, E., WALZ, G. & SUKHATME, V. P. 1999. Specific association of the gene product of PKD2 with the TRPC1 channel. *Proc Natl Acad Sci U S A,* 96**,** 3934-9.

TSIOKAS, L., KIM, E., ARNOULD, T., SUKHATME, V. P. & WALZ, G. 1997. Homo- and heterodimeric interactions between the gene products of PKD1 and PKD2. *Proc Natl Acad Sci U S A,* 94**,** 6965-70.

VALENTINE, M. S., RAJENDRAN, A., YANO, J., WEERARATNE, S. D., BEISSON, J., COHEN, J., KOLL, F. & VAN HOUTEN, J. 2012. Paramecium BBS genes are key to presence of channels in Cilia. *Cilia,* 1**,** 16.

VAN HOUTEN, J. 1979. Membrane potential changes during chemokinesis in Paramecium. *Science,* 204**,** 1100-3.

VAN HOUTEN, J. L., YANG, W. Q. & BERGERON, A. 2000. Chemosensory signal transduction in paramecium. *J Nutr,* 130**,** 946S-9S.

WILSON, P. D. 2004. Polycystic kidney disease. *N Engl J Med,* 350**,** 151-64.

WRIGHT, M. V. & VAN HOUTEN, J. L. 1990. Characterization of a putative Ca2(+)-transporting Ca2(+)-ATPase in the pellicles of Paramecium tetraurelia. *Biochim Biophys Acta,* 1029**,** 241-51.

YANG, Y., COCHRAN, D. A., GARGANO, M. D., KING, I., SAMHAT, N. K., BURGER, B. P., SABOURIN, K. R., HOU, Y., AWATA, J., PARRY, D. A., MARSHALL, W. F., WITMAN, G. B. & LU, X. 2011. Regulation of flagellar motility by the conserved flagellar protein CG34110/Ccdc135/FAP50. *Mol Biol Cell,* 22**,** 976-87.

YOSHIBA, S., SHIRATORI, H., KUO, I. Y., KAWASUMI, A., SHINOHARA, K., NONAKA, S., ASAI, Y., SASAKI, G., BELO, J. A., SASAKI, H., NAKAI, J., DWORNICZAK, B., EHRLICH, B. E., PENNEKAMP, P. & HAMADA, H. 2012. Cilia at the node of mouse embryos sense fluid flow for left-right determination via Pkd2. *Science,* 338**,** 226-31.

ZAGULSKI, M., NOWAK, J. K., LE MOUEL, A., NOWACKI, M., MIGDALSKI, A., GROMADKA, R., NOEL, B., BLANC, I., DESSEN, P., WINCKER, P., KELLER, A. M., COHEN, J., MEYER, E. & SPERLING, L. 2004. High coding density on the largest Paramecium tetraurelia somatic chromosome. *Curr Biol,* 14**,** 1397-404.

ZHANG, P., LUO, Y., CHASAN, B., GONZALEZ-PERRETT, S., MONTALBETTI, N., TIMPANARO, G. A., CANTERO MDEL, R., RAMOS, A. J., GOLDMANN, W. H., ZHOU, J. & CANTIELLO, H. F. 2009. The multimeric structure of polycystin-2 (TRPP2): structural-functional correlates of homo- and hetero-multimers with TRPC1. *Hum Mol Genet,* 18**,** 1238-51.

ZHANG, Z. R., CHU, W. F., SONG, B., GOOZ, M., ZHANG, J. N., YU, C. J., JIANG, S., BALDYS, A., GOOZ, P., STEELE, S., OWSIANIK, G., NILIUS, B., KOMLOSI, P. & BELL, P. D. 2013. TRPP2 and TRPV4 form an EGF-activated calcium permeable channel at the apical membrane of renal collecting duct cells. *PLoS One,* 8**,** e73424.

Table 3.I. Changes in membrane potential (ΔV_m) for ciliated cells in 0.5 mM $MgCl_2$ + 1 mM KCl compared to 1 mM KCl and results for Mg^{2+}-induced behavior of the cells in Mg/TEA.

	0.5 mM $MgCl_2$ + 1 mM KCl, mV (N)	Mg^{2+}-induced behavior
ΔV_m , wild type	**9.8 ± 1.6 (5)^**	**Normal**
ΔV_m , XntA1 mutant	**1.2 ± 2.2 (7)****	**None**
ΔV_m , wild type *XNTA* RNAi	**4.7 ± 4.9 (7)***	**Reduced**
ΔV_m , wild type *PKD2* RNAi	**6.9 ± 3.4 (9)*,^**	**Reduced**
ΔV_m , wild type expressing FLAG	**10.8 ± 2.8 (6)**	**Normal**
ΔV_m , wild type expressing *PKD2*-FLAG	**20.9 ± 3.2 (6)†**	**Normal**
ΔV_m, XntA1 *PKD2* RNAi	**3.1 ± 1.8 (4)****	**None**
ΔV_m, XntA1 expressing FLAG	**2.0 ± 3.2 (6)****	**None**
ΔV_m, XntA1 expressing *PKD2*-FLAG	**11.9 ± 3.6 (6) ^^**	**Slight reaction**
ΔV_m , wild type *BBS8* RNAi	**12.7 ± 2.4 (6) *, ^^**	**Increased**
ΔV_m, XntA1 *BBS8* RNAi	**6.5 ± 0.8 (3)*,^**	**Slight reaction**

Data are averages ± standard deviation (N) in mV. ΔV_m is calculated by subtracting the resting membrane potential of the cell in 1 mM KCl from the newly established membrane potential in 0.5 mM $MgCl_2$ with 1 mM KCl. Cells were allowed 4 minutes in the solution before V_m was noted, recordings were continuous. * And ** = significantly different compared to wild type cells, $P<0.05$ and $P<0.01$, respectively. ^ And ^^ = significantly different compared to XntA1 mutant cells, $P<0.05$ and $P<0.01$, respectively. †= significantly different from all other cell types listed, $P<0.01$. Mg^{2+}-induced behavior describes the backward swimming phenotype of the cell type in Mg/TEA compared to the appropriate control cells.

Table 3.II. Changes in membrane potential (ΔV_m) for deciliated cells in 0.5 mM $MgCl_2$ + 1 mM KCl compared to 1 mM KCl.

	0.5 mM $MgCl_2$ + 1 mM KCl (mV, N)
ΔV_m , wild type	**17.9 ± 3.8 (5)**
ΔV_m , XntA1 mutant	**15.7 ± 6.8 (8)**
ΔV_m , wild type *XNTA* RNAi	**20.0 ± 7.5 (5)**
ΔV_m , wild type *PKD2* RNAi	**10.3 ± 5.3 (4)***
ΔV_m , wild type expressing FLAG	**17.4 ± 1.7 (5)**
ΔV_m , wild type expressing *PKD2*-FLAG	**23.9 ± 4.7 (7)*,^**
ΔV_m, XntA1 *PKD2* RNAi	**2.9 ± 3.2 (4)**,^^**
ΔV_m, XntA1 expressing FLAG	**14.0 ± 1.5 (4)**
ΔV_m, XntA1 expressing *PKD2*-FLAG	**16.0 ± 4.0 (4)**
ΔV_m , wild type *BBS8* RNAi	**20.3 ± 4.2 (4)**
ΔV_m, XntA1 *BBS8* RNAi	**10.1 ± 3.4 (6)***

Data are averages ± standard deviation (N) in mV. ΔV_m is calculated by subtracting the resting membrane potential of the cell in 1 mM KCl from the newly established membrane potential in 0.5 mM $MgCl_2$ with 1 mM KCl. Cells were allowed 4 minutes in the solution before V_m was noted, recordings were continuous. * And ** = significantly different compared to wild type cells, $P<0.05$ and $P<0.01$, respectively. ^ And ^^ = significantly different compared to XntA1 mutant cells, $P<0.05$ and $P<0.01$, respectively.

Figure 3.1. Depletion of *PKD2* results in a phenotype similar to XntA1 mutant cells.(A) Backward swimming times of wild type cells fed the control RNAi vector (L4440), depleted in *PKD2*, *XNTA* or both *PKD2* and *XNTA* in Mg/TEA solution. Data are averages ± standard error of the mean (SEM), N=60 to 77 cells in at least 3 separate experiments. Asterisks indicate significance compared to the control-fed cells ($P<0.001$, Mann-Whitney U test) and caret with line indicates the *PKD2* depleted cells showed longer backward swimming compared to the single depleted *XNTA* cells and the double depleted *PKD2* + *XNTA* cells ($P<0.001$, Mann-Whitney U test). **(B)** Percent of wild type cells fed L4440 (control) or depleted in *PKD2* or *XNTA* or XntA1 mutants still swimming in 100 μM $NiCl_2$ over time. Data points are average number of cells swimming compared to the starting number of cells in each depression ± SEM. Data are 3 depressions per experiment, at minimum 3 experiments (9 to 21 counts per time point per cell type). Significance is seen at and after 90 minutes (asterisk over the line) when compared to the control cells (ANOVA, multiple comparison test, $P<0.05$ at minimum). Time points at and after 150 minutes are $P<0.001$ (ANOVA, multiple comparison test).

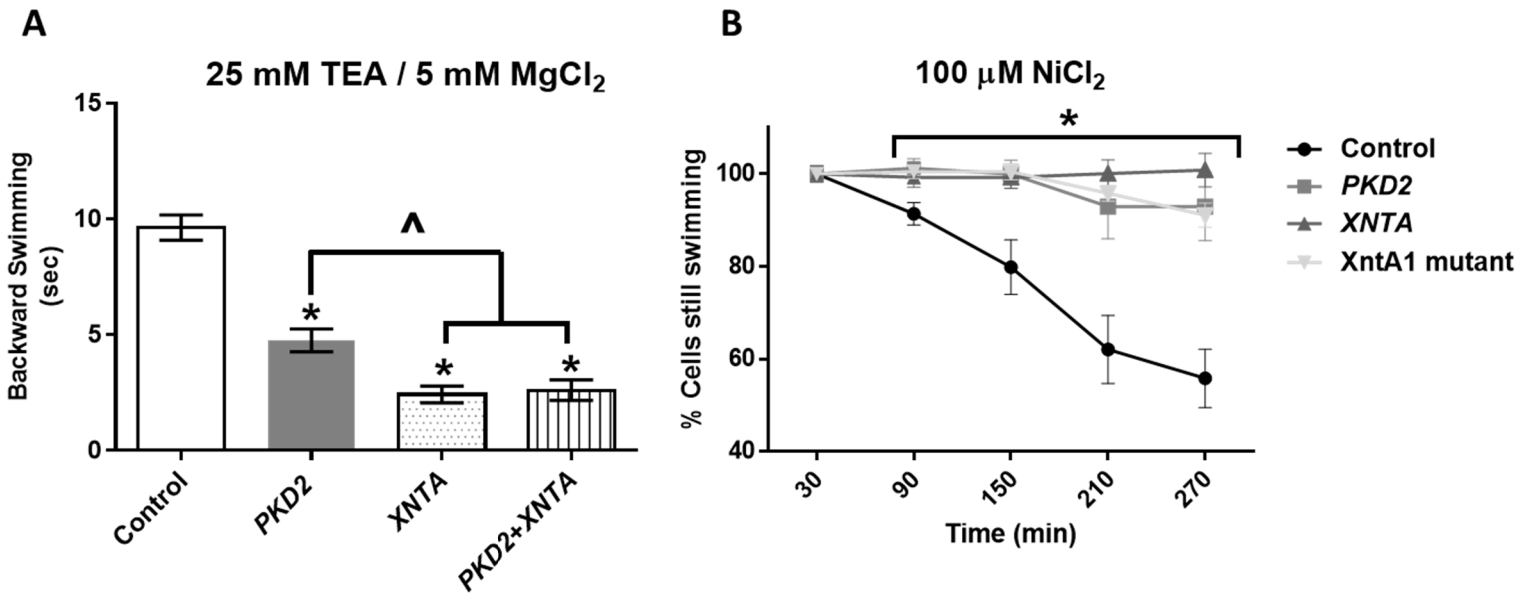
A
25 mM TEA / 5 mM MgCl2
Backward Swimming (sec)
15
10
5
0
*
*
*
^
Control
PKD2
XNTA
PKD2+XNTA
B
100 μM NiCl2
% Cells still swimming
100
80
60
40
*
30
90
150
210
270
Time (min)
Control
PKD2
XNTA
XntA1 mutant

Figure 3.2. Over-expression of FLAG-tagged genes and the effect on Mg^{2+}-induced behavior in wild type and XntA1 mutant cells. XntA1 mutants and wild type cells over-expressing *PKD2*-FLAG or *XNTA*-FLAG or the control plasmid (FLAG) were observed for backward swimming in Mg/TEA. All data seconds ± standard error of the mean, N=30 to 165. An asterisk over a bar indicates significant differences between samples (ANOVA, multiple T-tests, $P<0.001$). Caret indicates the wild type cells expressing FLAG-*PKD2* swim backward for significantly less time compared to all other cell types except the XntA1 mutants expressing *PKD2*-FLAG or FLAG. No bar is present for the XntA1 mutants expressing FLAG because these cells do not react to solutions with Mg^{2+}. Actual backward swimming times (sec) ± SD and sample sizes (N) are shown in the table on the right.

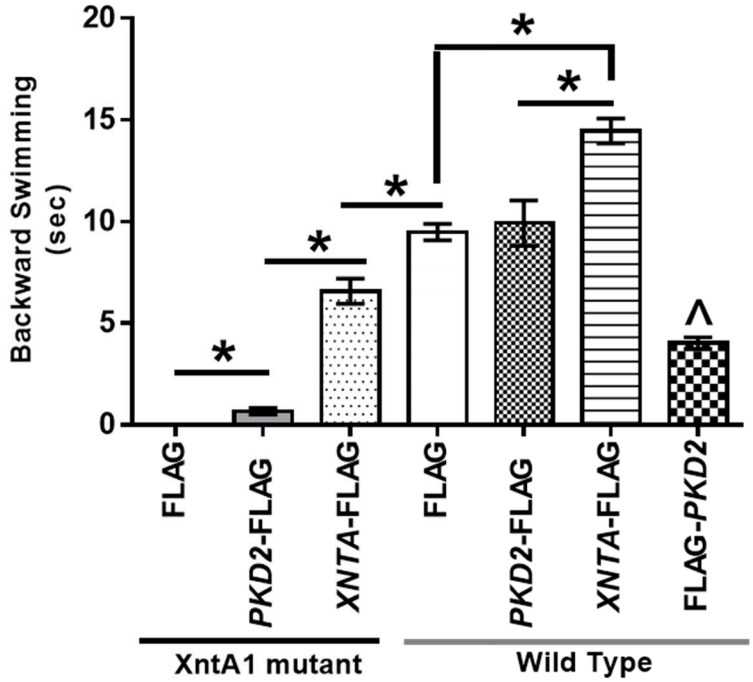

Cell Type	Expression plasmid	Backward swimming time (sec ± SD, N)
XntA1 mutant	FLAG	0±0, N=30
	PKD2-FLAG	0.7 ± 1.2, N=60
	XNTA-FLAG	6.6 ± 4.8, N=60
Wild Type	FLAG	9.5 ± 5.2, N=165
	PKD2-FLAG	9.9 ± 6.0, N=30
	XNTA-FLAG	14.5 ± 5.4, N=78
	FLAG-*PKD2*	4.0 ± 3.12, N=127

Figure 3.3. Immunoprecipitations of Pkd2-FLAG and XntA-myc from cell membrane (CM) and whole cilia (WC). Proteins were isolated from solubilized cell membrane (CM) or whole cilia (WC) of test cells (T) expressing (A) *PKD2*-FLAG or (B) *XNTA*-myc and the respective controls cells (C) expressing FLAG or myc. Blots were developed using Anti-FLAG (A, top panel; Pkd2-FLAG) or Anti-myc (B, center panel; XntA-myc). A representative set of tubulin loading controls (C, Anti-tubulin, bottom panel) is included. **(A)** Anti-FLAG identified bands for Pkd2-FLAG (black arrows) at 120 kD (WC only), 98 kD and 70 kD (both WC and CM) and 55 kD (CM only). The expected size of Pkd2-FLAG is 100 kD. **(B)** Anti-myc identified bands for XntA-myc (center panel, grey arrows) at 62 kD, which is the expected size of XntA-myc (61.5 kD). Anti-myc identified smaller fragments of XntA-myc at 46 kD (CM IP) and 37-38 kD (both CM and WC IPs). The robust bands in the WC IP at ~55 kD which are present in both the C and T lane for XntA-myc are antibody heavy chain; the IP and immunoblot were both done using primary antibodies produced in rabbit, and therefore should be ignored.

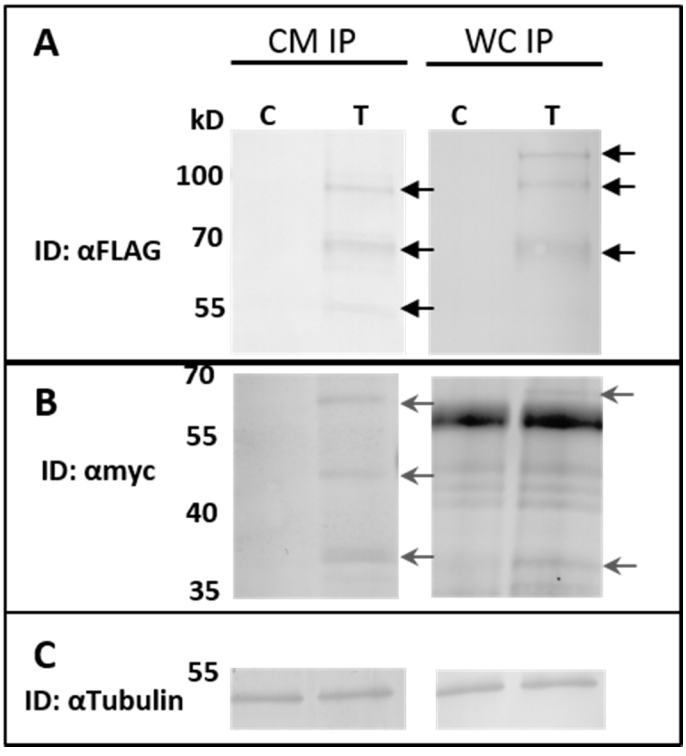

Figure 3.4. Immunolocalization of Pkd2-FLAG and XntA-FLAG in wild type cells and XntA1 mutants. Wild type **(A)** or XntA1 mutants **(B)** expressing FLAG (control cells, top row), *PKD2*-FLAG (center row) or *XNTA*-FLAG (bottom row). Centrin, shown in green, localizes the basal bodies and is a sub-cell membrane marker. FLAG staining can be seen in red. Also included is the merge image. Small amounts of non-specific FLAG staining can be seen in the control cells expressing FLAG. Scale bars are 15 μm; these cells are representative images of the population.

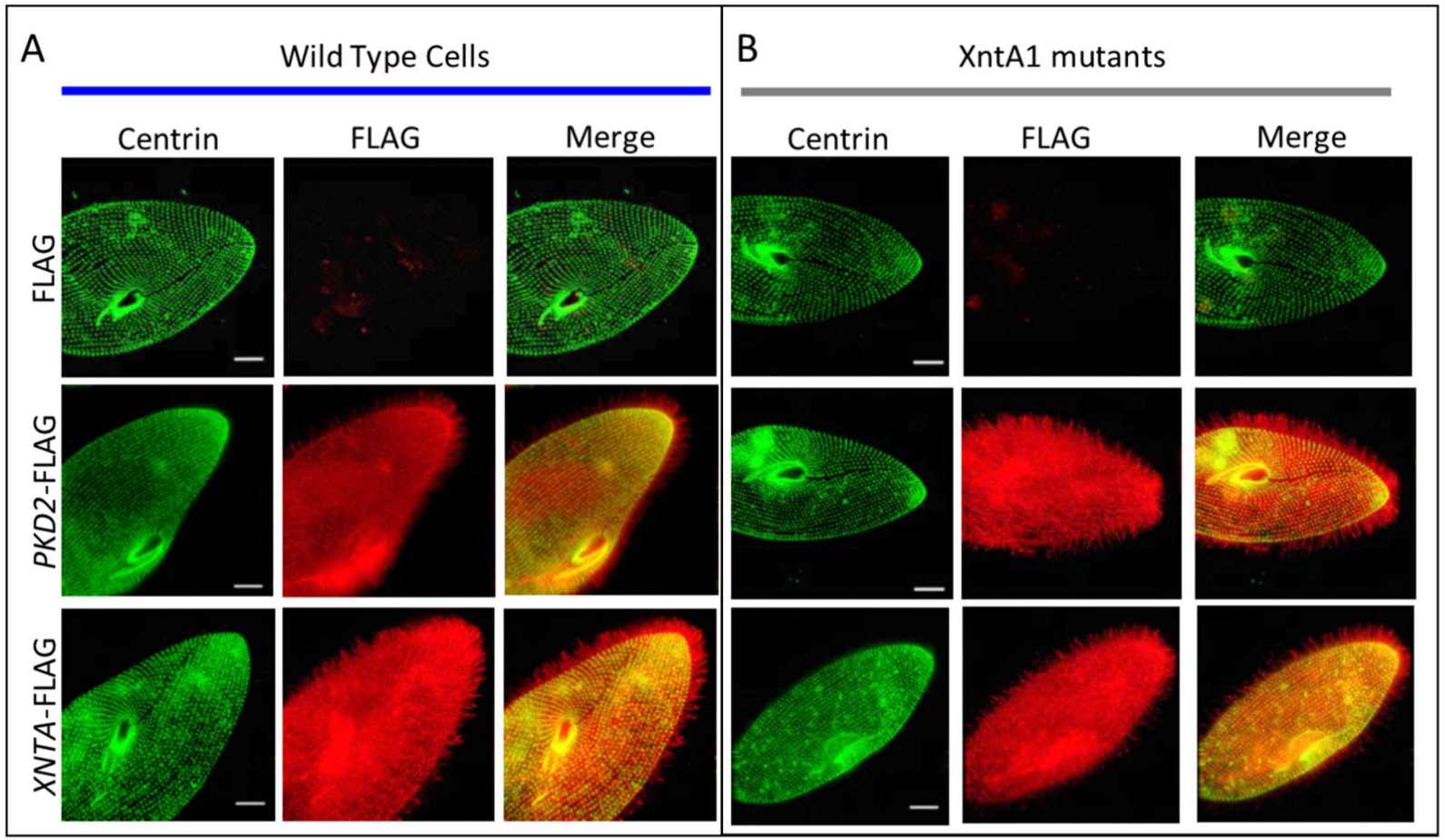
A
Wild Type Cells
B
XntA1 mutants
Centrin
FLAG
Merge
Centrin
FLAG
Merge
FLAG
PKD2-FLAG
XNTA-FLAG

Figure 3.5. Immunofluorescence of wild type cells expressing *PKD2*-FLAG or *XNTA*-FLAG depleted in *XNTA* or *PKD2*, respectively. Wild type cells expressing FLAG, *PKD2*-FLAG or *XNTA*-FLAG were fed the empty RNAi vector, L4440 (control) or were depleted in *XNTA* (*PKD2*-FLAG expressing cells) or *PKD2* (*XNTA*-FLAG expressing cells). Anti-FLAG (red) shows expressed proteins (Pkd2-FLAG or XntA-FLAG); Anti-centrin (green) marks the basal bodies just below the cell surface. Images are stacks of 20 to 30 Z sections (~ 10 to 15 μm thick), cells shown are representative of the population. Scale bars are 15 μm. Before immunostaining, cells were tested for Mg^{2+}-induced behavior in Mg/TEA to examine efficacy of RNAi. Graphs for each cell type are shown below images. Columns indicate average backward swimming time in seconds ± SEM, N=45 to 105 cells. Asterisk indicates significantly shorter backward swimming compared to the control cells (T-test, $P<0.01$).

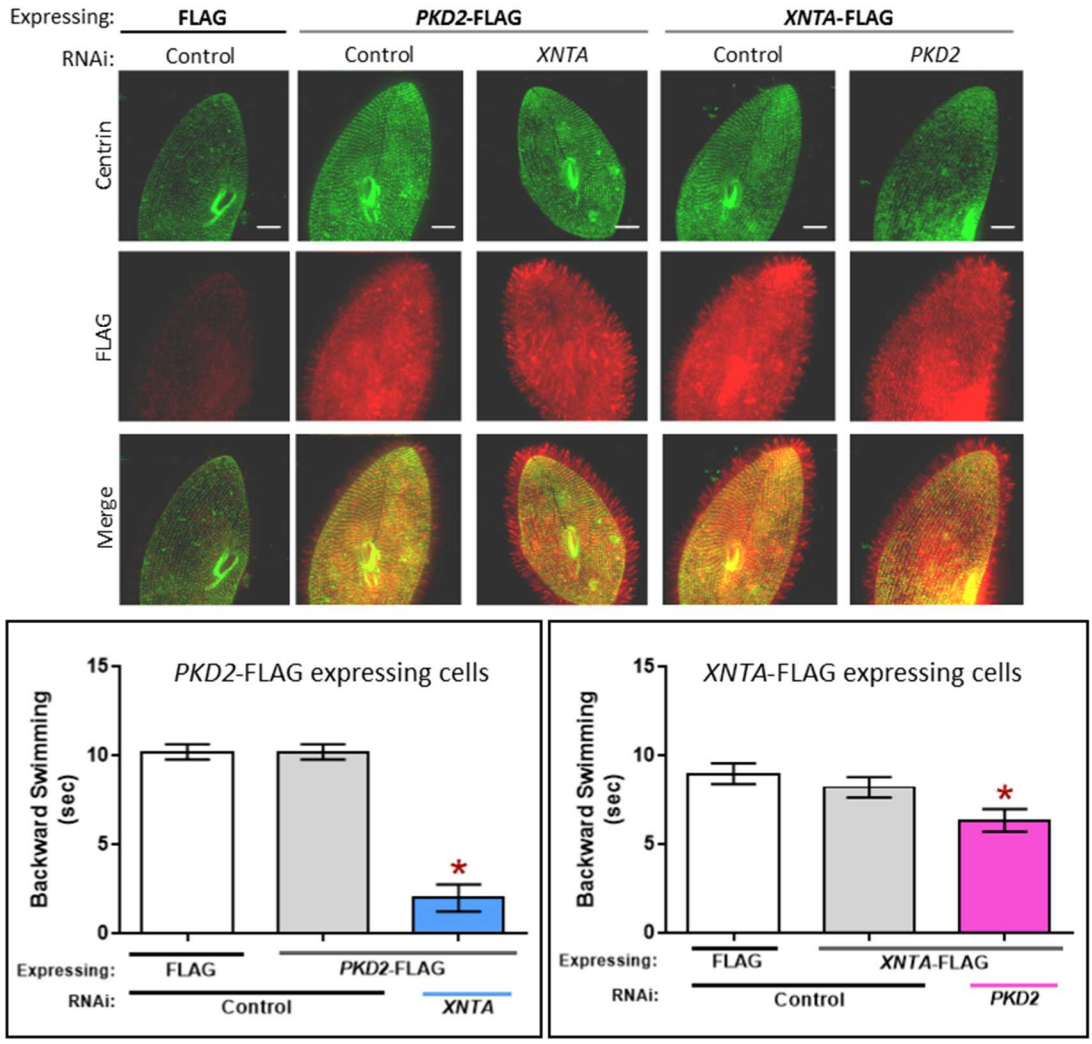
Expressing:
FLAG
PKD2-FLAG
XNTA-FLAG
RNAi:
Control
Control
XNTA
Control
PKD2
Centrin
FLAG
Merge
PKD2-FLAG expressing cells
Backward Swimming (sec)
15
10
5
0
*
Expressing:
FLAG
PKD2-FLAG
RNAi:
Control
XNTA
XNTA-FLAG expressing cells
Backward Swimming (sec)
15
10
5
0
*
Expressing:
FLAG
XNTA-FLAG
RNAi:
Control
PKD2

Figure 3.6. Depletion of *BBS8* shows Pkd2-FLAG is present at the cell surface in the cell membrane but is absent from the cilia. Cells expressing FLAG were fed the empty RNAi vector L4440 (negative control) and cells expressing *PKD2*-FLAG were fed L4440 (positive control) or were depleted in *BBS8* (test cells). Type of RNAi and plasmid being expressed are shown below the blots. Cell membranes **(A)** or whole cilia **(B)** were isolated, solubilized and used for IP. Blots were developed with Anti-FLAG using alkaline phosphatase (A) or enhanced chemiluminescence (B). Black arrows indicate Pkd2-FLAG protein from cell membrane (A) test cells (~120, 100, and 70 kD) depleted in *BBS8*. Tubulin loading controls are present below indicating equal amounts of protein were solubilized before IP. Cells were tested for Mg^{2+}-induced behavior to test the efficacy of the RNAi. Cells isolated for the cell membrane or whole cilia showed longer backward swimming compared to the negative control cells as expected in Na/TEA and Mg/TEA (asterisk: T-test, $P<0.01$).

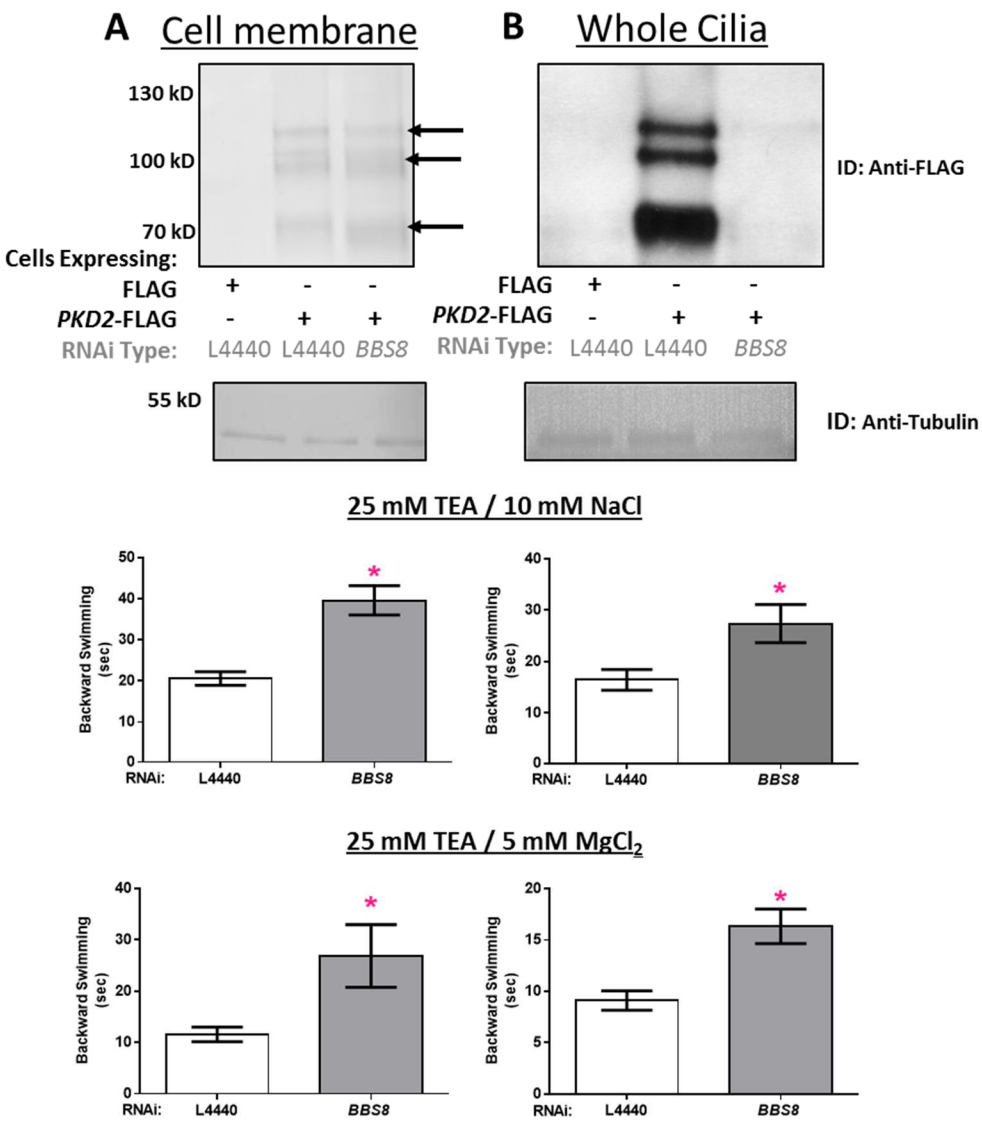
A Cell membrane
B Whole Cilia
130 kD
100 kD
70 kD
Cells Expressing:
FLAG + - -
PKD2-FLAG - + +
RNAi Type: L4440 L4440 BBS8
ID: Anti-FLAG
55 kD
ID: Anti-Tubulin
25 mM TEA / 10 mM NaCl
Backward Swimming (sec)
RNAi: L4440 BBS8
25 mM TEA / 5 mM MgCl2

Figure 3.7. The XntA-myc protein can co-IP Pkd2-FLAG from solubilized cell membrane (A) and whole cilia (B). Isolated cell membrane **(A)** or whole cilia **(B)** were solubilized for IP from cells expressing *PKD2*-FLAG and *XNTA*-myc (TEST) or the FLAG and myc epitopes (control). The resulting immunoblots were probed for the FLAG epitope (upper blots, Pkd2-FLAG, black arrows) followed by stripping the blots and probing for the myc epitope (lower blots, XntA-myc, grey arrows). The myc IP from both cell membrane and cilia show the heavy chain of the antibody at 50 kD (blots and IP were performed using antibody produced in rabbit.) IP for Pkd2-FLAG did not produce XntA-myc (Anti-myc blots, lower blots in A and B, left side.) IP for XntA-myc produced the Pkd2-FLAG protein in both the cell membrane and the cilia (upper right blots in both A and B.) Below are tubulin loading controls, samples were removed before solubilization to demonstrate TEST and control samples had approximately equal concentrations of proteins before solubilization.

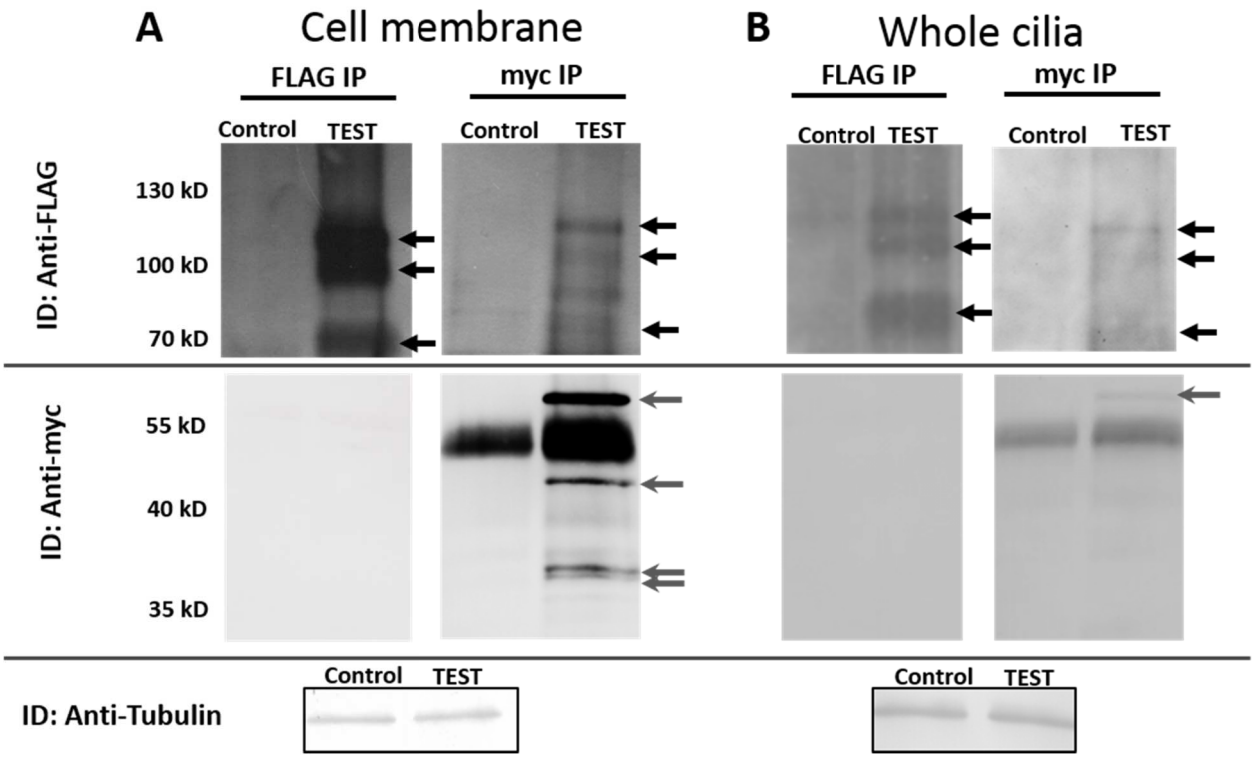
A
Cell membrane
B
Whole cilia
FLAG IP
myc IP
FLAG IP
myc IP
Control
TEST
Control
TEST
Control
TEST
Control
TEST
ID: Anti-FLAG
130 kD
100 kD
70 kD
ID: Anti-myc
55 kD
40 kD
35 kD
Control
TEST
Control
TEST
ID: Anti-Tubulin

Figure 3.8. Types of proteins identified in IPs for Pkd2-FLAG from cell membrane and cilia using LC-MS/MS. A total of 89 unique proteins were identified in three separate experiments. A breakdown of the proteins identified in the three preparations can be seen in the Venn diagram in **(A)**. The one peptide identified in all three preparations was Pkd2. The types of proteins identified in the cell membrane IP **(B)** and whole cilia IPs **(C)** are included. Two cilia Pkd2-FLAG IPs using different buffers were combined to create the chart for cilia (C). Including Pkd2, 31 proteins were identified in the cell membrane IP and 69 proteins were identified in the two cilia IPs. A complete list of the identified proteins can be seen in Supplement Table II.

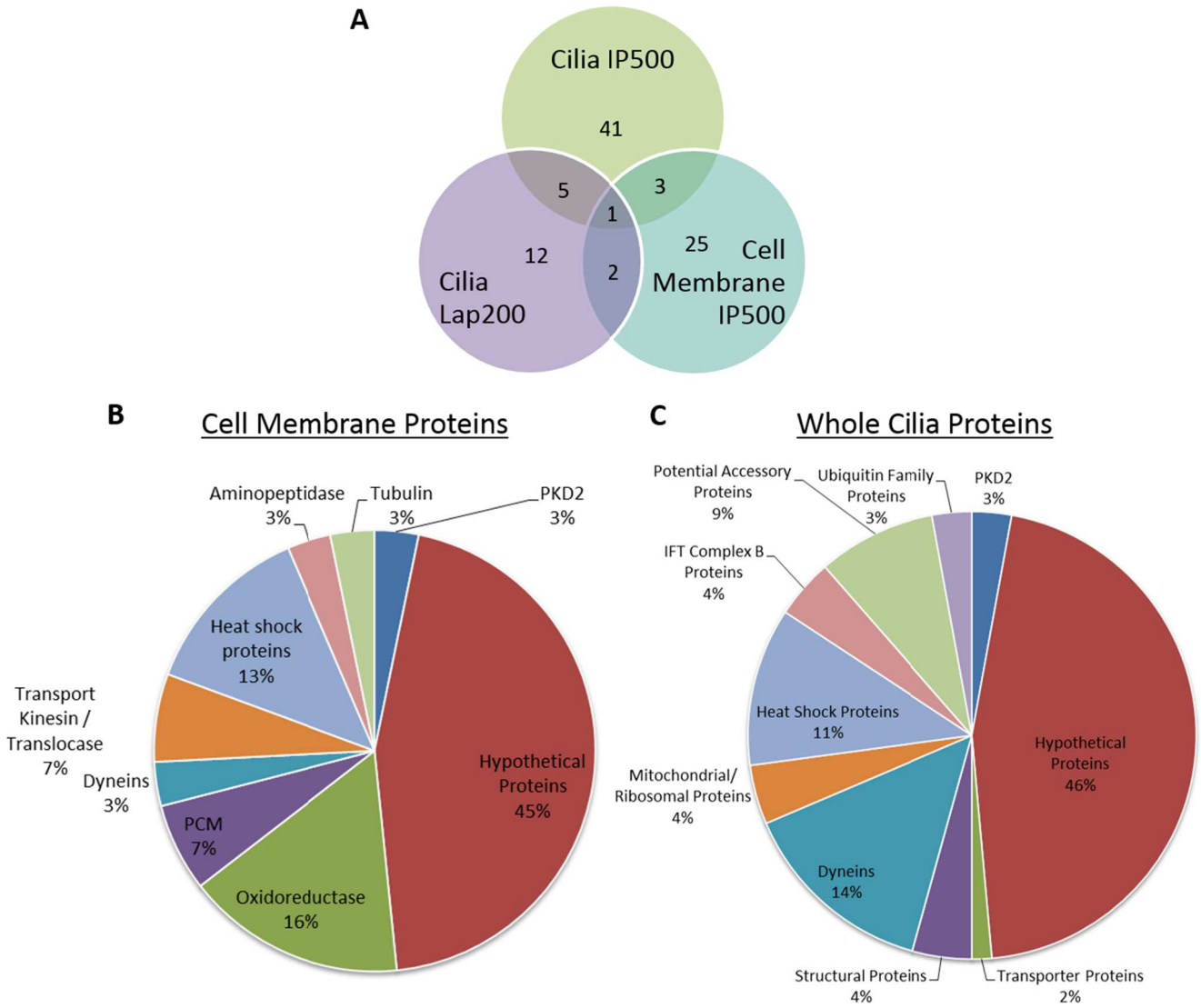
A
Cilia IP500
41
5
3
1
12
25
Cell
Membrane
IP500
Cilia
Lap200
2
B
Cell Membrane Proteins
Aminopeptidase
3%
Tubulin
3%
PKD2
3%
Heat shock
proteins
13%
Transport
Kinesin /
Translocase
7%
Dyneins
3%
PCM
7%
Oxidoreductase
16%
Hypothetical
Proteins
45%
C
Whole Cilia Proteins
Potential Accessory
Proteins
9%
Ubiquitin Family
Proteins
3%
PKD2
3%
IFT Complex B
Proteins
4%
Heat Shock Proteins
11%
Mitochondrial/
Ribosomal Proteins
4%
Dyneins
14%
Hypothetical
Proteins
46%
Structural Proteins
4%
Transporter Proteins
2%

Figure 3.9. Changes in membrane potential for ciliated (A) and deciliated (B) cells. Data are presented as average mV ± SEM (N are between 3 and 7 for each cell type). ΔV_m were obtained by comparing the resting membrane potential of the cells in the control solution of 1 mM KCl compared to the newly established membrane potential in the test solution of 0.5 mM $MgCl_2$ with 1 mM KCl. Some data sets are repeated on the graphs for comparison. Wild type is abbreviated WT and XntA1 mutant is XntA1. RNAi depletion (*PKD2, XNTA, BBS8*) follows the cell type or the gene being over-expressed (*PKD2*-FLAG or FLAG). Asterisk with bars indicates statistical significance (at least $P<0.05$, T-test). Caret indicates statistically different compared to all other cell types, $P<0.01$, T-test, except in the case of the deciliated cells. (The deciliated WT cells expressing *PKD2*-FLAG do not depolarize more than the WT cells depleted in *BBS8*.) All ΔV_m's for these cell types, both ciliated and deciliated, are shown in Table I and Table II, respectively.

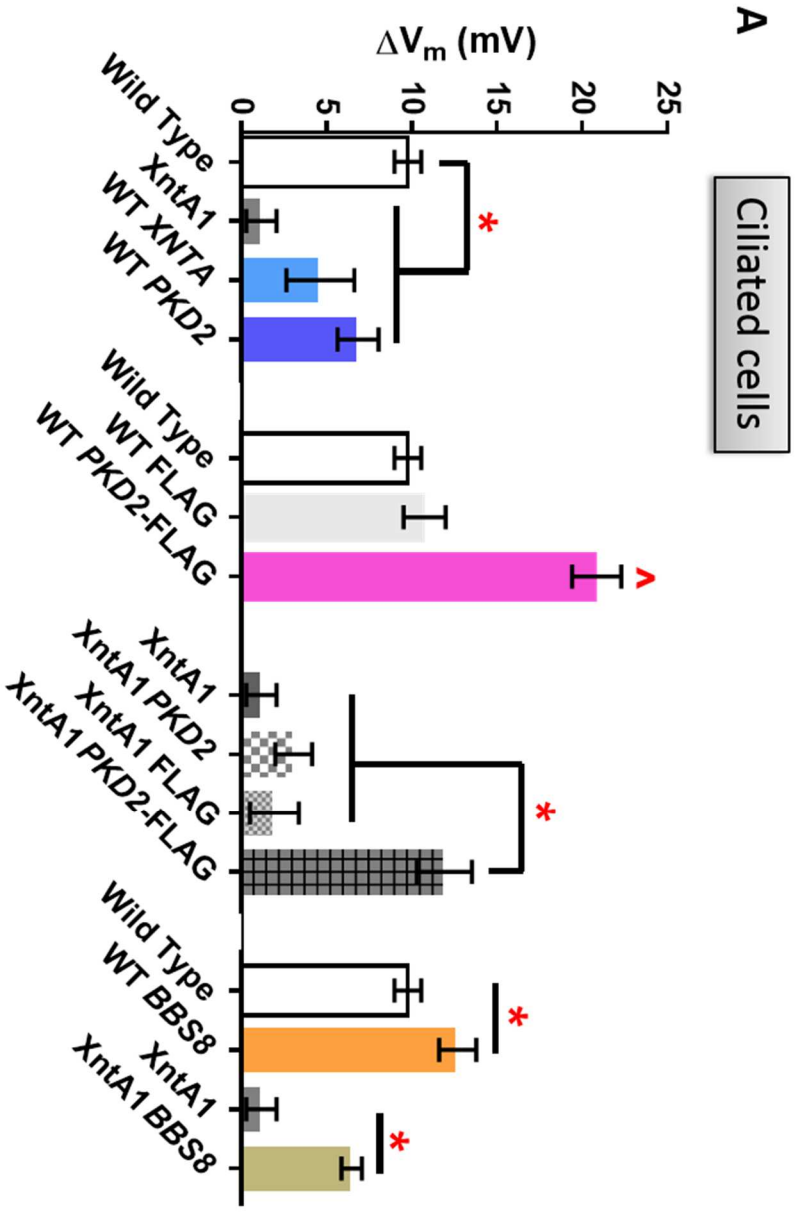
A
Ciliated cells
ΔVm (mV)
0
5
10
15
20
25
Wild Type
XntA1
WT XNTA
WT PKD2
Wild Type
WT FLAG
WT PKD2-FLAG
XntA1
XntA1 PKD2
XntA1 FLAG
XntA1 PKD2-FLAG
Wild Type
WT BBS8
XntA1
XntA1 BBS8
*
*
*
*
>

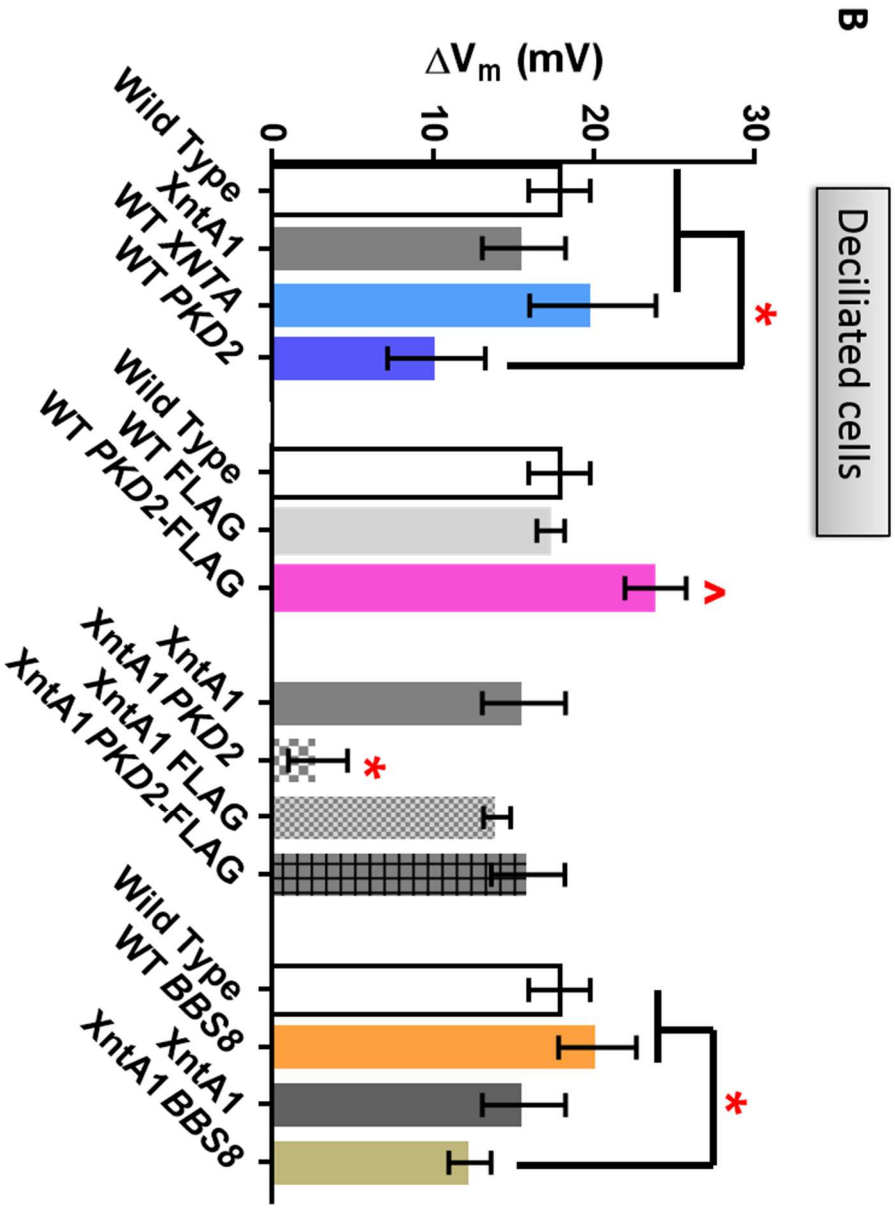
B
Deciliated cells
ΔVm (mV)
0
10
20
30
Wild Type
XntA1
WT XNTA
WT PKD2
Wild Type
WT FLAG
WT PKD2-FLAG
XntA1
XntA1 PKD2
XntA1 FLAG
XntA1 PKD2-FLAG
Wild Type
WT BBS8
XntA1
XntA1 BBS8
*
*
*

Figure 3.10. Summary of findings from electrophysiology. A summary of our findings from membrane potential recordings of ciliated and deciliated cells in 1 mM KCl solution with and without 0.5 mM $MgCl_2$. The cell type is described and depicted with proteins present, absent, or depleted. Deciliated cell results are summarized in the boxed out area. Changes in depolarization can be seen to the right of each image showing increases or decreases in membrane permeability to Mg^{2+}. Ciliated XntA1 mutants and deciliated XntA1 mutants depleted in *PKD2* show almost no membrane permeability to Mg^{2+}, shown by a straight line. Our conclusions (blue box) are that the concentration of the Pkd2 channel in the cell membrane and ciliary membrane and the presence or absence of the cilia and XntA protein impact the permeability of the Pkd2 channel. These data summarize our findings and support our proposal of the *Paramecium* Pkd2 channel being responsible for membrane Mg^{2+} permeability.

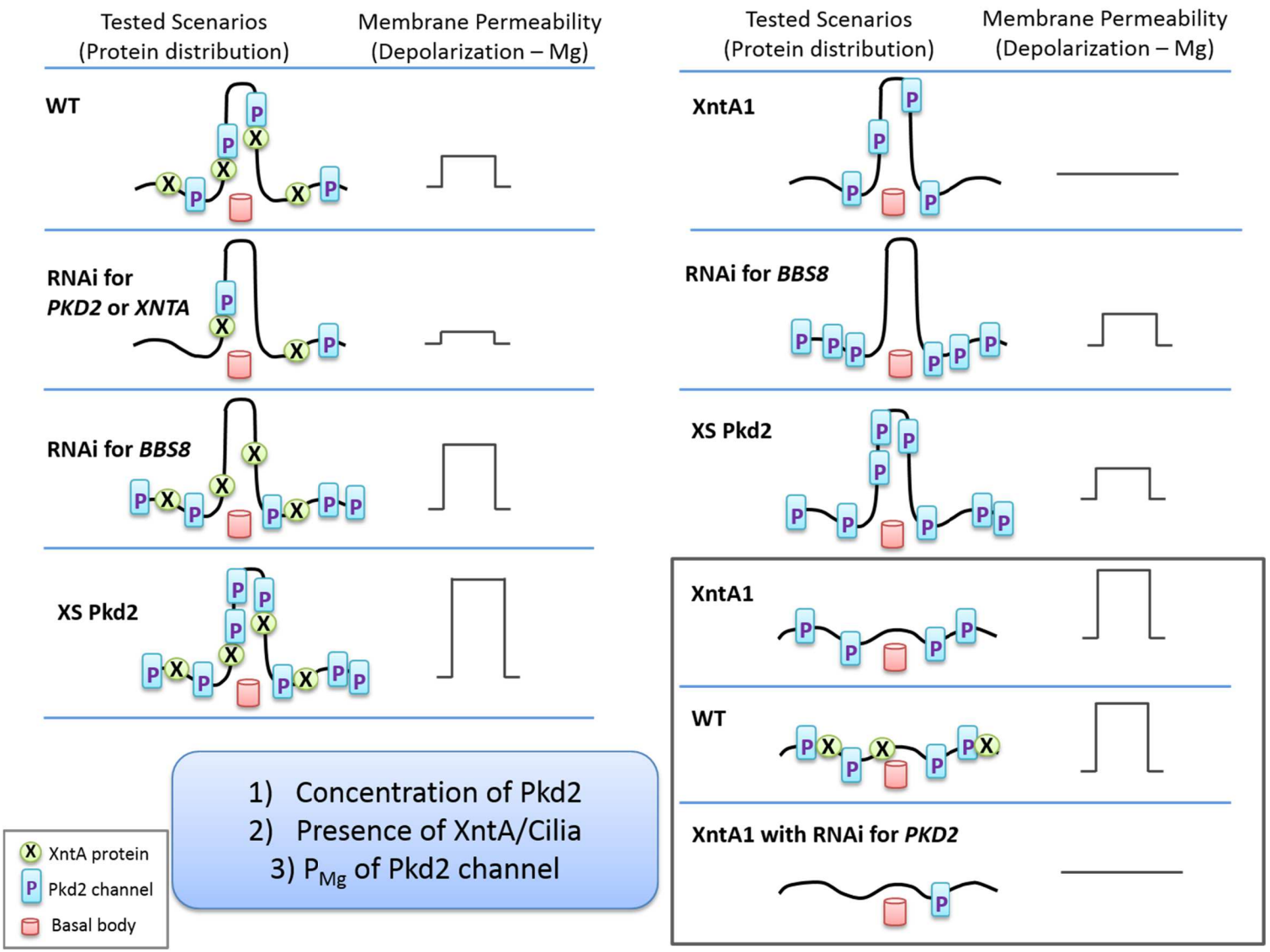
Tested Scenarios (Protein distribution)
Membrane Permeability (Depolarization – Mg)
WT
RNAi for PKD2 or XNTA
RNAi for BBS8
XS Pkd2
XntA1
RNAi for BBS8
XS Pkd2
XntA1
WT
XntA1 with RNAi for PKD2
X XntA protein
P Pkd2 channel
Basal body
1) Concentration of Pkd2
2) Presence of XntA/Cilia
3) P_{Mg} of Pkd2 channel

Supplement Table 3.I. Normalized backward swimming in ionic stimuli of different depleted cells.

	30 mM KCl	25 mM TEA / 10 mM NaCl	25 mM TEA / 5 mM $MgCl_2$
Control	100% ± 20.99% (107)	100% ± 35.52% (103)	100% ± 57.63% (102)
PKD2	86.18% ± 31.35% (61)	92.25% ± 32.21% (63)	**46.42% ± 36.42% (68) ***
XNTA	**120.13% ± 33.72% (62)***	81.74% ± 37.03% (62)	**25.05% ± 30.0% (66)***
XntA1 mutant	**284.24% ± 51.48% (60)***	**33.35% ± 11.68% (40)***	**0 ± 0% (65)***

Asterisk indicates statistically significant, Students T-Test (P<0.001) compared to the control cells. Bold red indicates shorter than the control cells and bold blue indicates longer than the control cells.

Supplement Table 3.II. Pkd2-FLAG co-IP proteins from two whole cilia IP's and one cell membrane IP

Cell Membrane IP500 Buffer

				# Peptides Found	
Protein ID*	**Protein Description**	**Mol. Mass**	**Predicted TM domains**	**Control**	**TEST**
G_00005599001	**PKD2**	**99 kD**	**6**	**0**	**14**
G_00004235001	Hypothetical Protein - huge extracellular domain	436 kD	1	0	14
G_00002466001	Hypothetical Protein - cell adhesion	110 kD	0	0	3
G_00002468001	Hypothetical Protein - concanavalin-A like lectin	530 kD	0	0	3
G_00006905001	Hypothetical Protein	136 kD	1	0	3
G_00032017001	Hypothetical Protein	143 kD	0	0	4
G_00029381001	Hypothetical Protein - ER to Golgi transport Kinesin	116 kD	0	0	3
G_00029949001	Dynein heavy chain	215 kD	0	0	2
G_00020020001	2-oxoglutarate dehydrogenase	113 kD	0	0	2
G_00006583001	2-oxoglutarate dehydrogenase	115 kD	0	0	2
G_00019968001	Alanyl aminopeptidase	112 kD	1	0	2
G_00027959001	Hsp70Pt08	72 kD	0	0	30
P_4000011001	Hsp70Pt07	72 kD	0	0	14
P_3300001001	Hsp70Pt01	72 kD	0	0	15
P_14200002001	PCM2 (*Paramecium* CaM-binding membrane-bound protein 2)	70 kD	0	0	2
G_00021676001	Hsp70	72 kD	0	0	2
G_00035998001	Succinate dehydrogenase	70 kD	0	0	2
G_00006368001	Hypothetical Protein - Nucleotide binding	56.8 kD	0	0	2
G_00012178001	Hypothetical Protein - possible protein peptidase M16 family	52.5 kD	0	0	2
G_00029566001	PCM1 (Paramecium CaM-binding membrane-bound protein 1)	70.5 kD	0	0	2
G_00006971001	Hypothetical Protein	42.7 kD	1	0	2
G_00013616001	Glyceraldehyde 3-phosphate dehydrogenase	39.8 kD	0	0	2
G_00012836001	Hypothetical Protein	43.5 kD	1	0	2
G_00023050001	Isocitrate dehydrogenase	37.6 kD	0	0	2

G_00036831001	Tubulin beta-1 chain	49.5 kD	0	0	3
G_00012123001	Hypothetical Protein	31.4 kD	0	0	2
G_00030389001	Hypothetical Protein	23.5 kD	0	0	3
G_00032183001	Hypothetical Protein	21.7 kD	1	0	2
G_00032072001	Hypothetical Protein	22.5 kD	2	0	2
G_00030301001	Hypothetical Protein	27.5 kD	0	0	2
G_00032993001	ADP/ATP translocase	58.8 kD	3	0	2

*Protein ID G_ = ID begins with GSPATP, Protein ID P_ = ID begins with PTETP.

Whole Cilia IP500 Buffer

				# Peptides Found	
Accession #*	**Protein Description**	**Mol. Mass**	**Predicted TM domains**	**Control**	**TEST**
G_00005599001	**PKD2**	**99 kD**	**6**	**0**	**8**
G_00012627001	Hypothetical Protein	437.6 kD	8	0	6
G_00002701001	Dynein Heavy chain protein *(Tetrahymena)*	231.5 kD	0	0	5
G_00017360001	Hypothetical Protein	380.3 kD	0	0	4
G_00038423001	Dynein heavy chain	307.5 kD	0	0	3
G_00038424001	Dynein Heavy chain protein *(Tetrahymena)*	50.8 kD	0	0	3
G_00002700001	Dynein Heavy chain protein family *(Tetrahymena)*	203.5 kD	0	0	3
P_700012001	Ubiquitin Family protein	92 kD	0	0	3
G_00020971001	Hypothetical Protein - ATPase/transposase	10 kD	0	0	3
G_00029949001	Dynein heavy chain family protein	214 kD	0	0	3
G_00008392001	Hypothetical Protein	177 kD	0	0	2
P_1100012001	Ubiquitin Family protein	97.8 kD	0	0	2
G_00001683001	Hypothetical Protein - conserved : coiled-coil domain (possible CG34110)	99 kD	0	0	4
G_00032013001	Hypothetical Protein - TPR domain containing protein	102 kD	0	0	3
G_00022879001	Hypothetical Protein - WD-40 repeats	101 kD	0	0	3
G_00020972001	Hypothetical Protein - ATPase/transposase	10 kD	0	0	2
G_00023151001	Radial spoke protein	80 kD	0	0	2
G_00002137001	Hypothetical Protein	102.5 kD	0	0	3

G_00018639001	Hypothetical Protein	183.8 kD	0	0	3
G_00029488001	Hypothetical Protein	75 kD	0	0	3
G_00030739001	Hypothetical Protein	75 kD	0	0	3
G_00028934001	Hypothetical Protein - Dynein intermediate chain WD-40 repeats	77 kD	0	0	2
G_00006874001	Hypothetical Protein - Adenylate kinase family protein (Tetrahymena)	88.6 kD	0	0	2
G_00006050001	IFT 81	81 kD	0	0	2
G_00007851001	Hypothetical Protein - oxidoreductase	84.8 kD	0	0	2
G_00027959001	HSP 70 pt8	72 kD	0	0	8
P_3300001001	HSP 70	70 kD	0	0	6
G_00022952001	Hypothetical Protein - Dynein Intermediate chain	75.8 kD	0	0	3
P_1200013001	IFT 72/74	67.5 kD	0	0	6
G_00011724001	Hypothetical Protein	70.1 kD	0	0	6
G_00014332001	Hypothetical Protein	68.4 kD	0	0	4
G_00023143001	Hypothetical Protein	69.1 kD	0	0	4
G_00001529001	Hypothetical Protein - contains Leucine rich repeats	59.4 kD	0	0	4
G_00003044001	Hypothetical Protein - outer dynein arm docking protein	65.6 kD	0	0	2
G_00010841001	Hypothetical Protein	11.4 kD	0	0	2
G_00004375001	Hypothetical Protein - flagellar associated protein	60.2 kD	0	0	2
G_00003522001	Fork head domain protein	60.7 kD	0	0	6
P_10600002001	Hypothetical Protein	75.8 kD	0	0	3
G_00010730001	Hypothetical Protein - contains conserved F-box and Leucine rich domain	60.5 kD	0	0	4
G_00005132001	Hypothetical Protein - cation channel family protein in *Tetrahymena*	61 kD	0	0	2
P_10700002001	Hypothetical Protein	76 kD	0	0	2
G_00033046001	IFT52	49.5 kD	0	0	2
G_00020334001	Hypothetical Protein	36.6 kD	0	0	4
P_13700002001	Hsp 40	37.8 kD	0	0	3

P_2700002001	Hypothetical Protein - Hsp40/DnaJ family of proteins	37.3 kD	0	0	2
G_00008057001	Hypothetical Protein - calmodulin or troponin protein	31 kD	0	0	2
G_00033919001	Hypothetical Protein - STOP conserved domain - stabilizes microtubules in neurons	49.1 kD	0	0	4
G_00036831001	Beta tubulin	49.5 kD	0	0	2
G_00008057001	Calmodulin-like protein; EF hand	31 kD	0	0	2
G_00004620001	Hypothetical Protein	26.5 kD	0	0	2

*Protein ID G_ = ID begins with GSPATP, Protein ID P_ = ID begins with PTETP.

Whole Cilia Lap200 Buffer

				# Peptides Found	
Protein ID*	**Protein Description**	**Mol. Mass**	**Predicted TM domains**	**Control**	**TEST**
G_00005599001	**PKD2**	**99 kD**	**6**	0	**13**
P_4000011001	HSP70, isoform 7	72.2 kD	0	0	14
P_10700002001	Hypothetical Protein	76 kD	0	0	9
P_3300001001	Hsp 70	72 kD	0	0	10
P_11000002001	Hsp 70 isoform 9	72 kD	0	0	8
G_00029765001	cytoplasmic dynein, WD-40 domain containing	81.6 kD	0	0	6
G_00024719001	HSP 70 protein, ER-type	30.3 kD	0	0	5
P_1900003001	cytoplasmic dynein, WD-40 domain containing protein	81.5 kD	0	0	3
G_00022677001	Hypothetical Protein - TPR-1 protein	51.8 kD	0	0	3
G_00034717001	Hypothetical Protein	168.1 kD	0	0	2
G_00026329001	Hypothetical Protein - HSP mitochondrial-like	72.2 kD	0	0	2
G_00029566001	PCM1 (*Paramecium* CaM-binding membrane-bound protein 1)	70.5 kD	0	0	2
G_00033610001	Ribosomal protein L4	44.8 kD	0	0	2
G_00012627001	Hypothetical Protein - ABC-transporter	437.5 kD	6 or 8	0	4

G_00034716001	Hypothetical Protein - adhesion/cell membrane (wall) protein	128.3 kD	2	0	2
G_00007851001	Hypothetical Protein - reductase	84.8 kD	0	0	2
G_00021916001	PKAr3-1	43 kD	0	0	2
G_00008057001	Calmodulin-like protein	31 kD	0	0	1
G_00004584001	60s ribosomal protein L7	28.6 kD	0	0	2
G_00017494001	ATP synthase	44 kD	0	0	2

*Protein ID G_ = ID begins with GSPATP, Protein ID P_ = ID begins with PTETP.

Chapter 4: Summary and Future Directions

Summary

The data presented in this work highlight the important contributions of our versatile model organism, *Paramecium tetraurelia* in the understanding of ciliopathy proteins, namely Polycystin-2 (Pkd2) and Meckelin (MKS3). Many of our findings would not have been possible using mammalian cells. Using techniques such as RNAi and electrophysiology, we have uncovered novel and intriguing roles for the proteins MKS3 and Pkd2. We also have a broadened knowledge of the XntA protein, suggesting a role other than a Mg^{2+} channel.

The distorted basal body rows and misshapen cortical units of the *MKS3* depleted cells would not have been visible or easily observed without the highly organized and patterned cell surface of *Paramecium*. Nor would we have been able to observe the misaligned basal bodies and propose the possible second pool of MKS3, important for guiding the daughter basal body along the kinetodesmal fiber. The novel contribution of this second pool of MKS3, important for the attachment and guidance of the basal body along the kinetodesmal fiber, must be investigated further. The involvement of MKS3 and its attachment points must be determined to better understand how the MKS3 protein is contributing in this guidance role.

Our use of electrophysiology and membrane potential recordings of *Paramecium* has shed new light on potential roles for the Pkd2 channel. Our observations of the Pkd2 protein acting as a Mg^{2+} channel are both novel and highlight the importance of a non-canonical research model to elucidate new functions of proteins. The Pkd2 channel is both promiscuous and versatile in mammalian cells, demonstrating that its interactions, function, and location are cell-type specific. Our findings here are no different. We show that the Pkd2 channel behaves and is most likely regulated differently in the cell and ciliary membranes. Also, Pkd2 utilizes different trafficking pathways to reach each membrane. The original findings we contribute from this study may prompt new avenues of investigations of the Pkd2 channel in other cell types. Our study may

also motivate new thinking concerning the contributions of Pkd2 to ciliopathies and human diseases. It is feasible that the Pkd2 channel passes Mg^{2+} in mammalian cells, but because of its established background as a non-selective calcium channel, the potential conductance of Mg^{2+} ions by the mammalian channel may be overlooked.

Our hypothesis that the XntA protein is not the Mg^{2+} channel, but instead is important for stabilizing or regulating Pkd2 in membrane microdomains is supported by other findings in our lab. Recent LC-MS/MS analyses of immunoprecipitations (IPs) of the voltage-gated calcium channels (VGCCs) from the cilia have co-IP'd the XntA protein. If XntA is stabilizing Pkd2 in or recruiting Pkd2 to membrane microdomains, XntA may also be stabilizing or recruiting other channels and proteins in the same domains. In addition, PMCAs 18 and 19 co-IP with the VGCC (Yano, unpublished data). PMCAs are crucial for the removal of calcium from the ciliary space (Saidu et al., 2009) and are expected to help sustain membrane hyperpolarization during chemoattraction (Wright and van Houten, 1990, Wright et al., 1993). The XntA1 mutants are unable to maintain their membrane hyperpolarization in the presence of certain attractants (see Appendix II). Together, these data suggest the possibility that the VGCCs and the PMCAs of the cilia are in membrane microdomains together with the XntA protein. Possibly, XntA is not only stabilizing or regulating Pkd2 in ciliary membrane domains, but also the PMCAs and VGCCs. The cooperation of the PMCAs, XntA, and the VGCCs could be vital to the stabilization and function of these proteins in the control and regulation of membrane potential.

To follow are proposed experiments which would be beneficial to further our knowledge and understanding of the proteins discussed in this study. Up to this point, our findings on XntA, Pkd2 and MKS3 have greatly expanded upon the understanding of the location and function of these proteins in *Paramecium*. The use of our model organism has provided intriguing new roles for MKS3 and Pkd2 which are applicable to mammalian cells. XntA, which is specific

to *Paramecium* and *Tetrahymena*, may have a distant relative with similar functions in mammalian cells, but this potential distant homolog has not yet been identified.

Further expansion on all of the projects presented in this work are either already underway or should be considered for further investigation. A complete understanding of the roles of their proteins, Mks3, Pkd2, and XntA, in *Paramecium* is not nearly complete. Further experiments to uncover the interacting partners and functions would help us to better understand the roles of MKS3, Pkd2, and XntA in human ciliopathies, as well as in our model organism *Paramecium*.

I. Further exploration of *MKS3* in *Paramecium*

The work presented on Meckelin (MKS3) in *Paramecium* has been a long and on-going research focus of our lab. My Master's work was focused on this project, as well as other collaborative efforts continuing over the years since. One re-appearing question which needs further investigation is the second proposed location of the MKS3 protein in *Paramecium*. Although we have published MKS3's first location (Picariello et al., 2014), the second transient pool of MKS3p has not yet been confirmed.

We have demonstrated that the N-terminal FLAG tagged MKS3 protein is located just above the plane of almost every basal body in the cell (Picariello et al., 2014). This location of FLAG-MKS3p above the basal body places it in the transition zone for *Paramecium*, which is in agreement with the localization of MKS3 in mammalian cells (Dawe et al., 2007, Williams et al., 2011, Chih et al., 2012). The transition zone is the area between where the triplet microtubules of the basal body become doublets to where the plate with the central pair of microtubules of the axoneme begins (Dute and Kung, 1978, Aubusson-Fleury et al., 2012, Garcia-Gonzalo et al., 2011).

However, we have not been successful as of yet in the identification of the MKS3 protein in the second proposed location: a transient pool of the protein, which is at or near the attachment point of the daughter basal body to the kinetodesmal fiber (Picariello et al., 2014). There could be many reasons for the difficulty and our lack of success in localizing MKS3p at the transient location near the kinetodesmal fiber.

For starters, we expect the transient pool of MKS3 to be just that; temporary or short-lived. The movement of the daughter basal body away from the mother basal body is not a prolonged event, taking perhaps only a few minutes. A *Paramecium* cell divides approximately every six hours. Of that six hours, the last 30 minutes encompasses the process of binary fission (Ruiz et al., 1987). Before division can begin, all dikinetids (two basal body units) must convert to monokinetids (single basal body units) (Iftode and Fleury-Aubusson, 2003). That is to say that all daughter basal bodies, which are anterior to the mother basal bodies in the anterior-posterior axis of the cell, must move anteriorly, away from their mother basal bodies. Connection points that exist during this migration include the bone node and the foot of the bone node (Iftode and Fleury-Aubusson, 2003). One might expect the location of the proposed transient pool of MKS3p to be located near the foot of the bone node of daughter basal body. The bone node connection point to the striated rootlet is also transient; once the daughter basal body has migrated anteriorly from the mother basal body, the bone node will disappear and the connection to the kinetodesmal fiber will appear (Iftode and Fleury-Aubusson, 2003). The expeditious migration of the daughter basal bodies as well as the short-lived nature of the bone node and foot connections to the kinetodesmal fiber may hamper the identification of the MKS3 protein at this location.

It would be helpful to attempt to "stop time" to capture the cells at just the right time point in their life cycle to obtain images of the transient pool of MKS3p. For starters, our current use of immunofluorescence using the DeltaVision microscopy system would not give appropriate

resolution to detect such a finite and precise location of a protein. One approach to tackle this problem would be to utilize immunogold labeling of thin sections using transmission electron microscopy of cells expressing the FLAG-MKS3 protein. Although the expression of FLAG-MKS3 has proven difficult and also short-lived, without an antibody to specifically recognize *Paramecium* MKS3, this may be the best approach. To begin, the *Paramecium* cells would need to be in the correct stage of growth in an attempt to isolate the temporary attachment point of the bone node and the foot to the kinetodesmal fiber. Cells can be synchronized by isolating cells at a specific point in division after control autogamy (Ruiz et al., 1987) or by incubating the cells at 37°C for approximately 30 minutes to an hour. Synchronizing the cells would place them at approximately the same point in their growth stage. Although the cells would be in the right stage of growth, there would be great difficulty in obtaining the correct section of the cell using TEM fixation techniques to visualize the bone node and the foot. I would expect many sections would need to be examined cut from a single block of fixed cells. The sections could first be screened to see 1) if cells are in the correct orientation and 2) if the bone node can be visualized and identified. Only then should consecutive sections be isolated and immune-gold labelled to possibly identify the presence of FLAG-MKS3. This approach would take a great deal of time and patience.

Another approach would be to use super resolution microscopy to obtain a more detailed image of the location of FLAG-MKS3p or the endogenous protein using an antibody to recognize *Paramecium's* MKS3 protein. Super resolution microscopy allows for the detection of particles with a resolution of 50 to 20 nm (Huang et al., 2009). An antibody was developed against the *Paramecium* MKS3 protein, but has not yet been optimized for use on Western blots or immunofluorescence. Regardless, the use of super resolution could more closely pinpoint the endogenous or FLAG-MKS3p in *Paramecium*. Subcellular markers to help with this localization could be to stain the basal body with ID5 (Synaptic systems, Goettingen, Germany) or the Anti-

centrin antibody which was made against *Tetrahymena* centrin 1 and recognizes *Paramecium* centrin 2 (Gift of Dr. Mark Winey, University of Colorado, Boulder, CO). We also have kinetodesmal fiber antibody (Gift of Dr. Janine Beisson, Gif-Sur-Yvette, France). Therefore, we have numerous markers for the subcellular structures and could again synchronize the cells in their growth, maximizing our chances of obtaining cells in the process of division to obtain images of the transient pool of MKS3p.

In Chapter 2, we showed results from a glutathione sepharose transferase (GST) pull down using the coiled coil domain of *Paramecium* MKS3. In this pull-down, kinetodesmal fiber (Kd) proteins were included, specifically KdB2. Work continues on these findings of a potential interaction of the MKS3 protein with the Kd elements. Numerous sequences within the *Paramecium* genome were identified as being members of the Kd family, many of which were subsequently tagged with N-FLAG and expressed *Paramecium*. Immunoprecipitations of these proteins from whole cell extracts of paramecia expressing the tagged Kd genes did not yield, as of yet, the MKS3 protein. Although, the IPs for the tagged Kd fiber proteins have produced other Kd proteins. This work is on-going and will hopefully yield more information concerning the interaction of the Kd proteins with other intracellular proteins and possibly MKS3.

An important contribution to the study of MKS3 and *Paramecium* would be the investigation of the identification of the *Paramecium* transition zone complex proteins. Some of the proteins found within the transition zone form a filter to selectively allow passage of certain proteins in and out of the cilium. The filter complex includes the tectonic proteins (Tctn), MKS1, Tmem267, Cep290, B9d1, and others (Garcia-Gonzalo et al., 2011). The MKS1 protein has been researched in *Paramecium*. Depletion of MKS1 leads to a separation of the cell membrane from the underlying cytoskeleton, leaving the depleted cells without defined cortical units and a membrane that is easily aspirated from the underlying cytoskeleton compared to wild type cells

(Campillo et al., 2012). The MKS1 protein has not yet been localized in the cells. MKS1 has no predicted transmembrane domains, so one might expect it to be found in many locations within the cell. When expressed in HEK293 cells, mammalian MKS1 is localized at the basal bodies (Dawe et al., 2007). Other proposed complex proteins, including MKS5, or RIPGRIP1L, has a homolog in *Paramecium* (GSPATG00016244001). Some groups have localized MKS5 to the transition zone as a component of the NPHP complex (Sang et al., 2011, Williams et al., 2011). Others have characterized MKS5/RPGRIP1L as a component of the basal body (Garcia-Gonzalo et al., 2011). The location of the MKS5 protein in *Paramecium* using epitope-tagging and over-expression may help to collaborate our findings of MKS3p. It may also facilitate the co-IP of the MKS3 protein from isolated membranes, which may contain the transition zone or transition zone components. Currently, work is undergoing to further study *Paramecium* MKS5 in our lab while researchers in France are currently attempting to identify and characterize the transition zone proteins in *Paramecium*.

We are currently able to perform membrane potential recordings in our lab which could shed light on the impacted channels that reside in the remaining cilia on *MKS3* depleted cells. Appendix I discusses the changes in swimming behavior of *MKS3* and *IFT88* depleted cells compared to control cells. *IFT88* depleted cells provide an important comparison because we expect a global shortening and loss of cilia from the depleted cells. This differs from the *MKS3* depleted cells, where we expect a change in their channel proteins because we have disturbed the transition zone. The change in channel composition is apparent from the altered backward swimming of the *MKS3* depleted cells from both the control cells and the *IFT88* depleted cells. We are able to use membrane potential measurements and backward swimming assays as an indirect measurement of membrane permeability to an ion and ion conductance, respectively. It would be very interesting to examine the membrane potential of *MKS3* depleted cells and the ability of these cells to depolarize or hyperpolarize under certain ionic conditions. Again, the

IFT88 depleted cells provide a valuable control for this study. The *IFT88* depleted cells demonstrate long backward swimming in depolarizing solutions containing TEA, suggesting an ineffective $I_{K(Ca)}$, while the *MKS3* depleted cells showed backward swimming that was sodium-specific. The *MKS3* depleted cells displayed backward swimming consistent with an overly active $I_{Na(Ca)}$. Measuring the membrane potential of these cells in varying ionic solutions may shed more light on the defective or over-active channels that exist in these cells.

Clearly further investigation into the MKS3 protein as well as other possible interacting partners, such as MKS5 and the kinetodesmal fiber proteins in *Paramecium* are needed. Many of these projects are already underway. Hopefully the current *Paramecium* MKS3 antibody can be further cleaned to become useful for immunostaining or immunoprecipitation studies. This would greatly increase the chances of teasing apart the *Paramecium* transition zone component proteins as well as clearly identifying both proposed populations of MKS3p. We have begun to explore the proteins important for anchoring the basal bodies below the cell surface, namely the kinetodesmal fiber proteins. Work on the *Paramecium MKS5* gene and protein are also underway, starting with an RNAi construct to deplete the cells of MKS5 and observe for phenotypes. Our continued work on MKS3p and proteins that may complex with it will surely yield new insights into the importance and function of these proteins.

II. Further exploration of *PKD2* in *Paramecium*

Our investigation of the Pkd2 protein in *Paramecium* began with a curiosity about the presence and function of transient receptor potential (TRP) family proteins in *Paramecium*. We were initially looking to identify the possible mechanoreceptor channel in *Paramecium*. Because of the interactions of Pkd2 with Pkd1 for mechanosensation in mammalian systems, Pkd2 seemed to be a promising channel to investigate. Our search for TRP channels in general within the

Paramecium database turned up very few homologs. The three candidate *PKD2* genes named in Chapter 3, *PKD2a* (GSPATG00005599001), *PKD2b* (GSPATG00024265001), and what we refer to as *PKD2L* (GSPATG0001264001), were some of the only genes we were able to suggest were potential TRP channels.

When we depleted *PKD2* from *Paramecium* using RNAi and observed short backward swimming specific to Mg^{2+} solutions, it was apparent that we had found a protein with some involvement in the Mg^{2+}-induced behavior. Our further investigation into Pkd2 and its functions in *Paramecium* provided novel roles for the Pkd2 protein. Our studies have identified candidate interacting partners that are worth investigating further. Our persistence has also provided the opportunity to revive to use of electrophysiology in the lab, providing us with invaluable information on the *Paramecium* Pkd2 channel. The continued use of electrophysiology in the lab will allow further study of other *Paramecium* channels and receptors we have investigated in the past as well as those being investigated currently. That includes the glutamate receptor (See Appendix II), the cAMP receptor for chemoattraction, and the voltage-gated calcium channels.

Based on our findings in Chapter 3, we have proposed that Pkd2 is both necessary and sufficient for Mg^{2+}-induced behavior in *Paramecium* contributing to both membrane potential changes and $I_{Mg(Ca)}$. In the cilia, we propose the Pkd2 protein is regulated by the XntA protein probably in microdomains, although more research is needed to determine how this occurs. Previous work (Preston and Kung, 1994, Haynes et al., 2002) combined with our findings show that in cilia, XntA is sufficient for apparent Mg^{2+} permeability. We suggest that XntA in cilia interacts with the Pkd2 protein, directly or indirectly. Pkd2 in the cell membrane is negatively regulated by XntA in the cilia or another protein in the cilia which has yet to be identified. Although XntA has been proposed to be a Mg^{2+} channel, we suggest that Pkd2 is the Mg^{2+} channel while XntA is a regulator of that channel.

Our proposal that the Pkd2 protein is present in microdomains where it may be regulated by the XntA protein is an important avenue to explore. The microdomains, sometimes referred to as lipid rafts or detergent-resistant membranes (DRMs), are small microdomains that are tightly packed with sphingolipids and cholesterol. The term "lipid rafts" is still a highly debated topic as to whether or not they exist. Recent evidence, as reviewed by Kraft (2013), discussed that although there is an existence of membrane microdomains where areas in the membrane are enriched in sphingolipids, that cholesterols are evenly distributed in the membrane and not concentrated in these microdomains (Kraft, 2013). However, the author then goes on to mention that the size of the cholesterol microdomains could be less than 85 nm and undetectable by current detection techniques.

Regardless, microdomains that are detergent-resistant appear to be important for cell signaling processes. Interference with or removal of cholesterol or the sphingolipids from the cell membrane hampers signaling pathways and the proteins involved (Radeva and Sharom, 2004, Foster et al., 2003). These microdomains are expected to be tightly packed with signaling proteins, including glycosylphosphatidyl inositol (GPI)-anchored proteins and tyrosine kinases. These membrane microdomains are typically detergent resistant, meaning that they are not easily solubilized in cold non-ionic detergents, such as Triton X-100 or Brij-96, hence the name detergent-resistant membranes (DRMs). However, because of their light buoyant density, these microdomains will float up on sucrose or OptiPrep™ gradients when spun at very high speeds (Radeva and Sharom, 2004, Pike, 2003).

To begin to answer the question of whether XntA recruits or stabilizes Pkd2 in microdomains, we would first need to establish that Pkd2 is present in the membrane microdomains. We would begin with cell membrane and cilia isolated from Pkd2-FLAG expressing cells. These different membranes would then be disrupted by incubating with cold

Triton X-100 along with heavy vortexing to disrupt the membranes. The use of OptiPrep™ or sucrose gradients and centrifugation would then allow us to separate the microdomains from the triton soluble portions of the membrane and dense cytoskeletal elements. Once the isolated fractions are concentrated, separated by SDS-PAGE and transblotted to nitrocellulose, the blots can be probed for the Pkd2-FLAG protein using anti-FLAG. We also have antibodies available to mark for GPI-anchored proteins in *Paramecium* such as the surface A and B i-antigens (Kind Gift of Dr. J. Forney, Perdue University, West Lafayette, Indiana) and the GPI-anchored Folate receptor (Weeraratne, 2007). Higher fractions, toward the top of the gradient, would contain light fractions where we would expect to find GPI-anchored proteins. Fractions toward the bottom of the gradient, would indicate heavy or more dense fractions. These experiments would allow us to determine if Pkd2 is present in the microdomains as well as if Pkd2 is associated with light or heavy fractions from the sucrose or OptiPrep™ density gradients

To determine if XntA is important for the positioning of Pkd2-FLAG in these microdomains, we could do two experiments. Both experiments would be similar to the one described above. Instead of wild type cells, we would express *PKD2*-FLAG in XntA1 mutant cells or we could deplete wild type cells expressing the Pkd2-FLAG protein of *XNTA* using RNAi. We could then observe changes in the location of the Pkd2-FLAG protein in the OptiPrep™ or sucrose gradients from what we observed without disturbing the XntA protein. If the XntA protein is important for positioning Pkd2 in the microdomains, the Pkd2 protein may not be found in or its distribution may change in the gradients when the XntA protein is missing or depleted.

Another approach is to disrupt the lipid rafts or microdomains in *Paramecium* using Methyl-β-cyclodextrin (MβCD). Incubation with MβCD will selectively remove cholesterol from the membrane (Rodal et al., 1999). MβCD is very effective at removing the cholesterol without

harming the cells (Foster et al., 2003). Incubation of *Paramecium* cells in a buffer containing MβCD can be compared to cells that have been incubated in the same buffer, but without the MβCD. The cilia and cell membranes can be isolated and separated on the density gradients and the distribution of the Pkd2-FLAG protein can be observed on GPI-anchored folate receptor (Weeraratne, 2007). With the depletion of cholesterol from the membranes using MβCD, we expect many of the microdomain-associated proteins to collapse into the more-dense fractions of the density gradient. Previous work in our lab has shown that MβCD incubation will easily deplete the cell membrane of sterols, but not the cilia. The removal of cholesterol from the ciliary membrane and disruption of ciliary microdomains has proven far more difficult (Ray, 2008). This may make it more difficult to determine if Pkd2 is acting in microdomains in the cilia. Cholesterol assays can also be performed on the gradient fractions to determine the effectiveness of the cholesterol depletion, such as the Amplex Red Cholesterol Assay kit (Life Technologies) or the Cholesterol Quantitation Kit (Sigma).

To accompany the immunoblots of cells depleted in MβCD, it would also be important to examine the membrane potential of the cells treated with and without methyl-β-cyclodextrin. To my knowledge, this has not been done before in *Paramecium*. It would be important to examine the cells not only in solutions with and without magnesium, but to also examine the cells in solutions containing known attractants for *Paramecium* that typically cause the membrane to hyperpolarize (See Appendix II). Work in our lab has been done to examine the chemoattraction of cells treated and mock-treated with MβCD using T-maze assays. To data, attraction to cAMP and glutamate have been shown to be diminished with MβCD treatment while attraction to folate, ammonia, and acetate appear unaffected (Pan, 2008). We now have an antibody against one of the cAMP receptors in *Paramecium*, pCAR3 (GSPATG00017916001). The protein is approximately 31 kD in size (Czapla, 2012). It is possible that the pCAR3 membrane receptor

would be useful in the microdomain studies. The attractant cAMP would also important to examine in T-maze assays using cells treated and mock-treated with MβCD.

Another important investigation that should take place is to look more closely at the multiple bands that are observed for the Pkd2 protein on Western blots. We have shown (Chapter 3) that multiple bands are observed for the Pkd2 protein and that using LC-MS/MS, the Pkd2 protein is present in these bands (See Appendix II). One of the bands is larger than the expected size of the Pkd2 protein (~120 kD). This higher band is most often found from the IPs obtained from solubilized whole cilia. In mammalian cells, Pkd2 has been shown to be N-glycosylated both when it is expressed in cell lines as well as endogenously in human kidney cells (Cai et al., 1999). To test for N-glycosylation, we can treat Pkd2 IP eluates with endoglycosidase H (EndoH). We would expect the larger band (120 kD) observed in the Western blots to collapse into the expected molecular mass (100 kD) or smaller. EndoH cleaves high-mannose oligosaccharides from proteins. To test the isolated proteins for EndoH-sensitivity, IP's from whole cilia of cells expressing *PKD2*-FLAG, and cilia from cells expressing FLAG as a control, would be collected and separated. One half would be mock-treated for EndoH, receiving the same treatment as the test cells but without receiving the EndoH enzyme. The other half of the IPs would be treated with EndoH. The treated and mock-treated IP eluates would then be separated by SDS-PAGE and probed with anti-FLAG. If the upper band observed in whole cilia IPs is indeed Pkd2 that has been N-glycosylated, we would expect the upper band, or perhaps even other bands, to collapse and blend with bands lower on the gel. The mock-treated sample should show no change in the distribution of Pkd2-FLAG from what we typically observe. The highest band at 120 kD should remain. N-glycosylation may explain the larger size we observe in blots of the Pkd2-FLAG protein, although other modifications are also possible.

We have presented data that suggest the Pkd2 protein is the Mg^{2+} channel. We have used backward swimming assays and membrane potential measurements to indirectly measure ion conductance and membrane ion permeability, respectively. It would be appropriate to use two electrode voltage clamp on Pkd2 depleted cells to measure Mg^{2+} ion conductance. Our lab is not currently able to perform these experiments, we do not have the necessary equipment. However, that is not to say we cannot obtain the equipment or use equipment from another lab. It is important to note that these experiments are not trivial. The successful impalement of a ciliated *Paramecium* cell which would be moving with not one, but two glass electrodes, is a technically challenging task.

To further test the function of the Pkd2 channel in *Paramecium*, it could be prudent to treat cells with known Pkd2 inhibitors while recording the membrane potential of cells in solutions with and without Mg^{2+}. Compounds such as lanthanum (La^{3+}) or gadolinium (Gd^{3+}) have been shown to inhibit Pkd2 activity as well as amiloride. By adding these compounds to the bath solution, Mg^{2+}-induced membrane depolarization may be inhibited if Pkd2 is acting as a Mg^{2+} channel. Both La^{3+} and Gd^{3+} are heavy metals, shown to inhibit Pkd2 channel activity in reconstituted human term syncytiotrophoblast (hST) membranes (Gonzalez-Perrett et al., 2001). Gadolinium inhibits Pkd2 at a concentration of 400 μM (Giamarchi et al., 2010) and lanthanum at a concentration of 500 μM (Kottgen et al., 2005). Amiloride can be used to inhibit Pkd2 channel activity at a concentration of 100 μM (Giamarchi et al., 2010). In mammalian cells, amiloride appears to be an inhibitor of Pkd2 activity. The other compounds, La^{3+} and Gd^{3+} are better blocking compounds of Pkd2 activity. Lanthanum is a better blocking compound than amiloride (Giamarchi and Delmas, 2007).

Lanthanum has been used on *Paramecium* for a study of calcium-dependent exocytosis. The external application of 1 mM lanthanum caused the "explosive" release of trichocysts as well

as local cortical increases in intracellular calcium concentrations. The site of application of the La^{3+} also became deformed (Klauke et al., 2000). The concentration used in the exocytosis study was twice that of what has been published to be successful in blocking Pkd2 channel activity. Lower concentrations would most likely work to inhibit Pkd2 channel activity and not cause trichocyst discharge at the same time.

The application of these potential *Paramecium* Pkd2 channel inhibitors does pose a few issues. First, we are not sure if La^{3+}, Gd^{3+}, or amiloride will work to block Pkd2 channel activity. Second, it would be difficult to determine if these chemicals were blocking Pkd2 and not another protein or channel because we do not have a knock out available for Pkd2. The best approach we currently have is the ability to deplete cells of *PKD2* mRNA using RNAi. We would expect that if one of these chemicals were blocking Pkd2 channel activity, that membrane potential recordings would be similar to that of a *PKD2* depleted cell. We now know that a ciliated XntA1 mutant shows almost no change in resting membrane potential in a bath solution containing 0.5 mM $MgCl_2$, but that if that XntA1 mutant cell is expressing *PKD2*-FLAG, there is a depolarization of the membrane indistinguishable from that of a wild type cell (Chapter 3). If these Pkd2 channel blockers were working to inhibit Pkd2 channel activity, we would expect that their application to an XntA1 mutant cell expressing *PKD2*-FLAG would remove any depolarization of that cell in the presence of Mg^{2+}, making it appear like an XntA1 mutant again. If successful, these channel blockers could also help to determine if the Pkd2 protein is a channel and if it is contributing to Mg^{2+} conductance.

The application of these blockers to deciliated cells may help to demonstrate that Pkd2 is the channel protein in the cell membrane that is causing the large membrane depolarizations. Both wild type and XntA1 mutant cells show membrane depolarizations in the presence of Mg^{2+} when these cells are deciliated (Chapter 3). These findings were unexpected; we had no

indication that the membrane of a deciliated XntA1 mutant would depolarize at all in the presence of Mg^{2+}. To our surprise the deciliated XntA1 mutant depolarized by the same amount as the deciliated wild type cells in the presence of Mg^{2+}. Only when *PKD2* was depleted from the deciliated XntA1 mutants did we see the membrane depolarize as we expected, which was hardly at all. Application of La^{3+} or Gd^{3+}, assuming these compounds block Pkd2 channel activity in *Paramecium*, may prevent the membrane depolarization in Mg^{2+} solutions of the deciliated wild type and XntA1 mutant cells. The results may support, or refute, our notion that Pkd2 is acting as the Mg^{2+} channel in the cell membrane.

The *Paramecium* sequence for Pkd2 is different than that of mammals. The *Paramecium* amino acid sequence for Pkd2 is shorter than that of mammals, including humans (Accession number Q13563). The *Paramecium* sequence is 849 amino acids compared to the human sequence which is 968 amino acids. Similar to the mammalian Pkd2 sequences, Pkd2 in *Paramecium* does have two proposed coiled coil domains. One at the N-terminus (amino acids 1 to 56) and one at the C-terminus (amino acids 811 to 832) (PCOILS: http://toolkit.tuebingen.mpg.de/pcoils). These regions may be important for protein-protein interactions. Expression of truncated Pkd2 proteins in *Paramecium* using the pPXV plasmid could provide insight into these regions of the protein. Two truncated versions could be created for the study. The first where the first 56 amino acids of Pkd2 are removed and the second where the last 37 amino acids are removed. These truncated versions could be inserted into the pPXV plasmid and injected into the macronucleus of paramecia. The expression of the truncated versions of Pkd2 could shed light on whether the coiled coil regions are important for protein-protein interactions. If the coiled coil domains are important for interactions, their removal may interfere with the function of the endogenous Pkd2 protein. The interference with the endogenous protein function would most likely manifest as reduced backward swimming in Mg^{2+} solutions or a reduced amount of membrane depolarization in solutions containing Mg^{2+}. The pPXV-C-FLAG plasmid could also be used in

place of the pPXV plasmid to use immunofluorescence to determine if the trafficking of the truncated versions of the Pkd2 protein are altered.

Expressing mutated versions of the Pkd2 protein may also help to determine the pore region of the protein. The fifth and sixth transmembrane spanning regions for *Paramecium* Pkd2 are expected to be amino acids A655 to D678 and L759 to F781. The region between these two predicted transmembrane regions (D678 to L759) should contain the pore region. Within the mammalian sequene of the pore region, there are four amino acids that are conserved with the human *PKD2* and *PKD2L* sequences, position F626, F637, I640 and G657. These amino acids are spaced 0F, +11F, +14I, +31G. Amino acids with a similar spacing, but not exact, appear in the predicted pore region of *Paramecium* Pkd2. Amino acids F702, F712, I714 and I715 are found in the predicted *Paramecium* pore region that are similar to the mammalian sequences and may be important for the pore formation (Tsiokas et al., 1999, Nomura et al., 1998). The pore region could be mutated and expressed using the pPXV plasmid in *Paramecium* followed by backward swimming assays and membrane potential measurements. The results could help decipher whether these amino acids are important for channel function, ion permeability, or ion selectivity.

It could be highly beneficial to develop an antibody against the Pkd2 sequence in *Paramecium*. Although the C-terminal epitope tagging has been relatively successful, N-terminal tagging of the Pkd2 protein was not. We have proposed that the Pkd2-FLAG protein may be interacting with XntA at the C-terminus which may occlude the C-terminal FLAG tag preventing the co-immunoprecipitation of the Pkd2 and XntA proteins. Developing an antibody to recognize a region in the large extracellular loop between the first and second predicted transmembrane domains could be beneficial. An antibody to recognize this region could yield a

successful IP of the Pkd2 protein and would allow for co-immunoprecipitation of proteins that may interact with both the N- or C-terminus of Pkd2.

Although not discussed here, our lab has glutathione sepharose transferase (GST)-fusion proteins of the N- and C-terminus of Pkd2. The N-terminus GST-fusion includes M1 to S198 without any predicted transmembrane domains. The C-terminus GST-fusion protein is the final 215 amino acids, N638 to N849. The C-terminal Pkd2 sequence includes the putative fifth and sixth transmembrane spanning domains and the pore loop. These proteins have been expressed before in bacteria, although they are not easy to extract and purify. The GST-fusion proteins for Pkd2 require a special protocol to isolate and extract the expressed proteins from inclusion bodies. Special bacteria must also be used that are efficient at expressing sequences rich in adenines and thymines (BL21-CodonPlus (DE3)-RIL bacteria, Agilent Technologies, Santa Clara, CA). It is possible that these short GST-fusion proteins could be expressed and be used for GST pull-down assays, although those assays can be difficult. Precautions must be taken to prevent or remove bacterial proteins from binding to and occupying the expressed proteins.

A more fruitful and informative approach might be to use these purified expressed proteins for Far Western development. This could be performed on IPs from whole cells or IPs from whole cilia that are expressing the XntA-FLAG protein. An important control would be the successful IP and identification of the XntA-FLAG protein from these cells. Another IP separated by SDS-PAGE, transblotted and then re-natured would then be probed using the expressed GST-fusion N- or C-terminal Pkd2 purified proteins. The blot would then be probed with anti-GST to recognize the GST-fusion proteins which would hopefully correspond with the XntA-FLAG band on the corresponding blot. If N- or C-terminal Pkd2 interacted with the re-natured XntA or XntA-FLAG on the blot, it should bind to the XntA protein. Cells expressing FLAG would need to be used as a control as well as a blot that was developed by incubating it with expressed GST

to ensure it was the terminal end of Pkd2 interacting with XntA, not the GST. These experiments would provide very useful information concerning direct interaction of the Pkd2 protein and XntA. It would also provide information as to which termini of Pkd2 interacts with XntA. Based on our proposed model in Chapter 3, we would expect the C-terminal Pkd2-GST fusion protein would bind to the XntA protein.

We have clearly shown in our data that Pkd2 requires the BBSome to traffic to the cilia. However, what method is Pkd2 using to reach the cell membrane? This is a question I would like to investigate further and would contribute to the overall understanding of the movement of this protein within the cell. Other groups have also shown that Pkd2 requires the BBSome or components therein to reach the cilia (Hoffmeister et al., 2011, Valentine et al., 2012). It would be beneficial for our work to determine how Pkd2 reaches the cell membrane. Knowing how the protein reaches the cell membrane may allow for the interruption of membrane Pkd2 trafficking while leaving Pkd2 in the cilia undisrupted.

In mammalian cells, there are instances where Pkd2 requires a signal, typically from Pkd1, to traffic to the cilia or the cell membrane (Hanaoka et al., 2000, Nauli et al., 2003). However, our work suggests Pkd2 does not require XntA to traffic to the cilia or the cell membrane. That is not to say there is not another protein in the cilia or in the cell membrane that may need to signal for Pkd2 to be trafficked to these membranes. It is possible this signaling protein exists and we have not identified it as of yet. Hoffmeister and colleagues did describe two amino acids that were necessary for the movement of human Pkd2 from the trans-Golgi to the cell membrane in the fourth transmembrane spanning region of the protein, K572 and F576. When these amino acids were mutated to alanines, the mutated Pkd2 protein no longer trafficked to the cell membrane in non-ciliated COS-7 and LLC-PK cells (Hoffmeister et al., 2011). If we were able to somehow prevent Pkd2 from reaching the cell membrane of *Paramecium*, but allow it

to reach the cilia, this would be a very useful model to study the activity of Pkd2 and its contribution to Mg^{2+}-induced behavior in only the ciliary membrane. So far, we are unsure of what this membrane trafficking protein might be.

Our research on the Pkd2 protein in *Paramecium* has provided a great deal of information on the Pkd2 protein, its potential interacting partners (see Appendix III), and what its role might be in our ciliated model organism. We have shown the importance of the BBSome for the trafficking of the Pkd2 protein to the cilia (Valentine et al., 2012). Also, that when *BBS8* is depleted, Pkd2 is able to reach the cell membrane where it is able to contribute to Mg^{2+}-induced behavior. We have presented novel findings on the involvement of Pkd2 in Mg^{2+}-induced behavior and that Pkd2 interacts with the XntA protein, either directly or indirectly. Our indirect evidence that suggests Pkd2 is involved in Mg^{2+} conductance is novel and may not be unique to *Paramecium*. Our lab plans to continue research on Pkd2 in *Paramecium* to further understand the role of this protein in Mg^{2+}-induced behavior, involvement with XntA, and Pkd2 presence in membrane microdomains.

III. Further exploration of XntA in *Paramecium*

Magnesium conductance and regulation have been of interest for almost 25 years in *Paramecium*. Investigations into Mg^{2+} membrane permeability started in the 1990's when *Paramecium* was discovered to have a calcium-dependent magnesium conductance (Preston, 1990). The XntA protein is a small protein, 550 amino acids. Its name lends true to its moniker of *eccentric*, being quite unconventional in many ways. What the XntA protein is doing in *Paramecium* is still undecided but numerous other experiments could help to better understand

the roles and function of XntA. Some of the proposed experiments to follow are relevant to the work presented in Chapter 3, as well as the work shown in Appendix II.

One of the first areas of investigation to conclude would be to have a complete understanding of the expression of the mutated and truncated versions of the XntA protein in the XntA1 mutant (see Appendix II). It would be important to repeat these experiments and include electrophysiology to recorded the changes in membrane potential in solutions with and without Mg^{2+} to compare to the backward swimming assays. We were unable to perform membrane potential measurements when the expression experiments were being done. The outcomes may shed more light on the ability of the XntA protein to function in its role and contribute to Mg^{2+} conductance and membrane permeability by proxy.

An additional version of the *XNTA* gene to express in the XntA1 mutants would be one where the PEST sequence has been removed. The PEST sequence is brief (Haynes et al., 2002), characterized by a richness in prolines (P), glutamic acids (E), serines (S), and threonines (T). PEST sequences are common in proteins that are targeted for early or rapid degradation (Rogers et al., 1986, Rechsteiner and Rogers, 1996). If the PEST sequence targets the XntA protein for early degradation, its removal may allow for a longer life-span of the XntA protein. If the XntA protein is able function in the cells for a longer time and not be broken down or degraded rapidly, the cells may display longer backward swimming or more membrane depolarization in solutions containing Mg^{2+}. We have other instances that suggest when there is an excess of XntA, there is prolonged Mg^{2+}-induced behavior or increased membrane depolarization. We observed that over-expression of the *XNTA*-FLAG gene in the XntA1 mutants led to partial curing of the mutants. The XntA1 mutants expressing *XNTA*-FLAG showed significantly longer backward swimming in Mg^{2+} solutions compared to the XntA1 mutants expressing FLAG, but not as much as the control wild type cells. Also, wild type cells expressing *XNTA*-FLAG showed significantly

longer backward swimming in Mg^{2+} solutions than the wild type control cells, indirectly suggesting that the over-expression of the XntA protein increases the Mg^{2+} conductance.

It would also be on interest to examine the expression of both the N- and the C- term of *XNTA* to cure the XntA1 mutants. Individually, the N-term and C-term of XntA showed no curing or very little curing of the XntA1 mutant, respectively (See Appendix II). However, if they are expressed together within the cells, it is possible that the two fragments may be able to act together to rescue the mutant. Although we hypothesize that the protein must be full-length to properly function, the expression of the two separate fragments would help to confirm this hypothesis. If the expression of both fragments did not show any increase in backward swimming, we would have more support of our hypothesis that the XntA protein must be full-length to properly function.

We did not have the capabilities to record membrane potential when many of the injected cells were available. Although voltage clamp studies have been done previously on XntA1 mutants expressing the wild type *XNTA* gene (Haynes et al., 2002), it would be useful to use electrophysiology to record the membrane potential changes in Mg^{2+} solutions of XntA1 mutants expressing *XNTA*-FLAG and FLAG-*XNTA*, as well as FLAG-*PKD2*. We have membrane potential recordings of wild type cells and XntA1 mutants expressing the *PKD2*-FLAG gene, but not of the wild type cells or XntA1 mutants expressing *XNTA*-FLAG. Now that were able to perform these membrane potential recordings, it would help complete the study of the XntA1 mutant if these recordings were performed.

As of yet, we have not identified any peptides from the XntA protein in any of our LC-MS/MS analyses. We are able to consistently visualize bands when using IP to precipitate XntA-FLAG or XntA-myc with antibodies against the epitope tags. We expect that because the same bands are identified on Western blots from the eluates of both the XntA-FLAG IP and the XntA-

myc IP that those bands are fragments of the expressed XntA protein with the C-terminal epitope tag intact. Additional attempts to IP the XntA-FLAG or XntA-myc protein are suggested where the entire silver stained gel from the IP eluates is sent for LC-MS/MS analysis, not just certain gel fragments. Dr. Junji Yano has identified two peptides belonging to XntA in his analysis of TritonX-114 phase separation of the ciliary membrane (Yano et al., 2013). These data, combined with our IPs and immunostaining data presented in Chapter 3, clearly demonstrate the XntA protein is in the cilia. Because the XntA protein has eleven predicted transmembrane domains, it is possible that Triton X-114 phase separation of the cell or ciliary membrane is needed to solubilize enough of the protein for LC-MS/MS analysis. Another possibility is that XntA is present in detergent resistant membranes (DRNs) and is not easily solubilized using cold non-ionic detergents. The presence of XntA in DNRs would be consistent with our proposed model that XntA may interact with Pkd2 in membrane microdomains. If XntA is found in the membrane microdomains of the cell and cilia membrane, then it should float up in our density gradients after the membrane is disrupted with Triton X-100 as described for Pkd2. It would be wise then to perform the same membrane microdomain studies using cells expressing XntA-FLAG or –myc to see if the XntA protein is found in the same fraction of the density gradient at Pkd2. If both proteins are found in the same fraction, it is possible they are interacting in the microdomains. Very similar experiments for XntA could be performed as what was described for the microdomain studies for the Pkd2 protein.

We have had a lot of difficulty in obtaining successful IPs with the full-length of XntA (~61 kD). The varied success in IP'ing the full length XntA has hampered our ability to do the reciprocal IP of Pkd2-FLAG and XntA-myc (Chapter 3), where we instead IP XntA-myc first to co-IP Pkd2-FLAG. We were unsuccessful in our last attempts to complete this experiment. An antibody to recognize the XntA protein in *Paramecium* may help facilitate these experiments. An antibody specific for the XntA protein might allow us to identify and IP the endogenous protein.

We could both visualize the protein on Western blots and perhaps even visualize the protein within the cells using immunofluorescence. There are no commercial antibodies for the XntA protein since the sequence is very unique to *Paramecium* and *Tetrahymena*. We don't believe the epitope tags are interfering with the function of the XntA protein, either endogenous or exogenous. We have shown some curing of the mutant when *XNTA*-FLAG is expressed. Wild type cells have shown an increase in Mg^{2+}-induced behavior with *XNTA*-FLAG is expressed. A section of the XntA protein to target for antibody development, however, would be a challenge. As mentioned, XntA has 11 predicted transmembrane spanning regions with an extraordinarily short N- and C- terminal tail, 15 and 1 amino acids, respectively (Haynes et al., 2002). There is one loop between the first and second predicted transmembrane spanning regions that is 26 amino acids in length which contains five acidic amino acids. Although the loop is short, a keyhole limpet hemocyanin (KLH)-conjugated antibody with these 26 amino acids could prove to be useful. Otherwise, the large intracellular loop could be used to develop a GST-fusion peptide for antibody development.

There is some indication that the XntA1 mutants are unable to hyperpolarize their membrane in response to attractants (See Appendix II). The same attractants cause a 5 to 10 mV hyperpolarization of the membrane potential in wild type cells (See Appendix II and (Van Houten, 1979, Preston and Van Houten, 1987)). It would be beneficial for the XntA1 mutants to be tested in T-maze assays to assess their attraction to typical attractants such as folate, glutamate, cAMP, ammonium, and acetate. These attractants cause the activation of different pathways to hyperpolarize the membrane of *Paramecium*. Two of the pathways, the glutamate pathway and the pathway that includes cAMP and folate, cause the hyperpolarization of the membrane by eventually activating the plasma membrane Ca^{2+}-ATPase pumps that remove calcium from the cells. Ammonium chloride crosses the membrane as ammonia and causes a hyperpolarization of the membrane (Van Houten, 1998). There is also evidence that the presence

of Mg^{2+} in the bath may alter the response of *Paramecium* to some of their attractants, specifically biotin, which paramecia are attracted to (Bell et al., 2007, Bell et al., 1998).

The XntA1 mutant cells can be tested for their reaction to these attractants using the T-maze assay which is a three-armed apparatus with a two-way stop cock. The cells are loaded into the center arm which is shorter and perpendicular to the other two horizontal arms. A control solution is loaded into one of the arms and the test solution containing the attractant is placed in the other arm. Importantly, the ions are balanced between the two arms so the cells do not swim in one direction or the other based on ionic concentrations, but on the presence/absence of the attractant. Cells are given 30 minutes to swim into either arm after being loaded, then the arms are emptied and the cells in each arm are counted. The cells in the average number of cells found in the test arm are divided by the total number of cells in the control and test arms to determine the index of chemoattraction (I_{Che}). An I_{Che} above 0.5 indicates attraction, below 0.5 indicates repulsion and an I_{Che} at 0.5 indicates neutrality (Van Houten et al., 1982).

The T-maze assays as well as more membrane potential recordings would be quite informative as to whether the XntA1 mutants are able to respond to the attractants the same way wild type cells are. T-maze assays would assess the ability of the XntA1 mutants to swim toward and attractant and maintain themselves within the T-maze arm containing the attractant. Measuring the membrane potential changes of these cells in solutions with and without the attractants has already hinted at the fact that these cells may not be able to maintain their membrane potentials in these solutions. Meaning, the XntA1 mutants may not be able to maintain a hyperpolarized membrane potential in solutions containing the attractants compared to solutions without the attractants (see Appendix II). This could be due to XntA stabilizing or recruiting proteins to the membrane microdomains. The plasma membrane calcium ATPases

(PMCAs), necessary for many of these maintained hyperpolarizations of the membrane, could also be stabilized in the microdomains by XntA, especially in the cilia.

It would also be interesting to test some of these attractants with and without the presence of Mg^{2+} in the T-maze solutions or the membrane potential solutions to see if there is any effect of Mg^{2+} on the reactivity of cells to attractants, both wild type and XntA1 mutants. The results could be informative concerning an influence of extracellular Mg^{2+} on the chemoresponsiveness of cells to chemoattractants and on the membrane potential changes that might occur. Although extracellular Mg^{2+} is an effective blocker of N-methyl D-aspartic acid (NMDA) ionotropic glutamate receptors (Nikolaev et al., 2012), previous work in our lab has shown that there was no effect of extracellular Mg^{2+} on glutamate chemoresponse (Jacobs, 2007). The results could yield insights into the function of the XntA protein being responsible for stabilizing other proteins in membrane microdomains other than the Pkd2 protein, such as the receptors or channels necessary for chemoattration processes. Also, if Mg^{2+} has any influence on the chemoresponse of the cells.

We do have evidence that the XntA protein co-immunoprecipitates with the voltage-gated calcium channels (VGCCs) of the cilia (Dr. Junji Yano, unpublished results). Our lab is currently investigating the presence of the VGCCs in membrane microdomains of the cilia. It is possible that the XntA protein is an important stabilizer of proteins in these membrane microdomains, not just the Pkd2 protein, maybe including the VGCCs and the PMCAs. The "eccentric" behavior of the XntA1 mutant cells could be explained by the instability of signaling pathways in membrane microdomains, both in the cell membrane and in the cilia, leading to an inability of the cell to regulate and control signaling pathways and swimming patterns. Eccentric received its moniker because of random bouts of backward swimming and odd behaviors in ionic solutions, not just those solutions with Mg^{2+}. Perhaps we have stumbled into the true nature of

the XntA protein as a stabilizer of signaling proteins in membrane microdomains. Continued research on this project using the approaches discussed here will continue to shed light on this unique protein and lead to a better understanding of these membrane microdomains.

References

AUBUSSON-FLEURY, A., LEMULLOIS, M., DE LOUBRESSE, N. G., LALIGNE, C., COHEN, J., ROSNET, O., JERKA-DZIADOSZ, M., BEISSON, J. & KOLL, F. 2012. The conserved centrosomal protein FOR20 is required for assembly of the transition zone and basal body docking at the cell surface. *J Cell Sci,* 125**,** 4395-404.

BELL, W. E., KARSTENS, W., SUN, Y. & VAN HOUTEN, J. L. 1998. Biotin chemoresponse in Paramecium. *Journal of Comparative Physiology a-Sensory Neural and Behavioral Physiology,* 183**,** 361-366.

BELL, W. E., PRESTON, R. R., YANO, J. & VAN HOUTEN, J. L. 2007. Genetic dissection of attractant-induced conductances in Paramecium. *J Exp Biol,* 210**,** 357-65.

CAI, Y., MAEDA, Y., CEDZICH, A., TORRES, V. E., WU, G., HAYASHI, T., MOCHIZUKI, T., PARK, J. H., WITZGALL, R. & SOMLO, S. 1999. Identification and characterization of polycystin-2, the PKD2 gene product. *J Biol Chem,* 274**,** 28557-65.

CAMPILLO, C., JERBER, J., FISCH, C., SIMOES-BETBEDER, M., DUPUIS-WILLIAMS, P., NASSOY, P. & SYKES, C. 2012. Mechanics of membrane-cytoskeleton attachment in Paramecium. *New Journal of Physics,* 14.

CHIH, B., LIU, P., CHINN, Y., CHALOUNI, C., KOMUVES, L. G., HASS, P. E., SANDOVAL, W. & PETERSON, A. S. 2012. A ciliopathy complex at the transition zone protects the cilia as a privileged membrane domain. *Nature Cell Biology,* 14**,** 61-U97.

CZAPLA, H. 2012. Cyclic adenosine monophoshate receptors in *Paramecium tetraurelia*. *MS thesis, Department of Biology, University of Vermont*.

DAWE, H. R., SMITH, U. M., CULLINANE, A. R., GERRELLI, D., COX, P., BADANO, J. L., BLAIR-REID, S., SRIRAM, N., KATSANIS, N., ATTIE-BITACH, T., AFFORD, S. C., COPP, A. J., KELLY, D. A., GULL, K. & JOHNSON, C. A. 2007. The Meckel-Gruber Syndrome proteins MKS1 and meckelin interact and are required for primary cilium formation. *Hum Mol Genet,* 16**,** 173-86.

DUTE, R. & KUNG, C. 1978. Ultrastructure of the proximal region of somatic cilia in Paramecium tetraurelia. *J Cell Biol,* 78**,** 451-64.

FOSTER, L. J., DE HOOG, C. L. & MANN, M. 2003. Unbiased quantitative proteomics of lipid rafts reveals high specificity for signaling factors. *Proc Natl Acad Sci U S A,* 100**,** 5813-8.

GARCIA-GONZALO, F. R., CORBIT, K. C., SIREROL-PIQUER, M. S., RAMASWAMI, G., OTTO, E. A., NORIEGA, T. R., SEOL, A. D., ROBINSON, J. F., BENNETT, C. L., JOSIFOVA, D. J., GARCIA-VERDUGO, J. M., KATSANIS, N., HILDEBRANDT, F. & REITER, J. F. 2011. A transition zone complex regulates mammalian ciliogenesis and ciliary membrane composition. *Nat Genet,* 43**,** 776-84.

GIAMARCHI, A. & DELMAS, P. 2007. Activation Mechanisms and Functional Roles of TRPP2 Cation Channels. *In:* LIEDTKE, W. B. & HELLER, S. (eds.) *TRP Ion Channel Function in Sensory Transduction and Cellular Signaling Cascades.* Boca Raton (FL).

GIAMARCHI, A., FENG, S., RODAT-DESPOIX, L., XU, Y., BUBENSHCHIKOVA, E., NEWBY, L. J., HAO, J., GAUDIOSO, C., CREST, M., LUPAS, A. N., HONORE, E., WILLIAMSON, M. P., OBARA, T., ONG, A. C. & DELMAS, P. 2010. A polycystin-2 (TRPP2) dimerization domain essential for the function of heteromeric polycystin complexes. *EMBO J,* 29**,** 1176-91.

GONZALEZ-PERRETT, S., KIM, K., IBARRA, C., DAMIANO, A. E., ZOTTA, E., BATELLI, M., HARRIS, P. C., REISIN, I. L., ARNAOUT, M. A. & CANTIELLO, H. F. 2001. Polycystin-2, the protein mutated in autosomal dominant polycystic kidney disease (ADPKD), is a Ca2+-permeable nonselective cation channel. *Proc Natl Acad Sci U S A,* 98**,** 1182-7.

HANAOKA, K., QIAN, F., BOLETTA, A., BHUNIA, A. K., PIONTEK, K., TSIOKAS, L., SUKHATME, V. P., GUGGINO, W. B. & GERMINO, G. G. 2000. Co-assembly of polycystin-1 and -2 produces unique cation-permeable currents. *Nature,* 408**,** 990-4.

HAYNES, W. J., KUNG, C., SAIMI, Y. & PRESTON, R. R. 2002. An exchanger-like protein underlies the large Mg2+ current in Paramecium. *Proc Natl Acad Sci U S A,* 99**,** 15717-22.

HOFFMEISTER, H., BABINGER, K., GURSTER, S., CEDZICH, A., MEESE, C., SCHADENDORF, K., OSTEN, L., DE VRIES, U., RASCLE, A. & WITZGALL, R. 2011. Polycystin-2 takes different routes to the somatic and ciliary plasma membrane. *J Cell Biol,* 192**,** 631-45.

HUANG, B., BATES, M. & ZHUANG, X. 2009. Super-resolution fluorescence microscopy. *Annu Rev Biochem,* 78**,** 993-1016.

IFTODE, F. & FLEURY-AUBUSSON, A. 2003. Structural inheritance in Paramecium: ultrastructural evidence for basal body and associated rootlets polarity transmission through binary fission. *Biol Cell,* 95**,** 39-51.

JACOBS, C. L. 2007. NMDA receptor associated protein in Paramecium and it involvement in glutamate chemoresponse. *MS thesis*.

KLAUKE, N., BLANCHARD, M. & PLATTNER, H. 2000. Polyamine triggering of exocytosis in Paramecium involves an extracellular Ca(2+)/(polyvalent cation)-sensing receptor, subplasmalemmal Ca-store mobilization and store-operated Ca(2+)-influx via unspecific cation channels. *J Membr Biol,* 174**,** 141-56.

KOTTGEN, M., BENZING, T., SIMMEN, T., TAUBER, R., BUCHHOLZ, B., FELICIANGELI, S., HUBER, T. B., SCHERMER, B., KRAMER-ZUCKER, A., HOPKER, K., SIMMEN, K. C., TSCHUCKE, C. C., SANDFORD, R., KIM, E., THOMAS, G. & WALZ, G. 2005. Trafficking of TRPP2 by PACS proteins represents a novel mechanism of ion channel regulation. *EMBO J,* 24**,** 705-16.

KRAFT, M. L. 2013. Plasma membrane organization and function: moving past lipid rafts. *Mol Biol Cell,* 24**,** 2765-8.

NAULI, S. M., ALENGHAT, F. J., LUO, Y., WILLIAMS, E., VASSILEV, P., LI, X., ELIA, A. E., LU, W., BROWN, E. M., QUINN, S. J., INGBER, D. E. & ZHOU, J. 2003. Polycystins 1 and 2 mediate mechanosensation in the primary cilium of kidney cells. *Nat Genet,* 33**,** 129-37.

NIKOLAEV, M. V., MAGAZANIK, L. G. & TIKHONOV, D. B. 2012. Influence of external magnesium ions on the NMDA receptor channel block by different types of organic cations. *Neuropharmacology,* 62**,** 2078-85.

NOMURA, H., TURCO, A. E., PEI, Y., KALAYDJIEVA, L., SCHIAVELLO, T., WEREMOWICZ, S., JI, W., MORTON, C. C., MEISLER, M., REEDERS, S. T. & ZHOU, J. 1998. Identification of PKDL, a novel polycystic kidney disease 2-like gene whose murine homologue is deleted in mice with kidney and retinal defects. *J Biol Chem,* 273**,** 25967-73.

PAN, Y. 2008. The role of plasma membrane calcium ATPase and its association with lipid rafts in chemoattraction in *Paramecium*. *Thesis Masters Degree, Department of Biology, University of Vermont*.

PICARIELLO, T., VALENTINE, M. S., YANO, J. & VAN HOUTEN, J. 2014. Reduction of meckelin leads to general loss of cilia, ciliary microtubule misalignment and distorted cell surface organization. *Cilia,* 3**,** 2.

PIKE, L. J. 2003. Lipid rafts: bringing order to chaos. *J Lipid Res,* 44**,** 655-67.

PRESTON, R. R. 1990. A magnesium current in Paramecium. *Science,* 250**,** 285-8.

PRESTON, R. R. & KUNG, C. 1994. Inhibition of Mg2+ current by single-gene mutation in Paramecium. *J Membr Biol,* 139**,** 203-13.

PRESTON, R. R. & VAN HOUTEN, J. L. 1987. Chemoreception in Paramecium tetraurelia: acetate and folate-induced membrane hyperpolarization. *J Comp Physiol A,* 160**,** 525-35.

RADEVA, G. & SHAROM, F. J. 2004. Isolation and characterization of lipid rafts with different properties from RBL-2H3 (rat basophilic leukaemia) cells. *Biochem J,* 380**,** 219-30.

RAY, K. 2008. Characterization of *Paramecium tetraurelia* ciliary membrane plasma membrane calcium pumps and lipid rafts. *Thesis Masters Degree, Department of Biology, University of Vermont*.

RECHSTEINER, M. & ROGERS, S. W. 1996. PEST sequences and regulation by proteolysis. *Trends Biochem Sci,* 21**,** 267-71.

RODAL, S. K., SKRETTING, G., GARRED, O., VILHARDT, F., VAN DEURS, B. & SANDVIG, K. 1999. Extraction of cholesterol with methyl-beta-cyclodextrin perturbs formation of clathrin-coated endocytic vesicles. *Mol Biol Cell,* 10**,** 961-74.

ROGERS, S., WELLS, R. & RECHSTEINER, M. 1986. Amino acid sequences common to rapidly degraded proteins: the PEST hypothesis. *Science,* 234**,** 364-8.

RUIZ, F., GARREAU DE LOUBRESSE, N. & BEISSON, J. 1987. A mutation affecting basal body duplication and cell shape in Paramecium. *J Cell Biol,* 104**,** 417-30.

SAIDU, S. P., WEERARATNE, S. D., VALENTINE, M., DELAY, R. & VAN HOUTEN, J. L. 2009. Role of plasma membrane calcium ATPases in calcium clearance from olfactory sensory neurons. *Chem Senses,* 34**,** 349-58.

SANG, L., MILLER, J. J., CORBIT, K. C., GILES, R. H., BRAUER, M. J., OTTO, E. A., BAYE, L. M., WEN, X., SCALES, S. J., KWONG, M., HUNTZICKER, E. G., SFAKIANOS, M. K., SANDOVAL, W., BAZAN, J. F., KULKARNI, P., GARCIA-GONZALO, F. R., SEOL, A. D., O'TOOLE, J. F., HELD, S., REUTTER, H. M., LANE, W. S., RAFIQ, M. A., NOOR, A., ANSAR, M., DEVI, A. R., SHEFFIELD, V. C., SLUSARSKI, D. C., VINCENT, J. B., DOHERTY, D. A., HILDEBRANDT, F., REITER, J. F. & JACKSON, P. K. 2011. Mapping the NPHP-JBTS-MKS protein network reveals ciliopathy disease genes and pathways. *Cell,* 145**,** 513-28.

TSIOKAS, L., ARNOULD, T., ZHU, C., KIM, E., WALZ, G. & SUKHATME, V. P. 1999. Specific association of the gene product of PKD2 with the TRPC1 channel. *Proc Natl Acad Sci U S A,* 96**,** 3934-9.

VALENTINE, M. S., RAJENDRAN, A., YANO, J., WEERARATNE, S. D., BEISSON, J., COHEN, J., KOLL, F. & VAN HOUTEN, J. 2012. Paramecium BBS genes are key to presence of channels in Cilia. *Cilia,* 1**,** 16.

VAN HOUTEN, J. 1979. Membrane potential changes during chemokinesis in Paramecium. *Science,* 204**,** 1100-3.

VAN HOUTEN, J. 1998. Chemosensory Transduction in Paramecium. *European Journal of Protistology,* 34**,** 301-307.

VAN HOUTEN, J., MARTEL, E. & KASCH, T. 1982. Kinetic analysis of chemokinesis of Paramecium. *J Protozool,* 29**,** 226-30.

WEERARATNE, S. D. 2007. GPI receptors in folate chemosensortransduction in Paramecium tetraurelia. *PhD Thesis*.

WILLIAMS, C. L., LI, C. M., KIDA, K., INGLIS, P. N., MOHAN, S., SEMENEC, L., BIALAS, N. J., STUPAY, R. M., CHEN, N. S., BLACQUE, O. E., YODER, B. K. & LEROUX, M. R. 2011. MKS and NPHP modules cooperate to establish basal body/transition zone membrane associations and ciliary gate function during ciliogenesis. *Journal of Cell Biology,* 192**,** 1023-1041.

WRIGHT, M. V., ELWESS, N. & VAN HOUTEN, J. 1993. Ca2+ transport and chemoreception in Paramecium. *J Comp Physiol B,* 163**,** 288-96.

WRIGHT, M. V. & VAN HOUTEN, J. L. 1990. Characterization of a putative Ca2(+)-transporting Ca2(+)-ATPase in the pellicles of Paramecium tetraurelia. *Biochim Biophys Acta,* 1029**,** 241-51.

YANO, J., RAJENDRAN, A., VALENTINE, M. S., SAHA, M., BALLIF, B. A. & VAN HOUTEN, J. L. 2013. Proteomic analysis of the cilia membrane of Paramecium tetraurelia. *J Proteomics,* 78**,** 113-22.

Comprehensive Bibliography

ADAMS, M., SIMMS, R. J., ABDELHAMED, Z., DAWE, H. R., SZYMANSKA, K., LOGAN, C. V., WHEWAY, G., PITT, E., GULL, K., KNOWLES, M. A., BLAIR, E., CROSS, S. H., SAYER, J. A. & JOHNSON, C. A. 2012. A meckelin-filamin A interaction mediates ciliogenesis. *Hum Mol Genet,* 21**,** 1272-86.

ADOUTTE, A., RAMANATHAN, R., LEWIS, R. M., DUTE, R. R., LING, K. Y., KUNG, C. & NELSON, D. L. 1980. Biochemical studies of the excitable membrane of Paramecium tetraurelia. III. Proteins of cilia and ciliary membranes. *J Cell Biol,* 84**,** 717-38.

ADPKD 2014. Autosomal Dominant Polycystic Kidney Disease: Mutation Database. *PKD Foundation Web site*.

AGRAWAL, N., DASARADHI, P. V., MOHMMED, A., MALHOTRA, P., BHATNAGAR, R. K. & MUKHERJEE, S. K. 2003. RNA interference: biology, mechanism, and applications. *Microbiol Mol Biol Rev,* 67**,** 657-85.

ALLEN, R. D. 1971. Fine structure of membranous and microfibrillar systems in the cortex of Paramecium caudatum. *J Cell Biol,* 49**,** 1-20.

ALLEN, R. D. 1988. Chapter 2: Cytology. *Paramecium***,** 4-40.

ALLEN, R. D. & FOK, A. K. 1980. Membrane recycling and endocytosis in Paramecium confirmed by horseradish peroxidase pulse-chase studies. *J Cell Sci,* 45**,** 131-45.

ALLEN, R. D. & HAUSMANN, K. 1976. Membrane behavior of exocytic vesicles. I. The ultrastructure of Paramecium trichocysts in freeze-fracture preparations. *J Ultrastruct Res,* 54**,** 224-34.

ALVAREZ-LEEFMANS, F. J., GIRALDEZ, F. & GAMINO, S. M. 1987. Intracellular free magnesium in excitable cells: its measurement and its biologic significance. *Can J Physiol Pharmacol,* 65**,** 915-25.

ANDREWS, O. E., CHA, D. J., WEI, C. & PATTON, J. G. 2014. RNAi-mediated gene silencing in zebrafish triggered by convergent transcription. *Sci Rep,* 4**,** 5222.

ANYATONWU, G. I., ESTRADA, M., TIAN, X., SOMLO, S. & EHRLICH, B. E. 2007. Regulation of ryanodine receptor-dependent calcium signaling by polycystin-2. *Proc Natl Acad Sci U S A,* 104**,** 6454-9.

ARIYUREK, Y., LANTINGA-VAN LEEUWEN, I., SPRUIT, L., RAVINE, D., BREUNING, M. H. & PETERS, D. J. 2004. Large deletions in the polycystic kidney disease 1 (PKD1) gene. *Hum Mutat,* 23**,** 99.

ARNAIZ, O., CAIN, S., COHEN, J. & SPERLING, L. 2007. ParameciumDB: a community resource that integrates the Paramecium tetraurelia genome sequence with genetic data. *Nucleic Acids Res,* 35**,** D439-44.

ARNAIZ, O. & SPERLING, L. 2011. ParameciumDB in 2011: new tools and new data for functional and comparative genomics of the model ciliate Paramecium tetraurelia. *Nucleic Acids Res,* 39**,** D632-6.

AUBUSSON-FLEURY, A., LEMULLOIS, M., DE LOUBRESSE, N. G., LALIGNE, C., COHEN, J., ROSNET, O., JERKA-DZIADOSZ, M., BEISSON, J. & KOLL, F. 2012. The conserved centrosomal protein FOR20 is required for assembly of the transition zone and basal body docking at the cell surface. *J Cell Sci,* 125**,** 4395-404.

BAALA, L., ROMANO, S., KHADDOUR, R., SAUNIER, S., SMITH, U. M., AUDOLLENT, S., OZILOU, C., FAIVRE, L., LAURENT, N., FOLIGUET, B., MUNNICH, A., LYONNET, S., SALOMON, R., ENCHA-RAZAVI, F., GUBLER, M. C., BODDAERT, N., DE LONLAY, P., JOHNSON, C. A., VEKEMANS, M., ANTIGNAC, C. & ATTIE-BITACH, T. 2007. The Meckel-Gruber syndrome gene, MKS3, is mutated in Joubert syndrome. *Am J Hum Genet,* 80**,** 186-94.

BAE, Y. K., QIN, H., KNOBEL, K. M., HU, J., ROSENBAUM, J. L. & BARR, M. M. 2006. General and cell-type specific mechanisms target TRPP2/PKD-2 to cilia. *Development,* 133**,** 3859-70.

BAI, C. X., GIAMARCHI, A., RODAT-DESPOIX, L., PADILLA, F., DOWNS, T., TSIOKAS, L. & DELMAS, P. 2008. Formation of a new receptor-operated channel by heteromeric assembly of TRPP2 and TRPC1 subunits. *EMBO Rep,* 9**,** 472-9.

BARGMANN, C. I. 2006. Chemosensation in C. elegans. *WormBook***,** 1-29.

BARR, M. M., DEMODENA, J., BRAUN, D., NGUYEN, C. Q., HALL, D. H. & STERNBERG, P. W. 2001. The Caenorhabditis elegans autosomal dominant polycystic kidney disease gene homologs lov-1 and pkd-2 act in the same pathway. *Curr Biol,* 11**,** 1341-6.

BASU, B. & BRUECKNER, M. 2008. Cilia multifunctional organelles at the center of vertebrate left-right asymmetry. *Curr Top Dev Biol,* 85**,** 151-74.

BEISSON, J., CLEROT, J. C., FLEURY-AUBUSSON, A., GARREAU DE LOUBRESSE, N., RUIZ, F. & KLOTZ, C. 2001. Basal body-associated nucleation center for the centrin-based cortical cytoskeletal network in Paramecium. *Protist,* 152**,** 339-54.

BEISSON, J. & SONNEBORN, T. M. 1965. Cytoplasmic Inheritance of the Organization of the Cell Cortex in Paramecium Aurelia. *Proc Natl Acad Sci U S A,* 53**,** 275-82.

BEISSON, J. & WRIGHT, M. 2003. Basal body/centriole assembly and continuity. *Curr Opin Cell Biol,* 15**,** 96-104.

BELL, W. E., KARSTENS, W., SUN, Y. & VAN HOUTEN, J. L. 1998. Biotin chemoresponse in Paramecium. *Journal of Comparative Physiology a-Sensory Neural and Behavioral Physiology,* 183**,** 361-366.

BELL, W. E., PRESTON, R. R., YANO, J. & VAN HOUTEN, J. L. 2007. Genetic dissection of attractant-induced conductances in Paramecium. *J Exp Biol,* 210**,** 357-65.

BERBARI, N. F., LEWIS, J. S., BISHOP, G. A., ASKWITH, C. C. & MYKYTYN, K. 2008. Bardet-Biedl syndrome proteins are required for the localization of G protein-coupled receptors to primary cilia. *Proc Natl Acad Sci U S A,* 105**,** 4242-6.

BERNSTEIN, E., CAUDY, A. A., HAMMOND, S. M. & HANNON, G. J. 2001. Role for a bidentate ribonuclease in the initiation step of RNA interference. *Nature,* 409**,** 363-6.

BHOGARAJU, S., ENGEL, B. D. & LORENTZEN, E. 2013. Intraflagellar transport complex structure and cargo interactions. *Cilia,* 2**,** 10.

BRANCATI, F., IANNICELLI, M., TRAVAGLINI, L., MAZZOTTA, A., BERTINI, E., BOLTSHAUSER, E., D'ARRIGO, S., EMMA, F., FAZZI, E., GALLIZZI, R., GENTILE, M., LONCAREVIC, D., MEJASKI-BOSNJAK, V., PANTALEONI, C., RIGOLI, L., SALPIETRO, C. D., SIGNORINI, S., STRINGINI, G. R., VERLOES, A., ZABLOKA, D., DALLAPICCOLA, B., GLEESON, J. G. & VALENTE, E. M. 2009. MKS3/TMEM67 mutations are a major cause of COACH Syndrome, a Joubert Syndrome related disorder with liver involvement. *Hum Mutat,* 30**,** E432-42.

BRAUNREITER, K., HAMLIN, S. & LYMAN-GINGERICH, J. 2014. Identification and characterization of a novel allele of Caenorhabditis elegans bbs-7. *PLoS One,* 9**,** e113737.

BREHM, P., DUNLAP, K. & ECKERT, R. 1978. Calcium-dependent repolarization in Paramecium. *J Physiol,* 274**,** 639-54.

BROKAW, C. J. & KAMIYA, R. 1987. Bending patterns of Chlamydomonas flagella: IV. Mutants with defects in inner and outer dynein arms indicate differences in dynein arm function. *Cell Motil Cytoskeleton,* 8**,** 68-75.

BRONSEMA, K. J., BISCHOFF, R. & VAN DE MERBEL, N. C. 2013. High-sensitivity LC-MS/MS quantification of peptides and proteins in complex biological samples: the impact of enzymatic digestion and internal standard selection on method performance. *Anal Chem,* 85**,** 9528-35.

BUONANNO, F., HARUMOTO, T. & ORTENZI, C. 2013. The defensive function of trichocysts in Paramecium tetraurelia against metazoan predators compared with the chemical defense of two species of toxin-containing ciliates. *Zoolog Sci,* 30**,** 255-61.

CAI, Y., ANYATONWU, G., OKUHARA, D., LEE, K. B., YU, Z., ONOE, T., MEI, C. L., QIAN, Q., GENG, L., WIZTGALL, R., EHRLICH, B. E. & SOMLO, S. 2004. Calcium dependence of polycystin-2 channel activity is modulated by phosphorylation at Ser812. *J Biol Chem,* 279**,** 19987-95.

CAI, Y., MAEDA, Y., CEDZICH, A., TORRES, V. E., WU, G., HAYASHI, T., MOCHIZUKI, T., PARK, J. H., WITZGALL, R. & SOMLO, S. 1999. Identification and characterization of polycystin-2, the PKD2 gene product. *J Biol Chem,* 274**,** 28557-65.

CAMPILLO, C., JERBER, J., FISCH, C., SIMOES-BETBEDER, M., DUPUIS-WILLIAMS, P., NASSOY, P. & SYKES, C. 2012. Mechanics of membrane-cytoskeleton attachment in Paramecium. *New Journal of Physics,* 14.

CAPDEVILLE, Y., CHARRET, R., ANTONY, C., DELORME, J., NAHON, P., AND ADOUTTE, A. 1993. Ciliary and Plasma Membrane Proteins in *Paramecium*: Description, Localization, and Intracellular Transit. *Advances in Cell and Molecular Biology of Membranes,* 2A**,** 181-226.

CELIC, A. S., PETRI, E. T., BENBOW, J., HODSDON, M. E., EHRLICH, B. E. & BOGGON, T. J. 2012. Calcium-induced conformational changes in C-terminal tail of polycystin-2 are necessary for channel gating. *J Biol Chem,* 287**,** 17232-40.

CHAPIN, H. C. & CAPLAN, M. J. 2010. The cell biology of polycystic kidney disease. *J Cell Biol,* 191**,** 701-10.

CHEN, C. P. 2007. Meckel syndrome: genetics, perinatal findings, and differential diagnosis. *Taiwan J Obstet Gynecol,* 46**,** 9-14.

CHIH, B., LIU, P., CHINN, Y., CHALOUNI, C., KOMUVES, L. G., HASS, P. E., SANDOVAL, W. & PETERSON, A. S. 2012. A ciliopathy complex at the transition zone protects the cilia as a privileged membrane domain. *Nature Cell Biology,* 14**,** 61-U97.

CLEMENS, J. C., WORBY, C. A., SIMONSON-LEFF, N., MUDA, M., MAEHAMA, T., HEMMINGS, B. A. & DIXON, J. E. 2000. Use of double-stranded RNA interference in Drosophila cell lines to dissect signal transduction pathways. *Proceedings of the National Academy of Sciences of the United States of America,* 97**,** 6499-6503.

COLE, D. G., DIENER, D. R., HIMELBLAU, A. L., BEECH, P. L., FUSTER, J. C. & ROSENBAUM, J. L. 1998. Chlamydomonas kinesin-II-dependent intraflagellar transport (IFT): IFT particles contain proteins required for ciliary assembly in Caenorhabditis elegans sensory neurons. *J Cell Biol,* 141**,** 993-1008.

COOK, S. A., COLLIN, G. B., BRONSON, R. T., NAGGERT, J. K., LIU, D. P., AKESON, E. C. & DAVISSON, M. T. 2009. A mouse model for Meckel syndrome type 3. *J Am Soc Nephrol,* 20**,** 753-64.

CORNEC-LE GALL, E., AUDREZET, M. P., CHEN, J. M., HOURMANT, M., MORIN, M. P., PERRICHOT, R., CHARASSE, C., WHEBE, B., RENAUDINEAU, E., JOUSSET, P., GUILLODO, M. P., GRALL-JEZEQUEL, A., SALIOU, P., FEREC, C. & LE MEUR, Y. 2013. Type of PKD1 mutation influences renal outcome in ADPKD. *Journal of the American Society of Nephrology,* 24**,** 1006-13.

CRADDOCK, V. M. 1968. The reaction of N-methyl-N'-nitro-N-nitrosoguanidine with deoxyribonucleic acid. *Biochem J,* 106**,** 921-2.

CRONKITE, D. L. 1974. Genetics of chemical induction of conjugation in Paramecium aurella. *Genetics,* 76**,** 703-14.

CZAPLA, H. 2012. Cyclic adenosine monophoshate receptors in *Paramecium tetraurelia*. *MS thesis, Department of Biology, University of Vermont*.

CZARNECKI, P. G. & SHAH, J. V. 2012. The ciliary transition zone: from morphology and molecules to medicine. *Trends in Cell Biology,* 22**,** 201-210.

D'ANGELO, A. & FRANCO, B. 2009. The dynamic cilium in human diseases. *Pathogenetics,* 2**,** 3.

DAOUST, M. C., REYNOLDS, D. M., BICHET, D. G. & SOMLO, S. 1995. Evidence for a third genetic locus for autosomal dominant polycystic kidney disease. *Genomics,* 25**,** 733-6.

DAWE, H. R., ADAMS, M., WHEWAY, G., SZYMANSKA, K., LOGAN, C. V., NOEGEL, A. A., GULL, K. & JOHNSON, C. A. 2009. Nesprin-2 interacts with meckelin and mediates ciliogenesis via remodelling of the actin cytoskeleton. *J Cell Sci,* 122**,** 2716-26.

DAWE, H. R., SMITH, U. M., CULLINANE, A. R., GERRELLI, D., COX, P., BADANO, J. L., BLAIR-REID, S., SRIRAM, N., KATSANIS, N., ATTIE-BITACH, T., AFFORD, S. C., COPP, A. J., KELLY, D. A., GULL, K. & JOHNSON, C. A. 2007. The Meckel-Gruber Syndrome proteins MKS1 and meckelin interact and are required for primary cilium formation. *Hum Mol Genet,* 16**,** 173-86.

DELMAS, P., NAULI, S. M., LI, X., COSTE, B., OSORIO, N., CREST, M., BROWN, D. A. & ZHOU, J. 2004. Gating of the polycystin ion channel signaling complex in neurons and kidney cells. *FASEB J,* 18**,** 740-2.

DISHINGER, J. F., KEE, H. L., JENKINS, P. M., FAN, S., HURD, T. W., HAMMOND, J. W., TRUONG, Y. N., MARGOLIS, B., MARTENS, J. R. & VERHEY, K. J. 2010. Ciliary entry of the kinesin-2 motor KIF17 is regulated by importin-beta2 and RanGTP. *Nat Cell Biol,* 12**,** 703-10.

DU, J., DING, M., SOURS-BROTHERS, S., GRAHAM, S. & MA, R. 2008. Mediation of angiotensin II-induced Ca2+ signaling by polycystin 2 in glomerular mesangial cells. *Am J Physiol Renal Physiol,* 294**,** F909-18.

DU, J., MA, X., SHEN, B., HUANG, Y., BIRNBAUMER, L. & YAO, X. 2014. TRPV4, TRPC1, and TRPP2 assemble to form a flow-sensitive heteromeric channel. *FASEB J,* 28**,** 4677-85.

DU, Q., THONBERG, H., WANG, J., WAHLESTEDT, C. & LIANG, Z. 2005. A systematic analysis of the silencing effects of an active siRNA at all single-nucleotide mismatched target sites. *Nucleic Acids Res,* 33**,** 1671-7.

DUNLAP, K. 1977. Localization of calcium channels in Paramecium caudatum. *J Physiol,* 271**,** 119-33.

DUTE, R. & KUNG, C. 1978. Ultrastructure of the proximal region of somatic cilia in Paramecium tetraurelia. *J Cell Biol,* 78**,** 451-64.

ECKERT, R. 1972. Bioelectric control of ciliary activity. *Science,* 176**,** 473-81.

ECKERT, R. & BREHM, P. 1979. Ionic mechanisms of excitation in Paramecium. *Annu Rev Biophys Bioeng,* 8**,** 353-83.

FAN, S. & MARGOLIS, B. 2011. The Ran importin system in cilia trafficking. *Organogenesis,* 7**,** 147-53.

FENG, S., RODAT-DESPOIX, L., DELMAS, P. & ONG, A. C. 2011. A single amino acid residue constitutes the third dimerization domain essential for the assembly and function of the tetrameric polycystin-2 (TRPP2) channel. *J Biol Chem,* 286**,** 18994-9000.

FINETTI, F., PACCANI, S. R., RIPARBELLI, M. G., GIACOMELLO, E., PERINETTI, G., PAZOUR, G. J., ROSENBAUM, J. L. & BALDARI, C. T. 2009. Intraflagellar transport is

required for polarized recycling of the TCR/CD3 complex to the immune synapse. *Nat Cell Biol,* 11**,** 1332-9.

FIRE, A., XU, S., MONTGOMERY, M. K., KOSTAS, S. A., DRIVER, S. E. & MELLO, C. C. 1998. Potent and specific genetic interference by double-stranded RNA in Caenorhabditis elegans. *Nature,* 391**,** 806-11.

FLIEGAUF, M., BENZING, T. & OMRAN, H. 2007. Mechanisms of disease - When cilia go bad: cilia defects and ciliopathies. *Nature Reviews Molecular Cell Biology,* 8**,** 880-893.

FLOCK, A. & DUVALL, A. J., 3RD 1965. The Ultrastructure of the Kinocilium of the Sensory Cells in the Inner Ear and Lateral Line Organs. *J Cell Biol,* 25**,** 1-8.

FLOTENMEYER, M., MOMAYEZI, M. & PLATTNER, H. 1999. Immunolabeling analysis of biosynthetic and degradative pathways of cell surface components (glycocalyx) in Paramecium cells. *Eur J Cell Biol,* 78**,** 67-77.

FOSTER, L. J., DE HOOG, C. L. & MANN, M. 2003. Unbiased quantitative proteomics of lipid rafts reveals high specificity for signaling factors. *Proc Natl Acad Sci U S A,* 100**,** 5813-8.

GABOW, P. A. 1993. Autosomal dominant polycystic kidney disease. *N Engl J Med,* 329**,** 332-42.

GABRIDGE, M. G., DOUGHERTY, E. P., GLADD, M. F. & MECCOLI, R. A. 1982. Effects of heavy metals on structure, function, and metabolism of ciliated respiratory epithelium in vitro. *In Vitro,* 18**,** 1023-32.

GALVANI, A. & SPERLING, L. 2002. RNA interference by feeding in Paramecium. *Trends Genet,* 18**,** 11-2.

GARCIA-GONZALO, F. R., CORBIT, K. C., SIREROL-PIQUER, M. S., RAMASWAMI, G., OTTO, E. A., NORIEGA, T. R., SEOL, A. D., ROBINSON, J. F., BENNETT, C. L., JOSIFOVA, D. J., GARCIA-VERDUGO, J. M., KATSANIS, N., HILDEBRANDT, F. & REITER, J. F. 2011. A transition zone complex regulates mammalian ciliogenesis and ciliary membrane composition. *Nat Genet,* 43**,** 776-84.

GARCIA-GONZALO, F. R. & REITER, J. F. 2012. Scoring a backstage pass: mechanisms of ciliogenesis and ciliary access. *J Cell Biol,* 197**,** 697-709.

GENG, L., OKUHARA, D., YU, Z., TIAN, X., CAI, Y., SHIBAZAKI, S. & SOMLO, S. 2006. Polycystin-2 traffics to cilia independently of polycystin-1 by using an N-terminal RVxP motif. *J Cell Sci,* 119**,** 1383-95.

GERISCH, G. 1982. Chemotaxis in Dictyostelium. *Annu Rev Physiol,* 44**,** 535-52.

GIAMARCHI, A. & DELMAS, P. 2007. Activation Mechanisms and Functional Roles of TRPP2 Cation Channels. *In:* LIEDTKE, W. B. & HELLER, S. (eds.) *TRP Ion Channel Function in Sensory Transduction and Cellular Signaling Cascades.* Boca Raton (FL).

GIAMARCHI, A., FENG, S., RODAT-DESPOIX, L., XU, Y., BUBENSHCHIKOVA, E., NEWBY, L. J., HAO, J., GAUDIOSO, C., CREST, M., LUPAS, A. N., HONORE, E., WILLIAMSON, M. P., OBARA, T., ONG, A. C. & DELMAS, P. 2010. A polycystin-2 (TRPP2) dimerization

domain essential for the function of heteromeric polycystin complexes. *EMBO J,* 29**,** 1176-91.

GLEESON, J. G., KEELER, L. C., PARISI, M. A., MARSH, S. E., CHANCE, P. F., GLASS, I. A., GRAHAM JR, J. M., MARIA, B. L., BARKOVICH, A. J. & DOBYNS, W. B. 2004. Molar tooth sign of the midbrain-hindbrain junction: occurrence in multiple distinct syndromes. *Am J Med Genet A,* 125A**,** 125-34; discussion 117.

GODISKA, R., AUFDERHEIDE, K. J., GILLEY, D., HENDRIE, P., FITZWATER, T., PREER, L. B., POLISKY, B. & PREER, J. R., JR. 1987. Transformation of Paramecium by microinjection of a cloned serotype gene. *Proc Natl Acad Sci U S A,* 84**,** 7590-4.

GOGENDEAU, D., BEISSON, J., DE LOUBRESSE, N. G., LE CAER, J. P., RUIZ, F., COHEN, J., SPERLING, L., KOLL, F. & KLOTZ, C. 2007. An Sfi1p-like centrin-binding protein mediates centrin-based Ca2+ -dependent contractility in Paramecium tetraurelia. *Eukaryotic Cell,* 6**,** 1992-2000.

GOGENDEAU, D., KELLER, A. M., YANAGI, A., COHEN, J. & KOLL, F. 2005. Nd6p, a novel protein with RCC1-like domains involved in exocytosis in Paramecium tetraurelia. *Eukaryot Cell,* 4**,** 2129-39.

GONZALEZ-PERRETT, S., KIM, K., IBARRA, C., DAMIANO, A. E., ZOTTA, E., BATELLI, M., HARRIS, P. C., REISIN, I. L., ARNAOUT, M. A. & CANTIELLO, H. F. 2001. Polycystin-2, the protein mutated in autosomal dominant polycystic kidney disease (ADPKD), is a Ca2+-permeable nonselective cation channel. *Proc Natl Acad Sci U S A,* 98**,** 1182-7.

HANAOKA, K., QIAN, F., BOLETTA, A., BHUNIA, A. K., PIONTEK, K., TSIOKAS, L., SUKHATME, V. P., GUGGINO, W. B. & GERMINO, G. G. 2000. Co-assembly of polycystin-1 and -2 produces unique cation-permeable currents. *Nature,* 408**,** 990-4.

HANSMA, H. G. 1979. Sodium uptake and membrane excitation in Paramecium. *J Cell Biol,* 81**,** 374-81.

HARDT, M. & PLATTNER, H. 2000. Sub-second quenched-flow/X-ray microanalysis shows rapid Ca2+ mobilization from cortical stores paralleled by Ca2+ influx during synchronous exocytosis in Paramecium cells. *Eur J Cell Biol,* 79**,** 642-52.

HAYNES, W. J., KUNG, C., SAIMI, Y. & PRESTON, R. R. 2002. An exchanger-like protein underlies the large Mg2+ current in Paramecium. *Proc Natl Acad Sci U S A,* 99**,** 15717-22.

HILDEBRANDT, F., BENZING, T. & KATSANIS, N. 2011. Ciliopathies. *N Engl J Med,* 364**,** 1533-43.

HOEFELE, J., MAYER, K., SCHOLZ, M. & KLEIN, H. G. 2011. Novel PKD1 and PKD2 mutations in autosomal dominant polycystic kidney disease (ADPKD). *Nephrol Dial Transplant,* 26**,** 2181-8.

HOFFMEISTER, H., BABINGER, K., GURSTER, S., CEDZICH, A., MEESE, C., SCHADENDORF, K., OSTEN, L., DE VRIES, U., RASCLE, A. & WITZGALL, R. 2011. Polycystin-2 takes different routes to the somatic and ciliary plasma membrane. *J Cell Biol,* 192**,** 631-45.

HOLMES, L. B., DRISCOLL, S. G. & ATKINS, L. 1976. Etiologic heterogeneity of neural-tube defects. *N Engl J Med,* 294**,** 365-9.

HU, J., BAE, Y. K., KNOBEL, K. M. & BARR, M. M. 2006. Casein kinase II and calcineurin modulate TRPP function and ciliary localization. *Mol Biol Cell,* 17**,** 2200-11.

HUAN, Y. & VAN ADELSBERG, J. 1999. Polycystin-1, the PKD1 gene product, is in a complex containing E-cadherin and the catenins. *J Clin Invest,* 104**,** 1459-68.

HUANG, B., BATES, M. & ZHUANG, X. 2009. Super-resolution fluorescence microscopy. *Annu Rev Biochem,* 78**,** 993-1016.

HUANG, K., DIENER, D. R., MITCHELL, A., PAZOUR, G. J., WITMAN, G. B. & ROSENBAUM, J. L. 2007. Function and dynamics of PKD2 in Chlamydomonas reinhardtii flagella. *J Cell Biol,* 179**,** 501-14.

HUGHES, J., WARD, C. J., PERAL, B., ASPINWALL, R., CLARK, K., SAN MILLAN, J. L., GAMBLE, V. & HARRIS, P. C. 1995. The polycystic kidney disease 1 (PKD1) gene encodes a novel protein with multiple cell recognition domains. *Nat Genet,* 10**,** 151-60.

HUSSER, M. R., HARDT, M., BLANCHARD, M. P., HENTSCHEL, J., KLAUKE, N. & PLATTNER, H. 2004. One-way calcium spill-over during signal transduction in Paramecium cells: from the cell cortex into cilia, but not in the reverse direction. *Cell Calcium,* 36**,** 349-58.

IFTODE, F., ADOUTTE, A., AND FLEURY, A. 1996. The Surface Pattern of Paramecium tetraurelia in interphase: An Electron Microscopic Study of Basal Body Variability, Connections with Associated Ribbons and their Epiplasmic Environment. *European Journal of Protistology,* 32**,** 1.

IFTODE, F., COHEN, J., RUIZ, F., RUEDA, A. T., CHENSHAN, L., ADOUTTE, A. & BEISSON, J. 1989. Development of Surface Pattern during Division in Paramecium .1. Mapping of Duplication and Reorganization of Cortical Cytoskeletal Structures in the Wild-Type. *Development,* 105**,** 191-211.

IFTODE, F., COHEN, J., RUIZ, F., RUEDA, A. T., CHEN-SHAN, L., ADOUTE, A., AND BEISSON, J. 1989. Development of surface pattern during division in Paramesium. *Development,* 105**,** 191-211.

IFTODE, F., ADOUTTE, A., AND FLEURY, A. 1996. The Surface Pattern of Paramecium tetraurelia in interphase: An Electron Microscopic Study of Basal Body Variability, Connections with Associated Ribbons and their Epiplasmic Environment. *European Journal of Protistology,* 32**,** 12.

IFTODE, F. & FLEURY-AUBUSSON, A. 2003. Structural inheritance in Paramecium: ultrastructural evidence for basal body and associated rootlets polarity transmission through binary fission. *Biol Cell,* 95**,** 39-51.

IGARASHI, P. & SOMLO, S. 2002. Genetics and pathogenesis of polycystic kidney disease. *J Am Soc Nephrol,* 13**,** 2384-98.

IWADATE, Y. & KIKUYAMA, M. 2001. Contribution of calcium influx on trichocyst discharge in Paramecium caudatum. *Zoological Science,* 18**,** 497-504.

JACOBS, C. L. 2007. NMDA receptor associated protein in Paramecium and it involvement in glutamate chemoresponse. *MS thesis*. University of Vermont, Burlington, VT.

JENNINGS, H. S. 1906. *Behavior of the lower organisms,* New York,, The Columbia university press, The Macmillan company, agents; etc.

JIN, H., WHITE, S. R., SHIDA, T., SCHULZ, S., AGUIAR, M., GYGI, S. P., BAZAN, J. F. & NACHURY, M. V. 2010. The conserved Bardet-Biedl syndrome proteins assemble a coat that traffics membrane proteins to cilia. *Cell,* 141**,** 1208-19.

JOHNSON, K. A. & ROSENBAUM, J. L. 1992. Polarity of flagellar assembly in Chlamydomonas. *J Cell Biol,* 119**,** 1605-11.

KANESHIRO, E. S. 1987. Lipids of Paramecium. *J Lipid Res,* 28**,** 1241-58.

KEE, H. L. & VERHEY, K. J. 2013. Molecular connections between nuclear and ciliary import processes. *Cilia,* 2**,** 11.

KIM, E. J. & CERUTTI, H. 2009. Targeted gene silencing by RNA interference in Chlamydomonas. *Methods Cell Biol,* 93**,** 99-110.

KLAUKE, N., BLANCHARD, M. & PLATTNER, H. 2000. Polyamine triggering of exocytosis in Paramecium involves an extracellular Ca(2+)/(polyvalent cation)-sensing receptor, subplasmalemmal Ca-store mobilization and store-operated Ca(2+)-influx via unspecific cation channels. *J Membr Biol,* 174**,** 141-56.

KLINGER, M., WANG, W., KUHNS, S., BARENZ, F., DRAGER-MEURER, S., PEREIRA, G. & GRUSS, O. J. 2014. The novel centriolar satellite protein SSX2IP targets Cep290 to the ciliary transition zone. *Mol Biol Cell,* 25**,** 495-507.

KOBORI, T., SMITH, G. D., SANDFORD, R. & EDWARDSON, J. M. 2009. The transient receptor potential channels TRPP2 and TRPC1 form a heterotetramer with a 2:2 stoichiometry and an alternating subunit arrangement. *J Biol Chem,* 284**,** 35507-13.

KOTTGEN, M., BENZING, T., SIMMEN, T., TAUBER, R., BUCHHOLZ, B., FELICIANGELI, S., HUBER, T. B., SCHERMER, B., KRAMER-ZUCKER, A., HOPKER, K., SIMMEN, K. C., TSCHUCKE, C. C., SANDFORD, R., KIM, E., THOMAS, G. & WALZ, G. 2005. Trafficking of TRPP2 by PACS proteins represents a novel mechanism of ion channel regulation. *EMBO J,* 24**,** 705-16.

KOTTGEN, M., BUCHHOLZ, B., GARCIA-GONZALEZ, M. A., KOTSIS, F., FU, X., DOERKEN, M., BOEHLKE, C., STEFFL, D., TAUBER, R., WEGIERSKI, T., NITSCHKE, R., SUZUKI, M., KRAMER-ZUCKER, A., GERMINO, G. G., WATNICK, T., PRENEN, J., NILIUS, B., KUEHN, E. W. & WALZ, G. 2008. TRPP2 and TRPV4 form a polymodal sensory channel complex. *J Cell Biol,* 182**,** 437-47.

KOULEN, P., CAI, Y., GENG, L., MAEDA, Y., NISHIMURA, S., WITZGALL, R., EHRLICH, B. E. & SOMLO, S. 2002. Polycystin-2 is an intracellular calcium release channel. *Nat Cell Biol,* 4**,** 191-7.

KOZMINSKI, K. G., BEECH, P. L. & ROSENBAUM, J. L. 1995. The Chlamydomonas kinesin-like protein FLA10 is involved in motility associated with the flagellar membrane. *J Cell Biol,* 131**,** 1517-27.

KOZMINSKI, K. G., JOHNSON, K. A., FORSCHER, P. & ROSENBAUM, J. L. 1993. A motility in the eukaryotic flagellum unrelated to flagellar beating. *Proc Natl Acad Sci U S A,* 90**,** 5519-23.

KRAFT, M. L. 2013. Plasma membrane organization and function: moving past lipid rafts. *Mol Biol Cell,* 24**,** 2765-8.

KUNG, C. 1971. Genic mutants with altered system of excitation in Paramecium aurelia. II. Mutagenesis, screening and genetic analysis of the mutants. *Genetics,* 69**,** 29-45.

KUNG, C., CHANG, S. Y., SATOW, Y., HOUTEN, J. V. & HANSMA, H. 1975. Genetic dissection of behavior in paramecium. *Science,* 188**,** 898-904.

KUNG, C. & NAITO, Y. 1973. Calcium-induced ciliary reversal in the extracted models of "Pawn", a behavioral mutant of Paramecium. *Science,* 179**,** 195-6.

KUNG, C. & SAIMI, Y. 1982. The physiological basis of taxes in Paramecium. *Annu Rev Physiol,* 44**,** 519-34.

KUO, I. Y., KEELER, C., CORBIN, R., CELIC, A., PETRI, E. T., HODSDON, M. E. & EHRLICH, B. E. 2014. The number and location of EF hand motifs dictates the calcium dependence of polycystin-2 function. *FASEB J,* 28**,** 2332-46.

LENTINE, K. L., XIAO, H., MACHNICKI, G., GHEORGHIAN, A. & SCHNITZLER, M. A. 2010. Renal function and healthcare costs in patients with polycystic kidney disease. *Clin J Am Soc Nephrol,* 5**,** 1471-9.

LEITCH, C. C., ZAGHLOUL, N. A., DAVIS, E. E., STOETZEL, C., DIAZ-FONT, A., RIX, S., ALFADHEL, M., LEWIS, R. A., EYAID, W., BANIN, E., DOLLFUS, H., BEALES, P. L., BADANO, J. L. & KATSANIS, N. 2008. Hypomorphic mutations in syndromic encephalocele genes are associated with Bardet-Biedl syndrome. *Nat Genet,* 40**,** 443-8.

LI, H. & DURBIN, R. 2009. Fast and accurate short read alignment with Burrows-Wheeler transform. *Bioinformatics,* 25**,** 1754-60.

LI, Y., WRIGHT, J. M., QIAN, F., GERMINO, G. G. & GUGGINO, W. B. 2005. Polycystin 2 interacts with type I inositol 1,4,5-trisphosphate receptor to modulate intracellular Ca2+ signaling. *J Biol Chem,* 280**,** 41298-306.

LIEBERMAN, S. J., HAMASAKI, T. & SATIR, P. 1988. Ultrastructure and motion analysis of permeabilized Paramecium capable of motility and regulation of motility. *Cell Motil Cytoskeleton,* 9**,** 73-84.

LING, K. Y. & KUNG, C. 1980. Ba2+ influx measures the duration of membrane excitation in Paramecium. *J Exp Biol,* 84**,** 73-87.

LUO, Y., VASSILEV, P. M., LI, X., KAWANABE, Y. & ZHOU, J. 2003. Native polycystin 2 functions as a plasma membrane Ca2+-permeable cation channel in renal epithelia. *Mol Cell Biol,* 23**,** 2600-7.

MACHEMER-ROHNISCH, S. & MACHEMER, H. 1989. A Ca paradox: Electric and behavioural responses of Paramecium following changes in external ion concentration. *Eur J Protistol,* 25**,** 45-59.

MACHEMER, H. & ECKERT, R. 1973. Electrophysiological control of reversed ciliary beating in Paramecium. *J Gen Physiol,* 61**,** 572-87.

MACHEMER, H. & OGURA, A. 1979. Ionic conductances of membranes in ciliated and deciliated Paramecium. *J Physiol,* 296**,** 49-60.

MAGUIRE, M. E. & COWAN, J. A. 2002. Magnesium chemistry and biochemistry. *Biometals,* 15**,** 203-10.

MAZELOVA, J., ASTUTO-GRIBBLE, L., INOUE, H., TAM, B. M., SCHONTEICH, E., PREKERIS, R., MORITZ, O. L., RANDAZZO, P. A. & DERETIC, D. 2009. Ciliary targeting motif VxPx directs assembly of a trafficking module through Arf4. *EMBO J,* 28**,** 183-92.

MOCHIZUKI, T., WU, G., HAYASHI, T., XENOPHONTOS, S. L., VELDHUISEN, B., SARIS, J. J., REYNOLDS, D. M., CAI, Y., GABOW, P. A., PIERIDES, A., KIMBERLING, W. J., BREUNING, M. H., DELTAS, C. C., PETERS, D. J. & SOMLO, S. 1996. PKD2, a gene for polycystic kidney disease that encodes an integral membrane protein. *Science,* 272**,** 1339-42.

NACHURY, M. V. 2008. Tandem affinity purification of the BBSome, a critical regulator of Rab8 in ciliogenesis. *Methods Enzymol,* 439**,** 501-13.

NACHURY, M. V., LOKTEV, A. V., ZHANG, Q., WESTLAKE, C. J., PERANEN, J., MERDES, A., SLUSARSKI, D. C., SCHELLER, R. H., BAZAN, J. F., SHEFFIELD, V. C. & JACKSON, P. K. 2007. A core complex of BBS proteins cooperates with the GTPase Rab8 to promote ciliary membrane biogenesis. *Cell,* 129**,** 1201-13.

NAITOH, Y. 1966. Reversal response elicited in nonbeating cilia of paramecium by membrane depolarizatin. *Science,* 154**,** 660-2.

NAITOH, Y. 1968. Ionic control of the reversal response of cilia in Paramecium caudatum. A calcium hypothesis. *J Gen Physiol,* 51**,** 85-103.

NAITOH, Y., ECKERT, R. & FRIEDMAN, K. 1972. A regenerative calcium response in Paramecium. *J Exp Biol,* 56**,** 667-81.

NAULI, S. M., ALENGHAT, F. J., LUO, Y., WILLIAMS, E., VASSILEV, P., LI, X., ELIA, A. E., LU, W., BROWN, E. M., QUINN, S. J., INGBER, D. E. & ZHOU, J. 2003. Polycystins 1 and 2 mediate mechanosensation in the primary cilium of kidney cells. *Nat Genet,* 33**,** 129-37.

NIKOLAEV, M. V., MAGAZANIK, L. G. & TIKHONOV, D. B. 2012. Influence of external magnesium ions on the NMDA receptor channel block by different types of organic cations. *Neuropharmacology,* 62**,** 2078-85.

NOMURA, H., TURCO, A. E., PEI, Y., KALAYDJIEVA, L., SCHIAVELLO, T., WEREMOWICZ, S., JI, W., MORTON, C. C., MEISLER, M., REEDERS, S. T. & ZHOU, J. 1998. Identification of PKDL, a novel polycystic kidney disease 2-like gene whose murine homologue is deleted in mice with kidney and retinal defects. *J Biol Chem,* 273**,** 25967-73.

NONAKA, S., TANAKA, Y., OKADA, Y., TAKEDA, S., HARADA, A., KANAI, Y., KIDO, M. & HIROKAWA, N. 1998. Randomization of left-right asymmetry due to loss of nodal cilia generating leftward flow of extraembryonic fluid in mice lacking KIF3B motor protein. *Cell,* 95**,** 829-37.

OGURA, A. & MACHEMER, H. 1980. Distribution of Mechanoreceptor Channels in the Paramecium Surface-Membrane. *Journal of Comparative Physiology,* 135**,** 233-242.

PAN, Y. 2008. The role of plasma membrane calcium ATPase and its association with lipid rafts in chemoattraction in *Paramecium*. *Thesis Masters Degree, Department of Biology, University of Vermont*.

PAZOUR, G. J., AGRIN, N., LESZYK, J. & WITMAN, G. B. 2005. Proteomic analysis of a eukaryotic cilium. *J Cell Biol,* 170**,** 103-13.

PAZOUR, G. J., DICKERT, B. L., VUCICA, Y., SEELEY, E. S., ROSENBAUM, J. L., WITMAN, G. B. & COLE, D. G. 2000. Chlamydomonas IFT88 and its mouse homologue, polycystic kidney disease gene tg737, are required for assembly of cilia and flagella. *J Cell Biol,* 151**,** 709-18.

PAZOUR, G. J., DICKERT, B. L. & WITMAN, G. B. 1999. The DHC1b (DHC2) isoform of cytoplasmic dynein is required for flagellar assembly. *J Cell Biol,* 144**,** 473-81.

PAZOUR, G. J., SAN AGUSTIN, J. T., FOLLIT, J. A., ROSENBAUM, J. L. & WITMAN, G. B. 2002. Polycystin-2 localizes to kidney cilia and the ciliary level is elevated in orpk mice with polycystic kidney disease. *Curr Biol,* 12**,** R378-80.

PEDERSEN, L. B. & ROSENBAUM, J. L. 2008. Intraflagellar transport (IFT) role in ciliary assembly, resorption and signalling. *Curr Top Dev Biol,* 85**,** 23-61.

PICARIELLO, T., VALENTINE, M. S., YANO, J. & VAN HOUTEN, J. 2014. Reduction of meckelin leads to general loss of cilia, ciliary microtubule misalignment and distorted cell surface organization. *Cilia,* 3**,** 2.

PIKE, L. J. 2003. Lipid rafts: bringing order to chaos. *J Lipid Res,* 44**,** 655-67.

PIPERNO, G. & MEAD, K. 1997. Transport of a novel complex in the cytoplasmic matrix of Chlamydomonas flagella. *Proc Natl Acad Sci U S A,* 94**,** 4457-62.

PLATTNER, H. & KISSMEHL, R. 2003. Molecular aspects of membrane trafficking in paramecium. *Int Rev Cytol,* 232**,** 185-216.

PORTER, M. E., BOWER, R., KNOTT, J. A., BYRD, P. & DENTLER, W. 1999. Cytoplasmic dynein heavy chain 1b is required for flagellar assembly in Chlamydomonas. *Mol Biol Cell,* 10**,** 693-712.

PRATT, A. J. & MACRAE, I. J. 2009. The RNA-induced silencing complex: a versatile gene-silencing machine. *J Biol Chem,* 284**,** 17897-901.

PRESTON, R. R. 1990. A magnesium current in Paramecium. *Science,* 250**,** 285-8.

PRESTON, R. R. 1998. Transmembrane Mg2+ currents and intracellular free Mg2+ concentration in Paramecium tetraurelia. *J Membr Biol,* 164**,** 11-24.

PRESTON, R. R. & KUNG, C. 1994a. Inhibition of Mg2+ current by single-gene mutation in Paramecium. *J Membr Biol,* 139**,** 203-13.

PRESTON, R. R. & KUNG, C. 1994k. Isolation and characterization of paramecium mutants defective in their response to magnesium. *Genetics,* 137**,** 759-69.

PRESTON, R. R. & USHERWOOD, P. N. R. 1988. Characterization of a Specific L-[H-3]Glutamic Acid Binding-Site on Cilia Isolated from Paramecium-Tetraurelia. *Journal of Comparative Physiology B-Biochemical Systemic and Environmental Physiology,* 158**,** 345-351.

PRESTON, R. R. & VAN HOUTEN, J. L. 1987. Chemoreception in Paramecium tetraurelia: acetate and folate-induced membrane hyperpolarization. *J Comp Physiol A,* 160**,** 525-35.

RADEVA, G. & SHAROM, F. J. 2004. Isolation and characterization of lipid rafts with different properties from RBL-2H3 (rat basophilic leukaemia) cells. *Biochem J,* 380**,** 219-30.

ROMANOVITCH, M. 2012. The L-glutamate receptor in Paramecium tetraurelia. *MS thesis*.

RASBAND, W. S. 1997-2009. ImageJ. *U.S. National Institute of Health.*

RAY, K. 2008. Characterization of *Paramecium tetraurelia* ciliary membrane plasma membrane calcium pumps and lipid rafts. *Thesis Masters Degree, Department of Biology, University of Vermont*.

RECHSTEINER, M. & ROGERS, S. W. 1996. PEST sequences and regulation by proteolysis. *Trends Biochem Sci,* 21**,** 267-71.

REEDERS, S. T., BREUNING, M. H., DAVIES, K. E., NICHOLLS, R. D., JARMAN, A. P., HIGGS, D. R., PEARSON, P. L. & WEATHERALL, D. J. 1985. A highly polymorphic DNA marker linked to adult polycystic kidney disease on chromosome 16. *Nature,* 317**,** 542-4.

RHOADS, D. E. & KANESHIRO, E. S. 1979. Characterizations of Phospholipids from Paramecium-Tetraurelia Cells and Cilia. *Journal of Protozoology,* 26**,** 329-338.

RINGO, D. L. 1967. Flagellar motion and fine structure of the flagellar apparatus in Chlamydomonas. *J Cell Biol,* 33**,** 543-71.

RODAL, S. K., SKRETTING, G., GARRED, O., VILHARDT, F., VAN DEURS, B. & SANDVIG, K. 1999. Extraction of cholesterol with methyl-beta-cyclodextrin perturbs formation of clathrin-coated endocytic vesicles. *Mol Biol Cell,* 10**,** 961-74.

ROGERS, S., WELLS, R. & RECHSTEINER, M. 1986. Amino acid sequences common to rapidly degraded proteins: the PEST hypothesis. *Science,* 234**,** 364-8.

RUIZ, F., BEISSON, J., ROSSIER, J., DUPUIS-WILLIAMS, P. 1999. Basal Body duplication in Paramecium requires gamma-tubulin. *Current Biology,* 9**,** 43-46.

RUIZ, F., GARREAU DE LOUBRESSE, N., KLOTZ, C., BEISSON, J. & KOLL, F. 2005. Centrin deficiency in Paramecium affects the geometry of basal-body duplication. *Curr Biol,* 15**,** 2097-106.

SAHA, M., CARRIERE, A., CHEERATHODI, M., ZHANG, X., LAVOIE, G., RUSH, J., ROUX, P. P. & BALLIF, B. A. 2012. RSK phosphorylates SOS1 creating 14-3-3-docking sites and negatively regulating MAPK activation. *Biochem J,* 447**,** 159-66.

SAIDU, S. P., WEERARATNE, S. D., VALENTINE, M., DELAY, R. & VAN HOUTEN, J. L. 2009. Role of plasma membrane calcium ATPases in calcium clearance from olfactory sensory neurons. *Chem Senses,* 34**,** 349-58.

SAIMI, Y. & KUNG, C. 1980. A Ca-induced Na-current in Paramecium. *J Exp Biol,* 88**,** 305-25.

SALONEN, R. & NORIO, R. 1984. The Meckel syndrome in Finland: epidemiologic and genetic aspects. *Am J Med Genet,* 18**,** 691-8.

SALONEN, R. & PAAVOLA, P. 1998. Meckel syndrome. *J Med Genet,* 35**,** 497-501.

SAMMELS, E., DEVOGELAERE, B., MEKAHLI, D., BULTYNCK, G., MISSIAEN, L., PARYS, J. B., CAI, Y., SOMLO, S. & DE SMEDT, H. 2010. Polycystin-2 activation by inositol 1,4,5-trisphosphate-induced Ca2+ release requires its direct association with the inositol 1,4,5-trisphosphate receptor in a signaling microdomain. *J Biol Chem,* 285**,** 18794-805.

SANG, L., MILLER, J. J., CORBIT, K. C., GILES, R. H., BRAUER, M. J., OTTO, E. A., BAYE, L. M., WEN, X., SCALES, S. J., KWONG, M., HUNTZICKER, E. G., SFAKIANOS, M. K., SANDOVAL, W., BAZAN, J. F., KULKARNI, P., GARCIA-GONZALO, F. R., SEOL, A. D., O'TOOLE, J. F., HELD, S., REUTTER, H. M., LANE, W. S., RAFIQ, M. A., NOOR, A., ANSAR, M., DEVI, A. R., SHEFFIELD, V. C., SLUSARSKI, D. C., VINCENT, J. B., DOHERTY, D. A., HILDEBRANDT, F., REITER, J. F. & JACKSON, P. K. 2011. Mapping the NPHP-JBTS-MKS protein network reveals ciliopathy disease genes and pathways. *Cell,* 145**,** 513-28.

SASNER, J. M. & VAN HOUTEN, J. L. 1989. Evidence for a *Paramecium* folate chemoreceptor. *Chemical Senses,* 14**,** 587-595.

SATIR, B., SALE, W. S. & SATIR, P. 1976. Membrane renewal after dibucaine deciliation of Tetrahymena. Freeze-fracture technique, cilia, membrane structure. *Exp Cell Res,* 97**,** 83-91.

SATOW, Y. 1978. Internal calcium concentration and potassium permeability in Paramecium. *J Neurobiol,* 9**,** 81-91.

SATOW, Y. & KUNG, C. 1976. A 'TEA+-insensitive' mutant with increased potassium conductance in Paramecium aurelia. *J Exp Biol,* 65**,** 51-63.

SATOW, Y. & KUNG, C. 1980. Ca-induced K+-outward current in Paramecium tetraurelia. *J Exp Biol,* 88**,** 293-303.

SCHULTZ, J. E., KLUMPP, S., BENZ, R., SCHURHOFF-GOETERS, W. J. & SCHMID, A. 1992. Regulation of adenylyl cyclase from Paramecium by an intrinsic potassium conductance. *Science,* 255**,** 600-3.

SCHWARZ, D. S., TOMARI, Y. & ZAMORE, P. D. 2004. The RNA-induced silencing complex is a Mg2+-dependent endonuclease. *Curr Biol,* 14**,** 787-91.

SEPULVEDA, W., SEBIRE, N. J., SOUKA, A., SNIJDERS, R. J. & NICOLAIDES, K. H. 1997. Diagnosis of the Meckel-Gruber syndrome at eleven to fourteen weeks' gestation. *Am J Obstet Gynecol,* 176**,** 316-9.

SHARMA, N., BERBARI, N. F. & YODER, B. K. 2008. Ciliary dysfunction in developmental abnormalities and diseases. *Curr Top Dev Biol,* 85**,** 371-427.

SMITH, E. F. & SALE, W. S. 1992. Structural and functional reconstitution of inner dynein arms in Chlamydomonas flagellar axonemes. *J Cell Biol,* 117**,** 573-81.

SMITH, U. M., CONSUGAR, M., TEE, L. J., MCKEE, B. M., MAINA, E. N., WHELAN, S., MORGAN, N. V., GORANSON, E., GISSEN, P., LILLIQUIST, S., ALIGIANIS, I. A., WARD, C. J., PASHA, S., PUNYASHTHITI, R., MALIK SHARIF, S., BATMAN, P. A., BENNETT, C. P., WOODS, C. G., MCKEOWN, C., BUCOURT, M., MILLER, C. A., COX, P., ALGAZALI, L., TREMBATH, R. C., TORRES, V. E., ATTIE-BITACH, T., KELLY, D. A., MAHER, E. R., GATTONE, V. H., 2ND, HARRIS, P. C. & JOHNSON, C. A. 2006. The transmembrane protein meckelin (MKS3) is mutated in Meckel-Gruber syndrome and the wpk rat. *Nat Genet,* 38**,** 191-6.

SONNEBORN, T. M. 1970. Gene action in development. *Proc R Soc Lond B Biol Sci,* 176**,** 347-66.

SPERLING, L., KERYER, G., RUIZ, F. & BEISSON, J. 1991. Cortical morphogenesis in Paramecium: a transcellular wave of protein phosphorylation involved in ciliary rootlet disassembly. *Dev Biol,* 148**,** 205-18.

STELLY, N., MAUGER, J. P., CLARET, M. & ADOUTTE, A. 1991. Cortical alveoli of Paramecium: a vast submembranous calcium storage compartment. *J Cell Biol,* 113**,** 103-12.

STEWART, A. P., SMITH, G. D., SANDFORD, R. N. & EDWARDSON, J. M. 2010. Atomic force microscopy reveals the alternating subunit arrangement of the TRPP2-TRPV4 heterotetramer. *Biophys J,* 99**,** 790-7.

SUI, G., SOOHOO, C., AFFAR EL, B., GAY, F., SHI, Y., FORRESTER, W. C. & SHI, Y. 2002. A DNA vector-based RNAi technology to suppress gene expression in mammalian cells. *Proc Natl Acad Sci U S A,* 99**,** 5515-20.

TAMMACHOTE, R., HOMMERDING, C. J., SINDERS, R. M., MILLER, C. A., CZARNECKI, P. G., LEIGHTNER, A. C., SALISBURY, J. L., WARD, C. J., TORRES, V. E., GATTONE, V. H., 2ND & HARRIS, P. C. 2009. Ciliary and centrosomal defects associated with mutation and depletion of the Meckel syndrome genes MKS1 and MKS3. *Hum Mol Genet,* 18**,** 3311-23.

TORRES, V. E., CHAPMAN, A. B., DEVUYST, O., GANSEVOORT, R. T., GRANTHAM, J. J., HIGASHIHARA, E., PERRONE, R. D., KRASA, H. B., OUYANG, J., CZERWIEC, F. S. & INVESTIGATORS, T. T. 2012. Tolvaptan in patients with autosomal dominant polycystic kidney disease. *N Engl J Med,* 367**,** 2407-18.

TORRES, V. E., HARRIS, P. C. & PIRSON, Y. 2007. Autosomal dominant polycystic kidney disease. *Lancet,* 369**,** 1287-301.

TSIOKAS, L., ARNOULD, T., ZHU, C., KIM, E., WALZ, G. & SUKHATME, V. P. 1999. Specific association of the gene product of PKD2 with the TRPC1 channel. *Proc Natl Acad Sci U S A,* 96**,** 3934-9.

TSIOKAS, L., KIM, E., ARNOULD, T., SUKHATME, V. P. & WALZ, G. 1997a. Homo- and heterodimeric interactions between the gene products of PKD1 and PKD2. *Proc Natl Acad Sci U S A,* 94**,** 6965-70.

TSIOKAS, L., KIM, E., ARNOULD, T., SUKHATME, V. P. & WALZ, G. 1997b. Homo- and heterodimeric interactions between the gene products of PKD1 and PKD2. *Proceedings of the National Academy of Sciences of the United States of America,* 94**,** 6965-6970.

VALENTINE, M. S., RAJENDRAN, A., YANO, J., WEERARATNE, S. D., BEISSON, J., COHEN, J., KOLL, F. & VAN HOUTEN, J. 2012. *Paramecium* BBS genes are key to presence of channels in Cilia. *Cilia,* 1**,** 16.

VAN HOUTEN, J. 1979. Membrane potential changes during chemokinesis in Paramecium. *Science,* 204**,** 1100-3.

VAN HOUTEN, J. 1998. Chemosensory Transduction in Paramecium. *European Journal of Protistology,* 34**,** 301-307.

VAN HOUTEN, J., MARTEL, E. & KASCH, T. 1982. Kinetic analysis of chemokinesis of Paramecium. *J Protozool,* 29**,** 226-30.

VAN HOUTEN, J. L., YANG, W. Q. & BERGERON, A. 2000. Chemosensory signal transduction in paramecium. *J Nutr,* 130**,** 946S-9S.

VAYSSIE, L., GARREAU DE LOUBRESSE, N. & SPERLING, L. 2001. Growth and form of secretory granules involves stepwise assembly but not differential sorting of a family of secretory proteins in Paramecium. *J Cell Sci,* 114**,** 875-86.

WATANABE, T. 1978. A scanning electron-microscopic study of the local degeneration of cilia during sexual reproduction in Paramecium. *J Cell Sci,* 32**,** 55-66.

WEERARATNE, S. D. 2007. GPI receptors in folate chemosensortransduction in Paramecium tetraurelia. *PhD Thesis*. University of Vermont, Burlington, VT.

WILLIAMS, C. L., LI, C. M., KIDA, K., INGLIS, P. N., MOHAN, S., SEMENEC, L., BIALAS, N. J., STUPAY, R. M., CHEN, N. S., BLACQUE, O. E., YODER, B. K. & LEROUX, M. R. 2011. MKS and NPHP modules cooperate to establish basal body/transition zone membrane associations and ciliary gate function during ciliogenesis. *Journal of Cell Biology,* 192**,** 1023-1041.

WILLIAMS, C. L., MCINTYRE, J. C., NORRIS, S. R., JENKINS, P. M., ZHANG, L., PEI, Q., VERHEY, K. & MARTENS, J. R. 2014. Direct evidence for BBSome-associated intraflagellar transport reveals distinct properties of native mammalian cilia. *Nat Commun,* 5**,** 5813.

WILSON, P. D. 2004. Polycystic kidney disease. *N Engl J Med,* 350**,** 151-64.

WRIGHT, M. V., ELWESS, N. & VAN HOUTEN, J. 1993. Ca2+ transport and chemoreception in Paramecium. *J Comp Physiol B,* 163**,** 288-96.

WRIGHT, M. V. & VAN HOUTEN, J. L. 1990. Characterization of a putative Ca2(+)-transporting Ca2(+)-ATPase in the pellicles of Paramecium tetraurelia. *Biochim Biophys Acta,* 1029**,** 241-51.

YANG, Y., COCHRAN, D. A., GARGANO, M. D., KING, I., SAMHAT, N. K., BURGER, B. P., SABOURIN, K. R., HOU, Y., AWATA, J., PARRY, D. A., MARSHALL, W. F., WITMAN, G. B. & LU, X. 2011. Regulation of flagellar motility by the conserved flagellar protein CG34110/Ccdc135/FAP50. *Mol Biol Cell,* 22**,** 976-87.

YANG, P., DIENER, D. R., YANG, C., KOHNO, T., PAZOUR, G. J., DIENES, J. M., AGRIN, N. S., KING, S. M., SALE, W. S., KAMIYA, R., ROSENBAUM, J. L. & WITMAN, G. B. 2006. Radial spoke proteins of Chlamydomonas flagella. *J Cell Sci,* 119**,** 1165-74.

YANO, J., RACHOCHY, V. & VAN HOUTEN, J. L. 2003. Glycosyl phosphatidylinositol-anchored proteins in chemosensory signaling: antisense manipulation of Paramecium tetraurelia PIG-A gene expression. *Eukaryot Cell,* 2**,** 1211-9.

YANO, J., RAJENDRAN, A., VALENTINE, M. S., SAHA, M., BALLIF, B. A. & VAN HOUTEN, J. L. 2013. Proteomic analysis of the cilia membrane of Paramecium tetraurelia. *J Proteomics,* 78**,** 113-22.

YOSHIBA, S., SHIRATORI, H., KUO, I. Y., KAWASUMI, A., SHINOHARA, K., NONAKA, S., ASAI, Y., SASAKI, G., BELO, J. A., SASAKI, H., NAKAI, J., DWORNICZAK, B., EHRLICH, B. E., PENNEKAMP, P. & HAMADA, H. 2012. Cilia at the node of mouse embryos sense fluid flow for left-right determination via Pkd2. *Science,* 338**,** 226-31.

ZAGULSKI, M., NOWAK, J. K., LE MOUEL, A., NOWACKI, M., MIGDALSKI, A., GROMADKA, R., NOEL, B., BLANC, I., DESSEN, P., WINCKER, P., KELLER, A. M., COHEN, J., MEYER, E. & SPERLING, L. 2004. High coding density on the largest Paramecium tetraurelia somatic chromosome. *Curr Biol,* 14**,** 1397-404.

ZHANG, P., LUO, Y., CHASAN, B., GONZALEZ-PERRETT, S., MONTALBETTI, N., TIMPANARO, G. A., CANTERO MDEL, R., RAMOS, A. J., GOLDMANN, W. H., ZHOU, J. & CANTIELLO, H. F. 2009. The multimeric structure of polycystin-2 (TRPP2): structural-functional correlates of homo- and hetero-multimers with TRPC1. *Hum Mol Genet,* 18**,** 1238-51.

ZHANG, Q., YU, D., SEO, S., STONE, E. M. & SHEFFIELD, V. C. 2012. Intrinsic protein-protein interaction-mediated and chaperonin-assisted sequential assembly of stable bardet-biedl syndrome protein complex, the BBSome. *J Biol Chem,* 287**,** 20625-35.

ZHANG, Z. R., CHU, W. F., SONG, B., GOOZ, M., ZHANG, J. N., YU, C. J., JIANG, S., BALDYS, A., GOOZ, P., STEELE, S., OWSIANIK, G., NILIUS, B., KOMLOSI, P. & BELL, P. D. 2013. TRPP2 and TRPV4 form an EGF-activated calcium permeable channel at the apical membrane of renal collecting duct cells. *PLoS One,* 8**,** e73424.

Appendix I: Depletion of Meckelin (*MKS3*) Leads to Short Cilia, Changes in Ciliary Ion Channels over Time, and a Loss of Trichocyst Discharge

Abstract

Meckelin (MKS3), a highly conserved integral membrane protein linked to Meckel-Gruber syndrome (MKS), assists in the migration of centrioles to the cell surface and ciliogenesis. In *Paramecium*, the MKS3 protein is located at the base of cilia, consistent with a role as a transition zone protein. In addition to its proposed role at the transition zone in *Paramecium*, we have also speculated that MKS3 is important for the guidance of daughter basal bodies along the striated rootlet before cell division. We have demonstrated previously that the reduction of *MKS3* leads to basal body rotation out of the anterior-posterior axis of the cell, a disruption of cortical rows and a disruption of the cell and ciliary surface, as well as a global loss of cilia. We present here additional and more detailed findings in *Paramecium* upon depletion of *MKS3*. Time-course studies of the RNAi treated cells, as well as the *IFT88* depleted cells, show short and missing cilia as soon as 24 hours after the start of the RNAi treatment. The ion channels of the ciliary membrane become unbalanced showing changes in the behavior of the *MKS3* depleted cells that are different from the *IFT88* depleted cells, suggesting further that MKS3 is important for regulating the proteins of the cilia. Lastly, trichocyst expulsion is inhibited in the *MKS3* depleted cells, presumably due to the disrupted cell surface. These results further highlight the importance of the MKS3 protein in proper ciliary maintenance and content and that depletion of MKS3 has global effects on the cell surface and the cilia which worsen over time.

Introduction

Abnormalities in the assembly, maintenance or function of cilia are collectively called ciliopathies. Ciliopathies can lead to defects in development, cysts in the kidneys and/or pancreas, fertility problems, and many other complications in mammals (reviewed in (D'Angelo and Franco, 2009)). In an effort to better understand the broad distribution of disorders and complications that arise from ciliopathies, research is needed to understand the function and involvement of the dysfunctional genes that contribute to the complications (Pazour et al., 2000, Pedersen and Rosenbaum, 2008, Sharma et al., 2008). One such ciliopathic gene, Meckelin (MKS3 or TMEM67), is linked to numerous ciliopathies. Presented here are additional results of the depletion of *MKS3* in the model organism *Paramecium tetraurelia*.

Cilia are highly conserved organelles that are vital for development and signal transduction in cells (Pedersen and Rosenbaum, 2008). These organelles are generally anchored by the basal body, which is positioned just below the cell surface. The basal body, as well as a closely related organelle, the centriole, are comprised of nine triplets of microtubules arranged in a circle to form a cartwheel pattern. The basal body is approximately 220 nm wide and 400 nm tall (Ringo, 1967). The cilia that emanate from the basal body are generally described as motile or non-motile, but all appear to have sensory functions. In general, non-motile or primary cilia lack the central pair of microtubules while motile cilia generally have a central pair of microtubules. However, there are examples of cilia that are motile and lack the central pair of microtubules, or have other configurations (Basu and Brueckner, 2008).

The cilium develops from the basal body using cargo that is transported via intraflagellar transport (IFT) complexes. These complexes were first described in *Chlamydomonas reinhardtii* (Kozminski et al., 1993, Rosenbaum et al., 1999). This transportation mechanism is bi-directional, using a kinesin-2 motor protein to carry cargo and proteins toward the tip (Kozminski et al.,

1995) and a dynein 2 motor protein to return cargo from the tip to the base (Pazour et al., 1999, Porter et al., 1999). Anterograde transport from base to tip relies on the IFT B complex while retrograde transport from the tip to base relies on the IFT A complex (Kozminski et al., 1995, Pazour et al., 1999). Complex B is comprised of at least eleven proteins, and complex A is made of at least six proteins (Cole et al., 1998, Piperno and Mead, 1997). IFT88, a component of complex B, leads to missing cilia or severely truncated ones when it is non-functional or missing (Nonaka et al., 1998). Defects in the IFT complexes are linked to ciliopathies (Pazour et al., 2000).

Previously, we demonstrated that the MKS3 protein is located above the plane of the basal body and is present at almost every basal body. Depletion of *MKS3* in *Paramecium* leads to missing cilia, disrupted basal body rows, and unorganized cortical units (Picariello et al., 2014). The thousands of cilia and organized cell surface of *Paramecium* has made it an ideal model organism for the study of MKS3. The surface of these cells is organized into a pattern of hexagonal polarized units arranged in rows that run longitudinally along the cell (Allen, 1971, Sonneborn, 1970). Each of these cortical units is outlined by a ridge and contains one or two basal bodies (Allen and Fok, 1980) with associated rootlets. The basal body in single basal body units, or the posterior (mother) basal body in two basal body units has three associated rootlets. The striated rootlet, or kinetodesmal fiber, projects toward the anterior of the cell and may pass through numerous cortical units. The other two associated rootlets are at 7 o'clock and 5 o'clock, as if looking down upon the basal body as if it were a clock face. The post ciliary rootlet is at 7 o'clock and the transverse microtubule is at 5 o'clock (Iftode, 1996). During division, all these components undergo a highly complex and organized process to create two daughter cells. Disruptions or arrest at certain stages in this process can cause the cells to stop their growth or to die (Iftode et al., 1989, Ruiz et al., 2005, Ruiz, 1999).

Also present just below the cell surface at the apex of the ridges that delineate the cortical units are secretory vesicles named trichocysts (Sonneborn, 1970, Allen, 1971, Iftode et al., 1989). The trichocysts are expected to be a defense mechanism (Buonanno et al., 2013). When a *Paramecium* cell comes into contact with a predatory, the trichocysts are rapidly expelled in a Ca-dependent manner (Buonanno et al., 2013, Hardt and Plattner, 2000). When the trichocysts are expelled, it also causes the cilia to reverse, propelling the cell backwards and away from the predator (Hardt and Plattner, 2000, Husser et al., 2004). There are *Paramecium* mutants that are unable to expel their trichocysts, called ND mutants for "non-discharge" (Gogendeau et al., 2005).

Ciliopathies can also arise from defects in the sensory function of cilia. Paramecia rely on their cilia not only for locomotion, but also for sensory perception of their environment. Defects in sensory perception can be monitored by the swimming behavior of these cells. The cilia of *Paramecium* are under the electrical control of the membrane which is dependent on the ion channels of the cell membrane and of the cilia (Eckert, 1972, Eckert and Brehm, 1979, Machemer and Ogura, 1979). The majority of the ion channels that are important for this behavior reside in the cilia (Machemer and Ogura, 1979). Changes to the channel content can easily be observed through changes in swimming behaviors of paramecia cells. Longer or shorter backward swimming in certain ionic stimuli can infer an overactive or underactive channel. This allows for the study of ionic conductances by proxy of swimming behavior in *Paramecium* (Machemer and Ogura, 1979, Brehm et al., 1978).

We present here additional studies of *MKS3* using RNAi beyond our previously published works (Picariello et al., 2014). Included are additional studies on *IFT88* RNAi that accompany the *MKS3* RNAi studies for comparison. Reduction of *IFT88* using RNAi is used as a positive control because the functions of IFT88 in ciliogenesis are well understood. We expect the observations of these depleted cells are from the global shortening and loss of cilia due to a loss

of IFT. This additional work examines the rate of loss of the cilia on *MKS3* and *IFT88* depleted cells as well as changes to the backward swimming behavior of these cells over time. Lastly, an analysis of trichocyst discharge of the cells is included, focusing on the central midline where we most commonly see disruptions of the basal bodies and cortical units (Picariello et al., 2014). This work supports *Paramecium* Mks3p having a role in the gating or passage of proteins into the cilia as well as in the organization of the cell surface.

Materials and Methods

Stocks, Cultures and Chemicals

Cells were grown in wheat grass medium inoculated with *Klebsiella pneumoniae* or *Aerobacter aerogenes* (adapted from (Sasner and Vanhouten, 1989)). Cell lines used were *Paramecium tetraurelia* (51-s, sensitive to killer) or *Paramecium tetraurelia* (ND6) non-discharge mutant (Gogendeau et al., 2005). All chemicals were from Sigma-Aldrich unless otherwise noted. In all experiments, cells were filtered and collected by low-speed centrifugation and washed two times in Dryl's solution (1 mM Na_2HPO_4, 1 mM NaH_2PO_4, 1.5 mM $CaCl_2$, 2 mM Na-citrate, pH 6.8).

Data Mining and Construct Design

Constructs were created as previously described (Picariello et al., 2014). Constructs were created from genomic DNA isolated using organic extraction and isopropanol precipitation. Sequence GSPATG00015939001 was used to create the RNAi construct to target *MKS3* mRNA, from positions +1100 to +2019, which is 31.9% of the gene. Primers were: 5'-GAAAACCCAAGCCAATCAATAC-3' and 5'-GGTCGACAATCTGAAGGATAAG-3'. The construct to target *IFT88* mRNA was designed from GSPATG00038505001 and is 91.9% of the

gene, including positions +48 to +2201. Primers were: 5′- CAATTAAGGAAAACCACCTG-3′ and 5′-AAAACTAACAGGATTGTCATCT-3′. The sequences used to create the RNAi constructs were analyzed by the ParameciumDB off-target tool (http://paramecium.cgm.cnrs-gif.fr/cgi/tool/alignment/off_target.cgi). The sequence used for the *MKS3* construct will only target GSPATG00015939001 while the construct designed for *IFT88* will target all five of the potential orthologs (Li and Durbin, 2009).

Samples were analyzed on a 0.75 or 1.0 % agarose gel and visualized with ethidium bromide. Bands were then cloned into pCR®2.1-TOPO® vector (Invitrogen), transformed into OneShot® cells (Invitrogen), and sequenced at the Vermont Cancer Center DNA Analysis Facility (University of Vermont, Burlington, VT). Sequences were cut from the plasmid and ligated into the double-T7 promoter vector L4440 (AddGene) using the Ligate-IT™ Kit (USB), as per the kit instructions. *Escherichia coli* strain Ht115 (DE3) which lacks RNase-III, were transformed with 50 ng of plasmid DNA for either *MKS3* or *IFT88*. As a control, Ht115 cells were transformed with empty L4440. Bacterial cultures were maintained with tetracycline (12.5 µg/mL) and ampicillin (AMP) (100 µg/mL).

RNAi by Feeding

Cultures were prepared as previously described (Nowacki et al., 2005) except bacteria were prepared in LB with 0.1 mg/mL AMP and were induced for three hours using a final concentration of IPTG of 0.125 mg/mL. Bacteria were then collected by centrifugation and resuspended in wheat grass medium. Paramecia were collected by centrifugation and resuspended in 10 mL of Dryl's solution for at least one hour before being added to the culture. The paramecia were added to each culture: 50 to 100 paramecia to the control culture, 4000 cells to the *MKS3* culture and 8000 cells to the *IFT88* culture. At 24 and 48 hours, an additional 0.125

mg/mL of IPTG, 0.1 mg/mL AMP, and 800 µg of stigmasterol were added. Growth rates of cultures were determined by counting cells at 24, 48, and 72 hours of growth.

Immunofluorescence and Scanning Electron Micrographs

Cells were collected, washed and reduced to 100 µL. Cells were permeabilized for 2 minutes in 1 mL of PHEM buffer [60 mM PIPES, 25 mM HEPES, 2 mM $MgCl_2$, 10 mM EGTA, and 0.1% Triton X-100] and fixed for one hour in 4% paraformaldehyde [Electron Microscopy Sciences (EMS)] in PBS (phosphate buffered saline). Cells were washed three times in PBS with 1% BSA and 0.1% Tween-20. Primary antibody for ciliary measurements, mouse anti-alpha-acetylated-tubulin 1:200 (Sigma). Cells were incubated in primary antibodies in 100 µL PBS for one hour, washed three times in PBS with 0.1% Tween-20, and incubated one hour with 1:200 dilution of secondary antibody AlexaFluor® goat anti-mouse 555 in PBS with 0.1% Tween-20. Cells were washed five times in PBS with 0.1% Tween-20 and mixed 1:1 with VectaShield® (Vector Labs), stored in aluminum foil at 4^{o}C until use.

The DeltaVision® Restoration Microscopy System (inverted Olympus IX70 microscope and a Kodak CH350E camera) at the Neuroscience COBRE Program (University of Vermont, Burlington, VT) was used at 20-22^{o}C using PlanApo 60x/1.40 oil-immersion objective. Images were deconvolved and analyzed using SoftWoRx® Pro software. Cilia length measurements were completed using ImageJ (Rasband, 1997-2009). Only straight cilia within the same z-section were used, the oral grove and caudal cilia were not used for measurements. Colocalization analysis was completed using SoftWoRx® Pro. All Statistical tests (unpaired T-tests) were completed using GraphPad Prism®, Excel, or R. Sample sizes were between 3 to 9 cells for each time point and between 191 and 482 cilia were measured.

To obtain cells for the scanning electron micrographs, RNAi cell cultures of 100 mL were staggered in order to collect cells of different times points (22, 46, and 70 hours) in the RNAi bacteria on the same day. Control cells fed the empty RNAi vector, L4440, were only collected at the longest time point, ~70 hours. RNAi bacteria were prepared as above and cells were imaged as previously described (Picariello et al., 2014).

Behavioral Assays

Each testing solution contained 1 mM calcium citrate, and ~1.3 mM Tris Base. Additional salts were added and pH adjusted using Tris Base to 7.05. Testing solutions included: 20 mM NaCl; 25 mM TEA with 10 mM NaCl; and 25 mM TEA with 5 mM $MgCl_2$; or 30 mM KCl. Cells were transferred to Resting Buffer (4 mM KCl in base buffer above) for 30 minutes then to a testing solution individually. The length of time the cell immediately swam backward or jerked in repetition upon a change in solution was measured using a stop-watch. Timing was stopped when the cell returned to a forward swimming direction. In each solution at each time point, between 48 and 96 cells were observed.

For presentation, the backward swimming data were normalized. Control cells' values were set to 100% and the mRNA reduced cells' time spent swimming backward were compared to this value. Data are presented as ± standard error of the mean (SEM). All statistical tests were performed on original non-normalized data. Because backward swimming in 20 mM NaCl is typically a fast turn, these data could not be normalized and therefore are presented as text within the results.

Secretion Assay

To elicit trichocyst secretion, we added a drop (~60 µL) of saturated picric acid solution to approximately 20 µL of each cell type which we observed for secreted trichocysts using an

Olympus CK2 microscope with an (LWD)CDPlan40FPL 0.55 NA 160/1 objective. Each cell was scored as S (secretion), PS (partial secretion), or NS (no secretion). Partial secretion was defined as showing trichocysts discharged outside but not completely around the periphery of the cell. The DIC images presented in Figure I.3 were taken using a BioRad Multiphoton Confocal system with an Olympus BX51W1 microscope using an XLumPlanFl 20x/0,95w dipping lens. The ND6 paramecia are non-discharge mutants unable to secrete their trichocysts (Gogendeau et al., 2005). Therefore, no secretion was expected in 100% of these cells. Cells from seven different experiments were examined with the totals of 426 control cells, 450 *MKS3* depleted cells, 416 *IFT88* depleted cells, and 249 ND6 cells.

Transmission Electron Microscopy (TEM)

100 mL cultures of RNAi treated cells were collected and washed twice in 100 mL Dryl's solution. Cells were then transferred to 1.5 mL Eppendorf tubes and fixed in 1% gluteraldehyde (EMS) in 0.05 M sodium cacodylate, pH 7.2 for 30 minutes on ice. Cells were washed three times in the same buffer and resuspended in 1% gluteraldehyde (EMS) in 0.05 M sodium cacodylate buffer, 1% osmium tetroxide, pH 7.2 on ice for 30 minutes. Cells were washed three times in the same buffer, 10 minutes each, and pre-embedded in 2% agarose (Invitrogen) in 0.05 M sodium cacodylate buffer. Samples were sliced into 1 mm x 1 mm blocks and placed in 50% ethanol and rocked for 30 minutes. Blocks were rinsed for 30 minutes in a series of ethanol concentrations (50%, 70%, 90%, two times with 100%) and two washes in propylene oxide. Cells were left overnight on specimen rotator in 1:1 of propylene oxide and Spurr's solution (EMS). Samples were washed in fresh Spurr's (EMS) for 6 hours, and placed in flat embedding molds with fresh Spurr's (EMS) at 60^{o}C for 48 hours. Thin sections (90 nm) were placed on copper 200 mesh grids, contrasted with 2% Uranyl acetate in 50% ethanol for 6 minutes, and then lead citrate for 4 minutes. Sections were imaged using a JEOL JEM-1210 Electron microscope.

Results

Ciliary Lengths

Scanning electron micrographs are shown to visualize this ciliary loss from the *MKS3* depleted cells at different time points in the RNAi bacteria. Figure I.1 shows the *MKS3* depleted cells after 22, 46, and 70 hours (Figure I.1B-D) in the RNAi bacteria compared to the control cells which were fed the L4440 bacteria for 70 hours (Figure I.1A). Cilia loss is observed by 22 hours and is very evident at the 70 hour mark. Cilia loss and shortening occurs globally and the oral grove cilia appear to be the last cilia lost from the *MKS3* depleted cells.

To quantify the lengths of the remaining cilia, the *MKS3* and *IFT88* mRNA depleted and control cells were permeabilized, fixed, and stained with anti-tubulin at 24-hour intervals. Our quantitative analysis of cilia length included only those cilia present on the cells and does not account for missing cilia. Many of the depleted cells had large bald patches and by 72 hours, the depleted cells were mostly bald, especially the *IFT88* depleted cells.

By 24 hours, both the *MKS3* and *IFT88* depleted cells had significantly shorter cilia than the controls ($P<0.0001$, multiple T-tests) and by 48 hours, the *IFT88* depleted cells showed shorter cilia than both the controls ($P<0.0001$, multiple T-tests) and the *MKS3* depleted cells ($P<0.001$, multiple T-tests) (Figure I.2A). At 72 hours, both depleted cell lines had significantly shorter cilia than the controls ($P<0.0001$, multiple T-tests), but no difference between each other. The measurements from these different time points are shown in Table I.I.

Swimming Assays of Ion Channel Function

There is a large body of research on *Paramecium* ion channels and the importance of those channels on swimming behavior (Eckert, 1972, Brehm et al., 1978, Eckert and Brehm, 1979, Kung and Saimi, 1982, Ling and Kung, 1980). By changing the ionic environment and monitoring

swimming behavior, we are able to decipher changes in ciliary ion channel function. Depolarizing solutions, such as high Na^+ (20 mM) or high K^+ (30 mM), will open the voltage gated calcium channels (Ca_V), which are found exclusively in the cilia (Dunlap, 1977), causing an action potential and backward swimming as long as Ca^{2+} remains high in the cilia. Repolarization of the cell by the activation of the voltage- and Ca^{2+}- activated K^+ channels (K_V and K_{Ca}, respectively) ends the action potential (Brehm et al., 1978). If Na^+ or Mg^{2+} is present in the surrounding solution, the action potential can be prolonged through the Ca^{2+}-activated Na^+ ($I_{Na(Ca)}$) (Saimi and Kung, 1980) or Ca^{2+}-activated Mg^{2+} ($I_{Mg(Ca)}$) (Preston and Kung, 1994b, Preston and Kung, 1994a) conductance.

MKS3 and *IFT88* depleted wild type cells were tested in 24-hour increments to account for changes over time. While the *MKS3* and *IFT88* depleted cells swam more slowly than control cells, they were able to reverse their cilia and respond to the different test solutions. Some of their responses to depolarizing stimuli were normal with the exceptions presented below.

20 mM NaCl: High Na^+ usually elicits a quick reversal of the power stroke that causes a turn in the swimming path, called an avoidance reaction. This solution tests the activity of Na^+ channels to cause backward swimming as well as K^+ channels to repolarize the cell. It does not distinguish between the K_V and K_{Ca} channels. Because the length of time of backward swimming by the control cells was shorter than can be timed by the stop-watch, the backward swimming durations for these cells are presented in Table I.II. However, at each time point, both the *MKS3* and *IFT88* depleted cells show easily measureable long backward swimming compared to the controls ($P<0.0001$, T-tests).

TEA solutions: Tetraethylammonium chloride (TEA) blocks the voltage-activated K^+ current ($I_{K(V)}$) when applied to the cells externally (Satow and Kung, 1976). When TEA solution is combined with a depolarizing stimulus, such as high Na^+ (10 mM) or high Mg^{2+} (5 mM), cells will

display long backward swimming and rely mostly on the K_{Ca} channels to repolarize the action potential.

When depolarized with 10 mM NaCl in 25 mM TEA, both depleted cell types demonstrated longer than normal backward swimming (Figure I.2B). The backward swimming of the *IFT88* depleted cells at 24 hours was significantly longer than both the control and *MKS3* depleted cells (P<0.0001, T-tests). Both the *MKS3* and *IFT88* depleted cells showed longer than normal backward swimming at 48 and 72 hours (P<0.0001, T-test). At 48 hours, the *IFT88* depleted cells swam backward even longer than the *MKS3* depleted cells (P <0.0001, T-test).

When the cells were depolarized with 5 mM $MgCl_2$ in 25 mM TEA, the only difference observed was by the *IFT88* depleted cells (Figure I.2C). These depleted cells showed significantly longer backward swimming at 24, 48, and 72 hours compared to both the controls and *MKS3* depleted cells (P <0.0001, T-tests).

30 mM KCl: In high K^+, paramecia depolarize beyond threshold and fire an action potential resulting in transient backward swimming due to the activity of the Ca_V channel. After 24 hours of feeding, the *IFT88* depleted cells showed significantly shorter backward swimming (P <0.0001, T-tests) (Figure I.2D). By 48 hours, both the *MKS3* and *IFT88* depleted cells showed shorter backward swimming (P<0.0001, T-tests) with no further decrease at 72 hours.

Secretion Assay

Cells were exposed to picric acid to stimulate the secretion of the trichocysts, small (3-4 μm) organelles that are part of a regulated calcium-controlled secretion system in *Paramecium* (Vayssie et al., 2001). Cells were scored as S (secretion), PS (partial secretion) or NS (no secretion). We included the ND6 mutant of *Paramecium*, which lacks a membrane associated protein vital for the last step of membrane fusion and exocytosis of trichocysts (Gogendeau et al., 2005). As

expected, one hundred percent of these cells showed no secretion (Figure I.3A). The *MKS3* depleted cells were statistically less likely to secrete their trichocysts and more likely to demonstrate NS or PS when compared to the control and *IFT88* depleted cells (ANOVA, post-hoc unpaired T-test, $P<0.05$; bar with asterisk, Figure I.3A). Differential Interference Contrast images (DIC) images show trichocyst secretion from the different cell types (Figure I.3B). The representative control cell and *IFT88* depleted cell both display secretions of the trichocysts (arrow heads) while the ND6 cell shows only cilia (arrow) around its edge (NS). The DIC image of the *MKS3* depleted cell shows there are secreted trichocysts only at the posterior end of the cell (arrow head). Of importance, of the *MKS3* depleted cells scored as PS, over 70% failed to secrete their trichocysts at the midline of the cell while none of the PS control cells shows such localized failure to secrete.

Ultrastructure Analysis

Transmission electron microscopy (TEM) and ImageJ analysis (Rasband, 1997-2009), showed no observable differences between the observed basal bodies of the control (Figure I.4A) and *MKS3* depleted cells (Figure I.4D). Cross sections of the control cilia, both transverse (Figure I.4B) and longitudinal (Figure I.4C), showed that the structures were the same compared to the *MKS3* depleted cells (Figure I.4E and F, respectively). The basal bodies were comparable in size and position: control basal bodies 379.6 ± 42.4 nm in length and 202.9 ± 22.8 nm wide (± SD, N=13) and *MKS3* depleted cell's basal bodies 367.7 ± 35.5 nm long and 191.8 ± 21.9 nm wide (± SD, N=14). However, a tangential section through the *MKS3* depleted cell shows cilia missing from cortical units (Figure I.4G, arrows).

Discussion

We used feeding RNAi to further examine cellular functions that were interrupted in *P. tetraurelia* upon depletion of the *MKS3* protein. We used *IFT88* as a positive control for our approach because it is a well characterized ciliopathy gene and reduction of its mRNA should result in short and missing cilia with no disruptions to the cell surface. While both depleted cell types have short and missing cilia, the phenotype of *MKS3* depleted cells differs from that of *IFT88* depleted cells. The differences cannot be explained simply by a reduction of ciliary length or IFT function alone.

Depletion of *MKS3* and *IFT88* quickly lead to short and missing cilia

Our study clearly shows that cells reduced in *MKS3* or *IFT88* mRNA have short and missing cilia. This phenotype for *MKS3* depletion have been previously reported by ourselves and others (Picariello et al., 2014, Dawe et al., 2007). Work by Dawe and colleagues (2007) suggests the migration of centrioles to the cell surface for cilium formation requires both MKS3 and MKS1, another MKS ciliopathy protein. *Paramecium* has a homologue for the mammalian MKS1 protein. The depletion of *MKS1* in *Paramecium* leads to a separation of the cytoskeleton from the cell membrane, essentially flattening the surface of the cells (Campillo et al., 2012). MKS1 is another component of the transition zone MKS complex in mammalian cells, which includes MKS3, to form a filter barrier between the cell and the cilia (Garcia-Gonzalo et al., 2011, Williams et al., 2011, Czarnecki and Shah, 2012, Chih et al., 2012).

The depletion of *MKS3* has been shown to create numerous cilia or centrioles when there should only be one cilium or centriole, which is in contrast to our findings. One group identified longer cilia when the *MKS3* gene was missing in the *bpck/bpck* mouse model for kidney disease (Cook et al., 2009). Another study by Tammachote et al. (2009) found that the MKS kidney cells

from patients and IMCD3 cultured cells had multiple centrosomes, multiple cilia per cell, or cilia of varying lengths on wpk rat kidney cells (Tammachote et al., 2009). In contrast, the confluent mutant-*MKS3* transfected HEK293 cells used by Dawe and colleagues (2007), while showing multiple centrioles, had short or missing cilia. At no point in our study did we see longer or more numerous cilia on the *MKS3* depleted cells. Cook *et al.* (2009) speculated that if the RNAi were allowed to run longer, that perhaps longer cilia would develop as seen in their *MKS3* knock out mouse model. However, in our experience, longer application of the *MKS3* RNAi in *Paramecium* by re-feeding is lethal. In *Paramecium*, it appears that depletion of *MKS3* leads to a shortening of cilia over time, which eventually disappear. Our study of *P. tetraurelia,* like that of Dawe and colleagues (2007), found that *MKS3* depletion causes short and missing cilia, but unlike Dawe and colleagues (2007), we have found no evidence of altered centrosome number, or in this case basal body number. There appears to be variations in reports of *MKS3* depletion perhaps due to cell types, state of confluence of cultured cells, and the methods used to disrupt MKS3 by using RNAi or knock out.

***MKS3* depleted cells show a deficiency in ciliary ion channel function**

In depolarizing stimuli, the *MKS3* and *IFT88* depleted cells displayed different phenotypes, even though both types have short and missing cilia. The *IFT88* depleted cells' behavior was consistent with the reduction of the Ca^{2+}-activated K^+ conductance ($I_{K(Ca)}$). Because there is abnormally longer backward swimming by the *IFT88* depleted cells both in solutions of TEA with Mg^{2+} and with Na^+, we interpret the longer backward swimming to be due to an ineffective $I_{K(Ca)}$ conductance rather than prolonged Na^+ or Mg^{2+} inward conductance. In contrast with *IFT88* depleted cells, the *MKS3* depleted cells' prolonged backward swimming was specific to Na^+ solutions. The cells' behavior was consistent with an overly long activation of the $I_{Na(Ca)}$ as

evidenced by prolonged backward swimming in solutions with NaCl with or without TEA, but not Mg^{2+} with TEA, which eliminates the $I_{K(Ca)}$ as the altered conductance.

Both depleted cell types have extremely short backward swimming in high K^+ solution. The short backward swimming could be from a reduced voltage-activated Ca^{2+} conductance ($I_{Ca(V)}$) of the Ca_V channels that are exclusively in the cilia (Dunlap, 1977) or an increased $I_{K(V)}$. Because our sodium data showed prolonged backward swimming, we expect $I_{K(V)}$ to be either normal or decreased, consistent with the observed prolonged backward swimming. Therefore, a decreased $I_{Ca(V)}$ is the most likely reason for the altered behavior in depolarizing K^+ solutions for both cell types.

The voltage dependent Ca^{2+} channels, other than being exclusively in the cilia membrane, are more concentrated at the distal end (Dunlap, 1977, Machemer and Ogura, 1979). Perhaps shortening the cilia in both depleted cell types contributed to short backward swimming in depolarizing K^+ solutions, but shortening alone cannot account for the differences between the depleted cell types in other solutions.

Interestingly, despite the decrease in $I_{Ca(V)}$ as the cilia shorten in both depleted cell types, there must be sufficient $I_{Ca(V)}$ to cause the reversal of the ciliary power stroke and to activate the K_{Ca} channels in the *MKS3* depleted cells. K_{Ca} channels must reside in the cilia in order to be activated (Husser et al., 2004). There is no spill-over of Ca^{2+} from action potentials from the cilia to the cell body (Husser et al., 2004), and the Ca^{2+} for activating this K_{Ca} channel comes from the ciliary Ca_V channels (Brehm et al., 1978, Satow and Kung, 1980).

These observations lead us to postulate that the *P. tetraurelia* IFT88 protein functions in transport of both structural ciliary proteins and membrane channels, and reduction of IFT88p leads to loss of the ciliary membrane proteins evenly as the cilia become shorter. The MKS3

protein, on the other hand, appears to be critical for positioning the components of the cortical units, including the basal bodies and ciliary cargo finding its way to the cell surface, including the ciliary membrane.

***MKS3*, but not *IFT88*, depleted cells have decreased secretion**

When exposed to picric acid to induce trichocyst secretion, the *MKS3* depleted cells demonstrated variable amounts of secretion while over 80% of the control and *IFT88* depleted cells showed full secretion of their trichocysts. The trichocysts dock at the plasma membrane at specific sites (rosettes) on the ridges between the basal bodies that outline each cortical unit (Allen and Hausmann, 1976). The majority of Ca^{2+} for this secretion is supplied by the alveolar sacs (Hardt and Plattner, 2000). The reduced secretion of trichocysts at the midline is most likely a secondary effect of the heavily disrupted membrane that does not allow for proper release of the trichocyst vesicles.

The *IFT88* depleted cells showed no disruption in their cell surface or secretion. Another IFT protein, IFT20 in a complex with IFT88 and IFT57, was linked to secretion in non-ciliated human lymphocytes (Finetti et al., 2009). We might have expected, based on these data, that the *IFT88* reduced paramecia would show reduced secretion compared to the controls, but this was not the case.

***MKS3* depleted cells have seemingly undisrupted basal bodies**

Our ultrastructure analysis of the *MKS3* depleted cells using TEM compared to the control cells showed no glaring abnormalities with the observed basal bodies or cilia. Although we did observe an instance where a tangential section of a *MKS3* depleted cell showed missing cilia (Figure I.4G), there were no other obvious abnormalities observed. The measurements of the observed basal bodies in the control cells and the *MKS3* depleted cells also showed no statistical

differences in height or width or positioning. We would suggest for any future analysis, that the population of cells used for ultrastructure studies be heavily hit with RNAi, possibly by re-feeding the cells. More sections of cells and if possible, consecutive sections, should be used for analysis to help to ensure what we were examining with TEM were highly depleted *MKS3* RNAi cells. Lastly, the concentration or cleaning of our *Paramecium* MKS3 antibody could be used to label the MKS3 protein for TEM immunogold labeling. The antibody is not currently up for this task, but in the future, the cleaning and concentration of the antibody using an ammonium sulfate purification could produce a more useful antibody against *Paramecium* MKS3.

Conclusions

The data presented here demonstrate that feeding RNAi to deplete the mRNA for *MKS3* and *IFT88* interferes with ciliary channels and secretion of membrane organelles, namely the trichocysts. *IFT88* and *MKS3* depleted cells share the phenotype of deficiencies in Ca_V channel function, most likely due to the global shortening of the cilia. However, the two depleted cell types differ in other apparent ciliary ion channel defects. The *IFT88* depleted cells showed defects in $I_{K(Ca)}$ while *MKS3* depleted cells showed prolonged activation of $I_{Na(Ca)}$. The reduced secretion of the *MKS3* depleted cells is most likely due to the disruption of their cell surface, interfering with the docking of the trichocysts. The hallmark of the *MKS3* depleted cells is disrupted basal body rows and cortical units, and short and missing cilia. Our structural analysis of the basal bodies demonstrates they are normal in their length and width. More information is needed concerning basal body orientation along the anterior-posterior axis of the cell. Current work is underway to investigate the interactions with the rootlet system of *Paramecium*.

Funding

The project described was supported in part by NIH Grant Numbers 5 P30 RR032135 from the COBRE Program of the National Center for Research Resources, 8 P30 GM103498 from the National Institute of General Medical Sciences, and NIH grant RO1 GM59988.

References

ALLEN, R. D. 1971. Fine structure of membranous and microfibrillar systems in the cortex of Paramecium caudatum. *J Cell Biol,* 49**,** 1-20.

ALLEN, R. D. & FOK, A. K. 1980. Membrane recycling and endocytosis in Paramecium confirmed by horseradish peroxidase pulse-chase studies. *J Cell Sci,* 45**,** 131-45.

ALLEN, R. D. & HAUSMANN, K. 1976. Membrane behavior of exocytic vesicles. I. The ultrastructure of Paramecium trichocysts in freeze-fracture preparations. *J Ultrastruct Res,* 54**,** 224-34.

BASU, B. & BRUECKNER, M. 2008. Cilia multifunctional organelles at the center of vertebrate left-right asymmetry. *Curr Top Dev Biol,* 85**,** 151-74.

BREHM, P., DUNLAP, K. & ECKERT, R. 1978. Calcium-dependent repolarization in Paramecium. *J Physiol,* 274**,** 639-54.

BUONANNO, F., HARUMOTO, T. & ORTENZI, C. 2013. The defensive function of trichocysts in Paramecium tetraurelia against metazoan predators compared with the chemical defense of two species of toxin-containing ciliates. *Zoolog Sci,* 30**,** 255-61.

CAMPILLO, C., JERBER, J., FISCH, C., SIMOES-BETBEDER, M., DUPUIS-WILLIAMS, P., NASSOY, P. & SYKES, C. 2012. Mechanics of membrane-cytoskeleton attachment in Paramecium. *New Journal of Physics,* 14.

CHIH, B., LIU, P., CHINN, Y., CHALOUNI, C., KOMUVES, L. G., HASS, P. E., SANDOVAL, W. & PETERSON, A. S. 2012. A ciliopathy complex at the transition zone protects the cilia as a privileged membrane domain. *Nature Cell Biology,* 14**,** 61-U97.

COLE, D. G., DIENER, D. R., HIMELBLAU, A. L., BEECH, P. L., FUSTER, J. C. & ROSENBAUM, J. L. 1998. Chlamydomonas kinesin-II-dependent intraflagellar transport (IFT): IFT particles contain proteins required for ciliary assembly in Caenorhabditis elegans sensory neurons. *J Cell Biol,* 141**,** 993-1008.

COOK, S. A., COLLIN, G. B., BRONSON, R. T., NAGGERT, J. K., LIU, D. P., AKESON, E. C. & DAVISSON, M. T. 2009. A mouse model for Meckel syndrome type 3. *J Am Soc Nephrol,* 20**,** 753-64.

CZARNECKI, P. G. & SHAH, J. V. 2012. The ciliary transition zone: from morphology and molecules to medicine. *Trends in Cell Biology,* 22**,** 201-210.

D'ANGELO, A. & FRANCO, B. 2009. The dynamic cilium in human diseases. *Pathogenetics,* 2**,** 3.

DAWE, H. R., SMITH, U. M., CULLINANE, A. R., GERRELLI, D., COX, P., BADANO, J. L., BLAIR-REID, S., SRIRAM, N., KATSANIS, N., ATTIE-BITACH, T., AFFORD, S. C., COPP, A. J., KELLY, D. A., GULL, K. & JOHNSON, C. A. 2007. The Meckel-Gruber Syndrome proteins MKS1 and meckelin interact and are required for primary cilium formation. *Hum Mol Genet,* 16**,** 173-86.

DUNLAP, K. 1977. Localization of calcium channels in Paramecium caudatum. *J Physiol,* 271**,** 119-33.

ECKERT, R. 1972. Bioelectric control of ciliary activity. *Science,* 176**,** 473-81.

ECKERT, R. & BREHM, P. 1979. Ionic mechanisms of excitation in Paramecium. *Annu Rev Biophys Bioeng,* 8**,** 353-83.

FINETTI, F., PACCANI, S. R., RIPARBELLI, M. G., GIACOMELLO, E., PERINETTI, G., PAZOUR, G. J., ROSENBAUM, J. L. & BALDARI, C. T. 2009. Intraflagellar transport is required for polarized recycling of the TCR/CD3 complex to the immune synapse. *Nat Cell Biol,* 11**,** 1332-9.

GARCIA-GONZALO, F. R., CORBIT, K. C., SIREROL-PIQUER, M. S., RAMASWAMI, G., OTTO, E. A., NORIEGA, T. R., SEOL, A. D., ROBINSON, J. F., BENNETT, C. L., JOSIFOVA, D. J., GARCIA-VERDUGO, J. M., KATSANIS, N., HILDEBRANDT, F. & REITER, J. F. 2011. A transition zone complex regulates mammalian ciliogenesis and ciliary membrane composition. *Nat Genet,* 43**,** 776-84.

GOGENDEAU, D., KELLER, A. M., YANAGI, A., COHEN, J. & KOLL, F. 2005. Nd6p, a novel protein with RCC1-like domains involved in exocytosis in Paramecium tetraurelia. *Eukaryot Cell,* 4**,** 2129-39.

HARDT, M. & PLATTNER, H. 2000. Sub-second quenched-flow/X-ray microanalysis shows rapid Ca2+ mobilization from cortical stores paralleled by Ca2+ influx during synchronous exocytosis in Paramecium cells. *Eur J Cell Biol,* 79**,** 642-52.

HUSSER, M. R., HARDT, M., BLANCHARD, M. P., HENTSCHEL, J., KLAUKE, N. & PLATTNER, H. 2004. One-way calcium spill-over during signal transduction in Paramecium cells: from the cell cortex into cilia, but not in the reverse direction. *Cell Calcium,* 36**,** 349-58.

IFTODE, F., ADOUTTE, A., AND FLEURY, A. 1996. The Surface Pattern of Paramecium tetraurelia in interphase: An Electron Microscopic Study of Basal Body Variability, Connections with Associated Ribbons and their Epiplasmic Environment. *European Journal of Protistology,* 32**,** 1.

IFTODE, F., COHEN, J., RUIZ, F., RUEDA, A. T., CHENSHAN, L., ADOUTTE, A. & BEISSON, J. 1989. Development of Surface Pattern during Division in Paramecium .1. Mapping of Duplication and Reorganization of Cortical Cytoskeletal Structures in the Wild-Type. *Development,* 105**,** 191-211.

KOZMINSKI, K. G., BEECH, P. L. & ROSENBAUM, J. L. 1995. The Chlamydomonas kinesin-like protein FLA10 is involved in motility associated with the flagellar membrane. *J Cell Biol,* 131**,** 1517-27.

KOZMINSKI, K. G., JOHNSON, K. A., FORSCHER, P. & ROSENBAUM, J. L. 1993. A motility in the eukaryotic flagellum unrelated to flagellar beating. *Proc Natl Acad Sci U S A,* 90**,** 5519-23.

KUNG, C. & SAIMI, Y. 1982. The physiological basis of taxes in Paramecium. *Annu Rev Physiol,* 44**,** 519-34.

LI, H. & DURBIN, R. 2009. Fast and accurate short read alignment with Burrows-Wheeler transform. *Bioinformatics,* 25**,** 1754-60.

LING, K. Y. & KUNG, C. 1980. Ba2+ influx measures the duration of membrane excitation in Paramecium. *J Exp Biol,* 84**,** 73-87.

MACHEMER, H. & OGURA, A. 1979. Ionic conductances of membranes in ciliated and deciliated Paramecium. *J Physiol,* 296**,** 49-60.

NONAKA, S., TANAKA, Y., OKADA, Y., TAKEDA, S., HARADA, A., KANAI, Y., KIDO, M. & HIROKAWA, N. 1998. Randomization of left-right asymmetry due to loss of nodal cilia generating leftward flow of extraembryonic fluid in mice lacking KIF3B motor protein. *Cell,* 95**,** 829-37.

PAZOUR, G. J., DICKERT, B. L., VUCICA, Y., SEELEY, E. S., ROSENBAUM, J. L., WITMAN, G. B. & COLE, D. G. 2000. Chlamydomonas IFT88 and its mouse homologue, polycystic kidney disease gene tg737, are required for assembly of cilia and flagella. *J Cell Biol,* 151**,** 709-18.

PAZOUR, G. J., DICKERT, B. L. & WITMAN, G. B. 1999. The DHC1b (DHC2) isoform of cytoplasmic dynein is required for flagellar assembly. *J Cell Biol,* 144**,** 473-81.

PEDERSEN, L. B. & ROSENBAUM, J. L. 2008. Intraflagellar transport (IFT) role in ciliary assembly, resorption and signalling. *Curr Top Dev Biol,* 85**,** 23-61.

PICARIELLO, T., VALENTINE, M. S., YANO, J. & VAN HOUTEN, J. 2014. Reduction of meckelin leads to general loss of cilia, ciliary microtubule misalignment and distorted cell surface organization. *Cilia,* 3**,** 2.

PIPERNO, G. & MEAD, K. 1997. Transport of a novel complex in the cytoplasmic matrix of Chlamydomonas flagella. *Proc Natl Acad Sci U S A,* 94**,** 4457-62.

PORTER, M. E., BOWER, R., KNOTT, J. A., BYRD, P. & DENTLER, W. 1999. Cytoplasmic dynein heavy chain 1b is required for flagellar assembly in Chlamydomonas. *Mol Biol Cell,* 10**,** 693-712.

PRESTON, R. R. & KUNG, C. 1994a. Inhibition of Mg2+ current by single-gene mutation in Paramecium. *J Membr Biol,* 139**,** 203-13.

PRESTON, R. R. & KUNG, C. 1994b. Isolation and characterization of paramecium mutants defective in their response to magnesium. *Genetics,* 137**,** 759-69.

RASBAND, W. S. 1997-2009. ImageJ. *U.S. National Institutes of Health, Bethesda, MD*.

RINGO, D. L. 1967. Flagellar motion and fine structure of the flagellar apparatus in Chlamydomonas. *J Cell Biol,* 33**,** 543-71.

ROSENBAUM, J. L., COLE, D. G. & DIENER, D. R. 1999. Intraflagellar transport: the eyes have it. *J Cell Biol,* 144**,** 385-8.

RUIZ, F., BEISSON, J., ROSSIER, J., DUPUIS-WILLIAMS, P. 1999. Basal Body duplication in Paramecium requires gamma-tubulin. *Current Biology,* 9**,** 43-46.

RUIZ, F., GARREAU DE LOUBRESSE, N., KLOTZ, C., BEISSON, J. & KOLL, F. 2005. Centrin deficiency in Paramecium affects the geometry of basal-body duplication. *Curr Biol,* 15**,** 2097-106.

SAIMI, Y. & KUNG, C. 1980. A Ca-induced Na-current in Paramecium. *J Exp Biol,* 88**,** 305-25.

SASNER, J. M. & VANHOUTEN, J. L. 1989. Evidence for a Paramecium Folate Chemoreceptor. *Chemical Senses,* 14**,** 587-595.

SATOW, Y. & KUNG, C. 1976. A 'TEA+-insensitive' mutant with increased potassium conductance in Paramecium aurelia. *J Exp Biol,* 65**,** 51-63.

SATOW, Y. & KUNG, C. 1980. Ca-induced K+-outward current in Paramecium tetraurelia. *J Exp Biol,* 88**,** 293-303.

SHARMA, N., BERBARI, N. F. & YODER, B. K. 2008. Ciliary dysfunction in developmental abnormalities and diseases. *Curr Top Dev Biol,* 85**,** 371-427.

SONNEBORN, T. M. 1970. Gene action in development. *Proc R Soc Lond B Biol Sci,* 176**,** 347-66.

TAMMACHOTE, R., HOMMERDING, C. J., SINDERS, R. M., MILLER, C. A., CZARNECKI, P. G., LEIGHTNER, A. C., SALISBURY, J. L., WARD, C. J., TORRES, V. E., GATTONE, V. H., 2ND & HARRIS, P. C. 2009. Ciliary and centrosomal defects associated with mutation and depletion of the Meckel syndrome genes MKS1 and MKS3. *Hum Mol Genet,* 18**,** 3311-23.

VAYSSIE, L., GARREAU DE LOUBRESSE, N. & SPERLING, L. 2001. Growth and form of secretory granules involves stepwise assembly but not differential sorting of a family of secretory proteins in Paramecium. *J Cell Sci,* 114**,** 875-86.

WILLIAMS, C. L., LI, C. M., KIDA, K., INGLIS, P. N., MOHAN, S., SEMENEC, L., BIALAS, N. J., STUPAY, R. M., CHEN, N. S., BLACQUE, O. E., YODER, B. K. & LEROUX, M. R. 2011. MKS and NPHP modules cooperate to establish basal body/transition zone membrane associations and ciliary gate function during ciliogenesis. *Journal of Cell Biology,* 192**,** 1023-1041.

Table I.I: Cilia length measurements over time for *MKS3* and *IFT88* depleted cells compared to the control cells.

	Control (µm)	*MKS3* (µm)	*IFT88* (µm)
24 hours	9.7 ± 0.1 (293; 8)	7.4 ± 0.1 (400; 9)*	7.0 ± 0.2 (377; 8)*
48 hours	9.6 ± 0.1 (339; 8)	4.5 ± 0.1 (482; 6)*	3.7 ± 0.1 (347; 9)*^
72 hours	9.6 ± 0.1 (191; 3)	3.7 ± 0.1 (412; 3)*	3.7 ± 0.2 (279; 3)*

All values are µm ± standard error of the mean. Values in parentheses are the number of cilia measured and the number of cells used to obtain those measurements, respectively. Bald patches and missing cilia were not quantified and are not reflected in these data. (*= $P<0.0001$ compared to the controls, unpaired T-test; ^=$P<0.001$ compared to *MKS3* depleted cells, unpaired T-test).

Table I.II: Backward swimming time for control and *MKS3* or *IFT88* depleted cells in 20 mM NaCl.

	24 hours	48 hours	72 hours
Control	0.65 ± 0.23 (85)	0.55 ± 0.23 (91)	0.02 ±0.02 (75)
MKS3	12.39 ± 1.39 (90)*	32.55 ± 3.00 (91)*	30.64 ± 3.28 (61)*
IFT88	22.43 ± 1.79 (93)*^	50.02 ± 3.10 (93)*^	34.70 ± 3.75 (48)*

Data are seconds ± standard error of the mean, (number of cells). *=P<0.0001, unpaired T-tests compared to the controls; ^=P<0.0001, unpaired T-tests, compared to *MKS3* depleted cells.

Figure I.1: Time course study of *MKS3* depleted cells compared to a control cell. Control cells were fed the bacteria for 70 hours **(A)** and *MKS3* depleted cells were fed the RNAi bacteria for 22 hours **(B)**, 46 hours **(C)** and 70 hours **(D)**. *MKS3* depleted cells show short and missing cilia at 22 hours and by 70 hours there are few cilia remaining and the surface is disrupted. Cells shown are representative of the population. Scale bars are 10 μm.

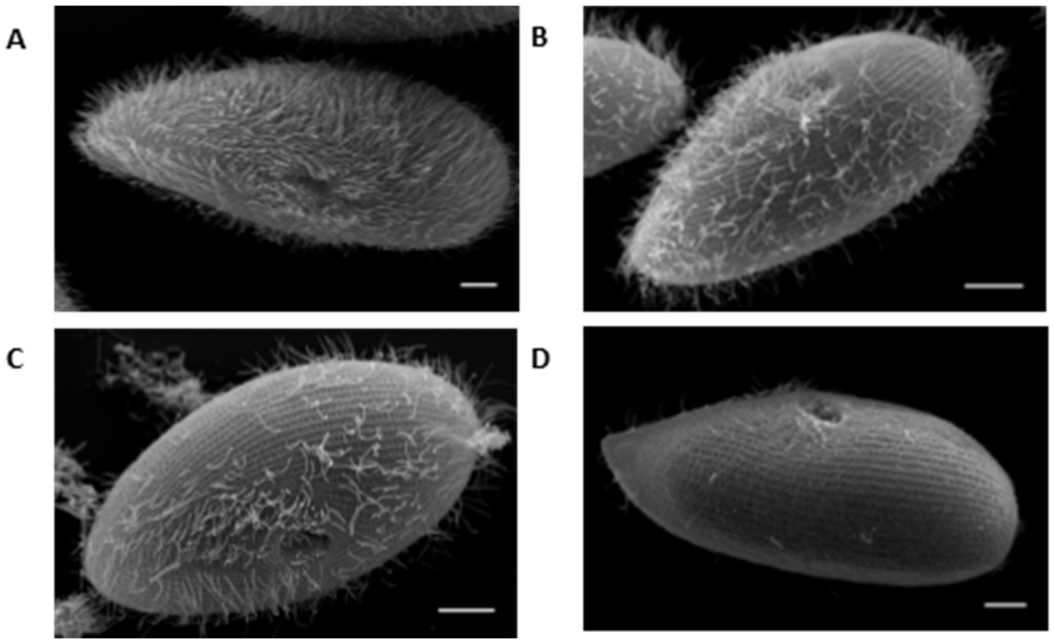

Figure I.2: Changes in cilia length and backward swimming over time in *MKS3* and *IFT88* depleted cells compared to control cells. (A) RNAi depleted cells were observed in 24 hour increments for shortening of the cilia using immunofluorescence. Short cilia on *MKS3* and *IFT88* depleted cells seen by 24 hours became shorter over time. Data are average μm ± standard error of the mean; tabulated data can be seen in Table I.I. **(B, C, D)** Normalized backward swimming (see Materials and Methods), averages are ± standard error of the mean in NaCl with TEA **(B)**, $MgCl_2$ with TEA **(C)** and KCl **(D)**. In all graphs, asterisk indicates statistical significance compared to the control (P<0.0001, unpaired T-test) or between the indicated data sets *MKS3* and *IFT88* (P<0.001, unpaired T-test). Statistical tests were performed on the raw data, not the normalized data.

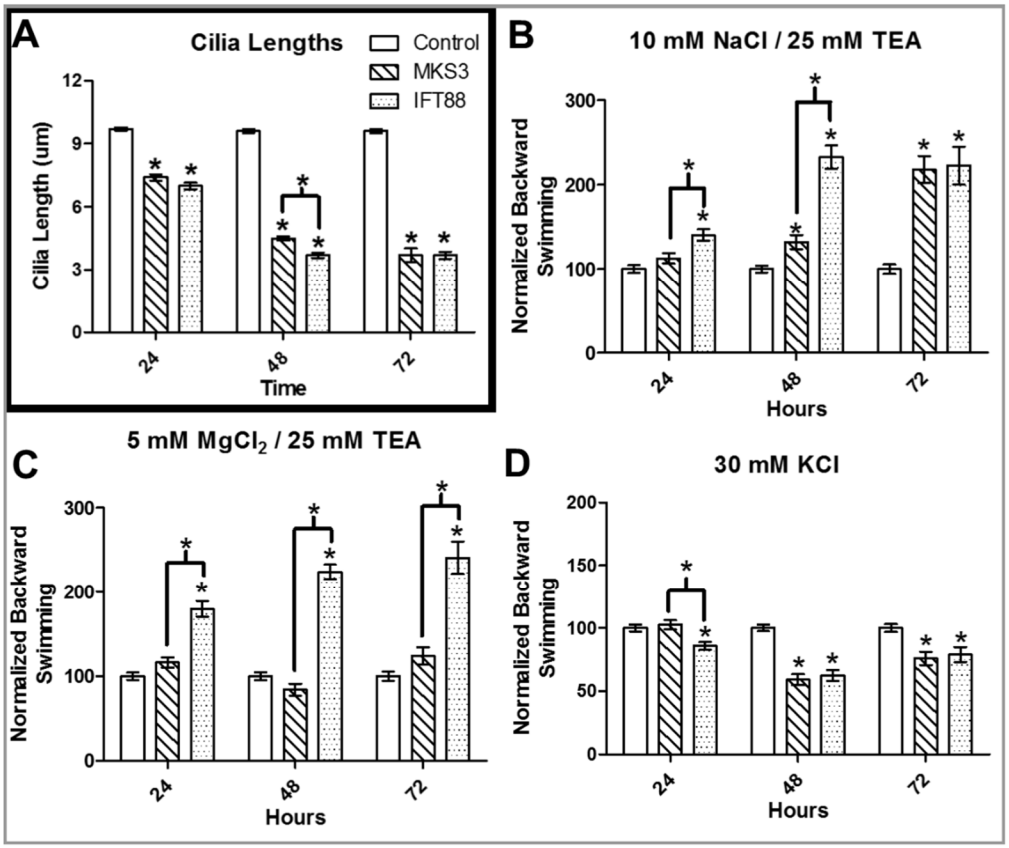

Figure I.3: Secretion of trichocysts induced by picric acid. Cells of each type (non-discharge 6 (ND6), control fed RNAi and MKS3 or IFT88 depleted) were concentrated, washed, and exposed to picric acid. Trichocyst secretion was classified as S (secretion), PS (partial secretion), or NS (no secretion). **(A)** Histogram shows the percentage of S, PS and NS of each cell type ± standard error of the mean, asterisk=$P<0.05$, ANOVA, post hoc unpaired T-tests). **(B)** DIC images show trichocyst secretion; scale bars: 20 μm. Arrows indicate cilia, arrow heads indicate discharged trichocysts. Cilia appear as a ring around the control and ND6 cells.

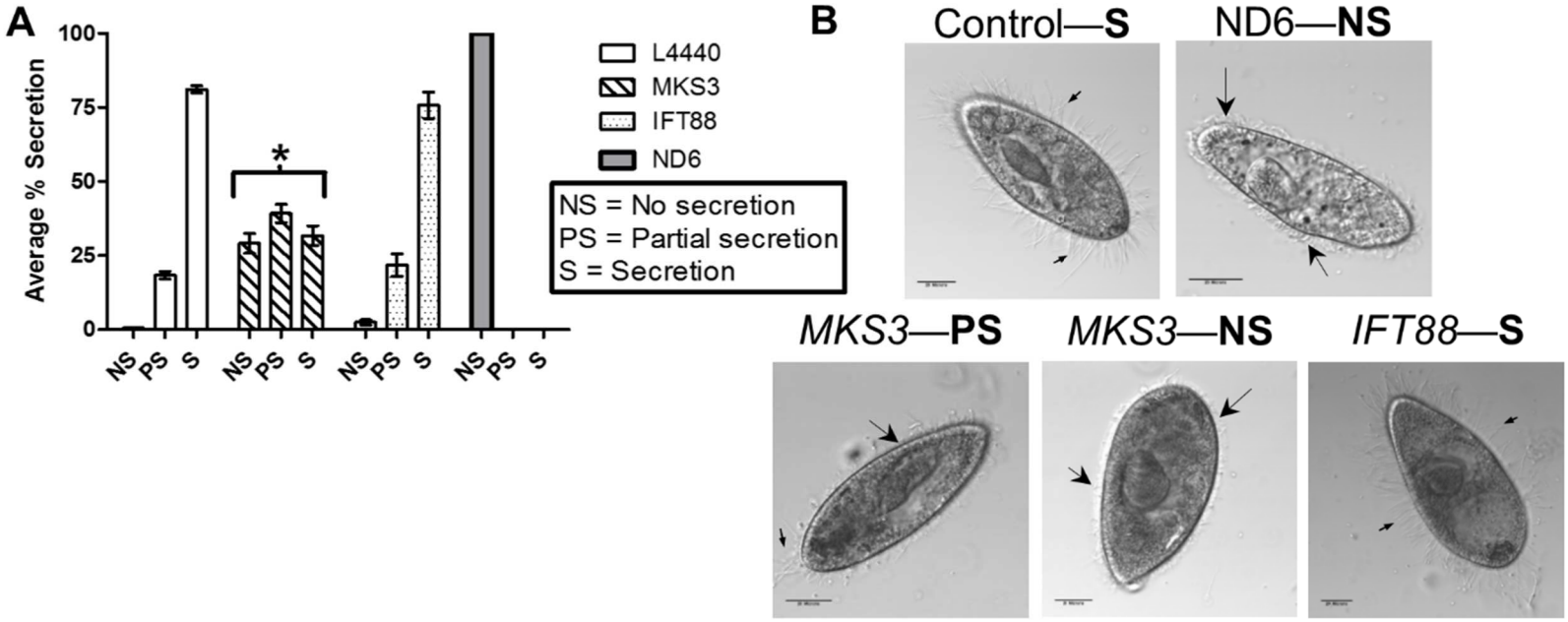
A
Average % Secretion
100
75
50
25
0
*
NS
PS
S
L4440
MKS3
IFT88
ND6
NS = No secretion
PS = Partial secretion
S = Secretion
B
Control—S
ND6—NS
MKS3—PS
MKS3—NS
IFT88—S

Figure I.4: Transmission Electron Micrographs of control fed and *MKS3* depleted RNAi cells. Control (A, B and C) and *MKS3* depleted cells (D-G). Of the basal bodies observed, there were no obvious ultrastructure differences between the control and *MKS3* depleted cells. However, a tangential section of an *MKS3* depleted cell demonstrates missing cilia (arrows). a=alveolar sac, bb= basal body, ax= axoneme. Scale bars: 100 nm except G, scale bar: 1 μm.

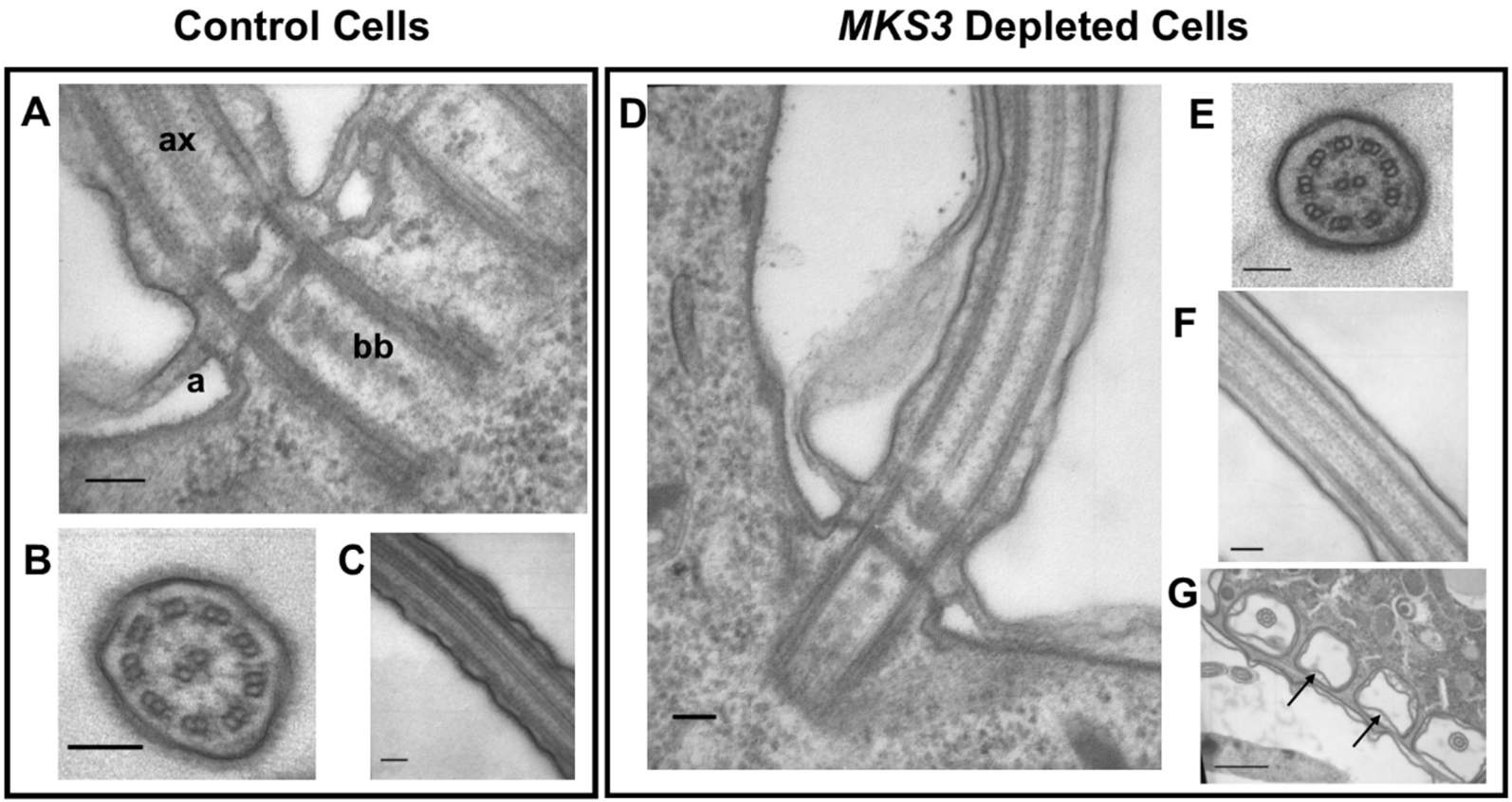
Control Cells
MKS3 Depleted Cells
A
ax
bb
a
B
C
D
E
F
G

Appendix II: The *eccentric* gene (*XNTA*) in *Paramecium*

Abstract

The XntA protein is a small protein of somewhat unknown function in *P. tetraurelia*. Although XntA has been described as a channel-like protein partially based on its predicted structure, it appears to be involved in numerous signaling pathways other than the Ca^{2+}-dependent Mg^{2+} conductance for which it is known. We have suggested previously (Chapter 3) that the XntA protein may be involved in stabilizing proteins, namely Pkd2, in membrane microdomains. In this work, we use expression of *XNTA* and truncated and mutated versions of *XNTA* in the XntA1 mutants, immunofluorescence, co-immunoprecipitations, and electrophysiology in an attempt to better understand the XntA protein and its function in *P. tetraurelia*. We demonstrate that the XntA protein must be full length to cure the mutant. We also show that XntA-myc and Pkd2-FLAG co-IP from whole cell extract but that although we observe epitope-tagged proteins on Western blots, we only identified peptides from Pkd2-FLAG when FLAG was the IP target using LC-MS/MS analysis. Lastly, we show that ciliated XntA1 mutant cells do not hyperpolarize their membrane in the presence of folate. When deciliated, the XntA1 cells do not hyperpolarize in the presence of acetate. Both of these actions were different than that of wild type cells. Hyperpolarization of the membrane in the presence of L-glutamate remains unchanged between the wild type cells and the XntA1 mutants but when these cells were deciliated, no hyperpolarization of the membrane was observed in the presence of L-glutamate. These data support the localization of the L-glutamate receptor in the cilia. The data presented here continue to suggest that the XntA protein is not a channel, but instead may be important in stabilizing proteins in membrane microdomains for important signaling pathways.

Introduction

Magnesium ions are important for numerous enzymatic reactions, including ATP and ADP synthesis, protein synthesis, and neurotransmitter release, to name a few (Maguire and Cowan, 2002). Magnesium is also required for the bending of cilia and is needed for the beating of the cilia in the model organism *Paramecium*. Previous research had also shown that extracted models of this cell, permeabilized with the non-ionic detergent Triton X-100, would reverse the orientation of the cilia on the cell surface toward the anterior of the cell in the presence of ATP and Mg^{2+} (Kung and Naito, 1973). In the '90's, researchers demonstrated that *Paramecium* has a robust inward Mg^{2+} current that is calcium dependent. When activated, it causes a depolarization of the cell (Preston, 1990). The membrane of *Paramecium* will depolarize in the presence of Mg^{2+} and Ca^{2+}, causing an influx of both ions, a prolonged action potential, and a reversal in the ciliary beat (Preston, 1990). The intracellular free Mg^{2+} concentration of *Paramecium*, shown to be ~0.4 mM (Preston, 1998, Preston, 1990) is not much different than that of other excitable cells, ~0.3 to 0.7 mM (Alvarez-Leefmans et al., 1987). *Paramecium* also has a second uncharacterized intracellular store of Mg^{2+} that is close to 8 mM (Preston, 1998, Preston, 1990).

In an attempt to better understand the regulation of Mg^{2+} across the membrane of *Paramecium*, Preston and colleagues (1994a,i) created mutants deficient in their Mg^{2+} conductance. Site-directed mutagenesis in *Paramecium* is essentially impossible due to the multiple nuclei of these cells. Therefore, a population of cells was mutated using a general mutagen, *N*-methyl-*N*'-nitro-*N*-nitrosoguanidine (MNNG) which causes the methylation of guanine residues, creating 7-methylguanines (Craddock, 1968). Those cells that survived the mutagen were then allowed to go through autogamy (Preston and Kung, 1994h, Preston and Kung, 1994a). The process of autogamy causes the breakdown of the somatic macronucleus followed by the meiotic division of

the germ line micronuclei. The four meiotic products are reduced to one which then divides mitotically to create a diploid cell that is homozygous for all genes (reviewed in (Kung et al., 1975)). The paramecia that survived the mutagen and autogamy were briefly cultured and then screened for cells deficient in their response to Mg^{2+}.

Two types of single-gene mutations were identified in the created mutants that were deficient in their response to Mg^{2+}. The recessive mutations were unlinked occurring in two separate genes, *XNTA* and *XNTB*. The XntA and XntB mutants showed no or reduced inward Mg^{2+} current (I_{Mg}), respectively (Preston and Kung, 1994h, Preston and Kung, 1994a). The XntA mutants showed a resistance to heavy metal paralysis of their cilia, a reduced ability to deactivate their depolarization activated Ca conductance ($I_{Ca(d)}$), and a rapidly deactivating Na^{+}-dependent Ca^{2+} current ($I_{Na(Ca)}$) (Preston and Kung, 1994h, Preston and Kung, 1994a). How the mutation in the *XNTA* gene leads to the slow deactivation of the Ca^{2+} conductance and the rapid deactivation of the $I_{Na(Ca)}$ is unknown. In 2002, when the gene *XNTA* gene was sequenced and identified, the authors speculated that perhaps XntA was an accessory protein that can affect the activity of other channels, such as a kinase or a regulatory protein. The authors concluded, based on the amino acid sequence analysis and their rescue studies, that XntA was a channel-like exchanger protein (Preston and Kung, 1994h, Preston and Kung, 1994a, Haynes et al., 2002). However, none of the rescue studies that were done addressed the two conductances other than the Ca^{2+}-dependent Mg^{2+}-conductance nor did they address the heavy metal resistance of the mutant. A complete understanding of the XntA protein and its function was incomplete.

The *XNTA* gene (PTETG4300006001) was identified through multiple injections into the XntA1 mutant of plasmids containing fragments of the wild type genomic library (Haynes et al., 2002). *XNTA* is 1707 nucleic acids long, with two introns located near the 5′ end. The mRNA is 1653 nucleic acids, coding for 550 amino acids. The sequence can be broken into two regions, an

α1 and an α2 region, with five and six predicted transmembrane spanning segments, respectively. These two regions have very low levels of homology to the K^+-dependent Na^+/Ca^{2+} exchangers. These two regions are connected by a large intracellular loop which contains a potential PEST sequence (Haynes et al., 2002) and a potential ubiquitination site at lysine (K) position 300. A PEST sequence is an amino acid sequence rich in proline, glutamic acid, serine, and threonine. These sequences serve as proteolytic signals, targeting proteins for rapid degradation (Rechsteiner and Rogers, 1996). Expression of wild type *XNTA* in the XntA1 mutant returns the $I_{Mg(Ca)}$ to these cells. The expression of the *XNTA* gene in the XntB mutant, however, does not show curing of the XntB mutant and *vice versa* (Haynes et al., 2002). The sequence of *XNTB* remains unknown.

The return of the $I_{Mg(Ca)}$ in the XntA1 mutant by expressing the *XNTA* gene has been demonstrated by both voltage clamp experiments as well as by measuring the backward swimming times of cells in solutions that contain Mg^{2+} (Haynes et al., 2002). The backward swimming of *Paramecium* can be used as a measurement of ion conductance by proxy. Paramecia cells typically swim forward, but if stimulated by a repellent or physical interaction at the anterior end of the cell, the membrane may depolarize beyond threshold causing an action potential. The increase in membrane potential causes the activation of the voltage-dependent calcium channels of the cilia and calcium to enter the cilia. The transient increase in the ciliary calcium concentration causes the cilia to reverse their power stroke from one towards the posterior of the cell to one that is toward the anterior. The cilia will remain beating strong toward the anterior of the cell as long as calcium remains high. The depolarization of the membrane is countered by the efflux of K^+ ions through the voltage-dependent and Ca^{2+}-dependent K^+ channels, also presumably in the cilia (Brehm et al., 1978, Satow and Kung, 1980). The duration of the action potential and therefore the length of time a cell swims backward can

be prolonged by the presence of other ions in the bath, such as Na^+ and Mg^{2+} which activate the Ca^{2+}-dependent Na^+ and Mg^{2+} conductances, respectively.

In this work, we examine the expression of the *XNTA* gene in the XntA1 mutants by expressing fragments of the gene in order to determine whether the entire gene is necessary for the return of $I_{Mg(Ca)}$ in the XntA1 mutant. We have also used immunofluorescence to look for the localization of some of the truncated versions of the XntA protein within the cell. Whole cell extracts of cells expressing *XNTA*-myc and *PKD2*-FLAG or control cells expressing FLAG and myc were used for immunoprecipitation (IP) in an attempt to co-IP the *PKD2*-FLAG and XntA-myc proteins. Gels were used for both silver staining and LC-MS/MS analysis of select bands while others were transferred to nitrocellulose and developed using antibodies against the epitope tags. Although these proteins appear to co-IP from whole cell lysate, only the Pkd2 protein was identified using LC-MS/MS analysis. Finally, we used electrophysiology to examine membrane potential changes in the wild type and XntA1 mutant cells. We determined that there is no difference between the wild type and XntA1 mutants in 5 mM and 1 mM KCl solutions. Examining both ciliated and deciliated cells in typical attractants for *Paramecium* such as folate, glutamate and acetate provided novel findings that deciliated cells did not show a significant hyperpolarization in glutamate solutions and also, that the XntA1 mutants were not as receptive to the attractants as the wild type cells. Our data suggest the XntA protein may have roles within the cell and ciliary membrane that are separate from XntA being a Mg^{2+} channel but instead perhaps as a stabilizer of proteins in membrane microdomains.

Materials and Methods:

All research was done using *Paramecium tetraurelia*, 51-s (sensitive to killer) or the mutant XntA1. Cells were cultured as previously described (Sasner and Vanhouten, 1989,

Valentine et al., 2012). Injected cells were maintained at 15°C and cultured at 22°C. Culture medium was inoculated with *Klebsiella pneumoniae* or *Aerobacter aerogenes*.

Plasmid Creation

The plasmids used for microinjection are a modified version of the pPXV-GFP plasmid (gift of Dr. W. John Haynes). The creation of this plasmid has been previously described (Valentine et al., 2012). Briefly, a GFP sequence was removed and a triple-FLAG sequence was inserted $(DYKDDDDK)^{x3}$. The Kpn I cut site at the 3'-end of the 3×FLAG sequence was mutated to create a stop codon. The existing restriction enzymes on the 5'-end of the 3×FLAG sequence were utilized to insert a linking sequence with the following order of restriction enzyme cut sites: SpeI – Apa I – Sac I – Nhe I. These restriction enzyme cut sites allowed for the cloning of the fragments of the *XNTA* gene to be inserted into the pPXV plasmid after primers were used to amplify the sequences and create the necessary restriction enzyme cut sites using Platinum®P*fx* Taq polymerase (Life Technologies, Grand Island, NY). The primer sequences used for DNA sequencing and for the creation of the different *XNTA* constructs are shown in Table II.I. The different combinations of the primers used to create the constructs and the positions in the *XNTA* sequence that the constructs consist of are shown in Table II.II. The PCR conditions used to create the inserts of *XNTA* were all the same (shown below). Template for the PCR was the previously made and sequenced XntA-FLAG plasmid DNA at 50 to 100 pg per PCR reaction. The N-terminus of XntA (N-term XntA) included the first five transmembrane spanning regions and the intracellular loop with the PEST sequence. The C-terminus of XntA (C-term XntA) included the entire 3'end of the DNA sequence starting just after the first five transmembrane spanning regions. The C-terminus plus two the last two transmembrane domains from the N-terminus (C+2N XntA) starts from position +390. The K300R plasmid contains a mutated lysine (K) to an arginine (R) at position 300. The lysine at position 300 was predicted to be a

ubiquitination site targeting the protein for degradation. The creation of the K300R version of the gene is described below. A diagram of each insert is shown in Figure II.1.

The following PCR cycles were used to create the constructs: 94°C for 5 minutes; then 5 cycles of 94°C for 1 min, 52°C for 1 min, 68°C for 2 min; 5 cycles of 94°C for 1 min, 58°C for 1 min, 68°C for 2 min; and twenty cycles of 94°C for 1 min, 61°C for 1 min, 68°C for 2 min. PCR reactions were checked on a 1% agarose gel stained with ethidium bromide and visualized using UV light. Resulting bands of expected sizes were removed using a razor blade and cleaned using the PrepEase® Gel Extraction kit (Affymetrix) as per the kit's instructions. Extracted and cleaned DNA was ligated into the prepared pPXV-C-FLAG plasmid using the restriction enzymes Spe I and Nhe I (New England BioLabs). Ligated plasmids were cloned into chemically competent DH5α bacteria as previously described (Valentine et al., 2012).

K300R was made by mutating the potential ubiquitination site at position 300 from a lysine (K) to an arginine (R). This was done using two primers to change an adenine to a guanine (bold), forward primer: 5'-CCTCAAAGTGCAATAA**G**ATAAAGAAATGATT-3', and reverse primer: 5'-TTATTCATCATTTAGTTATTATCTTTACTTCTATTTTGG-3'. The mutation was done using the Finnzymes Phusion® Site-Directed Mutagenesis Kit (Finnzymes/Thermo Fisher) as per the kit instructions. The primers were phosphorylated separately using 1 U (0.3 µL) T4 PNK (Life Technologies) in the appropriate buffer with 5 µL of 10 mM ATP in a 50 µL reaction at 37°C for 30 minutes. The T4 kinase was then deactivated by heating the reaction at 65°C for 20 minutes. 0.5 µM (2.5 µL) of each phosphorylated primer was mixed in a 50 µL reaction with 0.5 mM dNTPs, 700 pg of XntA-FLAG plasmid, 10 µL of 10x Phusion buffer, water and 0.5 µL HSII DNA Polymerase. The reaction was heated to 98°C for 30 seconds, followed by 98°C for 30 sec, 67°C for 30 sec, and 72°C for 3 minutes. A final extension of 72°C for 10 minutes was then completed and the reaction cooled to 4°C. 5 µL of this reaction was added to 100 µL of competent DH5α *E.*

coli bacteria and incubated on ice for 20 minutes. The bacteria were then heat-shocked at 42°C for one minute then plunged on ice. 250 µL of SOC media was added to the bacteria which were then shaken at 37°C for 1 hour. The bacteria were then spread on two LB-AMP plates for growth overnight at 37°C. The resulting bacteria colonies (10) were screened by isolating plasmid from three of the colonies and sending the plasmid for sequencing. All three colonies were positive for the mutation K300R.

We used previously described plasmids in this work, including *XNTA*-FLAG and *XNTA*-myc (Chapter 3). Also, the *PKD2*-FLAG plasmid was previously published (Valentine et al., 2012). A double-tagged XntA construct was also created for study, although it was not used. The C-FLAG plasmid that was digested with Spe I and ligated the 3×myc sequence into the plasmid. The 5'-end of the primer contained a start codon sequence (bold) followed directly by the 3xmyc sequence. The 3×myc sequence was created by fusing two complementary primers together as previously described (Valentine et al., 2012). The upper sequence primer: 5'-CTAGT**ATG**[GAACAAAAATTGATTTCAGAAGAAGATTT]$^{\times 3}$A-3' was fused to the lower sequence primer: 5'- CTAGT[CAAATCTTCTTCTGAAATCAATTTTTGTTC]$^{\times 3}$CATA. The double-stranded DNA was then ligated into the open pPXV-C-FLAG plasmid using LigateIT® (Affymetrix) as per the kits instructions.

Cracking Gel

To screen bacterial colonies, 30 overnight shaking cultures were started from the resulting bacterial colonies in 50 µL LB containing 100 µg/mL AMP. Five µL of the overnight shaking culture was mixed with 6 µL Lysis buffer [0.1 N NaOH, 10 mM EDTA, 1% sodium dodecyl sulfate (Life technologies), 10% glycerol (Affymetrix, Santa Clara, CA)] and 2 µL Loading buffer [0.25% bromophenol blue, 0.25% Xylene Cyanol FF, 30% glycerol (Affymetrix)]. Samples were loaded into a 0.75% Agarose (Affymetrix) gel and 2 µL of Supercoiled DNA ladder (Life

Technologies) was added in one lane as a standard. After being run at 100 mA for approximately 45 minutes, the gel was visualized by soaking in ethidium bromide for 40 minutes and visualized with UV light. Colonies producing bands of the appropriate size were used to start overnight cultures with 6 mL LB containing 100 µg/mL AMP.

Plasmid Extraction

Plasmids were extracted using the Wizard® Plasmid extraction kit (Promega, Madison, WI). Briefly, 5 mL of the overnight culture was centrifuged in a 15 mL sterile centrifuge tube at 1875 × g (3400 rpm) for 15 minutes. The resulting pellet was resuspended in 400 µL Cell Resuspension Buffer (50 mM Tris, 10 mM Na_2EDTA, and 0.1 mg/mL RNase I). The sample was moved to a 1.5 mL Eppendorf tube and mixed with 400 µL Cell Lysis Buffer [0.2 M NaOH and 1% sodium dodecyl sulfate (Life technologies)]. Samples were lysed at room temperature for 5 minutes, then the pH was neutralized using 400 µL of Neutralization buffer (0.13 M potassium acetate, pH 4.8). The tube was spun at 18,407 × g for 8 minutes (Eppendorf 5424 Centrifuge, Hauppauge, NY). A 3 mL Luer-lock syringe was prepared by placing a Wizard® Column (Promega) on the syringe and adding 1 mL of Resin Solution (Promega). The supernatant from the spun sample was then added to the resin and forced into the column using the plunger. The column was washed using 2 mL of Column Wash (80 mM potassium acetate, 8.3 mM Tris, 40 µM Na_2EDTA and 55% Ethanol). The column was dried by placing it on a 1.5 mL Eppendorf tube and spinning for 2 minutes at 18,407 × g. The column was then moved to a new tube and 25 µL of MilliQ water was added to the column to dissolve the plasmid. The sample was spun for 2 minutes at 18,407 × g. The collected water was passed through the column again to increase the yield. The concentration of the eluted plasmid was checked using the Agilent spectrophotometer (Agilent, Santa Clara, CA) (O.D. of 260 and 280 nm) and stored at -20^{o}C for later use. Twenty µg

of the plasmid at a concentration of 50 ng/µL was sent for sequencing at the Vermont Genetics Center DNA Facility (University of Vermont, Burlington, VT).

All plasmids were prepped for microinjection as previously described (Valentine et al., 2012). Approximately 5 pL were injected into the macronucleus of XntA1 mutants which were checked for Mg^{2+}-induced behavior before injection to ensure they had no reaction in that solution. Control cells were injected with the FLAG plasmid as all constructs contained a C-terminal FLAG tag. If cells were to receive a second plasmid for injection, they were first screened using genomic DNA extraction and PCR to ensure they contained the exogenous plasmid. Only then would some cells receive the second plasmid. After all injections, cells were maintained as individual clones at 15°C. All injected cells were tested for the exogenous plasmid by extracting genomic DNA and performing PCR using *XNTA* primers as well as primers specific to the exogenous pPXV plasmid. All primers can be found in Tables II.I and II.II. The PCR conditions were as follows: 94°C for 5 minutes, then 30 cycles of 94°C for 1 min, 42°C for 1 min, 68°C for 2 min, followed by a final extension of 68°C for 10 minutes. PCR products were visualized on a 1% agarose gel using ethidium bromide. Positive cell lines were maintained for no more than 4 weeks at 15°C with regular feeding to prevent autogamy.

Behavior Assays

We used different ionic stimuli to examine paramecia for ion channel defects. The swimming behavior of these cells are governed by their membrane potential. By exposing paramecia to different ionic solutions and observing their swimming behavior (i.e., backward swimming assays), we are able to infer ion conductances across the membrane. All the solutions contain the base buffer of 1 mM calcium citrate and ~1.3 mM Tris Base ([Tris(hydroxymethyl)aminomethane]). Additional salts were then added and the pH adjusted to 7.02 to 7.05 using 100 mM Tris Base. The following salts were added to the base buffer: 25 mM

TEA (tetraethylammonium chloride) with 5 mM $MgCl_2$ (Mg/TEA) and a resting buffer that contained 4 mM KCl.

After screening the cells for the injected plasmid, the cells were subjected to backward swimming assays in the $MgCl_2$ with TEA solution. The main phenotype of the XntA1 mutant is the inability to swim backward in Mg^{2+} solutions because of the missing $I_{Mg(Ca)}$ (Preston and Kung, 1994h, Preston and Kung, 1994a). We wanted to observe the ability of the small fragments of XntA to cure the XntA1 phenotype. Cells were transferred, approximately 20 at a time, to 500 µL of resting buffer (4 mM KCl in base buffer) and allowed to acclimate for at least 15 minutes. Cells were then transferred one at a time using specially made Pasteur pipettes to 100 µL of the test solutions and the time the cells spent swimming backward was timed using a stop watch. Once the cells returned to a forward swimming pattern, the stop watch was stopped and the time recorded. Test solutions were changed after ~5 cells had been tested in it. All tests were done in glass depression slides using dissecting microscopes.

Immunostaining

Immunostaining was done as previously described (Valentine et al., 2012). Merged images are shown. Primary antibodies used were 1:1000 rabbit anti-centrin (Gift from Dr. Mark Winey, University of Colorado, Boulder, CO) to highlight the basal bodies just below the cell surface and 1:500 mouse Anti-FLAG (Sigma M2 clone). Secondary antibodies were Alexa Fluor® donkey anti-mouse 488 and donkey Anti-rabbit 568, 1:250 dilution. Images were taken using the DeltaVision Microscope system using an Olympus IX70 microscope PlanApo 60x/1.4 oil lens. Images presented are stacks of Z-sections and are approximately 10 to 20 µM thick. Images are representative of the population.

Whole Cell Extract IP

Whole cell extract was adapted and completed as published in previous works (Nachury et al., 2007, Valentine et al., 2012). Briefly, cells were washed twice in 200 mL cold Lap200 Buffer (50 mM HEPES, 200 mM KCl, 1 mM EGTA, 1 mM $MgCl_2$, pH 7.8) and then in 100 mL cold Lap200 with protease inhibitors: 1 mM Phenylmethylsulfonyl fluoride (PMSF) (Sigma), 1 µg/mL Leupeptin (Research Products International) and 1 µg/mL Pepstatin A (Research Products International). Cells were then homogenized in less than 8 mL of Lap200 with protease inhibitors. The protein concentration of the homogenate was determined using a BCA protein assay (ThermoFisher) and the volumes and concentrations equalized between the two samples, test and control. Five µL of sample was removed from each for a loading control and enough Triton X-100 was added to each sample for the final concentration to be 1%. Proteins were solubilized while rocking for one hour on ice. Insoluble protein was removed by centrifugation at 31,000 × g for 20 minutes and then 100,000 × g for one hour, both at 4°C. The final supernatant was then used for immunoprecipitation (IP) using FLAG or myc affinity agarose (Sigma) as previously described (Valentine et al., 2012).

SDS-PAGE, Western Blots, Silver Staining, and LC-MS/MS

To examine proteins present in the IPs from whole cell extracts, the agarose affinity beads were mixed with 30-35 µL of sample buffer and 2 µL β-mercaptoethanol then boiled for 5 minutes. Samples were plunged into ice and then spun at 4°C for 5 minutes to pellet the beads. Samples were separated on 7-15% acrylamide gels using 10 µL of Thermo Scientific™ PageRuler™ prestained protein ladder or 30 µL of diluted Benchmark™ protein ladder (Life Technologies) as a molecular mass standard. For Western blots, proteins were transferred to Nitrocellulose paper (Pall Gelman, Port Washington, NY). For mass spectrometry, gels were silver stained. Transfers to nitrocellulose paper was done using a wet tank transfer in transfer

buffer (40 mM glycine, 50 mM Tris Base, and 20% methanol). Gels were transblotted at 390 mA for an hour and 20 minutes, then 250 mA for an hour and 20 minutes at 4°C.

Blots were developed using either Enhanced Chemiluminescence (ECL) or alkaline phosphatase (AP). For ECL, blots were blocked in 10 to 20 mL 5% Non-fat Dry milk in TBS-T (15 mM Tris-HCl, 140 mM NaCl, 0.1% w/v TWEEN®-20 (Sigma), pH 7.5). For AP blots, 2% w/v Telost gelatin from fish (Sigma) and 3% Normal Goat Serum (Vector Labs, Burlingame, CA) was added to the milk and TBS-T mixture. Blots were blocked for one hour at room temperature before primary antibodies were added. ECL blots were rinsed three times, 1× 15 minutes, 2× 5 minutes, with approximately 20 mL of TBS-T before the primary antibodies were added in TBS-T. AP blots were given the primary antibody in the blocking buffer. Primary antibodies and their dilutions included: rabbit or mouse Anti-FLAG M2 clone (Sigma) 1:2500; rabbit or mouse Anti-C-myc (GenScript, Piscataway, NJ), 1:2000; mouse Anti-Tubulin, acetylated (Sigma), 1:10,000. Blots were incubated in primary antibody overnight at room temperature (TBS-T) or 4°C (milk blocking buffer). The following day, the blots were rinsed three times with ~20 mL TBS-T before the addition of the secondary antibodies in TBS-T, 1:10,000 dilution. Secondary antibodies included donkey Anti-rabbit IgG HRP conjugate (GE Healthcare), goat Anti-rabbit IgG AP conjugate (Sigma), goat Anti-mouse IgG HRP conjugate (Thermo Scientific), and goat Anti-mouse AP conjugate (Sigma). After one hour, blots were washed 4× with ~20 mL TBS-T and then developed using 15 mL BCIP/NBT substrate (Moss, Inc., Pasadena, MD) or SuperSignal West Pico Chemiluminescence Substrate (Thermo Scientific) as per the kit's instructions.

Silver staining was completed as previously described (Valentine et al., 2012) using the FASTSilver™ staining kit (G-Biosciences, St. Louis, MO). After stopping the reaction with 2% acetic acid, gels were stored at 4°C in fresh 2% acetic acid until they were processed. Gels were processed for LC-MS/MS analysis as soon as possible after silver staining. The gels were cut,

destained, and processed for LC-MS/MS as previously described in Chapter 2 and 3 and in other reports (Valentine et al., 2012, Yano et al., 2013, Picariello et al., 2014).

Electrophysiology

Cells used for electrophysiology were in early logarithmic growth phase. Glass electrodes for recording membrane potential were pulled using 1 mm borosilicate glass capillary tubes (with filament) (World Precision Instruments, Sarasota, FL) by a Narishige pipet puller (Japan). The pulled electrodes were back filled with 500 mM KCl, showing a resistance in the starting bath of between 40 and 110 MΩ. The resting membrane potential of the cells was continuously recorded using a Warner Intracellular Electrometer IE-251A (Warner Instruments, Hamden, CT) processed through AD Instruments PowerLab 4/35 and analyzed using LabChart Pro (AD Instruments, Colorado Springs, CO). The main chamber bath was filled with 5 mM KCl in base buffer (See Behavior Assays). The main chamber was grounded to a 3M KCl reference bath connected by a 3% agar in 3 M KCl bridge sealed with Vaseline. The main chamber bath was under a constant controlled flow of buffer using a Buchler polystaltic pump (Buchler, Fort Lee, NJ) set to a flow rate of ~3 mL/min. The membrane potential recordings began in 5 mM KCl and cells were allowed to acclimate for 4 to 6 minutes before the chamber bath was changed to an attractant solution. The cells was given four minutes in the test solution then returned to 5 mM KCl for another 4 minutes before the next attractant solution was applied. Membrane potentials were noted down after the four minutes. Attractant solutions were prepared in the base buffer previously described (Behavior Assays). The K^+ ion concentration was maintained between the resting solution and the attractant solution. Solutions included 5 mM K-acetate, 5 mM K-D-Glutamate, 5 mM K-L-Glutamate, and 2.5 mM K_2-Folate.

Results

The swimming speed and direction of ciliary beat in *Paramecium* is governed by its membrane potential (Naitoh, 1968, Van Houten, 1979). These cells will depolarize in strong ionic solutions, such as Mg^{2+} concentrations above 0.5 mM, which will activate the ciliary voltage-gated calcium channels (Preston, 1990, Preston, 1998). When these channels open, calcium enters the cilia causing them to reverse their power stroke, propelling the cell backward. As long as calcium remains high, the cell will continue to swim backward. The presence of Mg^{2+} in the bath allows for activation of the $I_{Mg(Ca)}$ which prolongs the depolarization (Preston, 1990) and therefore, the backward swimming duration. The addition of TEA further prolongs the backward swimming as this chemical blocks the fast-acting repolarizing K^+ conductance (Satow and Kung, 1976, Satow and Kung, 1980). The XntA1 mutant, which does not swim backward in Mg^{2+} solutions, lacks the $I_{Mg(Ca)}$ and does not depolarize in the presence of Mg^{2+} (Preston and Kung, 1994h, Preston and Kung, 1994a, Haynes et al., 2002).

The injection of the wild type *XNTA* gene into the macronucleus of this mutant has been shown previously to recover the $I_{Mg(Ca)}$ and backward swimming in the XntA1 mutant (Haynes et al., 2002). Our data also suggest that we were able to cure the mutant by expressing *XNTA*-FLAG, but not to the level of wild type cells (Figure II.1 and II.2). Our previous findings suggested this protein is cleaved into smaller fragments and could be degraded very quickly (See Chapter 3). A single potential ubiquitination site was identified at K300 using UbPred (www.ubpred.org) with a high confidence rating. XntA also has a predicted PEST sequence (302 RNDQQDNDQDDNPLIDSNPMESVH 325). The predicted PEST sequence was found using Emboss epestfind (http://emboss.bioinformatics.nl/cgi-bin/emboss/epestfind) and the sequence was published previously (Haynes et al., 2002). These two sites, the PEST sequence and the potential ubiquitination site, may target the XntA protein for early degradation which could

explain the smaller fragments that we find. In an effort to prevent ubiquitination, we mutated the lysine to an arginine. Arginine was chosen because it is similar to lysine, but ubiquitination cannot occur. After creating the truncated and mutated versions of the *XNTA* gene, we expressed these genes in the XntA1 mutant and examined the cells for a return Mg^{2+}-induced behavior. Depictions and backward swimming times of the different *XNTA* genes expressed in the XntA1 mutant as well as the wild type control data are shown in Figures II.1 and II.2. All backward swimming times were analyzed using unpaired T-tests.

Expression of the N-terminus of XntA (N-term, amino acids 1-357) showed no rescue of the mutant, essentially no backward swimming in Mg/TEA solution was observed (Figure II.1 and II.2). The expression of the C-terminus of XntA (C-term, amino acids 177 to 550, 353 amino acids in length) and the expression of the C-terminus plus the last two transmembrane spanning regions of the N-terminus (C+2N, amino acids 112-550, 438 amino acids in length) showed a small, but significant, amount of backward swimming in Mg/TEA solutions. These data suggest a small amount of functionality of the protein. However, none of the truncated versions of the protein showed the level of curing as the full length of the XntA protein as shown here or in previous work (Haynes et al., 2002).

There was no difference in the backward swimming times in Mg/TEA observed by XntA1 mutants expressing *XNTA*-FLAG or the mutated XntA, K300R (P=0.7). However, XntA1 mutants expressing FLAG-*XNTA* showed significantly longer backward swimming compared to the XntA1 mutants expressing *XNTA*-FLAG, K300R, and myc-*XNTA*-FLAG (P<0.001). The XntA1 mutants expressing K300R and *XNTA*-FLAG swim backward for significantly longer in Mg/TEA than the XntA1 mutants expressing myc-*XNTA*-FLAG cells. Regardless, none of these XntA1 expressing cells were able to swim backward as long as wild type cells expressing FLAG

in Mg/TEA solutions (P<0.001). All backward swimming times are shown in Figures II.1 and II.2.

To visualize the location of the different XntA epitope-tagged proteins in the XntA1 mutants, most of the different XntA1 expressing mutants were immunostained (Figure II.3). XntA1 mutants expressing the FLAG plasmid were used as the control. Anti-centrin, a stain for the basal bodies found just below the cell surface was also used as an intracellular marker (Anti-centrin was a kind gift from Dr. Mark Winey, University of Colorado, Boulder, CO). We saw no difference in the localization of the different truncated versions of the XntA protein in the XntA1 mutant. FLAG-*XNTA, XNTA*-FLAG, K300R-FLAG, and C+2N-FLAG all appear to be localized at the cell surface and in the cilia. Figure II.3 shows representative cells within the population that were immunostained for each of these expressing mutant cell types. These were the injected XntA1 mutants that demonstrated the best curing, meaning a return of Mg^{2+}-induced behavior. The N-term and C-term expressing XntA1 mutants showed so little curing at the time of testing, and were not immunostained.

To determine possible interacting partners for the XntA1 protein we expressed *XNTA*-myc in wild type cells as well as *PKD2*-FLAG. Our previous work suggests these two proteins are involved in Mg^{2+}-induced behavior and could be potential interacting partners. Control cells were expressing FLAG and myc. We performed a whole cell extract and solubilized the samples with 1% Triton X-100. Proteins were immunoprecipitated (IP'd) using myc affinity agarose. The resulting eluate was divided and separated by SDS-PAGE. One-tenth of the test and control IP eluates were run on a separate gel and used for Western blot. The remaining eluate was silver stained and used for LC-MS/MS analysis. The Western blot was first probed with Anti-myc antibody (Figure II.4A), the blot was then stripped and re-probed using ant-FLAG antibody to determine if the Pkd2-FLAG protein co-IP'd with XntA-myc (Figure II.4B, blue arrows). Figure

II.4C shows the resulting silver stained gel with blue and purple arrowheads and brackets with numbers to indicate the approximate regions of the gel that were cut and sent for LC-MS/MS corresponding to the bands on the Western blots. A tubulin loading control was also included to demonstrate that the solubilization of the test and control whole cell extracts started with approximately the same amount of protein.

Bands of the approximate sizes for the XntA-myc protein were observed by Western blot at approximately 61 kD (full length XntA-myc), as well as smaller fragments at 41 kD, 35 kD and 33 kD (Figure II.4A, purple arrow heads). The re-probed Western blot to identify the Pkd2-FLAG protein showed faint bands at 110 kD, 100 kD, 90-88 kD, and 65-63 kD (Figure II.4B, blue arrow heads). The expected full length of Pkd2-FLAG is 100 kD. The approximate areas of the silver stained gel that corresponded to the anti-myc and anti-FLAG bands were excised and processed for LC-MS/MS analysis. Although these bands appeared on the Western blot, no peptides from XntA or Pkd2 were identified in the LC-MS/MS analysis of the gel slices. A list of the proteins identified with the XntA-myc IP Are shown in Table II.III. These proteins were identified in the test lane only. Proteins that were identified in both the control and test lane were removed from the analysis.

The same IP experiment was done in the reverse orientation, where FLAG affinity agarose was incubated in the solubilized whole cell extract from cell expressing *PKD2*-FLAG and *XNTA*-myc. Control cells were expressing FLAG and myc. One-tenth of the resulting eluate was again used for Western blot while the remaining sample was separated by SDS-PAGE and silver stained. The blot was first probed with Anti-FLAG, then stripped and re-probed with Anti-myc. Similar to the results shown in Figure II.4B, Figure II.5A shows bands for Pkd2-FLAG at approximately 100 kD, 90-88 kD, 70-68 kD (Figure II.5A, blue arrow heads). This blot was stripped and re-probed using Anti-myc which identified bands at 61 kD, 41 kD and 35 kD (Figure

II.5B, purple arrow heads). A tubulin loading control is shown, demonstrating the protein used for the solubilization between the test and control samples was approximately equal (Figure II.5D). As before, the approximate areas of the silver stained gel that corresponded to the bands identified for XntA-myc and Pkd2-FLAG on the Western blots were excised and processed for LC-MS/MS (Figure II.5C). These areas are designated again by brackets and numbers as well as colored arrowheads that approximately match with bands on the Western blots. Note the grey arrows near brackets 1, 2, and 3. These bands were visually different between the two gels and therefore were excised and processed for LC-MS/MS. Because of the darkness of the ladder, the approximate mass of these bands is unknown, but we expect them to be at or above 100 kD. The LC-MS/MS analysis identified the Pkd2 protein in all of the upper excised bands (1 through 6). Disappointingly, no XntA peptides were identified in this analysis. A complete list of the proteins unique to the test lane are shown in Table II.IV which correspond to the gel slice, or band, they were identified in. Proteins that were identified in both the control and test lane were removed from the analysis; only proteins unique to the test lane are shown.

An important experiment was to ensure that the XntA-myc IP results we were observing were not due to the myc affinity agarose IP'ing the FLAG protein. This control experiment can also accompany the results from Chapter 3. To ensure the myc affinity agarose was not IP'ing the FLAG epitope of Pkd2-FLAG, whole cilia from cells expressing FLAG (control) and whole cilia from cells expressing *PKD2*-FLAG were solubilized and used for two IPs, one using FLAG affinity agarose and the other using myc affinity agarose. The results are shown in Figure II.6. The immunoblot for this developed using rabbit anti-FLAG. Because the myc affinity agarose beads use a rabbit polyclonal antibody and the primary antibody used to develop the blot was produced in rabbit, the heavy and light chain of the antibody are very robust, at ~50 and ~25 kD. While clear bands are observed in the FLAG affinity agarose IP lane for Pkd2-FLAG (Figure II.6,

white arrows), there are no Pkd2-FLAG bands observed in the lane using the myc affinity agarose on the whole cilia from cells expressing Pkd2-FLAG.

During the process of training on the electrophysiology equipment, we decided to measure the resting membrane potential of wild type cells and XntA1 mutants in multiple ionic solutions. Prior publications demonstrated that there was no difference between the resting membrane potentials of wild type cells and an XntA1 mutant cells in 1 mM KCl in buffer, -38 ± 1 mV and -39 mV ± 1 mV, respectively. However, when the bath solution was changed to 1 mM KCl with 0.5 mM $MgCl_2$, the wild type cells depolarized by 10 ± 1 mV while the XntA1 mutants depolarized only by 1 ± 7 mV (Preston and Kung, 1994a). To further investigate the depolarization ability of the XntA1 mutants' membrane, we measured the membrane potential of these mutant cells and of wild type cells in various attractant solutions and potassium solutions. All statistical comparisons were done using un-paired T-tests.

We first established the resting membrane potential of these cells in 5 mM KCl in buffer as well as how much the cells hyperpolarize when changed to 1 mM KCl in buffer. The wild type cells had a resting membrane potential in 5 mM KCl in buffer of -28 ± 5.6 mV (N=22). The XntA1 mutants had a resting membrane potential in 5 mM KCl in buffer of -27.2 ± 5.7 mV (N=9), not statistically different than the wild type cells (P=0.75). When these cells were changed to a bath containing 1 mM KCl in buffer from 5 mM KCl, the wild type cells hyperpolarized (become more negative) by -13.2 ± 7 mV (N=14) and the XntA1 mutants hyperpolarized by -14.3 ± 5.2 mV (N=9). There was no statistical difference between the membrane potential of the wild type and XntA1 mutants in 1 mM KCl (P=0.68). When the wild type and XntA1 mutant cells were deciliated, there was no difference observed in their resting membrane potential in 5 mM KCl. The deciliated wild type cells had a resting membrane potential of -29 ± 7.2 mV (N=8) and the deciliated XntA1 mutant cells -31.5 ± 6.5 mV (N=8) (P=0.52). These values are also not

statistically different from the resting membrane potential of the ciliated cells, as expected from previous published data (Machemer and Ogura, 1979).

Previous studies have shown that when exposed to attractants, such as glutamate or folate, the membrane of *Paramecium* will hyperpolarize (become more negative) (Van Houten, 1979, Preston and Van Houten, 1987). Bacteria are thought to expel these attractants into the environment which the paramecia then use as a food cue, swimming into the area where bacteria are inhabiting to ingest them (Preston and Usherwood, 1988). The hyperpolarization of the membrane would lead to fast, smooth forward swimming of the cell (Van Houten, 1979, Eckert, 1972). In the presence of 5 mM acetate, the membrane should hyperpolarize by ~7.5 mV and in the presence of 2.5 mM folate, there should be a hyperpolarization of ~11 mV. These values do not change if the cells are deciliated (Van Houten, 1979, Preston and Van Houten, 1987). Although the hyperpolarizations of the wild type cells we observed was not as large as in previously published work (Preston and Van Houten, 1987), the wild type cells did hyperpolarized by -5.3 ± 2.1 mV (N=13) in 5 mM K-acetate, and by -5.8 ± 3 mV (N=17) in 2.5 mM K_2-folate. The XntA1 mutants do not hyperpolarize as much in 5 mM K-acetate, -0.9 ± 3.5 mV (N=5), although the values are not significantly different. However, in 2.5 mM K_2-folate, the XntA1 mutants hyperpolarize significantly less than the wild type cells, -1.9 ± 1.3 mV (N=6) (P<0.001). All values for the change in membrane potential are shown in Table II.V.

An intriguing find was in the deciliated cells, both wild type and XntA1 mutants. First, the deciliated wild type cells hardly hyperpolarize at all in 5 mM K-L-Glutamate, a significantly smaller hyperpolarization that in the ciliated wild type cells (P<0.01). There were no difference in the amount of hyperpolarization by the ciliated and deciliated wild type cells in 5 mM acetate, which was expected (Preston and Van Houten, 1987). However, the deciliated XntA1 mutants

depolarized in 5 mM K-acetate, which was significantly different than the deciliated wild type cells (P<0.01). All values for the change in membrane potential are shown in Table II.VI.

Discussion

We have shown here that we were capable of partially curing the XntA1 mutant by expressing various full-length fragments of the *XNTA* gene. The expression of small truncated fragments of *XNTA* were able to return some Mg^{2+}-induced behavior to the mutant, but not to the degree of expressing the full length gene. Expressing the 5'- or 3'- end of the *XNTA* gene (N-term, C-term, or C+2N term) did not show a dramatic curing of the mutant, suggesting the full-length protein is required. The majority of the XntA mutants (seven out of eight) that were initially studied were shown to have mutations creating premature truncations in the first half of the gene or protein. These XntA mutants were completely devoid of $I_{Mg(Ca)}$, even with some of the N-terminus of the protein in some cases (Haynes et al., 2002). Therefore, we were not surprised by the lack of backward swimming in Mg^{2+} solutions by the XntA1 mutants expressing the N-term of *XNTA*. The expression of the C-term or the C+2N did show a significant increase in the backward swimming of the mutant, but not to the degree of full-length XntA. Further studies should be done to determine if the protein must be whole to be functional. For example, expression of the N-term and the C-term in the XntA1 mutant may show significantly more curing which might suggest the protein does not have to be whole to be functional. Also, removal of the PEST sequence may change the activity of the expressed protein. If the PEST sequence does indeed target XntA for rapid degradation, its removal from the sequence may allow the XntA protein to be over-active. The over-activity of the protein could be measured by swimming assays and by electrophysiology in solutions containing Mg^{2+}.

The immunostaining of the different versions of the *XNTA* gene in the XntA1 mutant show almost no change in the distribution of the protein within the cells, even though the protein is not full length. We might infer from these results that if there is a signal sequence that targets the XntA protein to the cilia, that this sequence would be found somewhere in the later 2/3 of the C-terminus of the protein. However, better evidence would be needed to make such a statement of a signal sequence or ciliary targeting sequence. So far, signal sequences are unknown in *P. tetraurelia*. One such sequence important for ciliary targeting in mammalian cells is the VxPx motif, necessary for engaging the Arf4 protein for ciliary trafficking (Mazelova et al., 2009). However, this was demonstrated in photoreceptor cells which contain a modified cilium. A VxPx motif is found at position V382 of XntA, between the sixth and seventh transmembrane sequences, which may target the protein to the cilia. We have no proof that this sequence is important for tagging XntA or any other *Paramecium* protein for ciliary localization. But if the VxPx motif does target the XntA protein to the cilia, expressing the N-term of *XNTA* with the FLAG tag should show no ciliary staining of the epitope tagged protein since the N-term sequence does not include the VxPx motif. Also, mutation of this site may prevent the full-length protein from trafficking to the cilia. The notion of a ciliary targeting sequence is not far-fetched and has not been closely examined before in *P. tetraurelia*.

Our Western blots of whole cell extract IP eluates from cells expressing both *XNTA*-myc and *PKD2*-FLAG suggest these two proteins interact, either directly or indirectly. However, the LC-MS/MS data do not support the IP of XntA-myc because no peptides from XntA were identified. These findings were surprising since we observed XntA-myc bands in the Western blots. Conversely, identifying peptides for Pkd2 selectively in the lanes where we anticipated finding them (based on where the silver stained gel lined up with the Western blot), suggests we were not miss-interpreting where to identify the proteins. However, that is not to say that we did not miss the sections of gel that contained the XntA protein. As we have mentioned, the XntA

protein is cleaved into smaller fragments and could have been missed. In the future, using the entire gel would be more beneficial to ensure no proteins were inadvertently excluded. It is also possible that the proteins present in the gel were too weak or in too low of a concentration to identify by LC-MS/MS. Although the XntA-myc protein was identified on a Western blot, ECL is able to detect proteins in the low picogram range. LC-MS/MS is also able to detect proteins around 50 pg, however, this becomes complicated when the sample is not pure, but is instead a mixture of proteins in a tryptic digest (Bronsema et al., 2013). It is possible that XntA was in too low of a concentration to have peptides identified via LC-MS/MS.

The results from these experiments differ from our other IP results in Chapter 3 where we were able to IP Pkd2-FLAG when we targeted XntA-myc for IP, but we were unsuccessful at IP'ing XntA-myc when we targeted Pkd2-FLAG for IP. We proposed in Chapter 3 that this is due to the occlusion of the FLAG peptide on the C-terminus of Pkd2-FLAG from direct or indirect interactions with the XntA-myc protein. However, the IP's in Chapter 3 were from cell membrane and whole cilia. We are showing here the results from whole cell extract. It is possible that the interaction between XntA and Pkd2 when Pkd2-FLAG is targeted for IP was not maintained when using solubilized membranes for IP as in Chapter 3. Perhaps by using whole cell extract, there were more proteins accessible for IP because we have access to many of the vesicles being trafficked within the cell. Because of the amount of accessible proteins in a whole cell extract, weak interactions may be maintained, sustaining interactions between the XntA-myc protein and Pkd2-FLAG when Pkd2 is IP'd. It is also possible that the IP of Pkd2-FLAG from whole cell extract has pulled proteins collectively that are in a vesicle being trafficked to the cell membrane or the cilia, yielding a "false positive." This could appear as a co-IP of these proteins, when in fact, they are simply in the same vesicle.

We have ensured that the myc beads are not recognizing the FLAG epitope on the Pkd2-FLAG protein by performing a necessary control experiment. We have demonstrated using solubilized whole cilia that the myc affinity agarose does not IP Pkd2-FLAG. This supports our findings that the co-IP results we observe here and in Chapter 3, where XntA-myc and Pkd2-FLAG co-IP using the myc affinity agarose. That the co-IP is not because the myc agarose is attaching to the FLAG epitope. This control experiment was done later, once the cell membrane and whole cilia were being used for IPs as in Chapter 3. However, it is still an important experiment demonstrating that the IP results we have observed are not due to the myc affinity agarose recognizing the FLAG epitope yielding a false positive result.

The electrophysiology findings support the XntA protein being involved in processes other than Mg^{2+}-induced behavior. The XntA1 mutants did not hyperpolarize in 2.5 mM K_2-folate like the wild type cells. This finding was extremely interesting since the *Paramecium* folate receptor is a glycosophosphatidyl inositol (GPI)- anchored protein (Weeraratne, 2007). We would expect GPI-anchored proteins to be enriched in membrane microdomains, or lipid rafts. If the XntA protein is stabilizing proteins in membrane microdomains, as we have proposed it does for the Pkd2 protein, perhaps these domains are interrupted without the XntA protein leading to altered chemoresponse to attractants. Further testing would be necessary, but examining the response of these cells further to attractants would be important and could be extremely informative as to the possible other functions of the XntA protein.

When the cells were deciliated and their membrane potentials measured in the attractants, we did not expect to see a difference in the acetate or folate hyperpolarization response based on previous work (Preston and Van Houten, 1987). Although we did not observe changes in the wild type cells or the mutant that were significant in folate, we did observe that deciliated XntA1 mutants depolarize (positive change in membrane potential) as opposed to

hyperpolarize in acetate, which was significantly different than the wild type cells. Acetate is expected to bind a surface receptor activating a calcium/calmodulin kinase which in turn hyperpolarizes the cell by activating a potassium conductance to release potassium and the plasma membrane calcium ATPases (PMCA) to expel calcium to maintain the hyperpolarization (Preston and Van Houten, 1987). We would expect these receptors to be located both on the cell surface and probably on the cilia because deciliation does not change the hyperpolarization of the cell in acetate, shown here and elsewhere (Preston and Van Houten, 1987). Also, the channels necessary for this behavior are expected to be localized in the cilia (Machemer and Eckert, 1973, Machemer and Ogura, 1979). Other research does suggest that the XntA1 mutants may have an altered response to Mg^{2+} which demonstrated the XntA1 mutants are not as attracted to acetate as wild type cells (Bell et al., 2007). However, why the XntA1 mutant is depolarizing in acetate when the cell is deciliated is unknown, and further investigation is needed.

Another important finding to point out was the loss of membrane hyperpolarization of the membrane in 5 mM K-L-glutamate when wild type cells were deciliated. The responses of the cells to D-Glutamate, both wild type and XntA1 mutants, were not robust. However, the lack of hyperpolarization of the membrane of wild type cells to L-glutamate when they were deciliated was significant. Work in the 1980's on the glutamate receptors on *Paramecium* using ^{3}H-L-glutamate showed the binding sites to be on the cilia (Preston and Usherwood, 1988). Other work in our lab has produced conflicting results on the location of the glutamate receptors. However, these data confirm the location of the L-glutamate receptors in the cilia, which is important for glutamate chemoresponse and membrane hyperpolarization.

It is clear from our work presented in this Appendix as well as Chapter 3 that we have uncovered more questions than answers concerning the XntA1 mutant and the XntA protein. We know that XntA is important for Mg^{2+}-induced behavior and that it most likely interacts with the

Pkd2 protein, either directly or indirectly (Chapter 3). We also now know that there are deficiencies in this mutant in its ability to respond to attractants with a sustained membrane hyperpolarization. We have shown that the XntA protein, although truncated when we IP it in many cases, needs to be full length in order to be functional. Further investigation into membrane potentials of the XntA1 mutant, both ciliated and deciliated, in attractants is needed to better establish the differences between the wild type cells and the mutant. As we have become more proficient with electrophysiology, we may be able to obtain more consistent measurements. It is not a far-fetched proposal that the XntA protein is in fact a stabilizer of membrane microdomains. The instability of these microdomains could explain the multitude of pathways that seem to be affected in this mutant.

References

ALVAREZ-LEEFMANS, F. J., GIRALDEZ, F. & GAMINO, S. M. 1987. Intracellular free magnesium in excitable cells: its measurement and its biologic significance. *Can J Physiol Pharmacol,* 65**,** 915-25.

BELL, W. E., PRESTON, R. R., YANO, J. & VAN HOUTEN, J. L. 2007. Genetic dissection of attractant-induced conductances in Paramecium. *J Exp Biol,* 210**,** 357-65.

BREHM, P., DUNLAP, K. & ECKERT, R. 1978. Calcium-dependent repolarization in Paramecium. *J Physiol,* 274**,** 639-54.

BRONSEMA, K. J., BISCHOFF, R. & VAN DE MERBEL, N. C. 2013. High-sensitivity LC-MS/MS quantification of peptides and proteins in complex biological samples: the impact of enzymatic digestion and internal standard selection on method performance. *Anal Chem,* 85**,** 9528-35.

CRADDOCK, V. M. 1968. The reaction of N-methyl-N'-nitro-N-nitrosoguanidine with deoxyribonucleic acid. *Biochem J,* 106**,** 921-2.

ECKERT, R. 1972. Bioelectric control of ciliary activity. *Science,* 176**,** 473-81.

HAYNES, W. J., KUNG, C., SAIMI, Y. & PRESTON, R. R. 2002. An exchanger-like protein underlies the large Mg2+ current in Paramecium. *Proc Natl Acad Sci U S A,* 99**,** 15717-22.

KUNG, C., CHANG, S. Y., SATOW, Y., HOUTEN, J. V. & HANSMA, H. 1975. Genetic dissection of behavior in paramecium. *Science,* 188**,** 898-904.

KUNG, C. & NAITO, Y. 1973. Calcium-induced ciliary reversal in the extracted models of "Pawn", a behavioral mutant of Paramecium. *Science,* 179**,** 195-6.

MACHEMER, H. & ECKERT, R. 1973. Electrophysiological control of reversed ciliary beating in Paramecium. *J Gen Physiol,* 61**,** 572-87.

MACHEMER, H. & OGURA, A. 1979. Ionic conductances of membranes in ciliated and deciliated Paramecium. *J Physiol,* 296**,** 49-60.

MAGUIRE, M. E. & COWAN, J. A. 2002. Magnesium chemistry and biochemistry. *Biometals,* 15**,** 203-10.

MAZELOVA, J., ASTUTO-GRIBBLE, L., INOUE, H., TAM, B. M., SCHONTEICH, E., PREKERIS, R., MORITZ, O. L., RANDAZZO, P. A. & DERETIC, D. 2009. Ciliary targeting motif VxPx directs assembly of a trafficking module through Arf4. *EMBO J,* 28**,** 183-92.

NACHURY, M. V., LOKTEV, A. V., ZHANG, Q., WESTLAKE, C. J., PERANEN, J., MERDES, A., SLUSARSKI, D. C., SCHELLER, R. H., BAZAN, J. F., SHEFFIELD, V. C. & JACKSON, P. K. 2007. A core complex of BBS proteins cooperates with the GTPase Rab8 to promote ciliary membrane biogenesis. *Cell,* 129**,** 1201-13.

NAITOH, Y. 1968. Ionic control of the reversal response of cilia in Paramecium caudatum. A calcium hypothesis. *J Gen Physiol,* 51**,** 85-103.

PICARIELLO, T., VALENTINE, M. S., YANO, J. & VAN HOUTEN, J. 2014. Reduction of meckelin leads to general loss of cilia, ciliary microtubule misalignment and distorted cell surface organization. *Cilia,* 3**,** 2.

PRESTON, R. R. 1990. A magnesium current in Paramecium. *Science,* 250**,** 285-8.

PRESTON, R. R. 1998. Transmembrane Mg2+ currents and intracellular free Mg2+ concentration in Paramecium tetraurelia. *J Membr Biol,* 164**,** 11-24.

PRESTON, R. R. & KUNG, C. 1994a. Inhibition of Mg2+ current by single-gene mutation in Paramecium. *J Membr Biol,* 139**,** 203-13.

PRESTON, R. R. & KUNG, C. 1994h. Isolation and characterization of paramecium mutants defective in their response to magnesium. *Genetics,* 137**,** 759-69.

PRESTON, R. R. & USHERWOOD, P. N. R. 1988. Characterization of a Specific L-[H-3]Glutamic Acid Binding-Site on Cilia Isolated from Paramecium-Tetraurelia. *Journal of Comparative Physiology B-Biochemical Systemic and Environmental Physiology,* 158**,** 345-351.

PRESTON, R. R. & VAN HOUTEN, J. L. 1987. Chemoreception in Paramecium tetraurelia: acetate and folate-induced membrane hyperpolarization. *J Comp Physiol A,* 160**,** 525-35.

RECHSTEINER, M. & ROGERS, S. W. 1996. PEST sequences and regulation by proteolysis. *Trends Biochem Sci,* 21**,** 267-71.

SASNER, J. M. & VANHOUTEN, J. L. 1989. Evidence for a Paramecium Folate Chemoreceptor. *Chemical Senses,* 14**,** 587-595.

SATOW, Y. & KUNG, C. 1976. A 'TEA+-insensitive' mutant with increased potassium conductance in Paramecium aurelia. *J Exp Biol,* 65**,** 51-63.

SATOW, Y. & KUNG, C. 1980. Ca-induced K+-outward current in Paramecium tetraurelia. *J Exp Biol,* 88**,** 293-303.

VALENTINE, M. S., RAJENDRAN, A., YANO, J., WEERARATNE, S. D., BEISSON, J., COHEN, J., KOLL, F. & VAN HOUTEN, J. 2012. Paramecium BBS genes are key to presence of channels in Cilia. *Cilia,* 1**,** 16.

VAN HOUTEN, J. 1979. Membrane potential changes during chemokinesis in Paramecium. *Science,* 204**,** 1100-3.

WEERARATNE, S. D. 2007. GPI receptors in folate chemosensortransduction in Paramecium tetraurelia. *PhD Thesis*.

YANO, J., RAJENDRAN, A., VALENTINE, M. S., SAHA, M., BALLIF, B. A. & VAN HOUTEN, J. L. 2013. Proteomic analysis of the cilia membrane of Paramecium tetraurelia. *J Proteomics,* 78**,** 113-22.

Table II.I: Table of primers.

Name	Forward Primer (5′ – 3′)
pPXV 5′	TAAGATGAATCCAATATAATG
pPXV 3′	TTATTTAAGTGTTGTTCATTTA
XNTA F	CTTGAAATGCCTAAAGAATC
XNTA R	GTAAATCCTTTAGCTAATGC
XntA 3′UTR	AGATATTGTTCTTAAATCAAC
XntA N-term F (Spe I)	GCGACTAGTATGACCTACAGAGAATTAGTCCC
XntA N-term R (Nhe I)	CGCGCTAGCAGATTCTTTAGGCATTTCAAGTTTTG
XntA C-term F (Spe I)	GCGACTAGTATGGAATGGCTGACCCTCAATAATG
C-term +2N XntA F (Spe I)	GCGACTAGTATGCCTAATTCGCATCATGGAGTC
XntA C-term R (Nhe I)	CGCGCTAGCCTTTAAAATATTCAATCC
XntA Ubiq mut F	CAAAGTGCAATAA**G**(A)ATAAAGAAATG
XntA Mut R	TTATTCATCATTTAGTTATTATCTTTACTTCTATTTTGG

Table II.II: Table of primers used to create fragments of *XNTA* for microinjection.

Construct	Forward Primer	Reverse Primer	Sequence Position
N-term XntA	XntA N-term F (Spe I)	XntA N-term R (Nhe I)	+1 - +1125
C-term XntA	XntA C-term F (Spe I)	XntA C-term R (Nhe I)	+586 - +1704
C-term+2N XntA	C-term +2N XntA F (Spe I)	XntA C-term R (Nhe I)	+390 - +1704
K300R	XntA N-term F (Spe I)	XntA C-term R (Nhe I)	+1 - +1704

Table II.III: Proteins identified in the XntA-myc IP from WCE that were unique to the test lane.

Gel slice	Accession number (GSPATG…)	Protein Description	# of Peptides	Molecular Mass
1	00012163001	Hypothetical protein, Pyruvate phosphate dikinase	2	82 kD
1	00028373001	Hypothetical protein, Amylo-alpha-1,6-glucosidase family protein	2	123 kD
5	00039636001	Hypothetical protein	3	162 kD
7	00013616001	Glyceraldehyde 3-phosphate dehydrogenase	2	
7	00005516001	Ribosomal protein L5	2	40 kD
7	00031832001	Ribosomal protein L10	2	35 kD

Table II.IV: Proteins identified in the Pkd2-FLAG IP from WCE that were unique to the test lane.

Gel Slice	Accession Number (GSPATG…)	Protein Description	# of Peptides	Molecular Mass
1,2,3,4,5,6	00005599001	Pkd2	5,3,8,9,6,6	99 kD
1	00006907001	Hypothetical Protein	3	412 kD
2	00038320001	Hypothetical Protein, HSP70-domain containing protein	6	93 kD
2	00037951001	Hypothetical Protein,	2	102 kD
2	00017485001	Hypothetical Protein, HSP70-domain containing protein	2	93 kD
3	00020752001	Hypothetical Protein, transitional ER ATPase	2	91 kD
3	00027959001	Hypothetical Protein, ER-type HSP70	2	72 kD
3	PTETP3300001001	Hypothetical Protein, Cytosol-type HSP70	2	72 kD
4	00031542001	Hypothetical Protein, Proteosome/cyclosome 26s subunit protein, chaperone	3	98 kD
4,5	00024718001	Hypothetical Protein, HSP70	2,3	35 kD
4	00029670001	Hypothetical Protein, Vacuolar protein sorting-associated protein 35 containing protein	2	89 kD
4	00020796001	Piwi-related protein PAP	2	87.5 kD
4	00029765001	Hypothetical Protein, W-40 repeat containing protein, possible cytoplasmic dynein	2	82 kD
5	00021392001	COPII vesicle coat, ER-Golgi transport, potential Sec23/24	3	87.5 kD
6	00015732001	Hypothetical Protein, GroEL conserved domain, chaperonin-like	3	61 kD
6	00035998001	Hypothetical Protein, succinate dehydrogenase	2	70 kD
6	00029912001	Arginine tRNA ligase	2	69 kD
7	00023050001	Hypothetical Protein, isocitrate dehydrogenase	3	38 kD
7	00012130001	Hypothetical Protein, Zn-dependent alcohol dehydrogenase	2	41 kD
8	00012567001	Hypothetical Protein, possible myosin heavy chain kinase	2	36 kD
8	00012836001	Hypothetical Protein	2	43 kD

8	00030068001	Hypothetical Protein, Probable 26s proteasome non-ATPase regulatory subunit 6	2	37 kD
9	00006971001	Hypothetical Protein	2	43 kD
10	00027576001	Hypothetical Protein, 40s Ribosomal protein, S4e	3	33 kD
10, 11	00035275001	Hypothetical Protein, Ribosomal S3Ae family protein	2,2	31 kD
11	00029689001	Hypothetical Protein	3	27 kD
11	00001379001	Hypothetical Protein	2	31.5 kD
11	00032074001	Hypothetical Protein, fibrillarin non-specific Ser/Thr kinase	2	30 kD
11	00009904001	14-3-3	2	28 kD

Table II.V: Changes in membrane potential (ΔV_m) of <u>ciliated</u> cells when changed from 5 mM KCl to testing solution. Positive values indicate a depolarization of the membrane and negative values indicate a hyperpolarization of the membrane compared to the resting membrane potential in the resting solution (5 mM KCl).

Cell Type	5 mM K-acetate	5 mM K-L-Glutamate	5 mM K-D-Glutamate	2.5 mM K_2-Folate
Wild Type	-5.3 ± 2.1 (13)	-4.8 ± 1.6 (10)	-2.4 ± 2 (12)	-5.8 ± 2.9 (17)
XntA1 mutant	-0.9 ± 3.5 (5)	-1.8 ± 3.1 (4)	-0.4 ± 1.8 (4)	-1.9 ± 1.3 (6)
***P*-Value (T-test)**	0.07	0.19	0.11	0.0006

Table II.VI: Changes in membrane potential (ΔV_m) of <u>deciliated</u> cells when changed from 5 mM KCl to testing solution. Positive values indicate a depolarization of the membrane and negative values indicate a hyperpolarization of the membrane compared to the resting membrane potential in the resting solution (5 mM KCl). * **I**ndicates significantly less hyperpolarization compared to ciliated wild type cell (P<0.01, T-test).

Cell Type	5 mM K-acetate	5 mM K-L-Glutamate	5 mM K-D-Glutamate	2.5 mM K_2-Folate
Wild Type	-3.9 ± 2.7 (4)	-0.32 ± 2.6 (8)*	-0.65 ± 2 (7)	-2.4 ± 0.7 (2)
XntA1 mutant	3.4 ± 2.6 (5)	-1.6 ± 2.0 (4)	1.3 ± 1.3 (3)	-2.0 ± 2.9 (3)
***P*-Value (T-test)**	0.01	0.43	0.18	0.86

Figure II.1: Chart of XntA1 mutants expressing epitope-tagged versions of *XNTA* with backward swimming times in 25 mM TEA with 5 mM $MgCl_2$. Cells were examined for Mg^{2+}-induced behavior in Mg/TEA solution. First row shows wild type cells expressing the FLAG epitope as a positive control for Mg^{2+}-induced behavior. Lower rows are the different versions of *XNTA* being expressed by the XntA1 mutant cells. Included are depictions of the different *XNTA* constructs. Grey blocks represent transmembrane domains, green star represents potential ubiquitination site (pink star is the K300R mutated ubiquitination site). Purple oval represents PEST sequence and also the position of the FLAG (blue rectangle) and myc (dark purple oval) epitope tag placement. Backward swimming times are average seconds ± standard deviation. Asterisks indicated statistical significance compared to all other expressing cell types ($P<0.001$, multiple T-tests), with one exception, there is no significant difference between XntA1 mutants expressing N-term and the XntA1 mutants expressing FLAG.

Cell types and gene being expressed	Backward swimming (sec) ± SD
Wild type cells + FLAG	9.85 ± 5.01 (N=43)*
XntA1 + FLAG or myc	0.0 ± 0.0 (N=181)
FLAG-*XNTA*	7.2 ± 6.9 (N=120)*
XNTA-FLAG	2.8 ± 2.7 (N=339)
Myc-*XNTA*-FLAG	2.1 ± 2.7 (N=192)
K300R	2.9 ± 2.6 (N=283)
N-term	0.2 ± 0.7 (N=433)*
C-term	0.8 ± 1.8 (N=419)
C-term + 2N	0.5 ± 1.1 (N=393)

Figure II.2: Graph of backward swimming in 25 mM TEA with 5 mM $MgCl_2$ of XntA1 mutants expressing tagged versions of the *XNTA* gene. Backward swimming times (seconds) ± standard error of the mean (N=43 to 433 cells). Cell type is shown below the graph and injected plasmid shown below each bar. Red asterisks indicate the four cell types that are statistically different from all others. Significance between the other expressing cell types are described in the results section. No statistical difference between C-term and C+2N. No difference between *XNTA*-FLAG and K300R. See Figure II.1 for constructs and backward swimming times (sec) ± standard deviation and N.

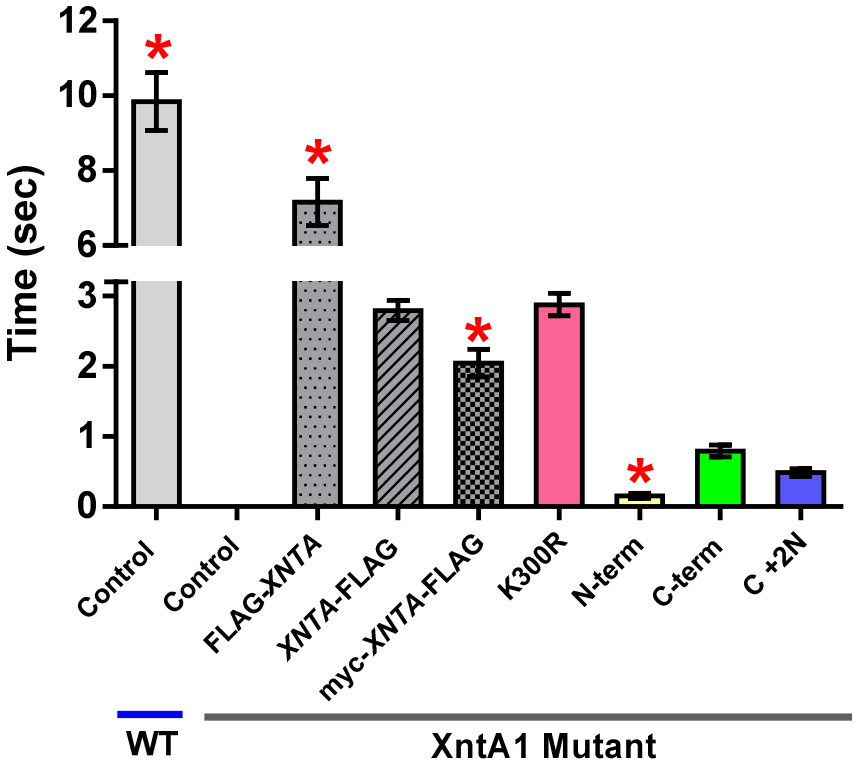

Figure II.3: Immunostaining of XntA1 mutants expressing epitope-tagged *XNTA*, truncated *XNTA* or mutated *XNTA*. Immunostaining of XntA1 mutants expressing FLAG (Control), FLAG-*XNTA*, *XNTA*-FLAG, C+2N-FLAG, or K300R-FLAG. Cells were immunostained with Anti-centrin to mark the basal bodies below the cell surface (green) and Anti-FLAG to show the expressed protein (red). Merged images are also shown, scale bar = 10 μm. Cells shown are representative of the population.

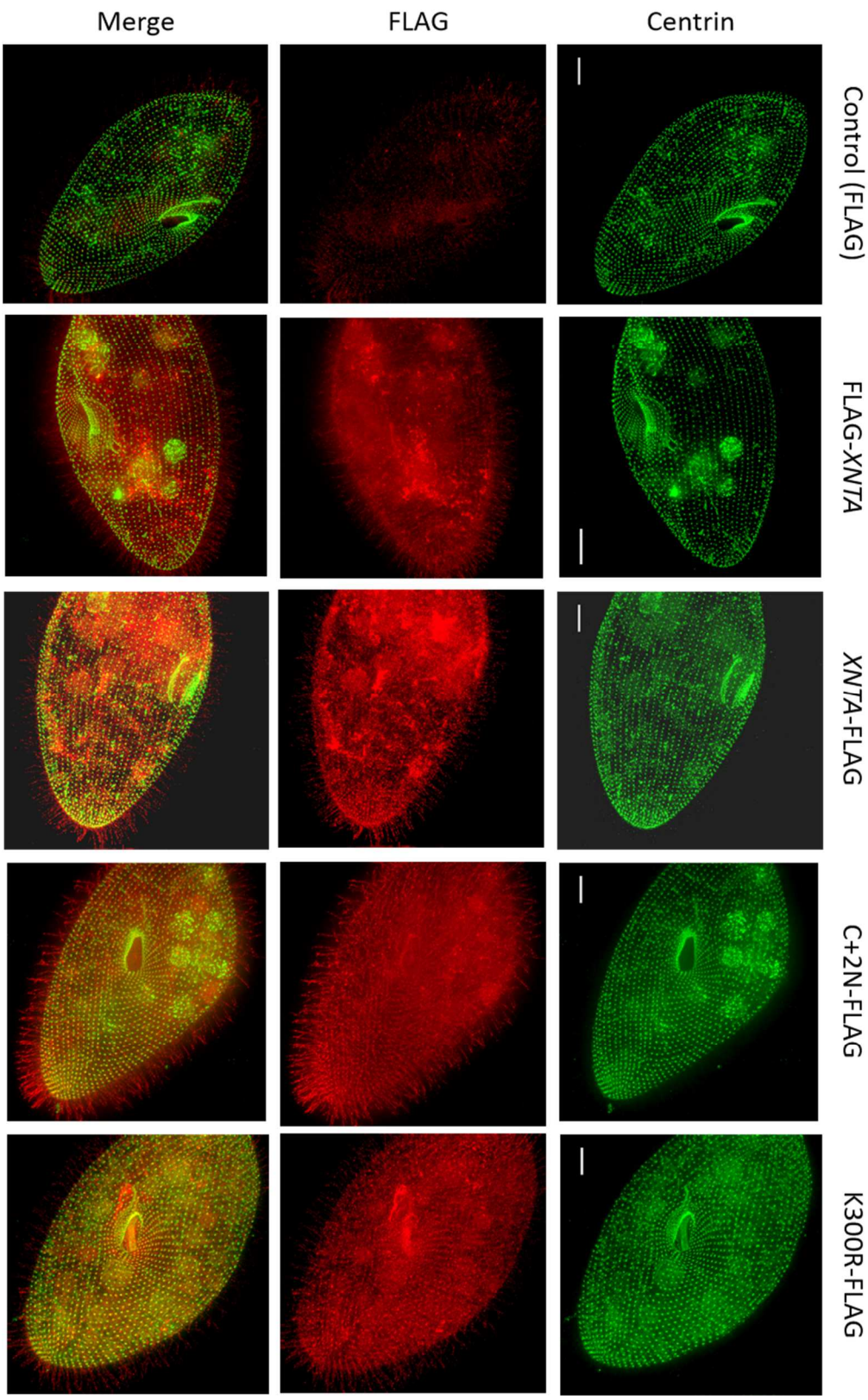
Merge
FLAG
Centrin
Control (FLAG)
FLAG-XNTA
XNTA-FLAG
C+2N-FLAG
K300R-FLAG

Figure II.4: Western blot and silver stained gel for whole cell extract XntA-myc IP. Wild type cells expressing myc and FLAG (Control; C) or XntA-myc and Pkd2-FLAG (Test; T) were homogenized, solubilized with Triton X-100 for IP using Anti-myc affinity agarose. **(A)** Western blot of one-tenth of anti-myc agarose eluate separated by SDS-PAGE and transblotted. Blot was first developed with Anti-myc to demonstrate the presence of the XntA-myc protein (purple arrow heads.) **(B)** The same blot was stripped and re-probed using Anti-FLAG to detect Pkd2-FLAG protein (blue arrow heads). Orange arrows indicate the heavy (upper) and light (lower) chain of the antibody. Primary and secondary antibodies used were both produced in rabbit. **(C)** The silver stained gel of the remaining eluate from the Anti-myc affinity agarose showing the approximate gel slices that were removed for tryptic digest and LC-MS/MS analysis (brackets with numbers). The molecular masses are shown on the left, these same masses do not correspond to the molecular masses on the immunoblots. Blue and purple arrow heads mark approximate regions of the gel where we would expect Pkd2-FLAG or XntA-myc to be found, respectively. **(D)** Blot developed with Anti-tubulin to demonstrate that the test and control samples were approximately the same concentration when solubilization began.

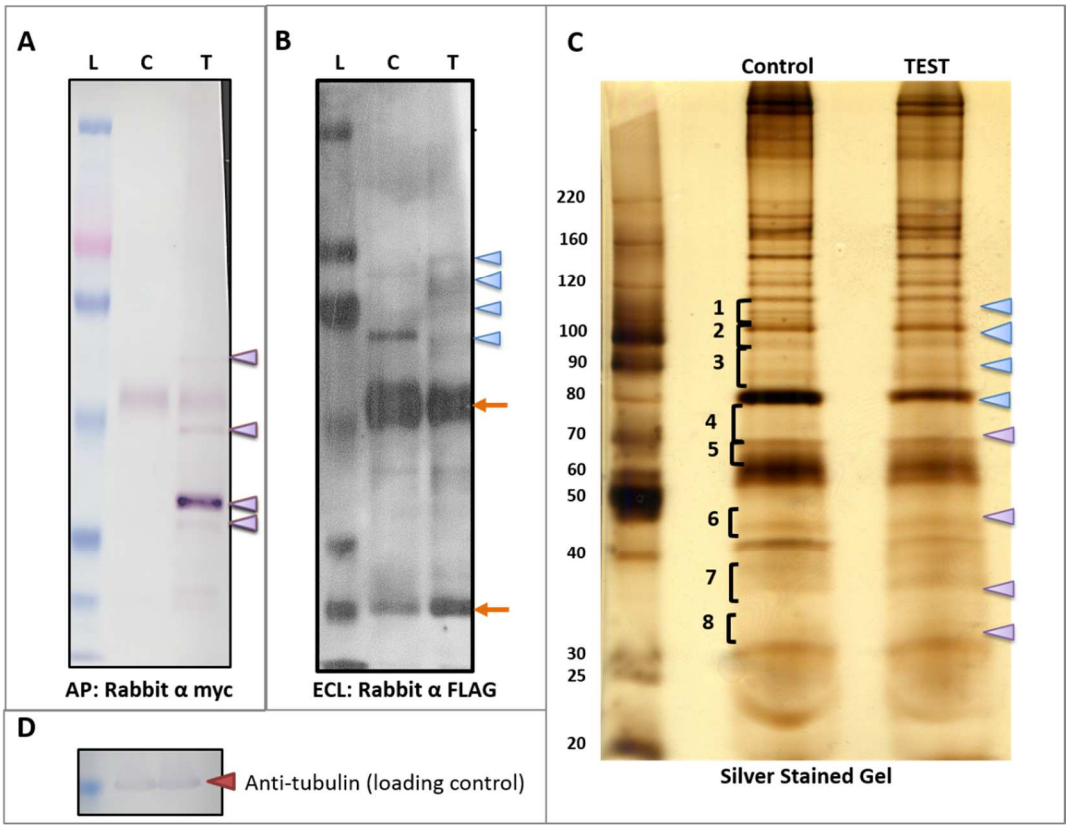
A
L C T
AP: Rabbit α myc
B
L C T
ECL: Rabbit α FLAG
C
Control
TEST
220
160
120
100
90
80
70
60
50
40
30
25
20
1
2
3
4
5
6
7
8
Silver Stained Gel
D
Anti-tubulin (loading control)

Figure II.5: Western blot and silver stained gel for whole cell extract Pkd2-FLAG IP. Wild type cells expressing myc and FLAG (Control; C) or XntA-myc and Pkd2-FLAG (Test; T) were homogenized, solubilized with Triton X-100 for IP using Anti-FLAG affinity agarose. **(A)** Western blot of one-tenth of anti-FLAG agarose eluate separated by SDS-PAGE and transblotted. Blot was first developed with Anti-FLAG to visualize the presence of the Pkd2-FLAG protein (blue arrow heads.) **(B)** The same blot was stripped and re-probed using Anti-myc to detect the XntA-myc protein (purple arrow heads). **(C)** The silver stained gel of the remaining eluate from the Anti-FLAG affinity agarose showing the approximate gel slices that were removed for tryptic digest and LC-MS/MS analysis (Brackets with numbers). The molecular masses are shown on the left, these same masses do not correspond to the molecular mass markers on the immunoblots. Blue and purple arrow heads mark approximate regions of the gel where we would expect Pkd2-FLAG or XntA-myc, respectively. **(D)** Blot developed with Anti-tubulin to demonstrate that the test and control samples were approximately the same concentration when solubilization began.

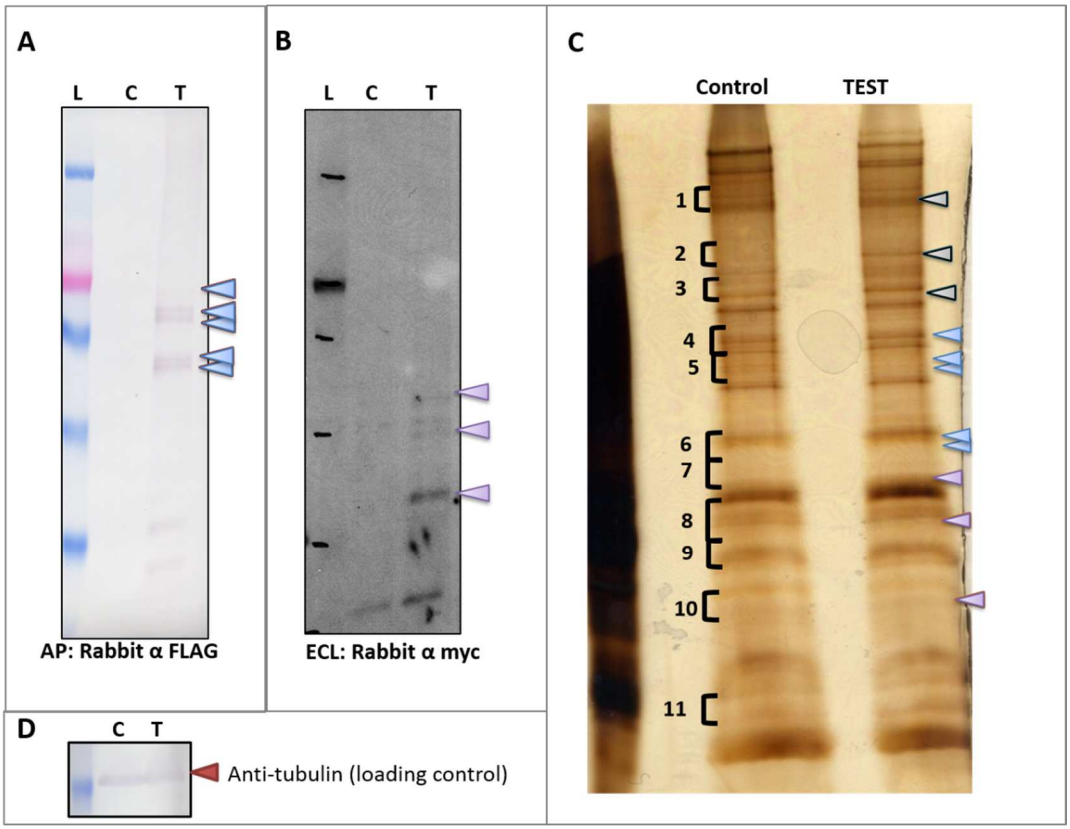
A
L C T
AP: Rabbit α FLAG
B
L C T
ECL: Rabbit α myc
C
Control
TEST
1
2
3
4
5
6
7
8
9
10
11
D
C T
Anti-tubulin (loading control)

Figure II.6: Control Western blot using myc affinity agarose on cells expressing *PKD2*-FLAG. Whole cilia were collected from cells expressing *PKD2*-FLAG and FLAG and solubilized. Two separate IPs were performed using FLAG affinity agarose (left) and myc affinity agarose (right). Molecular masses are shown on the left hand side, kD. Multiple Pkd2-FLAG bands are observed in the positive control lane (FLAG IP of *PKD2*-FLAG expressing cells), white arrow heads (~120, 100, and 70 kD). No bands other than non-specific bands and the heavy and light chain of the antibody are observed in the lanes using the myc affinity agarose.

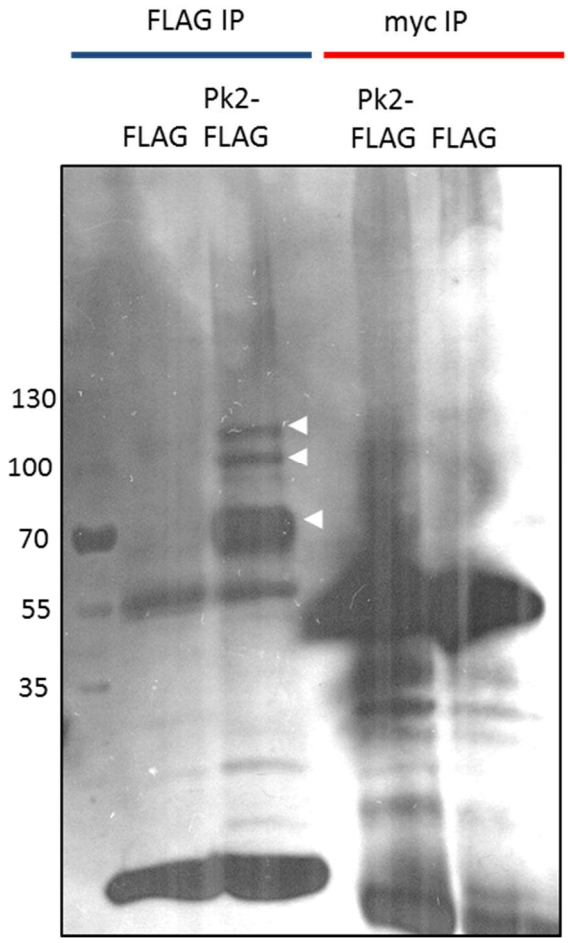

Appendix III: LC-MS/MS Data from Cell Membrane and Cilia Pkd2-FLAG Immunoprecipitations with Accompanying RNAi for Potential Interacting Partners

Overview and Materials and Methods

All information pertinent to the preparation of the Pkd2-FLAG plasmid, microinjection, isolation of cell membranes and cilia were done as previously described in Chapter 3 and (Valentine et al., 2012). Immunoprecipitation and LC-MS/MS analysis were performed as previously described in Chapter 3. The sequences chosen for RNAi construct creation were done so based on predicted function, prevalence, and number of times found in the analysis. Primers used to create the RNAi constructs are shown in Table III.I along with a brief description below. All relevant instructions for creating each of the RNAi constructs is included along with the restriction enzymes used. Amplification of each sequence was done using standard PCR protocols as preciously described using genomic DNA. All PCR products were ligated into the pCR®-2.1 TOPO® vector (Invitrogen/Life technologies), removed using restriction enzymes (New England BioLabs) and ligated into the double-T7 promoter RNAi plasmid L4440 (Addgene) as previously described (Chapter 2 and 3).

Feeding paramecia by RNAi was done as previously described (Chapter 2 and 3). The *PKD2* RNAi construct was also described previously in Chapter 3. Backward swimming assays were done as previously described (Chapter 3, (Valentine et al., 2012)) using 30 mM KCl to test the voltage-gated calcium channel function and potassium channel function. Also tetraethylammonium (TEA) with 10 mM NaCl or 5 mM $MgCl_2$ was used to examine the depleted cells for Mg^{2+}-specific behavior and potassium channel function. A description of all of these solutions, what channels are being examined in each solution, as well as how the cells are tested can be seen in Appendix I and in (Valentine et al., 2012).

Small Hypothetical Protein (SHyP) (PTETG10700002001): This sequence was chosen because it was identified in both of the buffers used for the cilia IPs (Lap200 and IP500 buffers). This gene has one paralog from the recent whole genome duplication (GSPATG00035837001) which is

87.2% identical at the nucleic acid level. The RNAi construct that was designed targets both paralogs. PCR Annealing temperature used was 52°C and extension time was 2 minutes 30 seconds. Restriction enzymes used to remove the sequence from pCR® 2.1-TOPO® vector and ligate into the L4440 plasmid were Sac I and Xho I.

Large Hypothetical Protein (LHyP) (GSPATG00012627001): This sequence was chosen because if was found in both of the Pkd2-FLAG cilia IPs in the different buffers. Four unique peptides were identified in the Lap200 IP and six peptides in the IP500 buffer IP. This proteins was one of the most abundant proteins identified in the Triton X-114 phase separation of the ciliary membrane proteins in *P. tetraurelia* (Yano et al., 2013). This protein is listed as a hypothetical protein of unknown function with 6 or 8 predicted transmembrane spanning domains. There are no off-target sequences for the RNAi construct for this gene and the sequence has no paralogs. It is a very large sequence, 11,458 nucleotides (nt) in length with a predicted protein length of 3,780 amino acids (438 kD). The PCR annealing temperature used was 52°C and extension time was 2 minutes 30 seconds (PCR was done at the same time as the SHyP). Restriction enzymes used to remove the sequence from pCR® 2.1-TOPO® vector and ligate into the L4440 plasmid were Sac I and Xho I.

Hypothetical adhesion protein (AHyP) (GSPATP00034716001): This protein was identified in the whole cilia Lap200 IP with two unique peptides. The protein is considered hypothetical with a distant relation to cell adhesion proteins in bacteria. The sequence was chosen for RNAi because we did not anticipate any involvement in Mg^{2+}-induced behavior based on the sequence and the predicted function of the protein. The gene is 3,465 nucleotides long coding for a protein of 1,146 amino acids in length with a predicted molecular mass of 128.3 kD. There is one recent whole genome duplication paralog for this gene (GSPATG00037540001). The paraogs are 88.1% identical and the protein sequences are 89% identical. The sequence used to create the RNAi

vector targets both paralogs. The PCR annealing temperature used was 52°C and extension time was 2 minutes. Restriction enzymes used to remove the sequence from pCR® 2.1-TOPO® vector and ligate into the L4440 plasmid were Sac I and Xho I.

WD40 hypothetical protein (WD40) (GSPATG00029765001): This sequence was chosen because the amino acid sequence for this protein has some similarities to cytoplasmic dynein with conserved WD40 repeats found between amino acids 212-620 (e-value: 1.7 e^{-9}). Six peptides were identified from this protein unique to the test lane from the whole cilia Lap200 IP. There are two intermediate whole genome duplication paralogs related to this sequence, GSPATG00007648001 (75% identical at the nucleic acid level and 86.6% identical at the amino acid level) and GSPATG00021536001 (74% identical at the nucleic acid level and 86.5% identical at the amino acid level). The gene sequence is 2,353 nucleotides long and codes for a predicted protein of 714 amino acids in length. The predicted molecular mass is 81.6 kD. The section of gene sequence used for RNAi has no off-target sequences and will not target the two paralogs. PCR Annealing temperature used was 50°C and extension time was 1 minute. Restriction enzymes used to remove the sequence from pCR® 2.1-TOPO® vector and ligate into the L4440 plasmid were Sac I and Xho I.

Hypothetical *Tetrahymena* cation channel protein (TtCC) (GSPATG00005132001): Two peptides from this protein were obtained in the IP500 whole cilia IP for Pkd2-FLAG. The closest homologous sequences found was for a putative *Tetrahymena* cation channel family protein sequence (e-values: $3e^{-18}$ and $2e^{-15}$). The protein has no predicted transmembrane domains and no conserved domains. The gene sequence is 1,681 nucleotides in length coding for a 61.1 kD protein of 536 amino acids. There is one recent whole genome duplication paralog for this sequence (GSPATG000027079001) which is 87.5% identical at the nucleic acid level and 92.6% identical at the amino acid level. The RNAi construct targets both paralogs. The PCR annealing temperature

used was 52°C and extension time was 2 minutes. Restriction enzymes used to remove the sequence from pCR® 2.1-TOPO® vector and ligate into the L4440 plasmid were Sac I and Xba I.

Predicted Lost Boys/CG34110/Ccdc135 protein (LOBO) (GSPATG00001683001): This protein was identified in the whole cilia IP500 Pkd2-FLAG IP. Four unique peptides were identified from this protein. The amino acid sequence for his protein (830 amino acids) was used in a BLAST search. The lobo homologues of *Crassostrea gigas* (Pacific Oyster) ($2e^{-100}$) and *Homo sapiens* ($2e^{-93}$) were identified. The *Drosophila* lobo homologue was a little more distant with an e-value of $2e^{-39}$. There are two intermediate whole genome duplication paralogs for this sequence (GSPATG00009014001 and GSPATG00025242001). These genes are both 82.6% identical to the *Paramecium* lobo sequence and neither is targeted using the sequence used to create the RNAi construct. The PCR annealing temperature used was 43°C and extension time was 1 minute. Restriction enzymes used to remove the sequence from pCR® 2.1-TOPO® vector and ligate into the L4440 plasmid were Sac I and Xba I.

Results

To further investigate other potential interacting partners of the Pkd2 protein other than XntA, we used feeding RNAi to deplete paramecia of proteins that were co-IP'd with Pkd2. We focused our efforts on proteins that were identified in the cilia IPs because we were interested in finding out more about the functions of Pkd2 in the cilia. We chose proteins to target with RNAi based on their abundance in the IP, if they were identified in IPs from both the buffers that were used (Lap200 and IP500, see Chapter 3), and also proteins that had interesting conserved domains or homologous proteins in other organisms. One gene, AHyP (GSPATP00034716001),

had predicted cell adhesion properties and we did not anticipate observing changes in swimming behavior in Mg^{2+} solutions or other solutions when this protein was depleted from the cells.

Figures III.1A-1C show the peptides that were identified in the different IPs and the peptide locations within the Pkd2 sequence. For the most part, identified tryptic peptides were distributed throughout the Pkd2 sequence, however, no peptides were identified in the first 73 amino acids of the Pkd2 protein in any of the IPs. Because the Pkd2-FLAG protein was being over-expressed in the cells, it was not surprising to find peptides throughout the gels. The fewest Pkd2 peptides were identified in the whole cilia IP500 IP, however, the most co-IP proteins were also idenitified in the same prep.

Once the constructs for RNAi were created, we began to examine the RNAi depleted cells for behavior changes in 30 mM KCl, 25 mM tetraethylammonium (TEA) with 10 mM NaCl, and 25 mM TEA with 5 mM $MgCl_2$. As discussed in other chapters, we are able to use changes in the ionic environment to examine paramecia cells. Changes in their swimming behavior can then be used to infer alterations in ion channels in the cilia or in the membrane (Eckert and Brehm, 1979, Kung and Saimi, 1982, Preston and Kung, 1994b, Preston and Kung, 1994a, Ling and Kung, 1980). *Paramecium* depolarizes in high ionic conditions, such as 30 mM KCl, which will cause the voltage gated calcium channels found exclusively in the cilia (Dunlap, 1977) to open. The transient increase in calcium will cause a reversal of the ciliary power stroke and the cell will be propelled backward. As long as Ca^{2+} remains high in the cilia, the cell will swim backward. The presence of TEA in the bath will block the corrective action of the fast-acting voltage-dependent K^+ conductance (Satow and Kung, 1976) forcing the cell to rely on the slower Ca^{2+}-dependent K^+ conductance to correct the membrane potential. The TEA in combination with the high Mg^{2+} or Na^+ allows for backward swimming of the cell that is easily timed using a stop watch. The presence of 5 mM $MgCl_2$ or 10 mM NaCl in the bath will prolong the backward swimming

further by activating the Ca^{2+}-dependent Mg^{2+}-conductance or Na^{+}-conductance, respectively. All statistical comparisons were done using a one-way ANOVA followed by non-parametric multiple comparison tests.

When we examined our different depleted cells in 30 mM KCl to examine the function of the voltage gated calcium channels, the *WD40*, *TtCC* and *LOBO* depleted cells showed short backward swimming compared to the control cells (asterisk, $P<0.001$). Interestingly, the double-fed cells depleted in both *PKD2* and *SHyP* showed short backward swimming in this solution (asterisk, $P<0.001$) while the individually depleted *PKD2* or *SHyP* cells showed no change in their swimming behavior in high K^{+}. All of these depleted cells, *WD40*, *TtCC*, *LOBO*, and *PKD2* and *SHyP*, swam backward for significantly less time in high K^{+} than the *PKD2* depleted cells (caret, $P<0.001$).

Very few changes in backward swimming were observed in 25 mM TEA with 10 mM NaCl. Only cells depleted in *LHyP* and the cells double-fed to deplete both *PKD2* and *SHyP* showed shorter backward swimming in this solution. None of the depleted cells were statistically different than the *PKD2* depleted cells. However, in 25 mM TEA with 5 mM $MgCl_2$, we saw far more changes in the backward swimming behavior of the depleted cell types. In fact, all the depleted cell types showed shorter backward swimming in Mg/TEA compared to the control cells (asterisk, $P<0.001$) except for the AHyP depleted cells. The control cells, *AHyP*, and *WD40* depleted cells were significantly different than the *PKD2* depleted cells (caret, $P<0.001$). All backward swimming times, number of cells tested (N), and standard deviations can be seen in Table III.II.

Discussion

In this Appendix, we attempted to further investigate potential interacting partners of the Pkd2 protein identified in the LC-MS/MS analysis of cilia Pkd2-FLAG IPs presented in Chapter 3. We identified one protein that when depleted showed changes in Mg^{2+}-induced behavior specifically, which was *SHyP*. We were able to demonstrate that some of the proteins that were depleted may contribute to the function of other ion channels, the trafficking or stabilization of proteins in the cilia, or proteins that may contribute to beating patterns of the cilia. It is important to remember that this was a preliminary study and that all depleted proteins would require extensive further testing to determine their true function in our ciliated model organism, *Paramecium tetraurelia*.

Our IP from the cell membrane and the two IPs from the cilia using different immunoprecipitation buffers did not have many proteins in common. We chose to focus on the proteins identified in the whole cilia IPs as opposed to the cell membrane because we felt those proteins would have more influence on backward swimming of *Paramecium* due to their location in cilia. We chose the proteins based on their abundance in the IPs as well as their conserved domains or potential proposed function. One of the proteins we chose to study was AHyP. When we depleted this proposed adhesion protein we did not expect any changes in behavior, that this depleted cell line would behave the same as the control cells, which was the case. However, it would be possible that this protein may be involved in conjugation. During conjugation, two cells of opposite mating types join to exchange genetic material. When the two cells come in contact with one another, the cilia are resorbed along both sides of the anterior suture and on the right side of the posterior suture. The cells are then able to come in close contact and conjoin to exchange genetic material (Watanabe, 1978). It is possible that the AHyP protein is involved in the adhesion, or conjoining of the two mating-reactive cells. It is feasible

that Pkd2 is important for this process. Pkd2 has been shown to be increased four-fold in gametogenesis of *Chlamydomonas reinhardtii* and is vital for the calcium-dependent coupling of flagellar adhesion during mating for these cells (Huang et al., 2007).

We included the depletion of *PKD2* as a positive control. We knew what to expect of the cells depleted in Pkd2 protein which was short backward swimming in Mg^{2+} solutions. Sure enough, Mg/TEA was the only solution where a change was observed in swimming behavior of *PKD2* depleted cells, not Na/TEA or high K^+. Interestingly, the depletion of *SHyP* only showed a change in backward swimming in Mg/TEA. However, when both *PKD2* and *SHyP* were depleted, we observed changes in all the swimming solutions, Na/TEA and high K^+ as well as Mg/TEA. The SHyP has no predicted transmembrane spanning domains but is significantly upregulated during reciliation (based on Microarray data, see ParameciumDB: http://paramecium.cgm.cnrs-gif.fr/cgi/). It is possible that when both *SHyP* and *PKD2* were depleted from the cells, that other channel pathways were affected. Another possibility is that these two channels together affect the backward swimming mechanisms of the cell. When both *SHyP* and *PKD2* were depleted, the shortening of the backward swimming times were not additive in Mg/TEA. It is unclear why the double-depletion of *PKD2* and *SHyP* would shorten the backward swimming times in all solutions. Possibly these two proteins are needed for the reversal of the ciliary beat or perhaps they act in microdomains with other channels that are important for backward swimming. If *SHyP* is important during reciliation of cells, it is feasible that *SHyP* has an important function in the construction, trafficking, regulation, or maintenance of proteins in the cilia. IPs using cells expressing an epitope-tagged version of SHyP may lead to the identification of other proteins that potentially interact with SHyP. The identification of more protein could bring clarity to the function or role of SHyP.

The depletion of *LHyP* showed short backward swimming in both solutions containing TEA compared to the control cells. Although this suggests a deficiency in the Ca^{2+}-dependent K^+ conductance which would be used to correct the depolarization of the cell membrane, we are not suggesting that LHyP is a Ca^{2+}-dependent K^+ channel. These K^+ channels typically consist of four subunits each consisting of 6 transmembrane spanning regions. These subunits would not correspond to the large size of the LHyP protein (438 kD). The LHyP protein has no conserved domains. It was one of the only proteins identified with potential transmembrane spanning domains. LHyP was also one of the most abundant proteins, based on the number of unique peptides identified, in the Triton X-114 phase separation and proteomic analysis of the ciliary membrane (Yano et al., 2013). It is possible that because of the abundance of this protein, it was immunoprecipitated based on its abundance in the cilia. LHyP may be found in close proximity to Pkd2, perhaps in the same microdomain. The protein was not identified in any of the control IPs from whole cilia of cells expressing FLAG so we can assume the result is not due to non-specific binding by the FLAG beads. We do not hypothesize that this protein is important for Mg^{2+}-induced behavior, however, based on its abundance in the cilia, the further investigation of LHyP is encouraged.

The depletion of *WD40* was very dramatic in the Mg/TEA and high K^+ solutions. This protein shows some homology to cytoplasmic dynein. Cytoplasmic dynein is known for its importance in retrograde transport as a part of intraflagellar transport system that move proteins and cargo from the tip of cilia and flagella to the base (Pazour et al., 1999, Porter et al., 1999). The predicted size of the WD40 protein is approximately 81 kD, which is an appropriate size for an intermediate chain dynein. Intermediate chains are expected to be important for binding the motor subunits, which are much larger, to the cargo the motor subunits are transporting. There are also the inner dynein arms of the cilia which are attached at specific points on the A tubule of the A and B outer ring of microtubule doublets (Smith and Sale, 1992). This WD40 *Paramecium*

predicted dynein does show homology to the *Chlamydomonas* flagellar inner arm intermediate dynein (1e-55) (accession number XP_00195786.1). Defects in the inner dynein arms of *Chlamydomonas* leads to decreased beat frequency and motility (Brokaw and Kamiya, 1987). It is feasible that depletion in *WD40* may contribute to an inability of the cells to swim backward for prolonged periods of time. However, depletion of *WD40* showed shortened backward swimming duration in solutions to test the voltage gated calcium channels (high K^+) and Mg^{2+}-induced behavior (Mg/TEA) and not Na/TEA. The data support a deficient transportation of channels to the cilia, namely the voltage-gated calcium channels (VGCCs) and the proposed Mg^{2+} channel, Pkd2. On the other hand, if there were deficient VGCCs in the cilia, backward swimming in all ionic solutions, including Na/TEA, would be expected. Further research is clearly required, the swimming assays of these depleted cells were only a preliminary examination. Immunofluorescence, electrophysiology, and numerous other studies would be required to further investigate the function of this protein in *Paramecium*.

The depletion of *TtCC* also led to short backward swimming in Mg/TEA and high K^+. This gene appears to be specific to *Tetrahymena* and *Paramecium*, much like the protein XntA. TtCC is a proposed cation channel protein in *Tetrahymena*, but it has no conserved domains and serves an unknown function in *Paramecium*. There are no predicted transmembrane spanning regions for this protein. It is feasible that TtCC, like WD40, may play some role in transporting proteins to the cilia or perhaps in the regulation of specific channels in the cilia. Again, however, far more research is needed before any conclusions can be made.

One of the most interesting finds was the protein with homology to the *Drosophila* lost boys, Lobo or CG34110. There is also a homologue for Lobo in mammals (Ccdc135) as well as in *Chlamydomonas* (FAP50). The Lobo/Ccdc135/FAP50 protein is highly conserved with tight associations to the microtubule outer doublets. The tight association with the axoneme, the

inability to solubilize the protein with NP-40, and the lack of both calcium and calmodulin binding domains led to the hypothesis that CG34110/Ccdc135/FAP50 is an intermediary protein (Yang et al., 2011). Knockout studies of CG34110 in *Drosophila* led to sperm that were unable to properly chemotax in the female reproductive track. Specifically, they were unable to move to the uterus through the seminal receptacle tubule. Pkd2 knockout sperm had the same phenotype while double knockouts were no worse. The authors suggested CG34110 (Lobo) was important for wave form stabilization in *Drosophila* sperm (Yang et al., 2011). Our work to deplete the *Paramecium* homologue of CG34110 showed short backward swimming in Mg^{2+} solutions and high K^+. If the lobo protein were important ciliary beating, we might have expected short backward swimming in all ionic stimuli. Regardless, the co-IP of these two proteins was exciting. Future studies would be useful to determine the subcellular location of Lobo in *Paramecium*. It would also be interesting to examine *LOBO* depleted cells in T-mazes. Although *Paramecium* does not chemotax, these cells are able to respond to ionic stimuli, including attractants, by hyperpolarizing their membrane and swimming fast and smooth forward (Kung et al., 1975). If a protein that is important for ciliary beat patterns is depleted, it is possible those depleted cells may show inappropriate chemoresponse.

Conclusion

The sequences used for depletion by feeding RNAi in *Paramecium* were chosen because of their possible interactions with the Pkd2 protein. We examined the backward swimming behavior of these depleted cells in Mg/TEA, Na/TEA, and high K^+ compared to control cells fed the empty RNAi vector to briefly investigate the possible functions of these genes in Mg^{2+} behavior. Only the SHyP depleted cells showed short backward swimming specific to Mg/TEA. Most of the depleted cells showed short backward swimming in Mg/TEA and high K^+, except

the AHyP depleted cells which we did not anticipate observing any differences in swimming behavior. The combined depletion of *SHyP* and *PKD2* showed dramatic changes in backward swimming in all solutions used for testing when the single depleted cell types showed only short backward swimming in Mg/TEA. At no point did any of the depleted cell types show longer backward swimming in any of the ionic stimuli. Further investigation into the location and function of Lobo in *Paramecium* would be of interest because of the connection of this protein to the axoneme in other systems. We have investigated further numerous co-IP proteins that may interact with the Pkd2 protein directly or indirectly. The function of these proteins may be important for other ion channels other than Pkd2. These potential interacting partners may also contribute to trafficking or stabilizing ciliary proteins or in proper ciliary beat form. Further investigation is needed in all cases, but as a preliminary screen of potential Pkd2 interacting partners, this screen was productive.

References

BROKAW, C. J. & KAMIYA, R. 1987. Bending patterns of Chlamydomonas flagella: IV. Mutants with defects in inner and outer dynein arms indicate differences in dynein arm function. *Cell Motil Cytoskeleton,* 8**,** 68-75.

DUNLAP, K. 1977. Localization of calcium channels in Paramecium caudatum. *J Physiol,* 271**,** 119-33.

ECKERT, R. & BREHM, P. 1979. Ionic mechanisms of excitation in Paramecium. *Annu Rev Biophys Bioeng,* 8**,** 353-83.

HUANG, K., DIENER, D. R., MITCHELL, A., PAZOUR, G. J., WITMAN, G. B. & ROSENBAUM, J. L. 2007. Function and dynamics of PKD2 in Chlamydomonas reinhardtii flagella. *J Cell Biol,* 179**,** 501-14.

KUNG, C., CHANG, S. Y., SATOW, Y., HOUTEN, J. V. & HANSMA, H. 1975. Genetic dissection of behavior in paramecium. *Science,* 188**,** 898-904.

KUNG, C. & SAIMI, Y. 1982. The physiological basis of taxes in Paramecium. *Annu Rev Physiol,* 44**,** 519-34.

LING, K. Y. & KUNG, C. 1980. Ba2+ influx measures the duration of membrane excitation in Paramecium. *J Exp Biol,* 84**,** 73-87.

PAZOUR, G. J., DICKERT, B. L. & WITMAN, G. B. 1999. The DHC1b (DHC2) isoform of cytoplasmic dynein is required for flagellar assembly. *J Cell Biol,* 144**,** 473-81.

PORTER, M. E., BOWER, R., KNOTT, J. A., BYRD, P. & DENTLER, W. 1999. Cytoplasmic dynein heavy chain 1b is required for flagellar assembly in Chlamydomonas. *Mol Biol Cell,* 10**,** 693-712.

PRESTON, R. R. & KUNG, C. 1994a. Inhibition of Mg2+ current by single-gene mutation in Paramecium. *J Membr Biol,* 139**,** 203-13.

PRESTON, R. R. & KUNG, C. 1994b. Isolation and characterization of paramecium mutants defective in their response to magnesium. *Genetics,* 137**,** 759-69.

SATOW, Y. & KUNG, C. 1976. A 'TEA+-insensitive' mutant with increased potassium conductance in Paramecium aurelia. *J Exp Biol,* 65**,** 51-63.

SMITH, E. F. & SALE, W. S. 1992. Structural and functional reconstitution of inner dynein arms in Chlamydomonas flagellar axonemes. *J Cell Biol,* 117**,** 573-81.

VALENTINE, M. S., RAJENDRAN, A., YANO, J., WEERARATNE, S. D., BEISSON, J., COHEN, J., KOLL, F. & VAN HOUTEN, J. 2012. Paramecium BBS genes are key to presence of channels in Cilia. *Cilia,* 1**,** 16.

WATANABE, T. 1978. A scanning electron-microscopic study of the local degeneration of cilia during sexual reproduction in Paramecium. *J Cell Sci,* 32**,** 55-66.

YANG, Y., COCHRAN, D. A., GARGANO, M. D., KING, I., SAMHAT, N. K., BURGER, B. P., SABOURIN, K. R., HOU, Y., AWATA, J., PARRY, D. A., MARSHALL, W. F., WITMAN, G. B. & LU, X. 2011. Regulation of flagellar motility by the conserved flagellar protein CG34110/Ccdc135/FAP50. *Mol Biol Cell,* 22**,** 976-87.

YANO, J., RAJENDRAN, A., VALENTINE, M. S., SAHA, M., BALLIF, B. A. & VAN HOUTEN, J. L. 2013. Proteomic analysis of the cilia membrane of Paramecium tetraurelia. *J Proteomics,* 78**,** 113-22.

Table III.I: Table of the gene name, primers, sequence position and percent coverage of the gene used to create the RNAi construct.

Name	Forward Primer	Reverse Primer	Position	% of the gene
SHyP	CACTGCACCAGTGTAATTGATG	GACTACCACTGAAGGCTTGTC	+30 - +2033 (2003 nt)	97.1%
LHyP	GGAGGCATTCTTGGCGTGGT	GATTTCAATTTCTCTTCTGTCGC	+10,013 - +11347 (1335 nt)	11.7%
WD40	AGTCACAACGATATGGCAGTAG	CAACTTTAGGAGCTATTCCAAG	+1637 - +2318 (681 nt)	29%
AHyP	CAGAGTCTTTGCCACAAAAGAG	GTGATAACTACCTGACTTGCTC	+1946 - +3442 (1496 nt)	43.2%
TtCC	CTTTTAAGGGAACACTCC	GATAAGGTGGTTTGTTGTACTCA	+27 - +1362 (1335 nt)	79.4%
LOBO	CAATCCATAATTCAAAGAGC	CCTAAGATTCAAATCTTATAG	+1880 - +2525 (645 nt)	25%

Table III.II: Backward swimming times for all depleted cells in the different ionic stimuli.

Cell Type	30 mM KCl	25 mM TEA with 10 mM NaCl	25 mM TEA with 5 mM $MgCl_2$
Control	13.8 ± 3.6 (221)^	19.3 ± 6.6 (148)	7.3 ± 3.1 (224)^
AHyP	14.3 ± 3.6 (65)	20.7 ± 7.1 (60)	6.9 ± 2.9 (70)^
PKD2	14.0 ± 4.9 (102)	17.6 ± 5.9 (98)	4.0 ± 3.1 (110)*
LHyP	13.8 ± 2.9 (81)	15.0 ± 4.7 (89)*	4.6 ± 3.2 (98)*
SHyP	15.0 ± 4.7 (96)	17.9 ± 6.3 (100)	3.3 ± 2.5 (106)*
PKD2* and *SHyP	10.1 ± 3.4 (64)*,^	13.5 ± 6.8 (64)*	3.9 ± 3.3 (64)*
WD40	2.1 ± 3.4 (66)*,^	21.6 ± 21.6 (66)	1.1 ± 2.6 (68)*,^
TtCC	8.6 ± 5.8 (61)*,^	17.2 ± 8.0 (61)	2.9 ± 3.2 (63)*
LOBO	6.4 ± 5.1 (63)*,^	20.9 ± 11.0 (60)	3.1 ± 2.7 (59)*

Figure III.1A-C: Pkd2 peptides identified in IPs from cell membrane and whole cilia. Peptides were identified in silver stained gels from the FLAG IP of solubilized cell membrane or whole cilia of cells expressing Pkd2-FLAG (test) or FLAG (control). Silver stained gels were processed for trypsin digestion and LC-MS/MS analysis. For full Materials and Methods and list of unique proteins identified in the test lanes, see Chapter 3. Peptides, their location within the Pkd2 sequence and the number of times they were found are shown for the cell membrane IP500 buffer IP (**III.1A**); the whole cilia IP500 buffer IP (**III.1B**); and the whole cilia Lap200 buffer IP (**III.1C**). The Pkd2 amino acid sequence is shown on the right and the peptides identified in the IP are shown on the left. Arginines (R) and Lysines (K) where trypsin cut are included in the peptides shown in the table. Peptides are highlighted within the sequence (blue). The number of times each peptide was identified is shown in the table as well as in the sequence (pink number near each highlighted peptide). Peptides were identified throughout the gel.

Figure III.1A: Cell membrane IP500 IP.

Peptide	# Times
K.YYISELQIQK.E	10
R.IAIIFLTYSK.S	10
K.DQGLSIGDLFK.W	10
K.YTIEGIEQGESSSFR.L	9
R.SNYEMIGGIQLR.I	9
R.DMTTEAFLEK.I	8
K.VIEFFTNR.G	8
R.GISNISQITLLLQK.K	8
R.LDQQTTFQNLK.E	5
K.TVRPALNSLQIDSIR.I	5
R.FSCFDVVYDSSK.A	3
K.YVNELQR.F	2
K.AQQQIKPHADQEEK.Q	2
K.AANYQGTFAVHK.N	1

MKNLQGEINKLHSEIDSKKREITKLKNDNTLRLEKINWIQEKVR
KMQREKKVLELNDQTLSIGHATTKHSTTTKEVQQQNEVQKPP
QQEIQLEKMQMLEFFNQYLDQTNKQMVKFQGNRNRKNGEK
DEYINPYPTINL[9]**KYTIEGIEQGESSSF[5]RLDQQTTFQNLK**ELAFY
YWNLAPYLRKFDEKDSEIMDDLELTDESHARIELKE[8]**KVIEFFTN**
[8]RGISNISQITLLLQKK[5]KTVRPALNSLQIDSIRITGGN[1]**KAANYQ**
GTFAVHKNRIKAIDTYNLFFEKFPGL[10]**KYYISELQIQK**EFQEQQ
KELEKGNQEKQEEKKFDLDDMNCLILSSIVVILVLALLSYTAYLSP
KYVNLNFTFINNLIGITSNGEYNKITSIPEFYYYMENFLGATMYN
SDKGDNPF[9]**RSNYEMIGGIQLRILR**SDLYECE[2]**KYVNELQ[3]RFSC**
FDVVYDSSKANKSQFLNYTYQTAEELGIMYFPKGNLTTYTDGG
YVVEFN[8]**RDMTTEAFLEK**INGLRKEQFLDAATAAIFLHFVIYNPS
INLWIQANFLLERNAQNKLTPYRAELTGFIPNVYSGQDGENLFQ
IDITKLIMASILLAFVAYRFYKIKFNTGKLGPAFLYITMEIGFFNCG
VGILTIISVAMSLQQSLQGRDPQELVNSEDFVHLELEADLYKKAE
LFLTISIMFLFLRLSYILKLND[10]**RIAIIFLTYSKSFK**ELLPFLAIEFPLF
LGFVMVFQIIYGNVFPQYSSFTLAIASQLTMIQGQLNITQFVNY
SPIVSMIVILFYYFFMLFFIISLFQAILIECFRIVIMKNGYPQD[10]**KD**
QGLSIGDLFKKWMFSWTQLFTSKKNTTEEKQ[2]**KAQQQIKPHA**
DQEEKQGINSATEN

Figure III.1B: Whole cilia IP500 IP.

Peptide	# Times
K.YYISELQIQK.E	3
R.SNYEMIGGIQLR.I	3
R.IAIIFLTYSK.S	3
K.VIEFFTNR.G	2
K.YVNELQR.F	1
R.LDQQTTFQNLK.E	1
K.YTIEGIEQGESSSFR.L	1
R.GISNISQITLLLQK.K	1

MKNLQGEINKLHSEIDSKKREITKLKNDNTLRLEKINWIQEK
VRKMQREKKVLELNDQTLSIGHATTKHSTTTKEVQQQNEV
QKPPQQEIQLEKMQMLEFFNQYLDQTNKQMVKFQGNR
NRKNGEKDEYINPYPTINL[1]**KYTIEGIEQGESSSF[1]RLDQQTT**
FQNLKELAFYYWNLAPYLRKFDEKDSEIMDDLELTDESHAR
IELKE[2]**KVIEFFTN[1]RGISNISQITLLLQKK**KTVRPALNSLQIDS
IRITGGNKAANYQGTFAVHKNRIKAIDTYNLFFEKFPGL[3]**KY**
YISELQIQKEFQEQQKELEKGNQEKQEEKKFDLDDMNCLIL
SSIVVILVLALLSYTAYLSPKYVNLNFTFINNLIGITSNGEYNKI
TSIPEFYYYMENFLGATMYNSDKGDNPF[3]**RSNYEMIGGIQL**
RILRSDLYECE[1]**KYVNELQR**FSCFDVVYDSSKANKSQFLNYT
YQTAEELGIMYFPKGNLTTYTDGGYVVEFNRDMTTEAFLEK
INGLRKEQFLDAATAAIFLHFVIYNPSINLWIQANFLLERNA
QNKLTPYRAELTGFIPNVYSGQDGENLFQIDITKLIMASILLA
FVAYRFYKIKFNTGKLGPAFLYITMEIGFFNCGVGILTIISVAM
SLQQSLQGRDPQELVNSEDFVHLELEADLYKKAELFLTISIM
FLFLRLSYILKLND[3]**RIAIIFLTYSKS**FKELLPFLAIEFPLFLGFV
MVFQIIYGNVFPQYSSFTLAIASQLTMIQGQLNITQFVNYSP
IVSMIVILFYYFFMLFFIISLFQAILIECFRIVIMKNGYPQDKD
QGLSIGDLFKWMFSWTQLFTSKKNTTEEKQKAQQQIKPH
ADQEEKQGINSATEN

Figure III.1C: Whole cilia Lap200 IP.

Peptide	# Times
K.VIEFFTNR	11
K.DQGLSIGDLF.K	10
K.YYISELQIQ.K	9
R.IAIIFLTYS.K	7
R.SNYEMIGGIQL.R	7
K.TVRPALNSLQIDSI.R	5
R.GISNISQITLLLQ.K	4
K.EVQQQNEVQKPPQQEIQLE.K	3
K.AQQQIKPHADQEE.K	3
K.YTIEGIEQGESSSF.R	2
R.LDQQTTFQNL.K	2
K.YVNELQ.R	1
K.AANYQGTFAVHK	1

MKNLQGEINKLHSEIDSKKREITKLKNDNTLRLEKINWIQEK
VRKMQREKKVLELNDQTLSIGHATTKHSTTT[3]**KEVQQQNE**
VQKPPQQEIQLEKMQMLEFFNQYLDQTNKQMVKFQGN
RNRKNGEKDEYINPYPTINL[2]**KYTIEGIEQGESSSF[2]RLDQQT**
TFQNLKELAFYYWNLAPYLRKFDEKDSEIMDDLELTDESHA
RIELKE[11]**KVIEFFTN[4]RGISNISQITLLLQKK[5]KTVRPALNSLQ**
IDSIRITGGN[1]KAANYQGTFAVHKNRIKAIDTYNLFFEKFPG
L[9]**KYYISELQIQKE**FQEQQKELEKGNQEKQEEKKFDLDDMN
CLILSSIVVILVLALLSYTAYLSPKYVNLNFTFINNLIGITSNGEY
NKITSIPEFYYYMENFLGATMYNSDKGDNPF[7]**RSNYEMIGG**
IQLRILRSDLYECE[1]**KYVNELQR**FSCFDVVYDSSKANKSQFL
NYTYQTAEELGIMYFPKGNLTTYTDGGYVVEFNRDMTTEA
FLEKINGLRKEQFLDAATAAIFLHFVIYNPSINLWIQANFLLE
RNAQNKLTPYRAELTGFIPNVYSGQDGENLFQIDITKLIMAS
ILLAFVAYRFYKIKFNTGKLGPAFLYITMEIGFFNCGVGILTIIS
VAMSLQQSLQGRDPQELVNSEDFVHLELEADLYKKAELFLTI
SIMFLFLRLSYILKLND[7]**RIAIIFLTYSKS**FKELLPFLAIEFPLFLG
FVMVFQIIYGNVFPQYSSFTLAIASQLTMIQGQLNITQFVNY
SPIVSMIVILFYYFFMLFFIISLFQAILIECFRIVIMKNGYPQD[10]
KDQGLSIGDLFKWMFSWTQLFTSKKNTTEEKQ[9]**KAQQQI**
KPHADQEEKQGINSATEN

Figure III.2: Backward swimming times of depleted cells in 30 mM KCl. Backward swimming time (seconds) ± standard error of the mean, N=61-221. Asterisk indicates statistical significance compared to the control cells, caret indicates significantly different compared to *PKD2* depleted cells (ANOVA, multiple comparison tests, $P<0.001$).

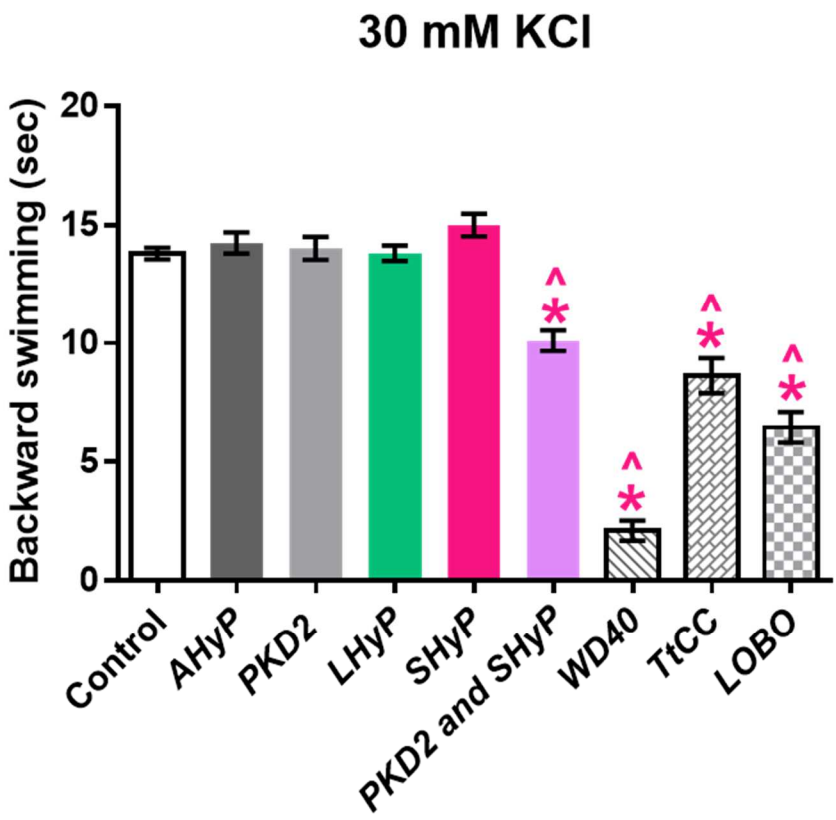

Figure III.3: Backward swimming times of depleted cells in 25 mM TEA with 10 mM NaCl. Backward swimming time (seconds) ± standard error of the mean, N=60-148. Caret and asterisk indicates statistical significance, ANOVA, multiple comparison tests, $P<0.05$ and $P<0.01$, respectively.

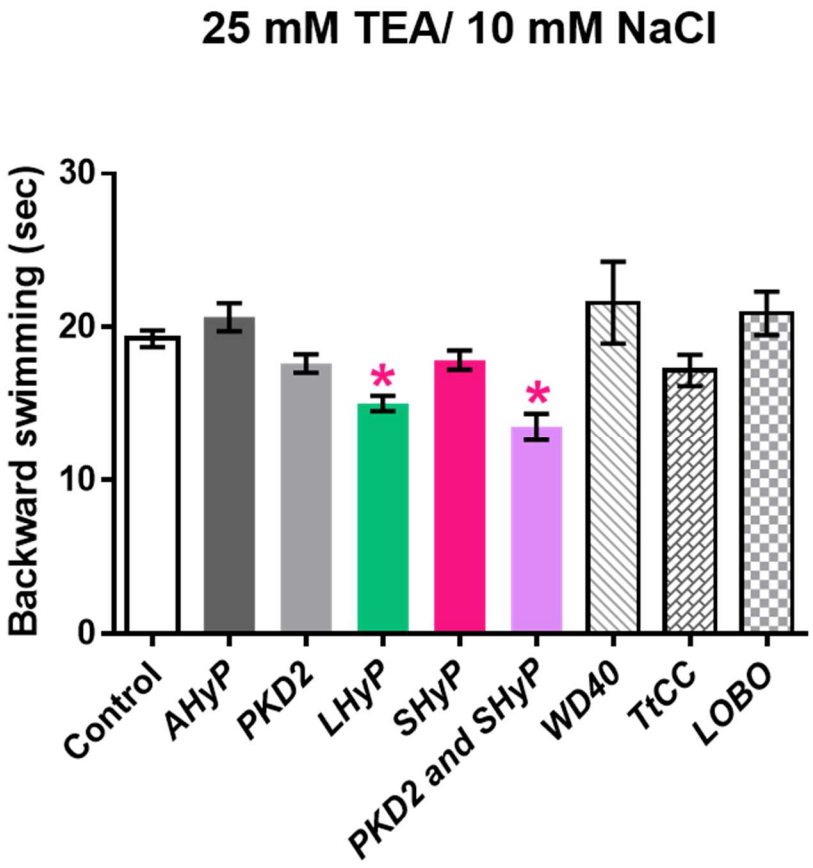

Figure III.4: Backward swimming times of depleted cells in 25 mM TEA with 5 mM $MgCl_2$. Backward swimming time (seconds) ± standard error of the mean, N=59-224. Asterisk indicates statistical significance compared to the control cells, caret indicates significantly different compared to *PKD2* depleted cells (ANOVA, multiple comparison tests, $P<0.001$).